

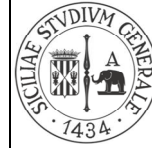
NOTA: anche questa pagina bianca fa parte del blocco di pagine della tesi

NOTA: tagliare il blocco di pagine della tesi (stampata fronte-retro) lungo le due linee qui tracciate prima di effettuare la rilegatura
La terza linea, sulla destra, indica il taglio finale che può essere fatto prima o dopo la rilegatura (io direi dopo, ma chiedete a chi fa la rilegatura).

DEPARTMENT OF CIVIL ENGINEERING AND ARCHITECTURE

*Ph.D. Thesis in Assessment and Mitigation of Urban and
Territorial Risks*

XXX cycle



UNIVERSITÀ
degli STUDI
di CATANIA

Francesca Barbagallo

**AN OVERDAMPED MULTIMODAL ADAPTIVE
NONLINEAR STATIC PROCEDURE FOR SEISMIC
ASSESSMENT OF RC INFILLED BUILDINGS**

Supervisor:

Prof. Edoardo M. Marino

Advisors:

Prof. E. M. Marino

Prof. A. Ghersi

Prof. M. Nakashima

INDEX

Introduction.....	7
Chapter 1.....	13
SEISMIC ASSESSMENT OF EXISTING STRUCTURES.....	13
1. State of the art of nonlinear methods of analysis.....	13
2. The conventional pushover analysis.....	19
3. Nonlinear static methods in seismic codes.....	22
3.1. The equivalent SDOF system according to the N2 method.....	24
3.2. The equivalent SDOF system according to the capacity spectrum method.....	25
4. The multimodal pushover analysis.....	26
4.1. The multimodal pushover analysis by Chopra and Goel.....	28
5. The adaptive pushover analysis.....	35
5.1. The adaptive pushover analysis by Gupta and Kunnath.....	38
5.2. The displacement adaptive pushover analysis by Antoniou and Pinho.....	40
6. The N1 method.....	46
7. The Advanced N1 method by Ghersi et al.	48
8. Evaluation of displacement demand of structures.....	51
8.1. Estimation of maximum displacement demand and influence of the equivalent viscous damping.....	51
8.2. Evaluation of the hysteretic damping.....	53
8.3. Formulations for the determination of equivalent viscous damping.....	54

Chapter 2.....	57
PROPOSAL OF THE OVER-DAMPED DISPLACEMENT ADAPTIVE PROCEDURE.....	57
1. Object	57
2. Description of the over-Damped Displacement Adaptive Procedure	58
2.1. Definition, application and scaling of the load vector	59
2.2. Association of the displacement demand to the peak ground acceleration.....	63
2.3. Application of the overdamping correction.....	64
3. Influence of the energy dissipation through equivalent damping	66
3.1. Definition of the set of accelerograms and evaluation of the parameter η	67
3.2. Influence of the equivalent viscous damping on the evaluation of seismic demand	72
4. Numerical example of the D-DAP	74
Chapter 3.....	81
DESIGN OF CASE STUDY FRAMES	81
1. Object	81
2. General description of the case study frames.....	84
3. Design of GL frames	88
3.1. Loads, materials and design procedure	88
3.2. Geometrical characteristics of GL frames	91
4. Design of SR frames	93
4.1. Loads, materials and design procedure	93
4.2. Geometrical characteristics of SR frames	96
Chapter 4.....	101
CALIBRATION OF THE D-DAP.....	101
1. Object and research methodology	101
2. Modelling of reinforced concrete frames	103
2.1. Set up of the numerical model	103
2.2. Loads and masses.....	104
2.3. Modelling of RC members	106
2.4. Modelling of infill panels.....	111
3. Sensitivity analysis of the parameters ruling the D-DAP	113
3.1. Evaluation of the number of modes enveloped.....	114

3.2. Evaluation of the displacement step size	117
4. Calibration of the equivalent damping law	120
Chapter 5.....	127
VALIDATION OF THE D-DAP	127
1. Object	127
2. Research methodology	128
3. Analysis of the results	129
3.1. Global response	130
3.2. Local response	133
4. Global evaluation of the D-DAP effectiveness	141
Chapter 6.....	149
APPLICATION OF D-DAP IN SEISMIC UPGRADING: AN EXAMPLE	149
1. Object	149
2. The base shear capping building: fundamental characteristics and experimental results	151
2.1. Basic behaviour of the base shear capping building	151
2.2. Experimental studies on the base shear capping system	154
3. Seismic assessment and upgrading of an existing RC frame	165
3.1. Assessment of the existing RC building	166
3.2. Effect of the seismic upgrading of RC building by the base shear capping system	168
Conclusions and future developments.....	171
References	179
Appendix A.....	189
Appendix B.....	199
Appendix C	209
Appendix D.....	229
Appendix E	249
Appendix F	269
List of abbreviations and variables	277

Introduction

The intense research activity of the previous century has focused mainly on the development of design processes that could effectively control the seismic behaviour of new buildings. Indeed, the large amount of data collected from previous seismic events, together with the development of sophisticated programs for structural calculations, improved the reliability of the design approaches of new buildings adopted by engineers in seismic areas. Furthermore, in order to increase even more the level of structural safety, modern seismic codes have imposed that new seismic resistant constructions fulfil very strict requirements, in terms of limit states to be verified and quality of construction details. As a consequence, today the seismic risk of new buildings should be deeply reduced.

Unfortunately, not every building in earthquake prone regions respond to the abovementioned design process. In particular, in the Mediterranean area, as well as other European countries, less than the 10% of the buildings were designed according to modern seismic approaches. Indeed, the main part of the existing building heritage is the product of the so called “economic boom”, that gave a strong impulse to the building activity in the second half of the XX century. The problem is that the seismic zonation at that time was very different from today, and many regions were not considered seismic areas yet, or were classified as sites with a lower seismic risk than today. Thus, the buildings that were constructed in those years were supposed to sustain gravity loads only, or to resist seismic actions lower than those expected today.

Despite their inadequacy to fulfil the requirements of modern seismic codes, those buildings are still fully in function, and are expected to face the earthquakes that will unavoidably occur in future years. However, because of the preservation oriented approach typical of the Mediterranean culture, and the recent economic crisis that has stopped the construction market, a complete renewal of the existing building heritage is not possible. Nonetheless, it is clear that the reduction of seismic risk of existing structures is a pressing need, to avoid inestimable human casualties and economic losses. Because of this, the process of seismic assessment and upgrading of existing structures has gained always more importance in recent years, as it is the most appropriate tool to detect the structural deficiencies and conceive the relevant retrofit interventions, which in turn reduce the seismic vulnerability. Recently, new national laws have been adopted to rule the process of seismic assessment, and to create a culture of seismic prevention even in the “non-technical” population. To this end, the Italian government has introduced in March 2017 a new national decree for the seismic classification of existing structures. According to this, buildings have to be classified into five seismic classes, from E to A. Low seismic classes (such as D or E), include buildings with very weak seismic resistance, while highest classes (up to A) include buildings capable of a better seismic performance. The seismic classification of every building depends on the maximum peak ground acceleration they can withstand and the economic losses expected in case of seismic events. If seismic upgrading interventions are introduced, the seismic class of the building can be improved. It is particularly interesting that, this classification is tightly related to the estimation of the capacity of the structure, and an accurate seismic assessment of the structure is necessary for a reliable evaluation of the seismic class. Based on the frame depicted above, it is clear that the seismic assessment of existing buildings is the fundamental step to (i) estimate the seismic capacity of the initial structure and identify the seismic class of the building, (ii) predict the collapse mechanism and the structural weakness, (iii) select the most appropriate seismic retrofitting technique and determine the seismic class of the upgraded building.

Recently, the scientific research has been devoting increasing efforts in developing methods of analysis to predict the seismic behaviour of existing structures. Since the XX century, linear analyses, such as modal response spectrum analysis or linear static analysis, were adopted as simplified approaches to predict the seismic response of structures. However, since real structures cannot keep an elastic behaviour under strong earthquakes, the prediction obtained by linear analysis cannot be accurate. Indeed, a reliable estimation of seismic performance of existing structures requires the determination of the inelastic deformation experienced by structural members during earthquakes. To this end, the nonlinear dynamic analysis is considered the most reliable tool, which provides high level of accuracy in the prediction of the structural response. Unfortunately, the main shortcomings of this type of analysis are the high computational effort and the significant time consuming character, that make this analysis not applicable for a daily professional use.

From the needing of a tool that accounts for the inelastic deformations of structures subjected to earthquake with the same accuracy of nonlinear dynamic analysis, but with a lower computational burden, the scientific research has developed the nonlinear static methods of analysis. Generally, all nonlinear static methods of analysis develop into two steps: firstly, the performance curve of the structure is obtained by a pushover analysis with a monotonically increasing invariant load vector, secondly the displacement demand is associated to a value of peak ground acceleration through an equivalent Single Degree of Freedom (SDOF) system. Among the approaches available in scientific literature, the Capacity Spectrum Method (CSM), proposed by Freeman et al. [14] and Freeman [15], and the N2 Method, proposed by Fajfar and Gaspersic[16] and Fajfar [17], are the most popular, as they were pioneering methods in this field and were recommended for the seismic assessment of structures by the American and the European seismic code, respectively. Since the use of nonlinear static analysis has been allowed by codes, this method has gained popularity among professional engineers, as a simplified tool to assess existing buildings. Although the results obtained by these analyses are generally considered reliable for

plane frames, however they are affected by the assumptions at the base of the methods. Indeed, common nonlinear static analyses do not take into account the contribution of higher modes of vibration to the seismic response, and do not consider the progressive reduction of the structural stiffness due to the nonlinear behaviour of the structure. To improve the level of accuracy, advanced nonlinear static methods of analysis were developed. Among others, Paret et al., Sasaki et al., Moghadam and Tso, Chopra and Goel, Sucuoglu and Gunay [18-22] developed nonlinear static methods of analysis with multimodal character, while Bracci et al, Gupta and Kunnath, Requena and Ayala, Skaheri et al. proposed an adaptive variant [23-26]. More innovative approaches are the DAP proposed by Antoniou and Pinho [27,28] and Pinho et al.[33], and the Advanced N1 method proposed by Ghersi et al. [34] and Lenza et al.[35]. Despite the innovative character of these methods, however the DAP still requires the approximation to a SDOF system for the evaluation of the displacement demand, whilst the Advanced N1 method neglects the effect of the energy dissipation due to the inelastic behaviour of the structure, which increases as the seismic excitation becomes stronger.

In addition to this, an important aspect is that existing structures are generally endowed with infill panels. Usually, infills are considered nonstructural elements, and because of this their contribution to the seismic response is “conservatively” neglected. However, frames with infill panels have a significantly larger stiffness, and their dissipative capacity and collapse mechanism are deeply influenced by the presence and the mechanical properties of infills. Despite this, neither the nonlinear static methods of analysis suggested by codes, nor the advanced nonlinear static methods were conceived to provide an accurate estimation of the nonlinear behaviour of infilled frames, which may be “unconservative”.

With the background depicted above, the main purpose of this thesis is the development of a nonlinear static method of analysis that, with acceptable computational costs, can accurately estimate the seismic response of RC frames, with and without infill panels. To this end, the thesis proposes a multimodal adaptive procedure named

overDamped Displacement Adaptive Procedure (D-DAP). This method has been developed by combining the approach adopted by Antoniou and Pinho[28] and Pinho et al [33], to update the load vector, and the procedure by Ghersi et al. [34] and Lenza et al. [35] for the association of the peak ground acceleration to the displacement demand without the SDOF approximation. In addition, the D-DAP explicitly considers the increase of the energy dissipation due the cumulated damage in the structure by means of a larger value of equivalent damping. In particular, the value of the equivalent damping is updated at each step, depending on the ductility demand of the structure and the elastic fundamental period, and it is calculated through a law, which has been specifically calibrated in this work on RC framed structures, with and without infills.

The development of the D-DAP followed two steps: first, the parameters ruling the method (i.e. number of modes to be enveloped and size of the incremental step) and the equivalent damping law were calibrated; second, the efficiency of the calibrated method in predicting the seismic response of RC frames was investigated. To this end, a set of 54 RC frames were designed to be representative of existing RC buildings, suffering from various types and levels of seismic deficiency. The sample of case studies includes frames endowed with infill panels with negligible, medium and large stiffness and strength. The adopted research methodology assumed the response obtained by Incremental nonlinear Dynamic Analysis (IDA) as target. The ruling parameters of the D-DAP and the equivalent damping law were calibrated by choosing the values that led to the minimum difference between the response for each cases study frame obtained by the D-DAP and that obtained by the IDA. The accuracy of the D-DAP in predicting the seismic behaviour of the case study frames was compared to the efficiency of other nonlinear static methods available in literature or suggested by seismic codes. This comparison was conducted considering local and global response parameters, and evaluating the error committed by the D-DAP in predicting the response of each case study frame.

In this thesis, the first Chapter is dedicated to the description of the nonlinear static methods drawn from literature and considered in

the preliminary study of the existing background. The second Chapter describes in detail the D-DAP. In the third Chapter the design procedure followed to build up the set of case study buildings is explained and the features of the designed frames are presented. The fourth and the fifth Chapter show the calibration and the validation process of the proposed method. Finally, the sixth Chapter is a practical example of seismic assessment, and consequent retrofitting intervention, of one case study frame by means of the D-DAP.

Chapter 1

SEISMIC ASSESSMENT OF EXISTING STRUCTURES

1. State of the art of nonlinear methods of analysis

Since the beginning of the XX century, some simplified approaches suggested the use of linear analyses, such as modal response spectrum analysis or linear static analysis, for the seismic assessment of structures. However, real structures cannot remain elastic under strong earthquakes. For this reason, a behaviour factor q is introduced to roughly estimate the nonlinear structural response and to reduce the reference pseudo-acceleration response spectrum. Several codes suggest the use of a behaviour factor q , such as EC8 [1]. Based on the structural type and the level of global and local ductility expected from the design of the structure, the value of q suggested for new structures may range between 1.5 and 9. However, the nonlinear structural response mainly depends on the collapse mechanism that the structure develops. Since for existing buildings this is not known *a priori*, the displacement and strain levels that the structure experiences during the seismic event are difficult to be determined. As a consequence, the ductility capacity of the structure, and in turn the behaviour factor q to be used in linear methods of analysis, cannot be accurately estimated. For this reason, seismic codes conservatively suggest q -values in a range between 1.5 and 3. Indeed, this makes the linear methods of analysis too conservative.

This limitation may be overcome if the inelastic deformation experienced by structural members during earthquake can be explicitly determined. In order to accurately assess the seismic performance of existing structures, a displacement-based approach is more advisable. According to this approach, the displacement capacity of the structure has to be compared to the displacement demand, that is the displacements and plastic deformations the structure can experience before reaching a given limit state have to be compared to the displacements and plastic deformations caused by earthquake. The nonlinear dynamic analysis is considered the most reliable tool to evaluate the inelastic response of structures. In particular, this method of analysis offers the advantages to provide the time-history of inelastic response of the structure subjected to a given accelerogram, and to ensure a high level of accuracy in the prediction of the structural response. Unfortunately, for a correct evaluation of the structural response, the nonlinear dynamic analysis requires the definition of several significant aspects. Firstly, the definition of a set of site-specific accelerograms compatible with the seismic spectrum for the considered site is a rather complicate task [2]. Indeed, the current guidelines, provided either by scientific research or by codes, regarding the generation of artificial accelerograms or the selection of natural accelerograms are not necessarily clear and consistent each other [2-5]. Furthermore, especially when incremental dynamic analysis are conducted [6], a big concern is often expressed about the validity of results obtained from records that have been scaled. The issue regards the question whether the seismic response of a structure predicted by using scaled accelerograms can estimate accurately the response of the same structure obtained from unscaled records. Many researchers have worked on this topic and the answers given to that question were not necessarily consistent each other. An additional complexity to run nonlinear dynamic analysis is given by the need of a correct modelling of the nonlinear cyclic behaviour of structural elements. In addition to those aspects, the nonlinear dynamic analysis is computationally demanding, especially when fibre models are employed to simulate multi-storey frames. This means that each nonlinear dynamic analysis has a long duration, which makes it difficult to be repeated.

Furthermore, each nonlinear dynamic analysis produces an extreme large amount of data. Thus, a post-processing work is always required to make the results available for physical interpretation. In conclusion, due to all those complex aspects, the nonlinear dynamic analysis can be considered accessible only for experts in seismic engineering, and it is not suitable for every day design use.

The need for a tool that explicitly considers the inelastic deformation experienced by the structural members during earthquakes without carrying out complex and computational costly nonlinear dynamic analysis led researchers to develop the nonlinear static methods of analysis. The main goal of these methods is to predict the seismic response of structures in a simplified way. Moreover, the use of nonlinear static methods is allowed by most seismic codes, for instance [1,7-13], because it generally provides reasonable results for plane frames. As a consequence, this method has gained popularity in the engineering community as a user friendly tool for seismic assessment of existing buildings.

Basically, the majority of nonlinear static procedures follow two main steps. In the first step the capacity curve of the structure, generally expressed in terms of base shear and top displacements, is evaluated by a pushover analysis. In pushover analysis, a mathematical model of the building is subjected to a monotonically increasing lateral load pattern until a pre-determined target displacement is reached, or the building reaches a collapse mechanism. The lateral load pattern can be assigned in terms of forces or displacement and it should approximate the inertial forces that the building experiences during a ground motion. In the second step, the displacement demand is associated to a value of Peak Ground Acceleration (PGA). Scientific literature offers a variety of approaches for nonlinear static analysis. Among others, the Capacity Spectrum Method (CSM) proposed by Freeman et al.[14] and Freeman [15], and the N2 Method proposed by Fajfar and Gasperic [16] and Fajfar [17] are considered the two fundamental approaches, and they were adopted by the American seismic code FEMA 440 [11] and ATC 40 [12], and the European seismic codes (EC8) [1], respectively.

Since all nonlinear static methods of analyses are quite simplified procedures, their predictions are affected by some assumptions adopted in the two steps. The capacity curve of the structure is determined by the pushover analysis run in the first step. In pushover analysis the static equilibrium equations are solved iteratively and incrementally, to determine the response of the structure undergoing monotonically increasing lateral load pattern. At each step of the pushover analysis, the structural resistance is evaluated, and the stiffness matrix is updated. Thus, each step of pushover analysis provides a complete description of the nonlinear state of the structure, both in terms of forces and displacements. To this end, one key issue is the selection of the lateral load pattern to be applied. In conventional pushover analysis, the distribution along the height of the lateral load pattern is invariant through the steps of the analysis. The invariant load patterns can be categorized in “semi-empirical” and “theoretical”. The “semi-empirical” load patterns are totally independent from the dynamic features of the frame. Instead, the “theoretical” load patterns are based only on the initial elastic dynamic features of the structure. Invariant load patterns commonly used have a linear distribution or a constant distribution along the height. Those two distributions aim at simulating the inertia forces that the structure develops when it vibrates with a predominant first mode or when it shows a soft storey mechanism, respectively.

However, the invariant load patterns generally neglect some important aspects. Firstly, the influence of higher modes of vibration is not taken into account. To overcome this limitation, a number of multimodal analysis have been developed by different researchers, among others Paret et al., Sasaki et al., Moghadam and Tso, Chopra and Goel, Sucuoglu and Gunay [18-22]. Those methods essentially perform a number of conventional pushover analysis equal to the number of significant modes of vibration. In each pushover, a different load pattern is applied, in order to simulate the effect of the considered mode of vibration. The structural response is estimated by combining the effects of each modal response. Although multimodal pushover analyses provide an important enhancement to traditional pushover analyses, however they are not able to consider the effect of the damage cumulated by the

structure on the structural dynamic properties. Because of this, the adoption of an invariant load pattern is likely to provide accurate predictions only for low to medium-rise framed structures. To overcome this drawback, adaptive pushover analysis have been developed by many researchers [23-26]. Basically, in adaptive approaches the loading pattern is updated at each step of pushover analysis, in order to consider the progressive reduction of the structural stiffness due to the nonlinear behaviour of the structure. An innovative approach that combines the multimodal and the adaptive character has been proposed by Antoniou and Pinho [27, 28]. In a first study, the authors suggested a force-based multimodal adaptive analysis (FAP) [27], based on an incremental modal analysis. Later, they developed a displacement-based adaptive pushover (DAP) [28], whereby a set of lateral displacements, rather than forces, is monotonically applied to the structure.

In the second step of the nonlinear static methods of analysis, the displacement demand for a given peak ground acceleration is obtained through the analysis of an equivalent Single Degree Of Freedom (SDOF) system subjected to a seismic input defined by the response spectrum. This step involves the idealization of the Multi Degree Of Freedom system (MDOF) into an equivalent SDOF system. Generally, nonlinear static methods of analyses start from a capacity curve of the MDOF system obtained by a single mode non-adaptive pushover analysis. According to the CSM method, the equivalent SDOF system is elastic with a reduced stiffness due to the spread of inelastic deformations. To take into account the beneficial effect of the energy dissipation in reducing the displacement demand, the equivalent SDOF system is assumed to have a value of damping ratio ξ higher than the nominal one, and it is related to the ductility demand μ . On the contrary, the N2 method assumes the equivalent SDOF system is elastoplastic, with a nominal value of damping ratio ξ , and it follows the equal displacement rule. An alternative simplified approach has been developed by Bosco et al. [29] and it is titled N1 method. According to this method, the nonlinear static analysis can be performed without an explicit reference to a SDOF system. Indeed, the displacement demand may be directly evaluated by the values provided by an elastic analysis (lateral forces or

modal response spectrum analysis), modified to take adequately into account the nonlinear behaviour.

Nevertheless, when the capacity curve of the MDOF system is obtained by adaptive pushover analysis, it is unrealistic to assume an equivalent SDOF system whose dynamic properties are only related to an invariant elastic modal shape. In order to consider the change of the structural properties during the analysis, an adaptive version of the CSM method has been recently developed. According to this variant, the displacement and the acceleration of the equivalent SDOF system are functions of the modal participation factor and the modal mass determined for a modal shape. The main innovation is that those parameters are calculated at each step of the pushover analysis based on the actual deformed pattern at the current step. Ferraioli et al. [30,31] and Pinho and Casarotti [32] proposed the application of such adaptive CSM method for the assessment of steel frames and r.c frames and bridges, respectively. In particular, Ferraioli et al. [30,31] suggested to obtain the inelastic demand response spectra in terms of pseudo-acceleration (S_a) and displacement (S_d) by scaling the 5%-damped elastic demand response spectra by means of ductility reduction factor R_μ . On the other side, Pinho et al. [33] adopted an increasing value of damping ratio evaluated as function of the ductility demand μ of the system. In addition to this, a response spectra scaling factor is evaluated as function of the fundamental period and the equivalent viscous damping. An alternative approach has been developed by Ghersi et al. [34] and Lenza et al. [35]. The authors proposed an advanced multi-modal and adaptive version of the N1 method, whereby a dynamic modal response analysis is run incrementally at each step. A displacement load, rather than force load, vector is determined at every step from the combination of the modal shapes. An elastic response spectra characteristic of the site considered is used. Differently from the previous methods, the evaluation of the displacement demand for a value of peak ground acceleration does not require neither the preliminary evaluation of the performance curve, nor the approximation to a SDOF.

Unfortunately, nonlinear static methods show a lower effectiveness in assessing the seismic behaviour of three-dimensional structures ir-

regular in plan, because they cannot provide a reliable estimate of the deck rotation. In order to overcome this limitation, the nonlinear static approaches suggested by seismic codes for asymmetric structures have been recently improved. For instance, Bhatt and Bento [36] presented an extended version of the Adaptive Capacity Spectrum (ACS) method for plan irregular buildings. In this approach, the ACS method starts from an adaptive displacement pushover and keeps the MDOF-to-SDOF transformation from the original ACS method, as proposed by [32]. The computation of the target displacement is made using the algorithm proposed in FEMA 440 for the calculation of the effective period, damping, reduction factor and the new modified acceleration displacement response spectrum (MADRS) [37]. The torsional effects are taken into account using the correction factors proposed by Fajfar et al. [38] in the extended N2 method for plan-asymmetric buildings. Alternatively, Bosco et al. [39] perform, for each direction of the seismic action, two nonlinear static analysis by applying the lateral forces to two points, which are different from the center of mass. The use of two analyses, rather than one as suggested by EC8, leads to a more accurate estimation of the real displacements at both sides of the deck. More references may be found in literature, however the seismic assessment of three-dimensional structures is beyond the limit of the present work and they will not be considered in the following sections.

2. The conventional pushover analysis

The main goal of pushover analysis is to describe the nonlinear behaviour of structures through the determination of the capacity curve, generally in terms of base shear and top displacement. Pushover analyses can be carried out by using invariant or adaptive load patterns. Invariant load patterns do not change within the structural analysis, whilst adaptive load patterns are updated through the analysis in the attempt of following the modification of the stiffness properties caused by the structural damage. Among the load patterns, a further classification, reported in Marino et al. [40], distinguishes the load patterns named semi-empirical from those defined as theoretical load patterns. Semi-

empirical load patterns are not directly connected to the dynamic properties of the structures or seismic events (e.g. constant and inverted triangular load patterns), and they are invariant. Differently, theoretical load patterns are strictly related to the aforementioned properties. When theoretical load patterns are related to the initial elastic dynamic features of the structure, they are considered invariant load patterns. However, theoretical load patterns can become adaptive if they are updated during the analysis.

Among the semi-empirical load patterns, it can be found:

- Equivalent static forces F_i proportional to the mass m and to the height of the i -th storey:

$$F_i = \frac{m_i}{\sum_j^{n_s} m_j} V_b \quad (1)$$

where n_s is the number of levels and V_b the design value of base shear.

- Equivalent static forces F_i proportional to the mass m and to the height h of the i -th storey with respect to the base of the structure:

$$F_i = \frac{m_i h_i}{\sum_j^{n_s} m_j h_j} V_b \quad (2)$$

If the mass and the storey drifts are the same at each level, then the first load pattern corresponds to the constant distribution, while the second one individuates the inverted triangular distribution.

Among the theoretical load patterns, it can be found:

- Equivalent static forces F_i proportional the eigenvector components of an equivalent mode of vibration [25] evaluated by means of the following equation:

$$\bar{\phi}_i = \sqrt{\sum_{j=1}^{n_m} (\phi_{ij} \Gamma_j)^2} \quad (3)$$

being Γ_j the participation factor and n_m the number of modes taken into account for the evaluation of the equivalent mode of vibration. The equivalent static forces may be calculated by means of the expression:

$$F_i = \frac{m_i \bar{\phi}_i}{\sum_{K=1}^{n_s} m_k \bar{\phi}_k} V_b \quad (4)$$

- The intensity of forces F_i [15] depends on the dynamic properties of the system and on the spectral pseudo-accelerations S_a of the j -th modes of vibration taken into account for the targeted evaluation:

$$F_i = \sqrt{\sum_{j=1}^{n_m} (\Gamma_j \phi_{ij} S_{aj} m_i)^2} \quad (5)$$

- The equivalent static forces are evaluated as the difference between modal storey shears V of contiguous levels [41]:

$$F_i = V_i - V_{i+1} \quad (6)$$

Where $V_i = \sqrt{\sum_{j=1}^n V_{ij}^2}$ is the modal shear force at the i -th level obtained as SRSS combination of the shear forces of the n modes of vibration.

- The horizontal forces are obtained as a function of the difference of the modal storey bending moments M of contiguous levels [40]:

$$F_i = \frac{M_i - M_{i+1}}{h} \quad (7)$$

Once the loading vector is applied along the height of the structure,

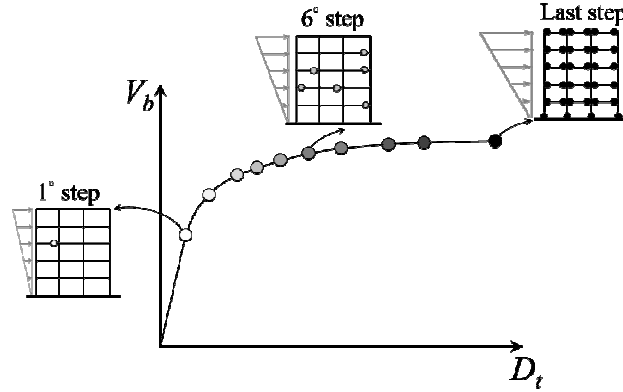


Figure 1 – Example of construction of the capacity curve by pushover analysis, assuming a model with rigid plastic hinges

it is increased progressively until the attainment of a predetermined limit state of the structure. In particular, if a model with rigid plastic hinges is adopted, each step of the pushover analysis ends when a new plastic hinge appears in the structure. Before increasing again the load vector, at the beginning of the following step the structural model is updated to take into consideration the yielding of the sections. At each step of the pushover analysis the seismic response of the structure is determined in terms of different response parameters. In particular, if the base shear and the top displacement corresponding to each single step are plot respectively on y and x axis of a plane, the performance curve of the structure is determined (Figure 1).

3. Nonlinear static methods in seismic codes

The N2 method and the CS method are considered the two main approaches among the existing nonlinear static methods of analysis, and they are suggested by EC8 and ATC40 for seismic assessment of structures. In spite of some important conceptual differences, both CS method and N2 method follow these steps:

- 1) determination of the performance curve
- 2) approximation of the structure under examination to an equivalent SDOF system
- 3) evaluation of the displacement demand of the equivalent SDOF system
- 4) evaluation of the displacement demand of the actual MDOF system.

The performance curve of the structure is obtained by pushover analysis. The vertical distribution of the horizontal forces F_i for pushover analysis is obtained by multiplying the floor masses m_i by a displacement profile Φ . Every reasonable profile Φ can be used. However, it is recommended that the analysis is repeated by two displacement profiles that bound the actual seismic response of the structure. Generally, seismic codes recommend displacement profiles proportional to the first mode of vibration and constant along the height.

Each point of the performance curve can be related to a value of peak ground acceleration. To do this, the displacement demand is preliminary evaluated for a SDOF system equivalent to the MDOF system, by means of elastic response spectra. Once that this relation is determined, given the value of peak ground acceleration, the corresponding top displacement demand of the actual Multi-Degree-Of-Freedom (MDOF) system can be immediately evaluated. If a modal displacement profile Φ is used, the mass m^* of the equivalent SDOF system is related to the effective modal mass M^* corresponding to the considered mode shape by the equation

$$m^* = \frac{M^*}{\Phi_n \Gamma} \quad (8)$$

where Φ_n is the value of the displacement profile at the top storey, and Γ is evaluated using the following equation:

$$\Gamma = \frac{\sum m_i \Phi_i}{\sum m_i \Phi_i^2} \quad (9)$$

Note that, if a single mode of vibration is considered, Γ is the modal participation factor. The performance curve of the MDOF system is scaled by means of the following equations:

$$F^* = \frac{V_b}{\Phi_n \Gamma} \quad (10)$$

$$D^* = \frac{D_t}{\Phi_n \Gamma} \quad (11)$$

where V_b and D_t are the base shear and the top displacement of the MDOF system.

The performance curve scaled by Equation 10 and 11 is used to determine the other features of the equivalent SDOF. The following sections show the determination of these features and the evaluation of the displacement demand D_{req}^* of the equivalent SDOF system according to N2 and CS method. Finally, the displacement demand of the equivalent SDOF system is transformed back to the top displacement demand D_{req} of the MDOF system by the inverse of Equation 11:

$$D_{req} = \Phi_n \Gamma D_{req}^* \quad (12)$$

The seismic response of the MDOF system, in terms of member internal forces, floor displacement, plastic deformations, etc. is then assumed as that obtained by pushover analysis at a top displacement equal to D_{req} . If any response quantity is larger for a top displacement smaller than D_{req} , this maximum value has to be used instead.

3.1. The equivalent SDOF system according to the N2 method

According to Fajfar [17], the equivalent SDOF system is an elastoplastic system. The force-displacement relationship of this system is obtained from the performance curve scaled by Equation 10 and 11. This curve is idealised, within the relevant range of displacements, by a bilinear relationship characterized by a lateral strength F_y^* and a yield displacement D_y^* . Different equivalence conditions have been suggested in literature or by codes. In this work, the post-yield slope is assumed null and the elastic branch of the bilinear curve is obtained by imposing the intersection with the point of the pushover curve corresponding to a value of lateral force equal to the 60% of the maximum lateral force, as suggested by NTC08 [13]. The coordinates of the yielding point are determined by equating the areas under the original and the idealised curve. The slope of the elastic branch is equal to the ratio $K_1 = F_y^* / D_y^*$ and the period of this SDOF system is:

$$T^* = 2\pi \sqrt{\frac{m^*}{K_1}} \quad (13)$$

In N2 method the displacement demand D_{req}^* of the equivalent SDOF system is related to the displacement of the corresponding elastic structure, which can be obtained as the spectral value $S_{de}(T^*)$. In particular, according to Vidic et al. [42], it is possible to assume:

$$R_\mu = \mu \quad \text{when } T^* \geq T_C \quad (14)$$

$$R_{\mu} = (\mu - 1) \frac{T^*}{T_c} + 1 \quad \text{when } T^* < T_c \quad (15)$$

where R_{μ} is the force reduction factor (ratio of the elastic strength demand to the actual strength of the bilinear system), μ is the ductility demand and T_c is the transition period that separates the constant acceleration branch of the spectrum from the constant velocity branch. Therefore, for structure with large frequency, the displacement D_{req}^* can be evaluated by amplifying the spectral displacement $S_{de}(T^*)$ by a coefficient depending on the force reduction factor R_{μ} , according to the following equations:

$$D_{req}^* = S_{de}(T^*) \quad \text{when } T^* \geq T_c \quad (16)$$

$$D_{req}^* = \frac{1}{R_{\mu}} \left[1 + (R_{\mu} - 1) \frac{T_c}{T^*} \right] S_{de}(T^*) \quad \text{when } T^* < T_c \quad (17)$$

The spectral displacement $S_{de}(T^*)$ may be calculated by the pseudo-acceleration $S_{ae}(T^*)$ as follows:

$$S_{de}(T^*) = \frac{T^{*2}}{4\pi^2} S_{ae}(T^*) \quad (18)$$

3.2. The equivalent SDOF system according to the capacity spectrum method

Differently from N2 method, the Capacity Spectrum Method [15] considers the reduction of the stiffness of the structure due to the formation of plastic hinges by an idealised elastic SDOF system with a reduced stiffness. Freeman assumes that the stiffness of the SDOF system reduces to an equivalent “global” secant stiffness K_g , which is evaluated as the slope of the line connecting the points of the performance curve corresponding to the zero-displacement and the peak displacement demand: $K_g = F_{max}^* / D_{max}^*$. The period of the equivalent SDOF system is:

$$T^* = 2\pi \sqrt{\frac{m^*}{K_g}} \quad (19)$$

Because of the hysteretic behaviour, the actual system is able to dissipate energy during the loading cycles. To take into account the beneficial effect of the energy dissipation in reducing the displacement demand, the equivalent SDOF system is assumed to have a value of damping ratio ξ higher than the nominal one and related to its ductility demand μ . In particular, Freeman provides the values of ξ to be adopted for a set of values of μ [43]. These values are here used to determine the following function, which relates the equivalent damping ratio ξ_{eq} to the ductility demand μ :

$$\xi_{eq} = 1.064\mu^3 - 9.984\mu^2 + 31.41\mu - 17.4122 < 15.715 \quad (20)$$

This function is obtained by minimizing the standard deviation of the differences between the values provided by the proposed function and those given by Freeman. The same bilinear relationship adopted in N2 method is used to evaluate the ductility demand μ .

The displacement demand D_{req}^* of the SDOF system is calculated by the pseudo-acceleration $S_{ae}(T^*)$ provided by an elastic response spectrum with the equivalent damping ratio ξ_{eq} :

$$D_{req}^* = \frac{T^{*2}}{4\pi^2} S_{ae}(T^*) \quad (21)$$

4. The multimodal pushover analysis

The multimodal pushover analyses have been developed in the attempt to improve the performance of nonlinear static analysis by considering the effect of higher modes of vibration on the seismic response. Such methods basically involve multiple pushover analyses, and the load patterns of each pushover analysis are related to the significant modes of vibration of the structure. The structural response is estimated combining the effects derived from each of the modal responses.

Sasaki et al. [19] suggested the Multi-Mode Pushover analysis (MMP). The MMP involves several pushover analyses whereby the load vectors represent the various modes deemed to be excited in the dynamic response. The load patterns are defined based on n significant modes of vibration, and any number n of modes can be used. However, since the mass participation factors become smaller at higher modes, usually only the first few modes are considered. For each mode of vibration, the load pattern is determined by multiplying the mass of each level by the modal shape amplitude at that level. Each pushover curve is converted into the Acceleration-Displacement Response Spectrum format and the Capacity Spectrum Method is applied to evaluate earthquake demand. This method identifies which mode is more critical and where any damage concentration occurs. Nevertheless, it does not provide any results on the overall response of the system since it does not consider any kind of modal combination rule.

A development of the MMP is the Pushover Results Combination (PRC), proposed by Moghadam and Tso [20]. According to this method, the structural response is estimated using the same approach of the MMP analysis, i.e. by combining the results of several pushover analyses carried out with load patterns that are related to the main modes of vibration. The overall response is obtained by weighting the results provided by each pushover analysis compared to the modal participation factors.

A Generalized Pushover Analysis (GPA) has been developed by Sucuoglu and Gunay [22]. This procedure conducts a set of pushover analysis with different generalized force vectors, which are applied incrementally until a prescribed seismic demand is attained for each vector. Each generalized force vector is obtained as a different combination of modal lateral forces and simulates the lateral force distribution acting on the system when a given response parameter reaches its maximum value during the dynamic response. To this end, any response parameter can be selected and the authors suggest the maximum interstorey drift. The target seismic demands for interstorey drifts at selected stories are calculated from the associated generalized drift expressions. The maximum value of any other response parameter is obtained

from the envelope of the results obtained by the GPAs. In case of elastic response, GPA and modal response spectrum analysis provide identical results. From the application to building frames, the authors found that this method is successful in estimating the maximum values of deformations and forces of structural elements with reference to the response history analysis.

Based on the MPA, an alternative procedure named Modal Pushover Analysis (MPA) has been proposed by Chopra and Goel [21]. Since this method has been considered as a term of comparison in the parametric study of the present work for the validation of the results of the proposed method, the following section will be dedicated to describe it in further details.

4.1. The multimodal pushover analysis by Chopra and Goel

In 2002 Chopra and Goel [21] developed an improved pushover analysis based on structural dynamics theory. The motivation of their research stems from the approximations induced by the assumptions adopted in conventional pushover analysis. Seismic demands of structures are generally computed by nonlinear static analysis of structures subjected to monotonically increasing lateral forces with an invariant height-wise distribution until a predetermined target displacement is reached. Both the force distribution and target displacement are based on the assumption that the response is controlled by the fundamental mode and that the mode shape remains unchanged after the structure yields. However, after the structure yields, both assumptions are approximate, and lead to inaccuracies, especially in case of high-rise structures. To overcome these limitations, the authors developed the Modal Pushover Analysis (MPA). Their research was conducted into two steps. As a first step, they demonstrated that the MPA procedure was equivalent to the response spectrum analysis for linearly elastic system. Afterwards, they extended the modal response spectrum analysis to inelastic buildings and presented the MPA for the estimation of the peak values of the response parameters. The same steps are followed in the current section of the thesis.

4.1.1. Dynamic and pushover analysis procedures for elastic systems

Considering a multistorey building, the following equation governs the response of the structure subjected to horizontal earthquake ground motion $\ddot{u}_g(t)$:

$$\mathbf{m}\ddot{\mathbf{u}} + \mathbf{c}\dot{\mathbf{u}} + \mathbf{k}\mathbf{u} = -\mathbf{m}\mathbf{i}\ddot{u}_g(t) \quad (22)$$

where \mathbf{u} is the vector of N lateral floor displacements relative to the ground, \mathbf{m} , \mathbf{c} and \mathbf{k} are the mass, classical damping and lateral stiffness matrices of the system, respectively. Each element of the vector \mathbf{i} is equal to unity. The right side of Equation 22 can be interpreted as effective earthquake forces:

$$\mathbf{p}_{eff}(t) = -\mathbf{m}\mathbf{i}\ddot{u}_g(t) \quad (23)$$

The vector $\mathbf{s} = \mathbf{m}\mathbf{i}$ defines the distribution of the effective forces over the height of the building, and $\ddot{u}_g(t)$ defines the intensity and time variation of the effective forces. This force distribution can be expanded as a summation of modal force distribution s_n , and the effective seismic force can be expressed as the summation of N modal contributions:

$$\mathbf{p}_{eff}(t) = \sum_{n=1}^N \mathbf{p}_{eff,n}(t) = \sum_{n=1}^N -s_n \ddot{u}_g(t) \quad (24)$$

where each n^{th} mode contribution to s and $\mathbf{p}_{eff}(t)$ are:

$$\mathbf{s}_n = \Gamma_n \mathbf{m} \phi_n \quad (25)$$

$$\mathbf{p}_{eff,n}(t) = -\mathbf{s}_n \ddot{u}_g(t) \quad (26)$$

The response of the MDOF system to $\mathbf{p}_{eff,n}(t)$ is entirely due to the n^{th} mode, without any contributions from the other modes. Thus, the response of the MDOF system in terms of top displacements is expressed as:

$$\mathbf{u}_n(t) = \phi_n q_n(t) \quad (27)$$

The modal coordinate $q_n(t)$ is determined as follows:

$$\ddot{q}_n + 2\xi_n \omega_n \dot{q}_n + \omega_n^2 q_n = -\Gamma_n \ddot{u}_g(t) \quad (28)$$

where ω_n and ξ_n are the natural vibration frequency and the damping ratio of n^{th} mode, respectively. Equation 28 represents the standard modal equation governing $q_n(t)$.

The total seismic response of the elastic structure can be described as the summation of n^{th} different contributions. Each n^{th} contribution represents the response of the structure subjected to a distribution of forces proportional to the n^{th} mode of vibration. Thus, the equation of motion is transformed from the nodal coordinates into the modal coordinates q_n . The solution to Equation 28 is provided by:

$$q_n(t) = \Gamma_n D_n(t) \quad (29)$$

The value of $D_n(t)$ is determined from the equation of motion of an equivalent SDOF system with natural frequency ω_n and damping ratio ξ_n equal to those of the n^{th} mode of the MDOF system subjected to $\ddot{u}_g(t)$:

$$\ddot{D}_n + 2\xi_n \omega_n \dot{D}_n + \omega_n^2 D_n = -\ddot{u}_g(t) \quad (30)$$

Finally, the top displacement of the MDOF system can be determined from the top displacement of SDOF system:

$$\mathbf{u}_n(t) = \Gamma_n \phi_n D_n(t) \quad (31)$$

Generally, any response quantity $r(t)$ can be expressed as the modal static response r_n^{st} due to external forces s_n , multiplied by the pseudo acceleration response $A_n(t)$ of the n^{th} mode SDOF system. Therefore, the total response of the system to the total excitation $\mathbf{p}_{eff}(t)$ is:

$$r(t) = \sum_{n=1}^N r_n^{st} A_n(t) \quad (32)$$

The presented equations represent the classical modal response history analysis. However, they were derived unconventionally from the modal expansion of the spatial distribution of the effective earthquake forces. This approach provides the basis for the development of the MPA.

The modal response spectrum analysis allows the evaluation of the peak value r_{n0} of the n^{th} mode contribution $r_n(t)$ as follows:

$$r_{n0} = r_n^{st} A_n \quad (33)$$

Where A_n is the pseudo-acceleration of the n^{th} mode SDOF system, and it is obtained from the pseudo-acceleration response spectrum in correspondence of the natural vibration period of the MDOF system. To estimate the peak value of the total response, the peak modal responses are combined according to the Square Root of Sum of Squares (SRSS) combination.

The same peak value r_{n0} of the n^{th} mode contribution can be obtained by a static analysis that pushes the structure to the roof displacement u_{rn0} due to the n^{th} mode, with a lateral force distribution along the height $\mathbf{s}_n^* = \mathbf{m}\boldsymbol{\phi}_n$. The peak values of modal responses r_{n0} are determined by separate modal pushover analysis and can be combined to estimate the peak of the total response. Indeed, the MPA for elastic system is equivalent to the response spectrum analysis procedure.

4.1.2. Dynamic and pushover analysis procedure for inelastic system

The previous considerations are now extended to the case of inelastic systems. In this case, the relations between lateral forces \mathbf{f}_s at a generic floor and the lateral displacements \mathbf{u} are not single-valued, but depend on the history of the displacements: $\mathbf{f}_s = \mathbf{f}_s(\mathbf{u}, \text{sign}\dot{\mathbf{u}})$. The differential equation governing the inelastic systems becomes:

$$\mathbf{m}\ddot{\mathbf{u}} + \mathbf{c}\dot{\mathbf{u}} + \mathbf{f}_s(\mathbf{u}, \text{sign}\dot{\mathbf{u}}) = -\mathbf{m}\ddot{u}_g(t) \quad (34)$$

Although classical modal analysis is not valid for inelastic systems, it is used to transform the previous equation to the modal coordinates of the corresponding linear system. This elastic system is defined to have the stiffness equal to the initial stiffness of the inelastic system. Both systems have the same mass and damping. Therefore, the natural vibration periods and modes of the corresponding linear system are the same to those of the inelastic system undergoing small oscillations, within the linear range. The displacements of the inelastic system can be expanded in terms of natural vibration modes of the corresponding linear system:

$$\mathbf{u}(t) = \sum_{n=1}^N \boldsymbol{\phi}_n q_n(t) \quad (35)$$

Combining Equation 34 and 35, the equation of motion of a MDOF system vibrating accordingly to the n^{th} mode is obtained:

$$\ddot{q}_n + 2\xi_n \omega_n \dot{q}_n + \frac{F_{sn}}{M_n} = -\Gamma_n \ddot{u}_g(t) \quad (36)$$

The resisting forces F_{sn} depend on all modal coordinates $q_n(t)$, and they imply the coupling of modal coordinates. This means that the equations of motion (36) are coupled for inelastic systems. To overcome this limit, the authors neglected the coupling of N (Equations 36) in modal coordinates and assumed this approximation to develop the Multimodal Pushover Analysis (MPA) for systems in the inelastic range. As in the elastic range, the spatial distribution s of the effective forces is expanded into the modal contributions s_n . The equations governing the response of the inelastic system to the effective seismic forces $\mathbf{p}_{\text{eff},n}(t)$ (Equation 26) are the following:

$$\mathbf{m}\ddot{\mathbf{u}} + \mathbf{c}\dot{\mathbf{u}} + \mathbf{f}_s(\mathbf{u}, \text{sign}\dot{\mathbf{u}}) = -\mathbf{s}_n \ddot{u}_g(t) \quad (37)$$

The solution of the Equation 37 could not be described by the separate contributions of n^{th} mode of vibration (Equation 27), because in the inelastic range the structure does not vibrate accordingly to one n^{th} mode of vibration only, but higher modes contribute to the solution as well. However, because for linear systems $q_r(t)=0$ for all modes other than the n^{th} mode, it is reasonable to expect that the n^{th} mode should be dominant even for inelastic systems. Based on this assumption, the equation of motion of the MDOF inelastic system in modal coordinates can be expressed with Equation 36, with the important approximation that F_{sn} now depends only on one modal coordinate q_n . The solution to Equation 36 can be expressed as:

$$q_n(t) = \Gamma_n D_n(t) \quad (38)$$

Where $D_n(t)$ and F_{sn} are described by:

$$\ddot{D}_n + 2\xi_n \omega_n \dot{D}_n + \frac{F_{sn}}{L_n} = -\ddot{u}_g(t) \quad (39)$$

$$F_{sn} = F_{sn}(D_n, \text{sign}\dot{D}_n) = \phi_n^T \mathbf{f}_s(D_n, \text{sign}\dot{D}_n) \quad (40)$$

Equation 39 may be interpreted as the governing equation of the inelastic SDOF system with the vibration properties of the n^{th} mode. This SDOF system has (1) natural vibration frequency ω_n and damping ratio ξ_n equal to those of the n^{th} mode of the corresponding linear MDOF system, and (2) F_{sn}/L_n-D_n relation between resisting force F_{sn}/L_n and modal coordinates D_n defined by Equation 39. The introduction of the n^{th} mode inelastic SDOF system allows the extension of the concepts established for elastic systems to inelastic systems. Indeed, the response of the system to the total excitation $\mathbf{p}_{eff}(t)$ can be determined by Equation 32. This is the Uncoupled Modal Response History Analysis (UMRHA) and further demonstrations may be found in [21].

The relationship between lateral forces F_s and D_n may be determined by a displacement-controlled non-linear static analysis. However, for the sake of simplicity a force-controlled, rather than displacement-controlled, nonlinear static analysis with an invariant distribution of lateral forces can be conducted. For an inelastic system, no invariant distribution of forces can produce displacements proportional to ϕ_n at all displacements or force levels. However, before any part of the structure yields, the only force distribution that produces displacements proportional to ϕ_n is given by $\mathbf{s}_n^* = \mathbf{m}\phi_n$. Therefore, this distribution seems to be acceptable to determine F_{sn} in Equation 40, even after the structure yields. Such nonlinear static analysis provides the so-called pushover curve, which is different than the F_{sn}/L_n-D_n curve. The structure is pushed to a predetermined roof displacement using the force distribution $\mathbf{s}_n^* = \mathbf{m}\phi_n$, and the base shear V_{bn} is plotted against roof displacement u_{rn} . Afterwards, the $V_{bn}-u_{rn}$ pushover curve has to be converted into to the F_{sn}/L_n-D_n relation. Thus, the two sets of forces and displacements are related as follows:

$$F_{sn} = \frac{V_{bn}}{\Gamma_n}, \quad D_n = \frac{u_{rn}}{\Gamma_n \phi_{rn}} \quad (41)$$

Equation 41 allows the conversion of the pushover curve to the F_{sn}/L_n-D_n bilinear relation represented in Figure 2, where the yield values of F_{sny}/L_n and D_{ny} are:

$$\frac{F_{sny}}{L_n} = \frac{V_{bny}}{L_n \Gamma_n}, \quad D_{ny} = \frac{u_{rny}}{\Gamma_n \phi_{rn}} \quad (42)$$

Knowing F_{sny}/L_n and D_{ny} , the vibration period T_n of the n^{th} mode inelastic SDOF system can be evaluated as follows:

$$T_n = 2\pi \sqrt{\frac{L_n D_{ny}}{F_{sny}}} \quad (43)$$

The estimation of the peak response r_{no} of the inelastic MDOF system to effective earthquake forces $\mathbf{p}_{eff,n}(t)$ can be obtained by increasing the horizontal forces of pushover analysis until the roof displacement is equal to u_{rno} . This value of the roof displacement is $u_{rno} = \Gamma_n \phi_{rn} D_n$, where D_n is the peak value of $D_n(t)$ and it is now determined by solving Equation 39. At this roof displacement, the pushover analysis estimates the peak value r_{no} of any response $r_n(t)$. The response value r_{no} is an estimate of the peak value of the response of the inelastic system to $\mathbf{p}_{eff,n}(t)$, and it also represents the exact peak value of the n^{th} mode contribution $r_n(t)$ to response $r(t)$. Each peak modal responses r_{no} is determined by a separate pushover analysis, and they are combined using an appropriate modal combination rule, to obtain an estimate of the peak value r_o of the total response.

The MPA implies some approximating assumptions. Firstly, this method neglects the coupling of modal coordinates after the yielding of structure. Secondly, although the structure behaves in the inelastic

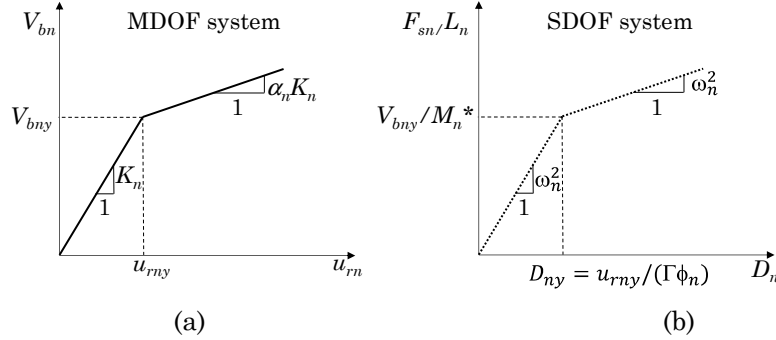


Figure 2 – Properties of the n^{th} mode inelastic SDOF system from the pushover curve: (a) MDOF system; (b) SDOF equivalent system

range, the superposition of the modal contribution in Equation 32 and the SRSS combination of the peak modal responses are considered applicable to evaluate the structural response. Finally, the equivalent SDOF system properties depend on the estimated displacement demand and the SDOF system law is simplified by means of a bilinear curve in UMRHA. Those approximations leads to inaccuracies in the total response in case of inelastic system, while the UMRHA corresponds to the response history analysis for elastic systems.

5. The adaptive pushover analysis

The major drawback of invariant load patterns is that they do not consider the change of dynamic properties of the structure, such as period elongation and stiffness degradation, due to structural yielding. This limitation stems from the inability of invariant load patterns to account for the progressive damage cumulation occurring in the full deformation range.

To go beyond the aforementioned limits and to follow more closely the time-variant distributions of inertia forces of the structure, several researchers (such as Bracci et al. [23], Gupta and Kunnath [24], Requena and Ayala [25], Shakeri et al. [26],) have proposed adaptive approaches to conduct pushover analysis. In adaptive pushover analyses the shape of the applied load vector (force or displacement) is updated at each analysis step, to reflect the dynamic properties of the system at the current step.

Bracci et al. [23] developed a procedure for a quick estimation of the safety margin from collapse of RC frames at a selected seismic demand level. In this procedure, the capacity of the structure is determined by means of an adaptive pushover analysis, whereby the force load vector is a function of the storey shear resistance. Any lateral distribution can be assumed as initial load pattern. At each step, the force applied at each storey is calculated from the storey shear resistance of the previous load step:

$$\Delta F_i^{j+1} = V^j \left(\frac{F_i^j}{V_b^j} - \frac{F_i^{j-1}}{V_b^{j-1}} \right) + \Delta V_b^{j+1} \left(\frac{F_i^j}{V_b^j} \right) \quad (44)$$

where i and j represent the storey location and analysis step respectively, ΔF_i^{j+1} is the incremental i -th storey force at step $j+1$, V^j and V^{j-1} are the total base shear at step j and $j-1$, respectively, F_i^j and F_i^{j-1} are the i -th storey forces applied at step j and $j-1$, respectively, ΔV_b^{j+1} is the incremental base shear at step $j+1$. The internal forces in each member is evaluated at the end of each step and the structural stiffness matrix is updated if any element changes state during that step. The load is applied in small increments until the drift at any level exceeds a specified level or a collapse is imminent. A range of site-specific seismic demand curves is established at different levels of nonlinear behaviour (i.e. from initial elastic response to final failure mechanism) and they are compared to the computed pushover capacities at each storey level of the structure.

An adaptive multiple-run pushover methodology was proposed by Gupta and Kunnath [24]. According to that method, an eigenvalue analysis is carried out before each load increment to determine the period, the eigenvalues of the system and the modal participation factors. Based on those parameters, a number of load patterns corresponding to the number of modes of interest is determined. To define the increment step, each load pattern is scaled based on the number of steps and the target base shear assumed. Then, a static analysis is carried out for each mode independently and the obtained responses for each mode are combined with SRSS and added to corresponding values from the previous step.

Requena and Ayala [25] investigated two variants of adaptive pushover (named approach 2-A and 2-B). Approach 2-A was formulated by Freeman and includes the contribution of higher modes of vibration in the distribution of the lateral loads by means of an SRSS combination of modal forces. The lateral loads are evaluated according to this equation:

$$F_i = \sqrt{\sum_{j=1}^N \left[\left(\frac{\sum_{k=1}^N m_k \phi_{kj}}{\sum_{k=1}^N m_k \phi_{kj}^2} \right) \phi_{kj} Sa_j m_i \right]^2} \quad (45)$$

where ϕ_{kj} is the modal shape of floor k and mode j and Sa_j is the pseudo spectral acceleration of mode j .

An alternative distribution takes into account higher modes of vibration by accepting the existence of an equivalent fundamental mode $\bar{\phi}_i$, determined as SRSS combination of the vibration mode shapes:

$$\bar{\phi}_i = \sqrt{\sum_{j=1}^N (\phi_{ij} \Gamma_j)^2} \quad (46)$$

where Γ_j is the modal participation factor. The equation that defines the distribution of equivalent static loads is the following:

$$F_i = \frac{m_i \bar{\phi}_i}{\sum_{k=1}^N m_k \bar{\phi}_k} V_b \quad (47)$$

The distribution of lateral loads is updated whenever the stiffness of the structure changes during the pushover analysis, due to the development of plastic hinges in some of the structural elements. Thus, the load pattern applied at each step is related to the current inelastic state of the structure.

Generally, load patterns with multimodal features are obtained by SRSS combination of modal loads. However, this approach suffers from an important limit, i.e. the effects of the sign reversal in the higher modes forces are not reflected in the applied load pattern, and thus only the amount of the modal forces is considered. Shakeri et al. [26] proposed a storey shear-based adaptive pushover method that explicitly takes into account the changes in the sign of the storey components in higher modes. At each analysis step, the storey shears V_{ij} associated to each considered mode are calculated as follows:

$$V_{ij} = \sum_{k=i}^n F_{kj} = \sum_{k=i}^n \Gamma_j \phi_{kj} m_k Sa_j \quad (48)$$

where i is the storey level, j is the mode considered, ϕ_{ij} is the i -th component of the j -th eigenvector (mode shape), m_i is the mass of the i -th storey, S_{aj} is the spectral acceleration corresponding to the j -th mode, Γ_j is the modal participation factor for the j -th mode, V_{ij} is the storey shear in level i associated with mode j . In the calculation of the storey shears for each mode using Equation 48, the sign reversal effects of the modal forces in the upper stories are considered. Then, the modal storey shears are combined using the SRSS rule, and the lateral forces required to generate the combined modal storey shears profile are assumed as the lateral load pattern. The required storey forces are calculated by subtracting the combined modal shear of consecutive stories.

An Adaptive Energy-based Pushover Analysis (AEPOA) has been proposed by Albanesi et al. [44]. The authors based their proposal on the consideration that an adaptive load pattern needs to be updated according to the inertial properties of the structure and its kinetic energy. Since every structural response path depends on the seismic intensity, in turn the adaptive pushover analysis depends on the seismic input adopted. The Energy based approach starts from the definition of a predominant response shape, which may be likely to represent the predominant dynamic behaviour of the structure. An effective damping value is assumed for the transient response. An initial velocity profile is calculated based on the previously determined response shape and on the Response Spectrum scaled to the effective damping. Then, a dynamic analysis is performed letting the structure deform under this initial velocity profile. The kinetic energy is dissipated based on the plastic behaviour of the structure. The imposed lateral (force or displacement) profiles at each step are supposed to take into account both the inertial properties of the structure and the kinetic energy dissipated during the earthquake.

5.1. The adaptive pushover analysis by Gupta and Kunnath

The adaptive method proposed by Gupta and Kunnath [24] is a load-controlled procedure. In this method, the distribution of forces is updated based on the dynamic properties of the system, and a site-specific spectrum is used to define the loading characteristics.

The procedure starts from an eigenvalue analysis of the structural model at the current stiffness state (in case of the first step this will be the initial stiffness). The periods of vibrations and the eigenvalues of the system are so determined. Using the storey masses and the eigenvalues, the modal participation factors are calculated. The forces at each storey level and for each of the n -th mode to be included in the analysis, are computed with the following relationship:

$$F_{ij} = \Gamma_j \phi_{ij} W_i S_a(j) \quad (49)$$

Where F_{ij} is the lateral storey force at i -th level for the j -th mode, and $S_a(j)$ is the spectral acceleration corresponding to the j -th mode.

For each mode of vibration, the modal base shears V_{bj} are evaluated as the summation of the lateral forces F_{ij} at all the levels. The building base shear V_b is assumed to be equal to the SRSS combination of the n modal base shears. Then, the storey forces V_{ij} are computed by scaling the base shear of the j -th mode by the factor S_n .

$$V_{ij} = S_n V_{bj} \quad (50)$$

$$S_n = \frac{V_B}{N_s V_b} \quad (51)$$

Where V_B is the base shear estimate for the entire structure and N_s is the number of uniform steps over which the base shear is to be applied. The process of applying lateral forces to the structural model starts from the first iteration. The lateral force is applied incrementally in small equal steps, which could be equal for simplicity.

A static analysis is performed using the scaled incremental storey forces corresponding to each mode independently. All the response parameters are computed by a SRSS combination of the respective modal quantities for this step and are added to the respective quantities of the previous step. At the end of each step, the accumulated value of each response parameter is compared to its respective yielding value. If any members yielded, the global stiffness has changed and the structural model is updated. The procedure starts the following step with a new modal analysis, to determine a new distribution of horizontal forces. In this way, the applied load pattern varies based on the instantaneous

dynamic characteristics of the structure. The entire procedure is repeated until the maximum base shear is reached or the global drift exceeds a specified limit.

5.2. The displacement adaptive pushover analysis by Antoniou and Pinho

Pushover analysis are usually conducted by applying an incremental distribution of forces along the height of the structure. However, the development of deformation- or displacement- based design and assessment methods led to an alternative approach in pushover analysis, where the input is assigned in terms of displacements rather than forces. The displacement loading seems to be the most appropriate option for nonlinear static analysis of structures subjected to earthquakes. Nonetheless, it may suffer from significant shortcomings. For example, if the displacement load vector is assumed invariant, it can neglect some structural characteristics, such as strength irregularities and soft storey mechanisms. To overcome the aforementioned limits, the Displacement Based Adaptive Procedure has been developed by Antoniou and Pinho [27, 28], whereby the displacement loading vector is applied adaptively.

The implementation of the DAP algorithm can be structured in four main steps: (i) definition of the nominal load vector and mass properties of the structure, (ii) computation of load factor, (iii) calculation of normalised scaling vector, (iv) update of loading displacement vector. The first step is carried out only at the beginning of the procedure, while the other three steps are repeated at every step.

5.2.1. Step 1 and 2: definition of the nominal load vector and computation of load factor

The nominal load vector U_o is defined at the start of the procedure. The magnitude of this vector is not relevant for the final results, since the procedure of pushover analysis scales the load vector to automatically meet the analysis target. The nominal load vector defines the structural nodes where the loads are applied to, and it characterizes the load shape throughout the analysis. In particular, in adaptive pushover the

shape of the loading vector is automatically defined and updated depending on the dynamic characteristics of the structure at the current step. For this reasons, the nominal vector at the start of the analysis is equal at all storeys. In addition, the DAP analysis requires the definition of the mass M of the structure, to carry out the eigenvalue analysis, that is employed to update the load vector shape.

The magnitude of the loading vector U at any analysis step is obtained by scaling the nominal vector U_0 by the load factor λ at that step (Eq. 52). The scale factor λ is increased at every step until a predefined analysis target is reached.

$$U = \lambda \cdot U_0 \quad (52)$$

The scale factor is evaluated through a response control incremental strategy. This means that the response of the structure (e.g. a given nodal displacement, or rotation) is directly controlled/incremented. Therefore, the load factor corresponding to such deformation can be evaluated. In this way, the applied loading vector at a particular increment corresponds to the attainment of the target response displacement/rotation at the controlled node.

5.2.2. Step 3: calculation of normalised scaling vector

The normalised modal scaling vector D' is computed at the beginning of every load increment to determine the shape of the load vector at every step. Such scaling vector has to be representative of the actual stiffness of the structure at the end of the previous step. To this end, an eigenvalue analysis is carried out to determine the modal shapes and participation factors of a number of modes deemed to be significant. SRSS combination rule is suggested to combine modal results.

Two approaches are proposed for scaling the load pattern: the displacement-based scaling and the storey-drift-based scaling. According to the displacement-based scaling, the displacement pattern D_i at each storey is obtained from the eigenvalue vectors as follows:

$$D_i = \sqrt{\sum_{j=1}^n D_{i,j}^2} = \sqrt{\sum_{j=1}^n (\Gamma_j \phi_{i,j})^2} \quad (53)$$

where i is the storey number and j is the mode number, Γ_j is the modal participation factor for the j -th mode, ϕ_{ij} is the mass normalised mode shape value for the i -th storey and the j -th mode, and n is the total number of modes.

An alternative scaling scheme is the storey-drift-based scaling. In this approach, the scaling displacement vector is computed from the maximum storey drift values that are obtained from modal analysis. Hence, the displacement pattern D_i at the i -th storey is obtained by summing the modal-combined storey drifts of the levels below the i -th storey, i.e. drifts Δ_1 to Δ_i . In particular, since the storey drifts Δ_{ij} at the i -th storey for the j -th mode are determined using the eigenvalue vectors, D_i is calculated as follows:

$$D_i = \sum_{i=1}^i \Delta_i, \quad \text{where } \Delta_i = \sqrt{\sum_{j=1}^n \Delta_{ij}^2} = \sqrt{\sum_{j=1}^n [\Gamma_j (\phi_{ij} - \phi_{i-1,j})]^2} \quad (54)$$

A further development of Equation 54 has been proposed by Antoniou and Pinho [28] by introducing an additional parameter $S_{d,j}$, i.e. a spectral amplification factor:

$$D_i = \sum_{k=1}^i \Delta_k \quad \text{where } \Delta_i = \sqrt{\sum_{j=1}^n \Delta_{i,j}^2} = \sqrt{\sum_{j=1}^n [\Gamma_j (\phi_{i,j} - \phi_{i-1,j}) S_{d,j}]^2} \quad (55)$$

The spectral amplification represents the displacement response spectrum ordinate corresponding to the period of vibration of the j -th mode. The use of such parameter allows weighting the modal storey drifts according to the instantaneous period of that mode. Thus, the response of the analysed structure is related to the effects that a particular input or spectrum may cause.

The displacements obtained by Equation 55 are normalised to keep the maximum displacement proportional to the load factor. The normalised modal scaling vector D' obtained defines the shape, not the magnitude, of the load (or increment of load) vector.

$$D'_i = \frac{D_i}{\max(D_i)} \quad (56)$$

When the structural response reaches its post-peak range, the shape of the load vector is no longer updated and only its magnitude is updated. This means that a conventional non-adaptive pushover analysis is employed thereafter.

5.2.3. Step 4: update of loading displacement vector

Being the normalised scaling vector D'_i , the scale factor λ and the nominal load vector U_0 determined, the loading displacement vector U_s at a given step s can be updated following two alternative approaches, that lead to significant differences in results: the total updating or the incremental updating.

According to the total updating approach, the load vector U_s at a given analysis step s is a newly derived load vector, that replaces the load vector of the previous step. The update load vector is computed as the product between the current total load factor λ_s , the current normalised modal scaling vector D'_s and the nominal load vector U_0 , as schematically represented in Figure 3 and numerically translated in Equation 57:

$$U_s = \lambda_s \cdot D'_s \cdot U_0 \quad (57)$$

According to the incremental updating approach, the load vector U_s at a given analysis step s is obtained by adding a newly derived load vector increment to the load vector U_{s-1} of the previous step. The increment is computed as the product between the current load factor increment $\Delta\lambda_s$, the current modal scaling vector D' and the nominal load vector U_0 , as schematically represented in Figure 4 and numerically translated in Equation 58:

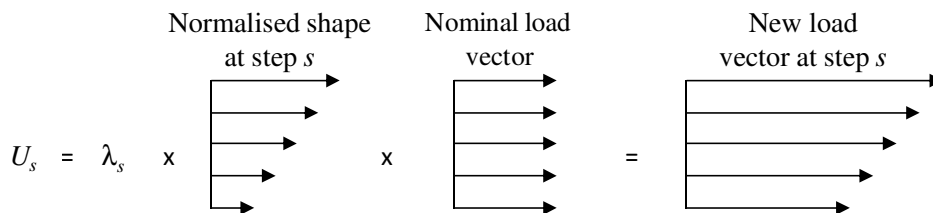


Figure 3 – Graphical representation of loading updating by total updating approach

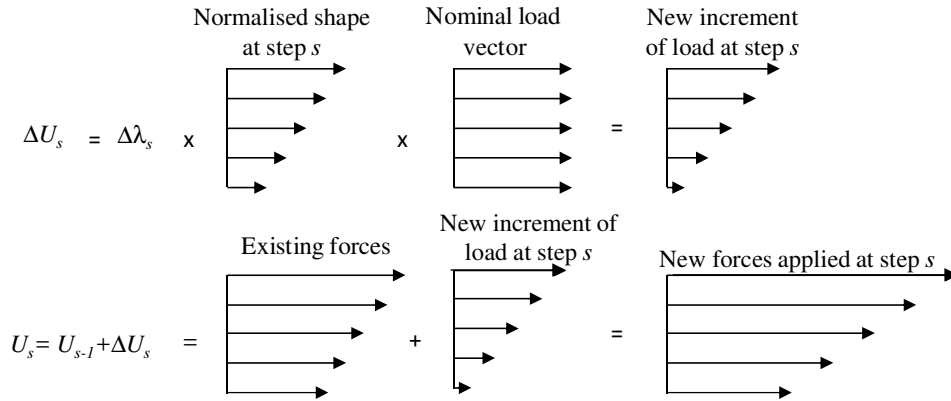


Figure 4 – Graphical representation of loading updating by incremental updating approach

$$U_s = U_{s-1} + \Delta \lambda_s \cdot D'_s \cdot U_0 \quad (58)$$

Thanks to the gradual modification of the load profile, the incremental updating avoids the occurrence of numerical instabilities, and is recommended for a more accurate estimate of the dynamic response characteristics for the examined structures.

5.2.4. Step 5: description of the assessment algorithm

Given the performance curve of the MDOF system, the seismic demand needs to be determined. To this end, Pinho and Casarotti [32] and Pinho et al. [33] have proposed a response-spectrum-based procedure that elaborates the main elements of the Capacity Spectrum Method within an adaptive perspective (named Adaptive Capacity Spectrum Method, ACSM). This procedure has been firstly developed for the seismic assessment of bridges [32], and later it has been updated and tested for the seismic assessment of buildings [33]. It employs the substitute structure methodology to model an inelastic system with equivalent elastic properties, and defines the seismic demand by an appropriately over-damped elastic response spectrum.

In the first step of the ACSM procedure, the equivalent SDOF adaptive performance curve is derived from the MDOF performance curve through a step-by-step determination of the equivalent system

displacements $\Delta_{sys,k}$ and accelerations $S_{a-cap,k}$. The values of $\Delta_{sys,k}$ and $S_{a-cap,k}$ are calculated based on the actual deformed shape at each analysis step k , according to the following equations:

$$\Delta_{sys,k} = \frac{\sum_i m_i \Delta_{i,k}^2}{\sum_i m_i \Delta_{i,k}} \quad (59)$$

$$S_{a-cap,k} = \frac{V_{b,k}}{M_{sys,k} g} \quad (60)$$

$$M_{sys,k} = \frac{\sum_i m_i \Delta_{i,k}}{\Delta_{sys,k}} \quad (61)$$

In the previous equations, $V_{b,k}$ is the total base shear of the system, m_i is the mass at the i -th storey, $\Delta_{i,k}$ is the deformed shape at the i -th storey at the k -th step of the analysis. It is noted that $\Delta_{sys,k}$ and $M_{sys,k}$ are defined as the inverse of the modal participation factor and the modal mass for a modal displacement shape. It is necessary to highlight that both these quantities are calculated step by step based on the current deformed pattern, rather than on an invariant elastic or inelastic modal shape.

In step two of the procedure, the developed adaptive capacity curve is intersected with an appropriately over-damped response spectrum, thus providing an estimate of the inelastic acceleration and displacement demand (i.e. performance point) on the structure. A swift iterative procedure is required at this stage to achieve convergence between the assumed value of equivalent viscous damping ξ_{eq} , used in the derivation of the over-damped spectrum, and that corresponding to the ductility level at the performance point. The authors suggest as a possible approach that combining the ductility-damping relationship proposed by Gulkan and Sozen [45] for Takeda degrading hysteretic response [46] (Equation 62), with the response spectra scaling factors introduced by Lin and Chang [47] as function of the period T of the equivalent SDOF system (Equation 63).

$$\xi_{eq-TakGulSoz} = \xi_0 + 0.2 \left[1 - \frac{1}{\sqrt{\mu}} \right] \quad (62)$$

$$B_{Lin-Change} = 1 - \frac{a \cdot T^{0.3}}{(T + 1)^{0.65}} \quad (63)$$

$$a = 1.303 + 0.436 \cdot \ln(\xi_{eq})$$

Finally, the displacement and acceleration/force of the equivalent SDOF system are transformed back to the MDOF system, and the inelastic seismic demand of the actual structural system is obtained.

6. The N1 method

The N1 Method is a nonlinear static analysis method proposed by Bosco et al. [29]. This method boasts the advantage of the direct evaluation of the displacement demand by the values provided by an elastic analysis (lateral forces or modal response spectrum analysis), modified to take adequately into account the nonlinear behaviour. Thus, any explicit reference to a SDOF system is required.

As for all nonlinear static methods, firstly the nonlinear behaviour of the real structure is determined by a pushover analysis. The base shear V_b versus top displacement D_t relationship represents the performance curve of the structure. In a second step, the displacement demand corresponding to a prefixed value of peak ground acceleration has to be determined. This second step develops into two sub-steps: the determination of the elastic response of the structure and the determination of the displacement demand by the elastic displacement. Assuming that the structure remains elastic, the modal response spectrum analysis provides the strength demand $V_{b,el}$ and the maximum displacement of the top floor D_{el} due to the seismic event for the prefixed peak ground acceleration. The bilinear (elastic-perfectly plastic) relationship equivalent to the performance curve of the actual structure is determined by the usual criteria proposed in literature. The elastic stiffness K_1 is determined as the ratio of the base shear to the top displacement provided by the elastic analysis. The ratio between the lateral strength and the displacement corresponding to the yielding point of the bilinear equivalent curve is defined secant stiffness K_s . After the elastic displacement D_{el} is evaluated, the displacement demand D_{req} can be obtained by cor-

recting D_{el} to take into account the difference between inelastic and elastic behaviour. Two corrections are required: the first one takes into account the reduction of the elastic stiffness of the structure due to the progressive damage of the structure, and the second one accounts for the potential increase of displacement due to the yielding of the structure. The difference between the elastic stiffness K_1 and the secant stiffness K_s is accounted for by evaluating the effective period T_e :

$$T_e = T_1 \sqrt{\frac{K_1}{K_s}} \quad (64)$$

and multiplying the displacement D_{el} by the ratio of the spectral displacements corresponding to the period T_e over the spectral displacements corresponding the fundamental period T_1 . The second correction is based on the equal displacements rule. This correction is necessary for periods shorter than T_c , and it depends on the coefficient R_μ given as ratio of the elastic strength demand to the maximum strength of the structure. Therefore, the following equations are obtained:

$$D_{req} = D_{el} \frac{S_{de}(T_e)}{S_{de}(T_1)} \quad \text{if } T_e \geq T_c \text{ or } R_\mu \leq 1 \quad (65)$$

$$D_{req} = D_{el} \frac{S_{de}(T_e)}{S_{de}(T_1)} \frac{1}{R_\mu} \left[1 + (R_\mu - 1) \frac{T_c}{T_e} \right] \quad \text{if } T_e < T_c \text{ and } R_\mu > 1 \quad (66)$$

Note that, analogously to all the other methods, R_μ is related to the bilinear idealization of the performance curve in the relevant range of displacements. Indeed, the strength demand is obtained by multiplying $V_{b,el}$ by the spectral accelerations ratio $S_{ae}(T_e)/S_{ae}(T_1)$, while the maximum strength is the yield value in the bilinear relationship.

It can be demonstrated that, when the distribution of horizontal forces along the height is proportional to the first mode of vibration of the structure (i.e. $\Phi = \Phi_1$), N2 and N1 methods provide identical results. Instead, when the assumed vector Φ is not proportional to the first mode of vibration, the mass m^* and the coefficient Γ considered by the N2 method are different from m_1^* and Γ_1 considered by the N1 method and, therefore, the two methods do not provide identical results.

Although static nonlinear methods are mainly used to determine the top displacement demand of a structure for a given peak ground acceleration, they can be also applied to obtain the peak ground acceleration corresponding to every point (D, V_b) of the performance curve. This approach leads to a global vision of the structural behaviour, individuating the values of peak ground acceleration corresponding to different limit states. The procedure to relate the points of the performance curve to the corresponding peak ground acceleration is quite straightforward. When the elastic top displacement D_{el} and the base-shear force $V_{b,el}$ are evaluated by modal spectrum response analysis for a chosen value a_g of peak ground acceleration, the values D_{el} and $V_{b,el}$ corresponding to any other value a_g of peak ground acceleration can be obtained by a scaling. Furthermore, when a point (D, V_b) of the performance curve of the structure is selected, the displacement is defined ($D_{req}=D$) and the bilinear idealization of the performance curve and the period T_e are determined. At the same time, also the ductility μ is known and the force reduction factor R_μ may be evaluated by Equation 14 and 15. Then, the corresponding displacement D_{el} is obtained by inverting Equation 65 and 66. Finally, the peak ground acceleration corresponding to D_{el} is evaluated by multiplying it by the ratio a_g/D_{el} according to the following equations:

$$a_g = a_g \frac{D}{D_{el}} \frac{S_{de}(T_e)}{S_{de}(T_1)} \quad \text{if } T_e \geq T_c \text{ or } R_\mu \leq 1 \quad (67)$$

$$a_g = a_g \frac{D}{D_{el}} \frac{S_{de}(T_e)}{S_{de}(T_1)} \frac{R_\mu}{1 + (R_\mu - 1)T_c / T_e} \quad \text{if } T_e < T_c \text{ and } R_\mu > 1 \quad (68)$$

7. The Advanced N1 method by Ghersi et al.

The procedure proposed by Ghersi et al. [34] and Lenza et al.[35] can be considered as a multimodal and adaptive development of the N1 method. The proposed method is named Advanced N1 method (AN1), and it requires a dynamic modal response analysis to be run incrementally at every step. The displacement load vector is determined at every step

from the combination of the modal shapes. The CQC is generally used to combine the modes of vibration, and the sign of the envelope is assumed equal to the sign of the first mode of vibration. Based on this, the proposed method has the following characteristics:

- It requires the use of an elastic response spectra which is characteristic of the site considered.
- It does not require the approximation to a Single Degree Of Freedom system (SDOF).
- It applies a displacement load vector, rather than a force load vector.
- It has a multimodal and adaptive character.
- It does not require the preliminary evaluation of the performance curve.

First, the proposed method is formulated for the assessment of RC plane frames and then it is extended to 3D framed structures. Furthermore, the proposed approach is re-elaborated as a displacement-based design method that does not require the use of the behaviour factor and takes into account explicitly the plastic deformation capacity of the structure.

The AN1 method requires a modal response analysis of the elastic frame. To do this, the reference elastic response spectra has to be scaled to a reference value $a_{g,ref}$ of peak ground acceleration, which is generally assumed equal to 1 g . The displacement load vector to be assigned in the following step is obtained from the envelope of the n modes of vibration deemed significant, following the displacement-based scaling approach proposed by Antoniou and Pinho. [28]. The displacement load vector is applied to the frame and it is monotonically increased until the attainment of the first plastic hinge. This corresponds to the end of the current step. The displacement attained at the end of the step is determined by the scaled load vector. Thus, the peak ground acceleration corresponding to the attained displacement can be determined by scaling the $a_{g,ref}$ with the same proportion of the load vector. Before the following step starts, the frame model is updated by replacing the yielded sections with plastic hinges. This is consistent with the modelling of concentrated plastic hinges with rigid plastic behaviour. A new modal

response analysis is carried out on the updated model to define the new displacement load vector of the following step. The updated displacement vector is assigned to the frame considering the stress and strain state that it has cumulated until the step before. The new steps can start and the load vector is increased until another yielding occurs and the dynamic properties of the frame change again. The displacement reached at the end of the step is evaluated as the summation of the displacement reached at the previous step and the increment of displacement ΔD at the current step. The increment of Δa_g causing the increment of displacement ΔD can be determined by linear proportion with the reference $a_{g,ref}$ and the increment of displacement of the modal shape ΔD_{mod} :

$$\Delta a_g = \frac{\Delta D}{\Delta D_{mod}} a_{g,ref} \quad (69)$$

The value a_g of peak ground acceleration at the current step is calculated by summing the peak ground acceleration at the previous step to the increment Δa_g of peak ground acceleration.

The AN1 repeats iteratively until a target limit state is achieved. If the structure becomes unstable, the modal response analysis cannot be run, and the displacement demand corresponding to that damage level cannot be determined. In such case, the structure is considered as a single degree of freedom system and the displacement demand is evaluated from the elastic displacement response spectra at a very large period. However, even in case of collapse, the authors recommend to assume the fundamental period around 5 s. This conservatively accounts for a possible residual stiffness of the frame due to the presence of infill panels.

Since the seismic vulnerability of the structure is evaluated step by step by the summation of the increase of peak ground acceleration, the performance curve is not required to this end.

8. Evaluation of displacement demand of structures

Generally, structural and nonstructural damages are caused by lateral displacements. Thus, a proper estimation of lateral displacement (or ductility) demand is a key issue for both design and seismic assessment of structures. The second step of nonlinear static methods of analysis is intended at evaluating the displacement (or ductility) demand of the structure beyond its elastic limit from the maximum displacement demand of a linear equivalent SDOF system. To this end, the estimation of maximum inelastic displacement demand of SDOF systems from the maximum displacement demand of linear elastic SDOF system is the underlying principle of most of nonlinear static procedures. Scientific literature has proposed different approaches to estimate the inelastic demand from maximum elastic displacement of SDOF system. Furthermore, some of those approaches have also demonstrated how the effect of the hysteretic behaviour of the structure may influence the prediction of the inelastic displacement. Thus, the use of the equivalent viscous damping is proposed to account for the dissipative capacity of the structure and to ensure a more accurate prediction of nonlinear behaviour.

8.1. Estimation of maximum displacement demand and influence of the equivalent viscous damping

Although several approximated methods have been proposed in literature, two main approaches to estimate maximum inelastic demands from maximum elastic displacement in SDOF systems can be distinguished [48]: methods based on a displacement modification factor and methods based on the equivalent linearization. According to the method based on a displacement modification factor, the maximum inelastic displacement is estimated as the product of the maximum deformation of a linear elastic system with stiffness and damping coefficient equal to those of the inelastic system (whose maximum displacement has to be determined) times a displacement modification factor. The displacement modification factor is a function of the ductility demand and the fundamental period of vibration, and it varies depending on the spectral

range where the initial period of the SDOF system falls in [48]. The N2 method adopts this approach and considers the influence of the dissipative capacity of structures by means of the equal displacement rule. According to the equivalent linearization method, the maximum deformation is evaluated as the maximum deformation of an equivalent linear elastic system with lower stiffness (generally assumed as secant stiffness) and higher damping coefficient than those of the system whose maximum displacement has to be evaluated. Capacity Spectrum method adopts this approach and takes into account the dissipative capacity of structures by means of the equivalent viscous damping.

Statistical studies [49] showed that the ratio of maximum inelastic to maximum elastic displacement demand is not generally affected by the earthquake magnitude or the distance to the source. However, methods based on the displacement modification factors generally tend to slightly overestimate the maximum displacement, and this occurs mainly in case of stiffness degrading systems. In particular, parametric comparisons showed a higher accuracy of the N2 method with respect to the CS method in case of the elastic perfectly plastic hysteretic systems [50]. Indeed, methods based on equivalent linearization indirectly cover the effect of different hysteretic behaviours and take into account the dissipative capacity of the structure through the equivalent viscous damping. The concept of equivalent viscous damping dates back to a study by Jacobsen [51]. In this study, the stiffness of the equivalent system was assumed equal to that of the real system, and the equivalent viscous damping ratio was obtained from the equation between the actual dissipated energy per cycle and the equivalent damping force. Based on this approach, several alternative contributions have related the equivalent viscous damping to the ductility demand of the system, with reference to various hysteretic models, and these relationships strongly influence the accuracy of the results. In particular, in a numerical investigation Miranda and Ruiz-Garcia [48] compared the capability of different performance based methodologies to estimate the inelastic displacements for various systems with different hysteretic loops. This study also suggested that Jacobsen's approach for the estimation of equivalent viscous damping was generally non conservative for struc-

tures with high hysteretic energy dissipation, and the level of accuracy depended on the specific damping law considered. Thus, the selection of a proper ductility demand-equivalent damping relation is a fundamental step for an adequate estimation of the displacement demand.

8.2. Evaluation of the hysteretic damping

The concept of viscous damping is generally employed to refer to the energy that the vibrating systems dissipate by various mechanisms. Since different damping mechanisms coexist in actual structures, they are all idealised in the concept of equivalent viscous damping. In literature, all the different approaches for the evaluation of the equivalent viscous damping provide the viscous damping ratio as the summation of two contributions: the inherent viscous damping in the elastic range ξ_0 , and the viscous damping ξ_{hyst} due to the hysteretic behaviour:

$$\xi_{eq} = \xi_0 + \xi_{hyst} \quad (70)$$

The value of the inherent viscous damping ξ_0 depends on the structural type, and for RC structures is generally assumed equal to 5%. The value of viscous damping due to the hysteretic response ξ_{hyst} is defined by equating the energy E_D dissipated in a cycle of the real structure (represented by the area E_D enclosed by the hysteresis loop) to the energy dissipated in an equivalent viscous system [52] (Figure 5):

$$\xi_{hyst} = \frac{1}{4\pi} \frac{\omega_n}{\omega} \frac{E_D}{E_{so}} \quad (71)$$

where E_{so} is the stored energy, ω and ω_n are the input frequency and the natural frequency of the structure, respectively. To adopt this approach, it is necessary to assume that both systems are subjected to harmonic excitations, loops are complete and the input frequency is equal to the natural frequency. Given those conditions, the hysteretic damping is evaluated as follows:

$$\xi_{hyst} = \frac{1}{4\pi} \frac{E_D}{E_{so}} \quad (72)$$

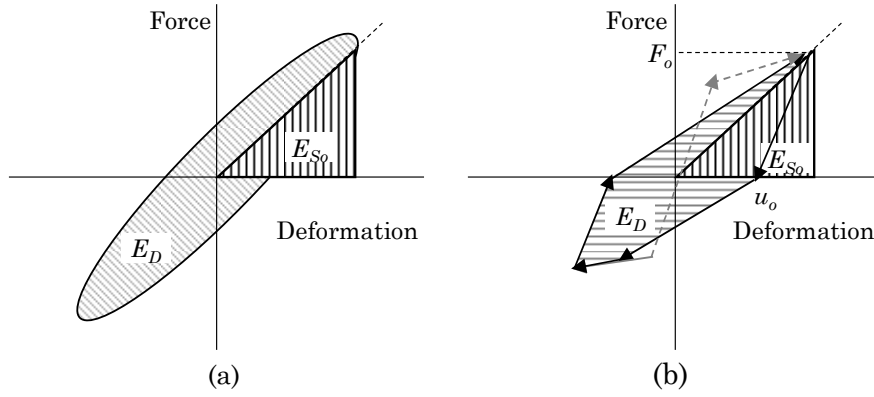


Figure 5 – Dissipated and stored energy in (a) viscous damping system, (b) nonlinear hysteretic behaviour

This energy balance, applied to an elastic-perfectly plastic system that experiences the ductility demand μ , leads to the following function of μ :

$$\xi_{eq} = \xi_0 + \frac{2}{\pi} \left(\frac{\mu - 1}{\mu} \right) \quad (73)$$

8.3. Formulations for the determination of equivalent viscous damping

Scientific literature provides a wide range of equations for the evaluation of the equivalent viscous damping.

Rosenblueth and Herrera [53] proposed a general equation, which is valid for elastic-plastic systems with kinematic strain hardening:

$$\xi_{eq} = \xi_0 + \frac{\frac{2}{\pi} (1 - r_{py}) (\mu - 1)}{\mu - r_{py} \mu + r_{py} \mu^2} \quad (74)$$

Where r_{py} is the ratio between the post-yielding stiffness and the elastic stiffness. This equation can be obtained by extending the approach suggested by Chopra (as explained in section 8.1) to elastic-plastic hardening systems. Indeed, if r_{py} is assumed null, i.e. if the system is perfectly plastic with no hardening, Equation 74 correspond to Equation 73.

Since both Rosenblueth's and Chopra's approaches were based on harmonic loadings, Gulkan and Sozen [45] noted that generally the dis-

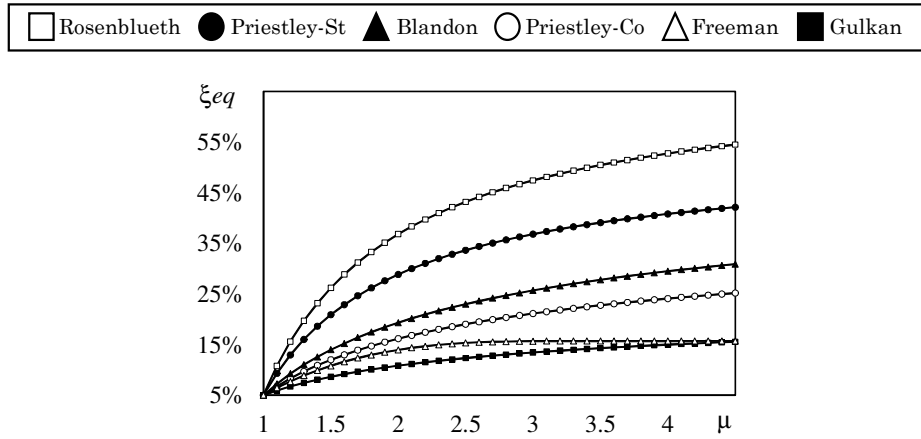


Figure 6 – Equivalent viscous damping laws

placement caused by earthquake motions is smaller than the maximum response predicted. This means that using Equations 73 or 74 would lead to an overestimation of the equivalent viscous damping, and in turn to an underestimation of displacement demand. Thus, considering the Takeda hysteretic model [46], Gulkan and Sozen [45] conducted some experimental shake table tests on small-scale RC frames and proposed an empirical equation (already reported in Equation 62) for the evaluation of the equivalent viscous damping.

Priestley [54] developed several formulations for the evaluation of equivalent damping, which depend on the material of structural members. The formulations reported in this study are referred to steel and concrete members and are expressed by Equation 75 and 76, respectively:

$$\xi_{eq} = \xi_0 + \frac{150}{\pi\mu}(\mu - 1) \quad (75)$$

$$\xi_{eq} = \xi_0 + \frac{120}{\pi} \left(1 - \frac{1}{\mu^{0.5}} \right) \quad (76)$$

More recently, Blandon and Priestley [55] investigated the accuracy of various damping laws by means of nonlinear dynamic analysis on SDOF systems with six different hysteretic models: elastic perfectly

plastic, bilinear type model, a narrow Takeda model, a fat Takeda model, a Ramberg Osgood model and a flag shape model. Based on the results obtained, the authors proposed a more general relationship between the equivalent viscous damping factor and the ductility demand:

$$\xi_{eq} = \xi_0 + \frac{a}{\pi} \left(1 - \frac{1}{\mu^b} - 0.1 r_{yp} \mu \right) \left(1 + \frac{1}{(T_1 + c)} \right) \frac{1}{N} \quad (77)$$

Where a , b , c , and d are numerical coefficients defined for various hysteretic behaviours, T_1 is the fundamental period and N is a normalization factor. First, this equation was calibrated to match as close as possible the values of the effective damping for an effective period of 0.5 s. Then, it was modified to match the damping in case of larger periods, and to adjust when the ductility values are larger than 4.

All these formulations are plotted in Figure 6. The formulation proposed by Rosenblueth provides the highest increase with respect to $\xi_{eq} = 5\%$. The equation developed by Priestley for the steel members provides a larger increase of damping compared to the formulation for concrete elements. The equation proposed by Blandon (plotted for $T_1=1$ s) leads to an intermediate increase of ξ_{eq} , while that one developed by Gulkan and Sozen provides the lowest increase of ξ_{eq} .

Chapter 2

PROPOSAL OF THE OVER-DAMPED DIS- PLACEMENT ADAPTIVE PROCEDURE

1. Object

The main object of this research is to develop a method of analysis that (i) provides a good estimation of the seismic behaviour RC framed buildings with or without infills, (ii) holding acceptable computational costs, (iii) so that it could be a useful tool not only for research purposes but also for professional applications. To this end, the multimodal adaptive nonlinear static methods of analysis, named overDamped Displacement Adaptive Procedure (D-DAP), is proposed. The D-DAP has been developed assuming the Displacement Adaptive Procedure proposed by Antoniou and Pinho [28] and the Advanced N1 method proposed by Ghersi et al. [34] and Lenza et al. [35] as reference starting points. The DAP proposed by Pinho has a multimodal and adaptive character, which allows to overcome some of the weaknesses of the nonlinear static methods of analysis suggested by seismic codes. However, this method adopts an adaptive version of the Capacity Spectrum Method that requires the approximation of the MDOF through the equivalent SDOF system. On the other hand, the AN1 proposed by Ghersi et al. keeps the multimodal and adaptive character of the load vector, and proposes a direct method for the association of the peak ground acceleration to the displacement demand, avoiding the approximation to a SDOF system. However, this method keeps a constant ref-

erence value of damping ratio and does not consider the energy dissipation due to the inelastic behaviour of the structure.

The D-DAP combines (i) the approach adopted by Pinho et al. for the definition of the displacement adaptive multimodal load vector, and (ii) the procedure suggested by Ghersi et al. for the direct association of the peak ground acceleration to the displacement demand. In addition to this, the D-DAP introduces the use of an equivalent damping step in order to consider the energy dissipation due to the damage cumulated in the structure. In principle, whichever damping law available in literature could be used in the D-DAP, but the level of accuracy of the results may significantly vary. Furthermore, depending on the structural type, one damping law may be more or less appropriate than another. In order to make the D-DAP effective for the prediction of RC framed structures, a new damping law has been specifically calibrated in the present work, and its description will be object of Chapter 4.

2. Description of the over-Damped Displacement Adaptive Procedure

The proposed D-DAP can be described in four main steps:

- 1- Definition of the load vector
- 2- Application and scaling of the load pattern
- 3- Association of the displacement demand to the corresponding peak ground acceleration
- 4- Application of the overdamping correction

The method repeats iteratively the steps, until the structural collapse or a target displacement are achieved.

Step 1 and 2 follow the same approach suggested by Pinho et al. and they have already been explained in details in Chapter 1 (Section 5.2). For the sake of simplicity, those steps will be briefly recalled in section 2.1, with emphasis on the details that have been included in the D-DAP. Step 3 and 4 will be described in sections 2.2 and 2.3, respectively.

2.1. Definition, application and scaling of the load vector

The D-DAP applies a load pattern that is assigned along the height of the structure in terms of displacements D . The load vector is updated at every step of the analysis according to the stiffness of the structure at the current step. To this end, every step of D-DAP starts with a modal response spectra analysis, which allows evaluating the fundamental period of vibration of the structure, and taking into account the reduction of the structural stiffness due to the progressive yielding of the structure. This updating process provides the D-DAP with the adaptive feature. The modal response spectra analysis is carried out using an elastic spectrum with a reference peak ground acceleration $a_{g,ref}$ and 5% of damping ratio, and taking into account the contributions of n modes of vibration to the seismic response. For every j -th mode of vibration, the modal shape ϕ_j , the modal participation factor Γ_j and the period of vibration T_j are calculated.

The displacement D_i of the load pattern at the i -th storey is obtained following the interstorey displacement-based scaling approach suggested by Pinho. According to this, the interstorey drift $\Delta_{i,j}$ at every i -th storey and for every j -th mode is calculated as the difference of the j -th modal shapes ϕ_j at the floors i -th and $(i-1)$ -th (Equation 55). Since for planar framed buildings the periods of the observed modes of vibration are generally sufficiently apart, the SRSS combination rule is employed to calculate the interstorey drift Δ_i at the i -th storey. The displacement D_i of the load pattern at every storey is obtained summing the interstorey drifts Δ_i from storey 1 to the i -th concerned storey

At every step of the analysis, a fixed increase of top displacement ΔD_t is imposed (for example, $\Delta D_t = 1$ mm). Thus, the displacement load pattern D obtained from the modal response spectrum analysis has to be scaled, so that the displacement at the top storey D_t corresponds to ΔD_t . The final load pattern applied at the current step s is given by the summation at each i -th storey of the displacement vector cumulated up to the previous step $D_{i,step-1}$ and the increase of the loading vector at the current step $\Delta D_{i,step}$. (following Equation 58).

2.1.1. Displacement response spectra

The definition of the displacement pattern depends on the spectral displacement S_{de} (Equation 55), which in turn is a function of the adopted displacement response spectra. EC8 prescribes that the displacement response spectra (showed in Figure 7(a) for soil type C) be obtained from the acceleration response spectra, according to the following equation:

$$S_{de}(T) = S_{ae}(T) \left[\frac{T}{2\pi} \right]^2 \quad (78)$$

The spectral acceleration S_{ae} (plotted in Figure 7(b) for soil type C) is evaluated according to the following equations:

$$S_{ae}(T) = a_{g,ref} \times S \times \left[1 + \frac{T}{T_B} \times (\eta \times 2.5 - 1) \right] \quad \text{if } 0 \leq T \leq T_B \quad (79)$$

$$S_{ae}(T) = a_{g,ref} \times S \times \eta \times 2.5 \quad \text{if } T_B \leq T \leq T_C \quad (80)$$

$$S_{ae}(T) = a_{g,ref} \times S \times \eta \times 2.5 \left[\frac{T_C}{T} \right] \quad \text{if } T_C \leq T \leq T_D \quad (81)$$

$$S_{ae}(T) = a_{g,ref} \times S \times \eta \times 2.5 \left[\frac{T_C T_D}{T^2} \right] \quad \text{if } T > T_D \quad (82)$$

Where $a_{g,ref}$ is the reference peak ground acceleration, S is the soil coeffi-

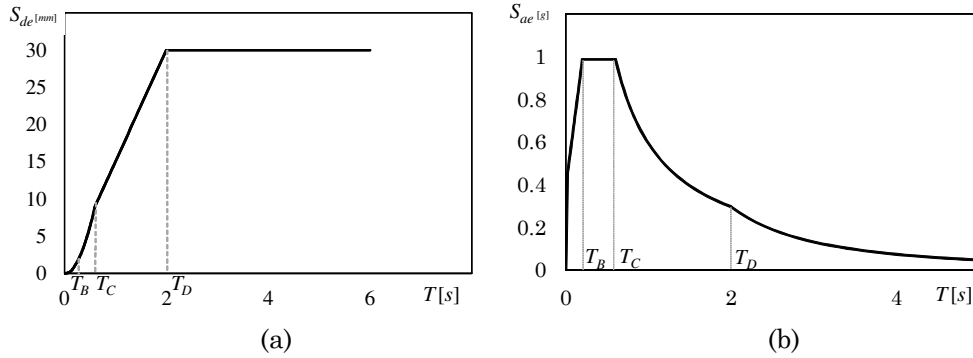


Figure 7 – (a) Displacement response spectra; (b) Acceleration response spectra for soil C

cient, T_B , T_C and T_D are the corner periods which depend on the type of soil considered (values are reported in EC8 – Part 1 – 3.2.2.2) and that define the shape of the spectra. In this case, the values adopted for S , T_B , T_C and T_D were those recommended by EC8 for soil C and type 1 response spectrum, i.e. 1.15, 0.2 s, 0.6 s, 2.0 s, respectively. The parameter η is the corrective factor that depends on the value of damping ratio ξ . Further details about η will be presented in Section 3.1.

2.1.2. Occurrence of collapse mechanism

The occurrence of the collapse mechanism requires additional considerations about the modal response spectra analysis at the beginning of the generic step. In the real world, when the structure becomes unstable, the displacements keep increasing according to the shape of the collapse mechanism that has formed. However, in the proposed procedure, when the structure becomes unstable, one of the eigenvalues tends to be zero and the fundamental period becomes infinite. Thus, the modal response spectrum analysis cannot be run, and therefore the load pattern cannot be updated. In order to overcome this numerical flaw, the structure is assumed unstable when its fundamental period reaches a value T_{NC} sufficiently large. After this period is attained, the D-DAP considers the system as an equivalent SDOF system, with modal participation factor Γ_1 of the first mode of vibration. The top displacement is evaluated using Equation 83

$$D_{MDOF} = S_d(T_{NC}) \cdot \Gamma_1 \cdot \phi_{1,n} \tag{83}$$

and the pattern displacement is not updated anymore. The pushover continues applying a constant increment of top displacement ΔD_t to the pattern load assigned in the following steps. Given the value of $D_{t,MDOF}$, the reference acceleration $a_{g,ref}$ and the increase ΔD_t , the increase of acceleration Δa_g can be evaluated assuming a linear behaviour inside the step:

$$\Delta a_g = a_{g,ref} \frac{\Delta D_t}{D_{t,MDOF}} \tag{84}$$

For RC framed buildings, $T_{NC} = 5$ s is assumed as a fundamental period representative of damaged structures close to the collapse, as

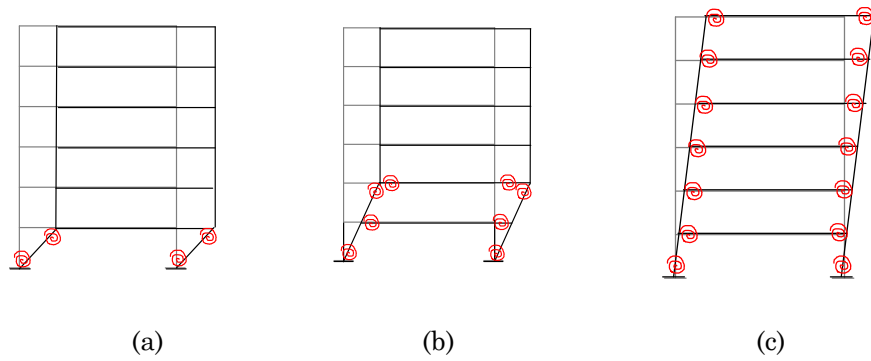
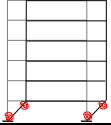
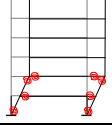
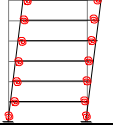


Figure 8 – Collapse mechanisms considered: (a) one storey soft storey, (b) multiple storeys soft storey, (c) global mechanism

suggested in [35], and used to switch from adaptive to constant load pattern.

In order to support this choice, the behaviour of the structure after the collapse mechanism has been investigated. For the sake of simplicity, a one bay six storey frame has been analysed. Three possible collapse mechanisms have been simulated, by introducing in the frame springs with a very low rotation stiffness (Figure 8). In particular, the stiffness of the spring has been assigned so that the structure has a fundamental period of 5 s, consistently with the abovementioned assumption. A modal response spectrum analysis has been conducted on each frame, and the response spectrum has been selected with a value of $a_{g,ref}$ that leads to a top displacement, evaluated from the envelope of all modes of vibration, of 1 mm. The modal mass m_l , the modal participation factor Γ_1 and the top displacement component $\phi_{1,n}$ of the first mode of vibration have been evaluated at the collapse of the structure. The obtained values are summarised in Table 1. Furthermore, the top displacement is determined assuming that the structure behaves as SDOF system, with mass equal to the mass of the entire structure and very low stiffness. Thus, the displacement of the structure obtained considering the contribution of the first mode of vibration only is evaluated by Equation 83. For a period of 5 s, the spectral displacement $S_d(T_1)$ is evaluated by replacing Equation 82 in Equation 78. The obtained values of top dis-

Table 1 – Modal mass and modal participation factor of the first mode of vibration, evaluation of displacement at the structural collapse

			
$a_{g,ref}$ (g)	0.001124	0.001070	0.000878
m_1	99.92%	95.21%	84.59%
$\Gamma_1 \times \phi_{1,n}$	1.0378	1.0889	1.2960
$D_{t,MDOF}$ (mm)	1.000	0.999	0.976
$D_{t,MDOF_modal\ envelope}$ (mm)	1.000	1.000	1.000

placement $D_{t,MDOF}$ are reported in Table 1, along with those obtained by modal response spectrum analysis (1 mm). From the comparison between the displacements obtained with the first mode of vibration and those obtained directly from the modal response spectra analysis combining all the significant modes, it can be noted that those two values are extremely close. Thus, it is reasonable to assume that when the structure collapses it vibrates as SDOF system according to the first mode of vibration, and the first mode of vibration basically follows the shape of the collapse mechanism. Note that the value of top displacement evaluated from the modal envelope equal to 1 mm has been chosen as an example and does not undermine the generality of the conclusion. Indeed, if a different value of this displacement were chosen, also the contribution to the top displacement of the first mode of vibration would change proportionally, and the comparison would lead to the same conclusion.

2.2. Association of the displacement demand to the peak ground acceleration

The final step of the D-DAP provides the association of the displacement to the corresponding Peak Ground Acceleration (PGA). Nonlinear static methods of analysis available in literature require the transformation of the MDOF system into an equivalent SDOF system. In the

proposed D-DAP the ground acceleration corresponding to every top displacement experienced by the structure is directly evaluated, without any other approximations.

As long as the increase of the load pattern is assigned small enough, it is reasonable to assume that the structure has a linear response within the single step of analysis. This allows the use of a linear interpolation to evaluate the increase of PGA $\Delta a_{g,s}$ that has caused the increase of load pattern $\Delta D_{t,s} = D_{t,s} - D_{t,s-1}$ at the step s (note that the increase of load pattern corresponds to the increase of the top displacement of the structure):

$$\Delta a_{g,s} = \frac{D_{t,s} - D_{t,s-1}}{D_t} a_{g,ref} \quad (85)$$

Where D_t is the displacement at the top of the structure obtained from the modal response spectra analysis with response spectra with reference acceleration $a_{g,ref}$. The acceleration $a_{g,s}$ that has caused the top displacement at the end of step s is:

$$a_{g,s} = a_{g,s-1} + \Delta a_{g,s} \quad (86)$$

2.3. Application of the overdamping correction

Because of the increase of the load pattern, the damage tends to cumulate in the structure that experiences an inelastic behaviour. Although the increasing damage in a structure may appear unfavourable, however thanks to the yielding of some structural and nonstructural elements the structure is able to dissipate a larger amount of energy. A higher dissipative capacity is a positive aspect, because it means that the structure has to be subjected to a larger ground acceleration a_g to reach a given top displacement D_t . This means that the equivalent damping ratio is not equal to a fix value, but increases at every step of the analysis along with the spread of the yielding in the structure.

So far, the increase of acceleration $\Delta a_{g,s}$ at a step s (Equation 85) has been evaluated with reference to a response spectrum, that is scaled according to a fix value (here assumed equal to 5%) of equivalent viscous damping ξ_{ref} . The value of ξ_{ref} is included in the factor η (as it will be explained in further detail in Section 3.1), which appears in the equation

proposed by EC8 for the determination of the spectral displacement S_{de} (Equation 79-82). Since in both Equations 85 and 86 the equivalent viscous damping is assumed equal to 5%, the energy dissipated by the structure through the yielding is not taken into account in the evaluation of the peak ground acceleration yet. In order to consider this, the peak ground acceleration evaluated by Equation 86 is corrected considering increasing values of equivalent damping ratios.

To this end, it should be noted that, regardless of the fundamental period T_l or the type of soil, the ratio of a spectral displacement $S_{d,e}^{5\%}$ obtained from the response spectra scaled with 5% damping and the spectral displacement $S_{d,e}^{\xi^*}$ obtained from the response spectra scaled with a larger damping ratio $\xi_{eq} = \xi^*$ is equal to the ratio of the corresponding parameters η :

$$\frac{S_{d,e}^{5\%}}{S_{d,e}^{\xi^*}} = \frac{\eta^{5\%}}{\eta^{\xi^*}} \quad (87)$$

Since η is equal to 1 when the damping ratio is 5% (as demonstrated in the following section), it follows that:

$$S_{d,e}^{\xi^*} = \eta^{\xi^*} S_{d,e}^{5\%} \quad (88)$$

The top displacement D_n is obtained from the summation of the drift evaluated by modal response spectra analysis with response spectra scaled to 5% damping ratio, according to the following equations:

$$D_t^{5\%} = \sum_{i=1}^n \Delta_i \text{ where } \Delta_i = \sqrt{\sum_{j=1}^n \Delta_{i,j}^2} = \sqrt{\sum_{j=1}^n [\Gamma_j (\phi_{i,j} - \phi_{i-1,j}) S_{d,j}^{5\%}]^2} \quad (89)$$

In light of Equation 88, the top displacement D_t can be evaluated considering a response spectra with a larger damping ξ^* by modifying Equation 89 as follows:

$$D_t^{\xi^*} = \eta^{\xi^*} \sum_{i=1}^n \Delta_i = \eta^{\xi^*} D_t^{5\%} \quad (90)$$

Thus, in order to take into account a larger equivalent damping ratio, the increment of acceleration evaluated by Equation 85 can be easily corrected according to the following expression:

$$\Delta a_{g,s}^{\xi^*} = \frac{D_{t,s} - D_{t,s-1}}{D_t^{5\%} \eta^{\xi^*}} a_{g,ref} \quad (91)$$

However, the effect of the equivalent viscous damping is the result of the entire damage cumulated by the structure not only during the single step, but from the beginning of the analysis until the considered step. Based on the demonstration abovementioned, the correction that accounts for the increase of the equivalent damping can be applied more straightforwardly to the total peak ground acceleration evaluated at the end of each step of the D-DAP, according to this equation:

$$a_{g,s} = \frac{a_{g,t}^{5\%}}{\eta(\xi^*)} \quad (92)$$

3. Influence of the energy dissipation through equivalent damping

The value assumed for the equivalent damping ratio ξ_{eq} has a fundamental role in the association of the peak ground acceleration to the displacement demand evaluated by pushover analysis. Indeed, by means of the factor $\eta(\xi_{eq})$, the equivalent damping ratio scales the ordinates of the response spectrum used in the modal analysis (Equation 79-82), or equivalently the ground acceleration associated to a displacement demand (Equation 92). The Italian code and the European code suggest their own equation for the evaluation of $\eta(\xi_{eq})$. However, to estimate more accurately the contribution of the equivalent damping ratio to the seismic response of the structure, a new equation of $\eta(\xi_{eq})$ has been developed in this work, based on the set of accelerograms adopted to run the nonlinear dynamic analysis on the frames considered later.

In the following sections, the adopted set of accelerograms is defined and the new equation of $\eta(\xi_{eq})$ is proposed. Furthermore, the developed equation of $\eta(\xi_{eq})$ is applied considering various damping laws available in literature, to show the influence of different equivalent

damping ratio on the evaluation of the peak ground acceleration corresponding to the displacement demand.

3.1. Definition of the set of accelerograms and evaluation of the parameter η

A set of ten artificial ground motions, compatible with the EC8 elastic spectrum for soil type C and characterized by 5% damping ratio and reference peak ground acceleration for soil type A equal to 0.35 g, is adopted as reference seismic input (Figure 9). In particular, the accelerograms have been generated so that the mean spectrum in terms of displacement is compatible with the displacement spectrum proposed by EC8 in Appendix A. The set of accelerograms included ten ground motion records to fulfil the requirement of EC8-Part 1 [56]. Indeed, according to the code, if the structural response is obtained from at least seven nonlinear time history analyses, with ground motions compatible with code response spectrum, the average of the response quantities from all of these analyses can be calculated.

Each ground motion is characterized by a total duration of 30.5 s and is enveloped by a three branch compound function: the first branch is an exponential increasing function, the second one is a constant function (strong motion phase), and the third one is a function with exponential decay. The duration of the strong motion phase of the accelero-

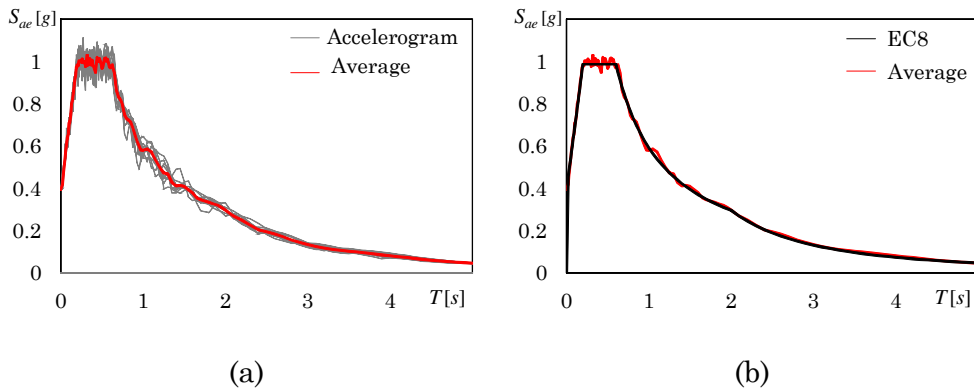


Figure 9 –Elastic response spectra: (a) ten accelerograms with the average elastic response spectra, (b) elastic response spectra of EC8 with the average elastic response spectra

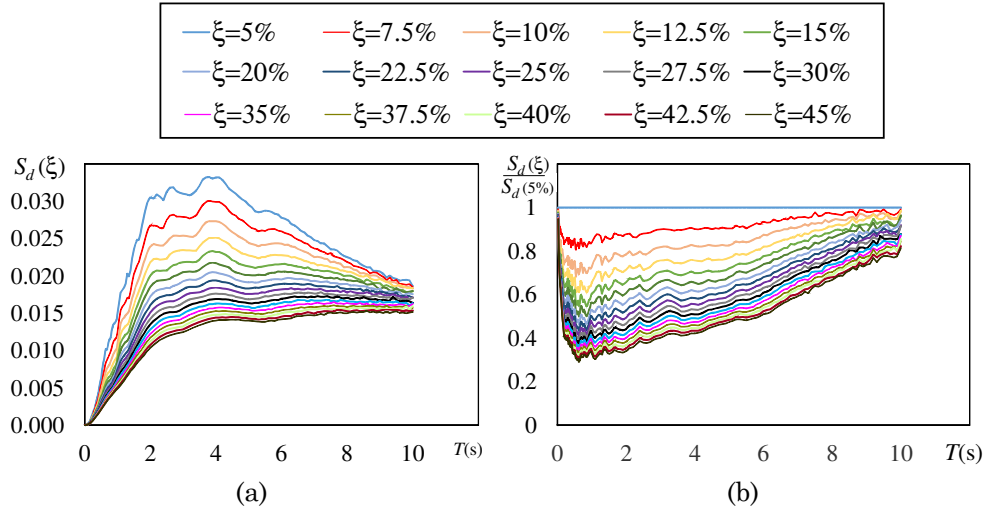


Figure 10 – (a) Mean elastic displacement (m) response spectra for increasing damping ratios; (b) relation between the ratio $\eta = S_d(\xi) / S_d(5\%)$ and the fundamental period T for increasing damping ratios

gram is equal to 7.0 s. Details about the envelope intensity function and the procedure for the determination of the lengths of the parts of the compound function may be found in [57]. The SIMQKE computer program [58] is used to generate these ground motions.

For each of the ten accelerograms, the corresponding elastic displacement response spectrum has been calculated. To this end, the damping ratio is fixed and linear dynamic analysis is conducted by applying each of the considered accelerograms on SDOF systems with increasing fundamental periods. Given a fixed accelerogram, the maximum displacement was evaluated for each of the SDOF considered. The maximum displacements thus recorded and the fundamental periods T of the corresponding SDOF systems provide the response spectra for the fixed accelerogram. When for every considered T , the maximum displacements obtained for every accelerogram are summated and divided by the number of accelerograms (10 in this case), the mean response spectrum of the ten accelerograms is obtained. The procedure is repeated for several values of the dampind ratio ξ_{eq} . Figure 10(a) shows the mean response spectra of the ten accelerograms, and each line refers to

a different value of damping ratio ξ_{eq} . As expected, for fixed values of T , larger damping ratios lead to lower spectral displacements S_d .

In order to investigate the influence of damping ratio on the seismic response of structures, useful information can be obtained considering the parameter η . This latter can be defined, for a fixed value of fundamental period, as the reduction of the spectral displacement due to larger damping ratios with respect to the spectral displacement obtained with a reference damping ratio. Since in the current work RC framed buildings are analysed, the reference value of damping ratio is assumed equal to 5%. Thus, for every considered value of T , η can be determined as the ratio of the spectral displacement obtained with a damping ratio $\xi_{eq} = \xi^*$, and the spectral displacement obtained with 5% damping ratio:

$$\eta(T) = \frac{S_d(\xi^*, T)}{S_d(\xi^{5\%}, T)} \quad (93)$$

For every value of T , the ratio η is calculated considering damping ratios ranging from 5% to 45% in steps of 2.5%. In Figure 10(b) the relation between η and the fundamental period T is plotted, and every line refers to a different damping ratio. Given a fixed T , larger damping ratios lead to lower displacements, and in turn to lower values of the ratio η . However, for a fixed damping ratio, the value of η shows a significant dependence from the fundamental period T . Indeed, three regions with different features of the dependence between the ratio η and the period T may be individuated. For periods lower than about 0.3 s, the ratio η decreases for increasing values of T . On the contrary, for periods larger than about 0.5 s, the ratio η increases with T . Finally, in a rather narrow range of periods, between 0.3 s and 0.5 s, the ratio η reaches its minimum value and keeps stable values close to the minimum.

Both the NTC08 [13] and the EC8-Part 1 [56], suggest to calculate η as function of the damping ratio ξ_{eq} :

$$\eta = \sqrt{\frac{5 + a}{a + \xi_{eq}}} \quad (94)$$

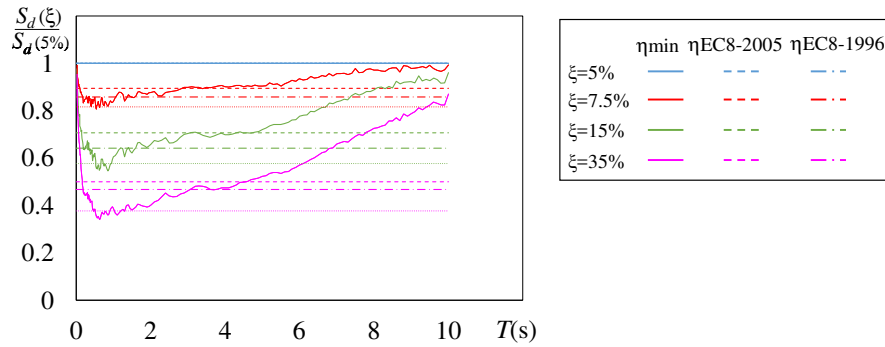


Figure 11 – Relation between $\eta = S_d(\xi) / S_d(5\%)$ and the fundamental period T for damping ratios equal to 5%, 7.5%, 15% and 35%

The value of the coefficient a is suggested equal to 5 by the NTC08 and by the latest version of EC8 (2005), whilst the EC8 draft of 1996 suggested a value of 2. Figure 11 compares the values of the ratio η obtained from the spectral displacement (continuous line) to the values of η evaluated by the Equation 94 with a equal to 5 (dashed line) and 2 (dashed-dotted line). For the sake of simplicity, only 4 values of damping ratios are considered: 5%, 7.5%, 15% and 35%. Generally, given a fixed damping ratio, for very low periods and for very large periods Equation 94 significantly underestimates the value of η compared to that obtained by spectral displacements. For intermediate periods, Equation 94 leads to overestimated values of η . The values of the turning periods that identify the aforementioned three tendencies depends on the value of a and the value of damping ratio. Lower values of a and lower values of ξ_{eq} tend to narrow the intermediate range of periods where η is overestimated. However, given a fixed damping ratio, generally the first turning period is around 0.15-0.20 s, whilst the second turning period is larger than 1.5-2.0 s.

Figure 11 evidences that Equation 94 neglects the dependence of the parameter η from the fundamental period T . In particular, when this leads to overestimated values of η , the contribution of the damping ratio to the evaluation of the seismic demand of the structure is underestimated. This means that in those cases the energy dissipation due to

the progressive yielding of the structure is only partly taken into account. In order to overcome this limit, a corrective factor of the ratio η evaluated by Equation 94 should be introduced, and it should be function of the period T . However, an important shortcoming of this approach is that the corrective factor is not univocally defined. Indeed, since Equation 94 overestimates or underestimates η depending on the value of T , the corrective factor should decrease or increase η in turn.

To simplify the approach, two assumptions were considered: (1) for a given damping ratio the minimum value of η is considered, (2) the dependence from the fundamental period T is introduced through the equivalent viscous damping ξ_{eq} , and to this end a new equation of ξ_{eq} will be calibrated in Chapter 4. Thanks to the first assumption, the value of η is always underestimated and the required correction has to increase η univocally. The second assumption was introduced in order to propose a new simple equation of η that was in accordance with the formulation provided by EC8. This approach is also consistent with other damping laws already available in literature that introduce the dependence from the period T in the equation of the equivalent viscous damping [55].

In order to define the new equation of η , for every value of the

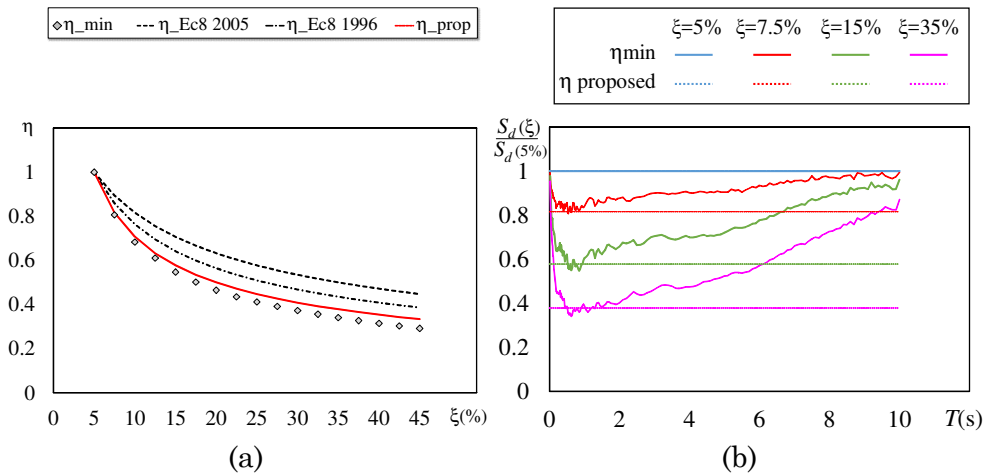


Figure 12 – (a) Relation between the minimum η and damping ratio ξ ; (b) relation between η and the fundamental period T for damping ratios equal to 5%, 7.5%, 15% and 35%

damping ratios considered in Figure 10, the minimum value of η was calculated. The results are depicted by the grey diamonds in Figure 12 (a). For increasing damping ratios, the dashed line and the dashed-dotted line in Figure 10(a) plot the value of η calculated by Equation 94 with a equal to 5 and 2, respectively. For fixed value of ξ_{eq} , both the equations overestimate the minimum value of η obtained from the spectral displacement. Thus, in order to predict more accurate those values, the following equation is proposed:

$$\eta = \sqrt{\frac{5}{\xi_{eq}}} \quad (95)$$

The values of η calculated by the proposed equation are plotted in Figure 12(a) (red line) and it shows that the prediction of the minimum values of the ratio η thus obtained is quite accurate. To better validate the proposed equation, Figure 12(b) compares the values of η obtained from the spectral displacement (continuous line) to the values of η evaluated by Equation 95 (dotted line) for damping ratios equal to 5%, 7.5%, 15% and 35%. This figure confirms that the proposed equation is able to estimate the minimum value of η with a good accuracy, almost regardless of the damping ratio value.

3.2. Influence of the equivalent viscous damping on the evaluation of seismic demand

Generally, formulations available in literature (such as those showed in Chapter 1) evaluate the equivalent viscous damping as function of the of the ductility demand μ . Given a performance curve in terms of base shear V_b and top displacement D_t (Figure 13(a)), the ductility demand μ at a generic step s is evaluated as the ratio of the top displacement $D_{t,s}$ at the considered step s and the yielding displacement D_y . To estimate the yielding displacement, the performance curve is bilinearised (Figure 13(a)). Scientific literature and seismic codes propose different criteria for the bilinearisation of the performance curve obtained by pushover analysis. In this work, given the top displacement corresponding to the final step of the inelastic branch of the bilinear curve (for example Point

A in Figure 13(a)), the elastic branch (starting from the origin 0) of the bilinear curve is obtained by intersecting the pushover curve in correspondence of a lateral force equal to the 60% of the maximum lateral force, as suggested by NTC08 [13]. The post-yield slope is assumed null and the coordinates of the yielding point are determined by equating the areas under the original and the idealised curve.

Figure 13(b) shows the values of the ground acceleration a_g associated to the displacement demand D_t at every step of the D-DAP. The continuous black line is obtained considering a fix value of equivalent damping ratio equal to 5%, thus neglecting the energy dissipation. On the contrary, other curves takes into account the dissipative capacity of the structure by correcting the ground acceleration a_g according to Equations 92 and 95, as explained in the previous sections. Since the estimation of η requires the evaluation of the equivalent viscous damping as function of the ductility demand μ , the influence of various equivalent damping laws was investigated. Thus, each curve refers to a different function adopted for the evaluation of the equivalent viscous damping. Specifically, the damping laws described in Section 8.2 of Chapter 1 are considered. When the damping ratio is kept at 5% and no

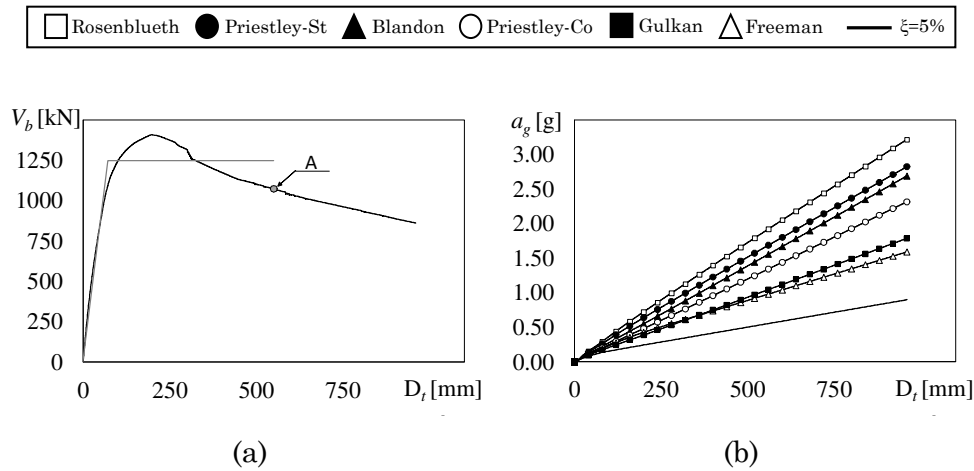


Figure 13 – Performance curve of an RC frame calculated by D-DAP in terms of (a) V_b - D_t and (b) a_g - D_t with various equations for the equivalent damping ratio

energy dissipation is considered, any given value of displacement D_t is reached for lower values of ground accelerations a_g . If the energy dissipation is accounted by means of one of the considered equivalent damping laws, the given displacement D_t is attained for larger ground accelerations a_g . In particular, for a fixed top displacement D_t , the largest and the lowest increases of a_g are obtained by correcting the ground acceleration (Equations 92) considering the equivalent damping laws of Rosenblueth (Equation 74) and Freeman (Equation 20), respectively. Overall, Figure 13(b) demonstrates the critical influence of the energy dissipation on the evaluation of the displacement demand in the D-DAP. Indeed, the selection of the law to evaluate the equivalent damping ratio can lead to a significantly under/over-estimated prediction of the displacement demand, which in turn misleads the assessment of the considered structure. To avoid this, a proper damping law has to be chosen to accurately estimate the displacement demand. To this end, an extensive study on the existing damping laws in literature has been conducted, and a new equation has been proposed in this work specifically for the seismic assessment of RC frames with various characteristics. Details on this part of the research are reported in Chapter 4.

4. Numerical example of the D-DAP

A numerical example is presented in this section to illustrate in details how the D-DAP proceeds to predict the response of RC frames. To do this, a 3-storey 5-span RC frame, with storey mass equal to 106.1 t and fundamental period $T_1=0.4$ s, has been considered. For the sake of simplicity, other details regarding the analysed RC frame are not reported in this section, because they are not necessary to follow the implementation of the numerical example. However, further information about this frame can be found in Chapter 3. The performance curve of this frame in terms of base shear and top displacement (V_b-D_t), and ground acceleration and top displacement (a_g-D_t) is showed in Figure 14(a) and (b), respectively. Those results are obtained by running a D-DAP analysis enveloping three modes of vibration, with top displacement step size of 1 mm, and considering the Priestley damping law for concrete for the

evaluation of the ground acceleration. All the calculations required by the D-DAP, already introduced in Section 2 and 3 of this Chapter, are here applied to a generic step of the analysis. In particular, step 100 is here considered, and the calculations show how the D-DAP acts to push the structure to the following step 101.

At step 100, the considered frame has reached a top displacement $D_t=100\text{ mm}$ and a base shear $V_b=867.6\text{ kN}$ at a peak ground acceleration $a_g=0.329\text{ g}$. The absolute displacements are equal to 20.4, 67.2 and 100.0 at first, second and third storey, respectively. In order to push the structure to the following top displacement (101 mm), the distribution of displacements along the height has to be updated and increased. To this end, a modal analysis of the frame at the last step is conducted. This permits to consider the damage cumulated by the structure until this step (100). The modal shapes and the periods corresponding to the three modes of vibration thus evaluated are reported in Table 2. Given the storey mass equal at all levels, the modal participation factor is calculated for each mode of vibration using Equation 9, and the values are showed in Table 2. The period corresponding to the first mode of vibration at the current step is equal to 3.140 s and is larger than the fundamental elastic mode (0.4 s). This means that the structure at the considered step has experienced a deep inelastic behaviour. To evaluate the spectral displacements corresponding to the periods of the three

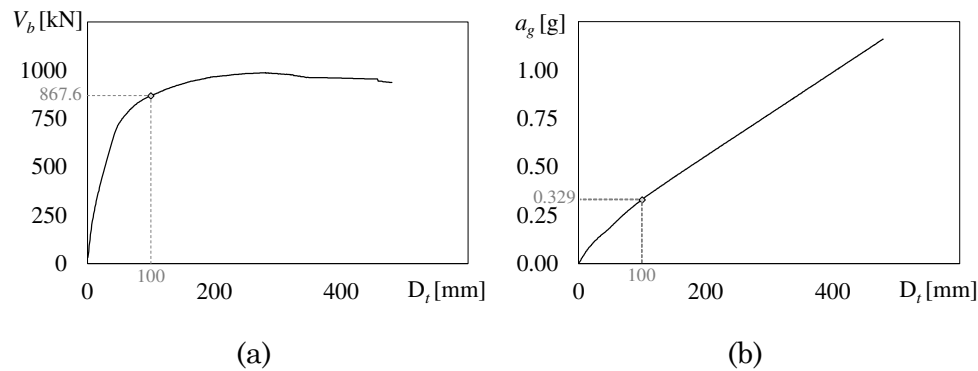


Figure 14 – Performance curve of an RC frame calculated by D-DAP in terms of (a) V_b - D_t and (b) a_g - D_t

Table 2 – Results of the modal analysis at the end of step 100

	Mode 1	Mode 2	Mode 3
Storey	ϕ_1	ϕ_2	ϕ_3
3	-1.000	0.642	0.274
2	-0.655	-0.899	-0.539
1	-0.0791	-0.661	1.000
T_1 [s]	3.140	0.629	0.432
Γ_1	-1.208	-0.554	0.538
S_d [m]	0.874	0.275	0.136

modes of vibration, the elastic response spectrum for soil C, scaled for 5% damping and with reference ground acceleration equal to 1 g is considered. The spectral ordinates corresponding to the periods of the first, second and third mode of vibration are 0.873 m , 0.275 m and 0.136 m , respectively.

Given the modal participation factors and the spectral displacements for all the considered modes, the drift at each i -th storey corresponding to each j -th mode of vibration are evaluated as follows:

$$\Delta_{i,j} = \Gamma_j (\phi_{i,j} - \phi_{i-1,j}) S_{d,j} \quad (96)$$

The values of drifts Δ thus evaluated at each storey and for each mode of vibration are reported in Table 3. Then, the envelope of modal drifts is obtained by SRSS combination of those values. Finally, the updated distribution of absolute displacements D is obtained by summing the enveloped drifts Δ_{env} . All these results are summarised in Table 3.

Table 3 – SRSS combination of drifts and absolute displacements

	Mode 1	Mode 2	Mode 3	SRSS	
Storey	Δ [m]	Δ [m]	Δ [m]	Δ_{env} [m]	D [m]
3	0.364	0.235	0.059	0.437	1.207
2	0.608	0.036	0.113	0.619	0.769
1	0.083	0.101	0.073	0.149	0.149

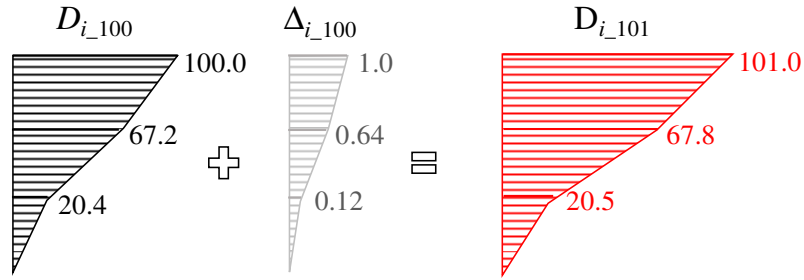


Figure 15 – Evaluation of the updated distribution of displacement

Since the displacement step size Δ_{step} is set equal to 1 mm, the distribution of absolute displacements D (Table 3) evaluated from modal envelope has to be scaled so that the top displacement D_t is 1 mm. To this end, the absolute displacement at each storey has to be scaled by the following factor Ω :

$$\Omega = \frac{\Delta_{step}}{D_t} = \frac{1}{1.207} = 0.000829$$

Thus, the increment of displacement Δ_t to be added to the displacement of the previous step is equal to 1 mm, 0.64 mm and 0.12 mm at the third, second and first storey respectively. Thus, at step 101 the displacements are equal to 101 mm, 67.8 mm and 20.5 mm at the third, second and first storey respectively (Figure 15). Given this displacement vector, the base shear is 869.1 kN.

The last stage of the calculation regards the association of the ground acceleration to the tops displacement of 101 mm. The increment of ground acceleration Δa_g corresponding to the increment of displacement Δ_{step} is evaluated by Equation 85 assuming a reference ground acceleration of 1 g, and it is equal to 0.000829.

$$\Delta a_g = \frac{D_{t,101} - D_{t,100}}{D_{t,101}} = \frac{101 - 100}{1.207} = 0.000829 g$$

With a reference damping ratio of 5%, the total acceleration corresponding to step 100 is 0.177 g, thus the total acceleration with 5% damping ratio at step 101 is 0.178 g (given by the summation 0.177+0.000829). However, to consider the energy dissipation, a larger

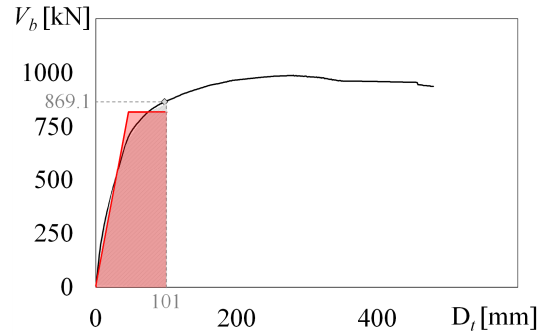


Figure 16 – Construction of the bilinear curve at step 101

equivalent damping ratio has to be evaluated and the peak ground acceleration so far calculated should be corrected consistently. To this end, the pushover curve is bilinearised (Figure 16) in correspondence of step 101, to determine the displacement corresponding to the yielding, and in turn the ductility demand. To build the bilinear curve these steps are followed: (1) the slope of the elastic branch is obtained by connecting the origin to the point of the pushover corresponding to a base shear equal to the 60% of the maximum base shear ($0.6 \times 869.1 = 521.4 \text{ kN}$); (2) the coordinates of the yielding point are obtained by equating the area under the bilinear curve to the area below the pushover curve, between the origin and $D_t = 101 \text{ mm}$, as showed in Figure 16. The yielding point of the bilinear curve is identified by a top displacement and a base shear equal to 46.3 mm and 817 kN , respectively. The ductility demand μ is obtained by dividing the maximum displacement (101 mm) to the yielding displacement (46.3 mm), and it is equal to 2.180. Given the ductility demand, and considering the equation proposed by Priestly for the evaluation of the equivalent damping ratio for concrete elements (Equation 76), the equivalent damping ratio at step 101 is 17.3%:

$$\xi_{eq} = \xi_0 + \frac{120}{\pi} \left(1 - \frac{1}{\mu^{0.5}} \right) = 5 + \frac{120}{\pi} \left(1 - \frac{1}{2.18^{0.5}} \right) = 17.3\%$$

The factor η calculated by Equation 95 is 0.537.

$$\eta = \sqrt{\frac{5}{17.3}} = 0.537$$

In conclusion, the overdamped ground acceleration corresponding to a top displacement of 101 *mm* is evaluated by Equation 92 and is equal to 0.332 *g*.

$$a_{g,101} = \frac{a_{g,101}^{5\%}}{\eta(\xi_{eq})} = \frac{0.178}{0.537} = 0.332 \text{ g}$$

Chapter 3

DESIGN OF CASE STUDY FRAMES

1. Object

The largest construction development occurred in Italy between the Sixties and the Eighties of the XX century. During those years, most of the Italian areas were not considered seismically active yet, thus many buildings were designed without considering seismic provisions, i.e., basically to sustain gravity loads only. Some other areas were already recognized as seismic zones, and the buildings located there were designed according to the seismic codes of that time. The city of Catania is an emblematic case, as it thoroughly exemplifies the situation of the country. In fact, Catania was recognized as seismic areas only in the Eighties, thus its building heritage includes both structures that were designed without considering seismic provisions and structures designed according to old seismic codes. Hence, in order to generate a set of case study frames that could be representative of the existing Italian building heritage, a preliminary survey has been conducted in the urbanized areas of the city of Catania. Figure 17 shows some of the pictures collected in Catania.

Based on the acquired information, it was possible to recognize some features common among the existing buildings. Generally, these RC buildings are rectangular in plan and rather regular in plan and in elevation. The number of storeys usually ranges from four to twelve. The structure is constituted by a 3D RC frame, which is very flexible



Figure 17 – Pictures of existing buildings collected in Catania

and weak in one direction. In fact, resisting elements are mainly disposed along a single direction. Generally, three or more RC frames are arranged along the longitudinal direction of the building and sustain the decks. In the orthogonal direction, frames are located only at the two sides of the building and next to the staircase. Hollow clay block-cement mix unidirectional slabs are generally used. The staircase is usually located in central position. The infill panels of these buildings do not have any structural function, although they interact with the structure during seismic events. Mechanical properties of infills may vary, because of the presence of openings or the low quality of material. Thin and weak walls always make partitions. Frames located in the interior part of the building are generally provided with flat beams, which allow a greater flexibility of the interior distribution of rooms. On the contrary, deep beams are typically used for the perimeter frames. Longitudinal reinforcement of decks and beams are made by bent-up bars.

Depending on the age of the building, smooth- or deformed-rebars were used. Deformed-rebars were mainly used in structures dated back to the seventies or later.

The main goal of the present work is to create an extended set of RC frames to properly calibrate the D-DAP and to broadly investigate its efficiency in predicting the seismic response of frames with different seismic performances. The case study frames are designed to simulate real existing buildings, suffering from different levels of seismic deficiencies and exhibiting various types of collapse mechanisms. To this end, two sets of frames are designed following the information collected in the preliminary survey conducted on real structures. The first set is composed of RC frames (named frames GL) designed for gravity loads only. The second set includes RC frames (named frames SR) designed according to the seismic force level and the provisions stipulated by the old Italian standards for low seismicity zone. All the frames are drawn from 3-, 6- and 9-storey existing RC framed buildings, which are endowed with one-way decks supported on two sides and main reinforcement in one direction only. The frames designed for gravity loads suffer from larger damage concentration and show a less dissipative collapse mechanism. On the contrary, the seismic resistant frames are stiffer and stronger than frames designed for gravity loads. Furthermore, the seismic resistant frames basically comply with the strong-column/weak-beam philosophy and show a more dissipative collapse mechanism. Each set is composed of three types of frames (Type 1, 2 and 3), which differ for the amount of gravity loads resting on beams and columns. The amount of gravity load depends on the location of the frame inside the plan layout of the building, and on the direction of the frame with respect to the orientation of the deck (direction of its main reinforcement).

A noteworthy issue is the role played by the infill panels in the evaluation of seismic response of existing buildings. The observation of post-earthquakes damages on RC buildings has showed that infill panels can significantly affect the seismic response of buildings. If infill panels are uniformly distributed throughout the structure, they usually have a beneficial effect on the seismic response of the structure. How-

ever, a negative effect on the structural performance may be caused by an irregular location of infill panels, especially in elevation. In particular, the soft storey mechanism is one of the typical collapse mechanisms that may generally occur in RC framed structures where infills are missing at one storey, such as the first storey. Nonetheless, soft storey mechanism can also occur in structures with a regular distribution of infill panels due to the weakness or the brittleness of the infills. Such cases were observed for instance during L'Aquila earthquake, which stressed the large vulnerability of RC infilled structures [59]. RC structures with masonry infills are generally widespread in many parts of Europe and around the world. However, the stiffness and strength of infill panels, as well as the connection between infill panels and structural elements, are strongly related to the building habits that were common in a specific geographical region at a certain time. Based on this consideration, infill panels may present a large variety of mechanical properties, which range from extremely large to very low stiffness and strength. In order to take into account such a large variability, the RC case study frames have been endowed with two kinds of infill panels: the first type is very stiff and strong, whilst the second type has lower stiffness and strength. Furthermore, the case study frames have been considered in the bare configuration as well. This allowed to simulate the limit case of RC frames where the presence of infill panels could be neglected because of their extremely low properties. In total, 54 RC frames are analysed.

2. General description of the case study frames

The GL frames are drawn from buildings that were designed to sustain gravity loads only. These buildings are representative of typical Italian residential buildings of the seventies. The SR frames are extracted from two RC framed buildings designed for earthquake resistance in low seismicity area according to the Italian standards for constructions and seismic resistance [60-61] in force in the nineties.

Two different plan layouts symmetric with respect to the y -axis have been considered for both the buildings the GL frames and the SR

frames belonged to, as shown in Figure 18(a - b) and (c - d), respectively. In the first arrangement of plan layout, the deck was orientated along the y -direction (Figure 18(a) and (c)), whilst in the second arrangement the deck was parallel to the x -direction (Figure 18(b) and (d)). In case of buildings designed for gravity loads only, the structure with the first plan layout (Figure 18(a)) presents four frames along the x -direction and four frames along the y -direction. Two of these latter frames enclose the staircase, and the other two are at the sides of the building. On the other hand, the building with the second plan configu-

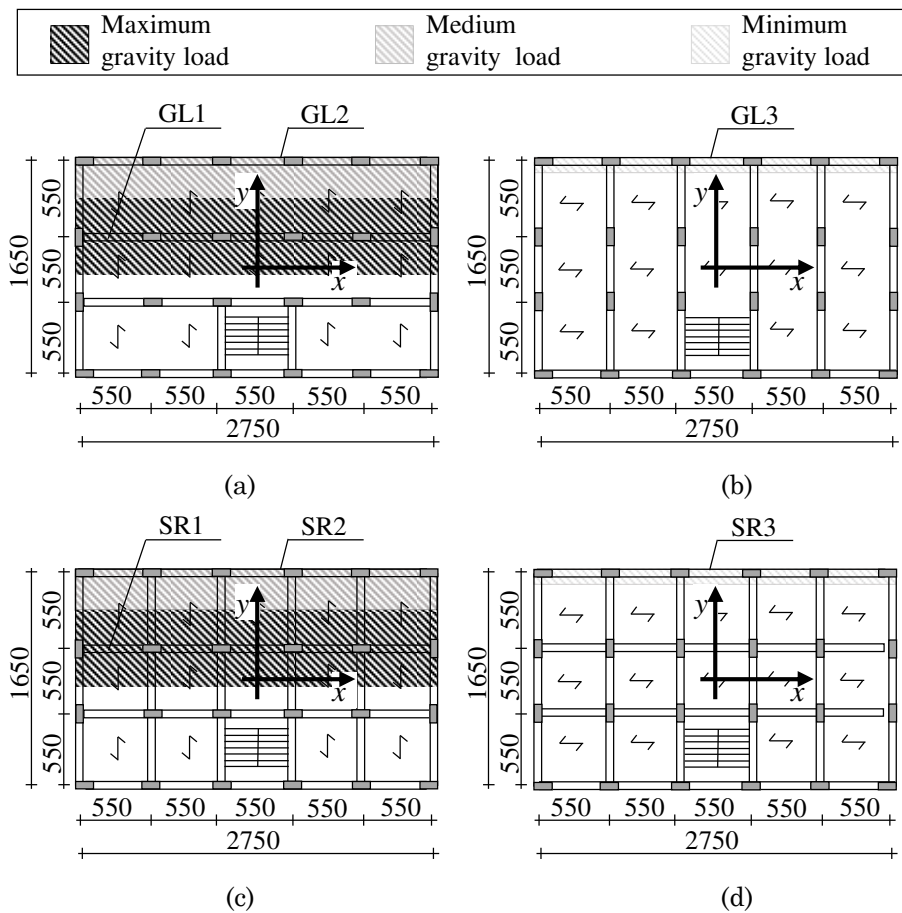


Figure 18 – Plan layout of buildings (units in cm): (a) GL building and (c) SR building with deck perpendicular to longitudinal frames; (b) GL building and (d) SR building with deck parallel to longitudinal frames

ration (Figure 18(b)) has two longitudinal frames on the outermost sides, and six frames along the y -direction. In case of buildings designed for seismic forces, both the plan layouts (Figure 18(c) and (d)) present four frames along the x -direction and six frames along the y -direction. All the analysed frames lay along the x -direction. The frame type 1 and 2 are the central and the outermost frames, respectively, extracted from the buildings where the deck orientation is parallel to y -direction. In particular, Frames GL1 and GL2 are drawn from the plan layout of the building in Figure 18(a), whilst frames SR1 and SR2 are drawn from the building shown in Figure 18(c). In consequence of the orientation of the deck, frame type 1 supports larger gravity loads than frame type 2. Frame type 3 is drawn from the building with the deck orientated along the x -direction (Figure 18(b) and (d)). Thus, this frame supports only the self-weight of beams, columns, infills and the weight of an additional 50 cm wide stripe of deck. Thus, frame GL3 and SR3 support the least amount of gravity loads among the GL frames and the SR frames, respectively.

Both the SR frames and the GL frames were designed with five 5.5 m wide bays and with a number of storeys equal to 6, 9 and 3. The interstorey height is equal to 3.2 m. In case the influence of the infill panels on the seismic response is taken into account, the distribution of infills is supposed to be uniform along the height of the frame. The geometrical characteristics of the frames are shown in Figure 19.

Hereinafter, each frame is identified by a label composed of two alphanumeric parts. In the first part, the two letters indicate which set the frame belongs to, the first number indicates the number of storeys and the last number the amount of gravity load. Frames designed for Seismic Resistance are labelled SR (frame), while frames designed for Gravity Loads are labelled GL (frame). Frames with the largest gravity loads are indicated with 1, frames with the lowest gravity loads are indicated with 3 and the intermediate loaded frames are indicated with 2. The second part of the label is not needed for bare frames, while it is required in case of infilled frames. In this part, the letter I indicates the presence of panel infills, while the number indicates the cracking strength of panel infills in MPa. As an example, SR61-I028 refers to the

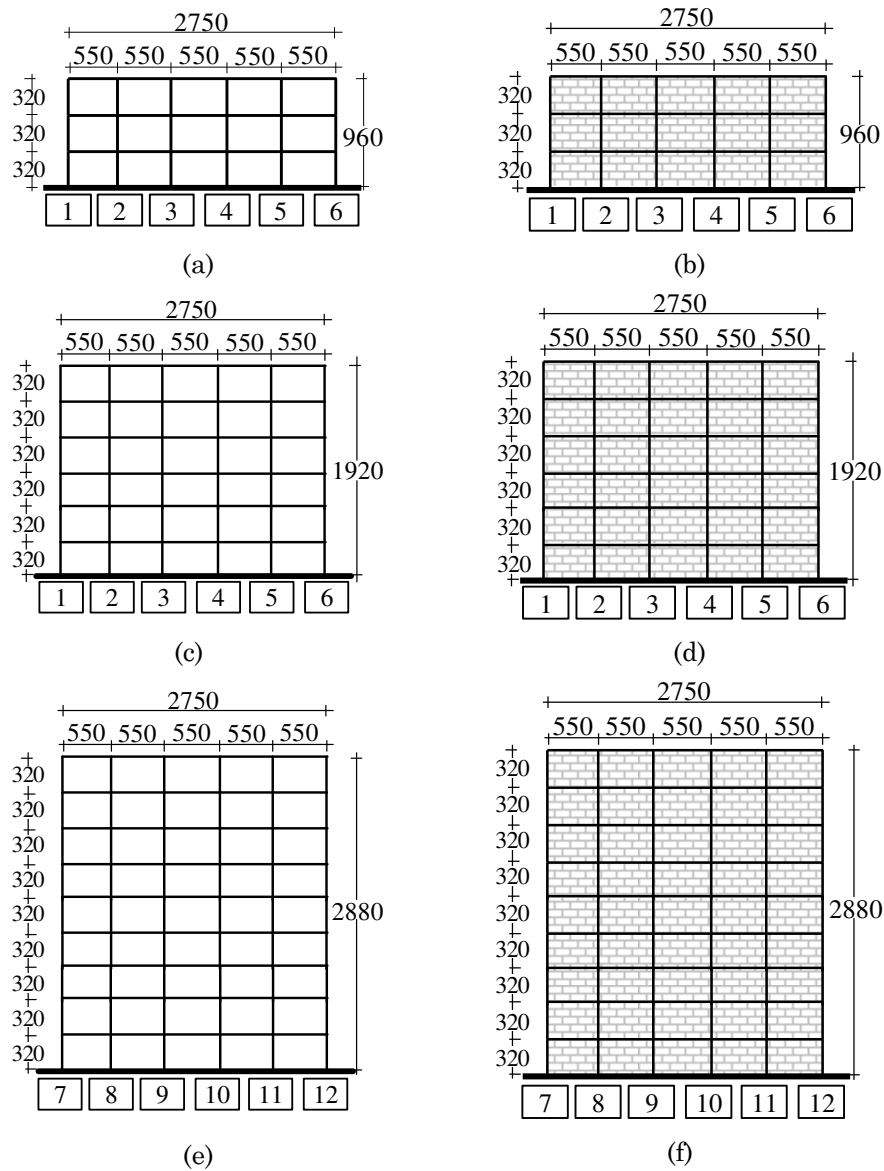


Figure 19 – Geometrical scheme of the case study frames (units in cm): (a) and (b) three storey high bare and infilled frame, (c) and (d) six storey high bare and infilled frame, (e) and (f) nine storey high bare and infilled frame

frame designed for seismic actions (SR), with 6 storeys (6), the largest gravity loads on beams (1) and infill panels (I) with cracking strength

equal to 0.28 MPa (028).

Section 3 and 4 show the design and the size of the cross section of beams and columns of SR frames and GL frames, respectively.

3. Design of GL frames

The design of beams and columns of GL frames followed the regulations in force during the seventies in Italy [60, 63 - 65]. The design assumptions, the adopted design procedure, and the results of the design are resumed in the following sections.

3.1. Loads, materials and design procedure

Only gravity loads are considered for the evaluation of the design internal forces of structural members. Dead loads (G) and live loads (Q) are determined per unit area considering the nominal values provided in [63]. The concentrated loads on columns and the distributed loads on beams are evaluated based on the tributary area concept. The concentrated loads on columns are determined by multiplying the tributary area of deck, the tributary length of beams and the tributary length of infill panels by the respective nominal values of dead and live loads per unit area. The tributary area (A_{tr}) of the deck and the corresponding load, the tributary length (L_{tr}) of beams and the corresponding load, the tributary length of infill panels and the corresponding load, the total gravity load (P_{tot}) and the self-weight load (P_{self}) are reported in Table 4 for each column of a generic floor of each GL frame. The number of each column is referred to Figure 19. The distributed loads resting on beams are reported in Table 5 per unit length and they are evaluated considering the weight of the deck, the self-weight of the beam itself and the weight of the infill panel.

The dimensions of the cross sections and the size of steel reinforcements of beams and columns are determined by the allowable stress method [64]. The minimum reinforcement ratio prescribed in [64] for the tension zone of beams is equal to 0.0015. Columns are designed to resist axial force only. Indeed, the bending moment was usually neglected by the design practice of the seventies. The design axial force of

the column N is evaluated according to the tributary area concept. The minimum cross section area of the column $A_{c,req}$ is calculated according

Table 4 – Concentrated loads on columns

GL1								
	Deck		Beam		Infill		P_{tot} (kN)	P_{self} (kN)
	A_{tr} (m^2)	Load (kN)	L_{tr} (m)	Load (kN)	L_{tr} (m)	Load (kN)		
Col.1	16.64	116.46	8.80	35.20	6.05	42.35	194.01	11.64
Col.2	36.60	256.22	6.05	24.20	-	-	280.42	16.83
Col.3	33.28	232.93	5.50	22.00	-	-	254.93	15.30
Col.4	33.28	232.93	5.50	22.00	-	-	254.93	15.30
Col.5	36.60	256.22	6.05	24.20	-	-	280.42	16.83
Col.6	16.64	116.46	8.80	35.20	6.05	42.35	194.01	11.64
GL2								
	Deck		Beam		Infill		P_{tot} (kN)	P_{self} (kN)
	A_{tr} (m^2)	Load (kN)	L_{tr} (m)	Load (kN)	L_{tr} (m)	Load (kN)		
Col.1	7.56	52.94	5.50	22.00	5.50	38.5	113.44	6.81
Col.2	16.64	116.46	6.05	24.20	6.05	42.4	183.01	10.98
Col.3	15.13	105.88	5.50	22.00	5.50	38.5	166.38	9.98
Col.4	15.13	105.88	5.50	22.00	5.50	38.5	166.38	9.98
Col.5	16.64	116.46	6.05	24.20	6.05	42.4	183.01	10.98
Col.6	7.56	52.94	5.50	22.00	5.50	38.5	113.44	6.81
GL3								
	Deck		Beam		Infill		P_{tot} (kN)	P_{self} (kN)
	A_{tr} (m^2)	Load (kN)	L_{tr} (m)	Load (kN)	L_{tr} (m)	Load (kN)		
Col.1	7.56	52.94	5.50	22.00	5.50	38.50	113.44	6.81
Col.2	16.64	116.46	8.80	35.20	6.05	42.35	194.01	11.64
Col.3	15.13	105.88	8.25	33.00	5.50	38.50	177.38	10.64
Col.4	15.13	105.88	8.25	33.00	5.50	38.50	177.38	10.64
Col.5	16.64	116.46	8.80	35.20	6.05	42.35	194.01	11.64
Col.6	7.56	52.94	5.50	22.00	5.50	38.50	113.44	6.81

to the aforementioned regulations by the following relation:

$$A_{c,req} = \frac{N}{0.7 \bar{\sigma}_c (1 + n \rho_l)} \quad (97)$$

where $\bar{\sigma}_c$ is the allowable stress of concrete, n is the homogenization coefficient for rebars assumed equal to 10, and ρ_l is the ratio of the longitudinal rebar area A_s to $A_{c,req}$ assumed not smaller than 0.006. The characteristic compressive cubic strength R_{ck} for concrete is assumed equal to 25 MPa (corresponding to the cylinder strength f_{ck} equal to 20 MPa for strength class C20/25) for the design of 3-storey and 6-storey frames, and equal to 30 MPa (corresponding to the cylinder strength f_{ck} equal to 25 MPa for strength class C25/30) for the design of 9-storey frames. Deformed-rebars made of steel grade Feb38K with a characteristic yield stress $f_{yk} = 375$ MPa is used for reinforcement. The values of the allowable stresses are 8.5 MPa and 9.75 MPa for concrete C20/25 and C25/30, respectively. The allowable stress of steel reinforcement is equal to 215 MPa. The area A_s of the longitudinal rebars of columns is

Table 5 – Distributed gravity loads on beams

	Length(m)	G _k (kN/m)	Q _k (kN/m)	G _k + Q _k
GL1				
Deck	5.50	30.3	12.1	
Beam	5.50	4.0		46.4
Infill	5.50			
GL2				
Deck	5.50	13.8	5.5	
Beam	5.50	4.0		30.3
Infill	5.50	7.0		
GL3				
Deck	5.50	2.5	1.0	
Beam	5.50	4.0		14.5
Infill	5.50	7.0		

not smaller than the minimum value $A_{s,min}$:

$$A_{s,min} = \max \begin{cases} 0.003 A_c \\ 0.006 A_{c,nec} \end{cases} \quad (98)$$

where A_c is the actual cross section area of concrete of the column. Stirrups with diameter of 8 mm and spacing of 150 mm are used for beams and columns.

3.2. Geometrical characteristics of GL frames

The design procedure reported in Section 3.1 led to the definition of the cross sections of columns and beams. Table 6 shows the size in cm of the cross sections of structural members at each storey of the GL frames; the numbers identifying the columns refer to Figure 19. The columns of all GL frames are characterized by a decreasing area of the

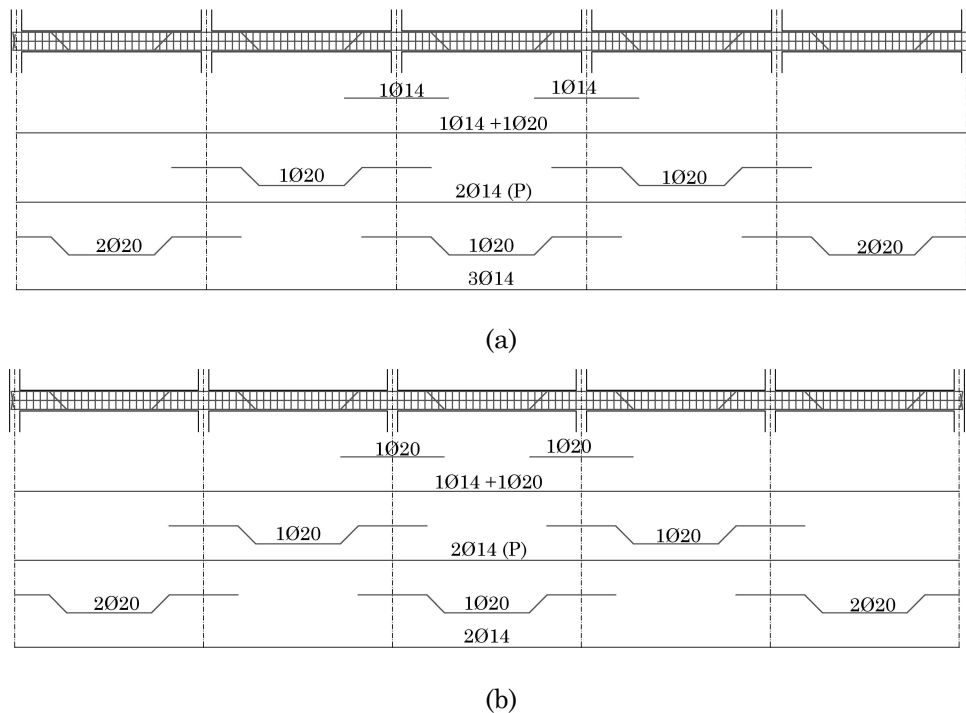


Figure 20 – Arrangement of rebars of beams at a generic floor of GL frame: (a) 9-storey frame; (b) 6- and 3-storey frame

cross section along the height. This result is consistent with the design practice that was common in Italy before the seismic codes entered in

Table 6 – Cross section of GL frame members

Frame	GL1			GL2			GL3		
Storey	Columns of the 9-storey frames								
	1, 6	2, 5	3, 4	1, 6	2, 5	3, 4	1, 6	2, 5	3, 4
9	30x30	30x30	30x30	30x30	30x30	30x30	30x30	30x30	30x30
8	30x30	30x40	30x30	30x30	30x30	30x30	30x30	30x30	30x30
7	30x30	30x50	30x40	30x30	30x30	30x30	30x30	30x30	30x30
6	40x30	30x60	30x50	30x30	30x30	30x30	30x30	30x30	30x30
5	50x30	30x70	30x60	30x30	30x40	30x40	30x30	30x40	30x40
4	60x30	30x80	40x60	40x30	30x50	30x40	40x30	30x50	30x40
3	70x30	40x80	40x70	40x30	30x50	30x50	40x30	30x60	30x50
2	80x30	40x80	40x80	50x30	30x60	30x50	50x30	30x60	30x60
1	90x30	40x90	40x90	50x30	30x70	30x60	50x30	30x70	30x60
Storey	Beams of the 9-storey frames								
All	30x60			30x60			30x60		
Storey	Columns of the 6-storey frames								
	1, 6	2, 5	3, 4	1, 6	2, 5	3, 4	1, 6	2, 5	3, 4
6	30x30	30x30	30x30	30x30	30x30	30x30	30x30	30x30	30x30
5	30x30	30x40	30x30	30x30	30x30	30x30	30x30	30x40	30x30
4	40x30	30x50	30x30	30x40	30x30	30x40	40x30	30x50	30x30
3	50x30	30x60	30x30	30x50	30x30	30x50	50x30	30x60	30x30
2	60x30	30x80	40x30	30x50	40x30	30x50	60x30	30x80	40x30
1	70x30	40x80	40x30	30x60	40x30	30x60	70x30	40x80	40x30
Storey	Beams of the 6-storey frames								
All	30x60			30x60			30x60		
Storey	Columns of the 3-storey frames								
	1, 6	2, 5	3, 4	1, 6	2, 5	3, 4	1, 6	2, 5	3, 4
3	50x30	30x60	30x30	30x50	30x30	30x50	50x30	30x60	30x30
2	60x30	30x80	40x30	30x50	40x30	30x50	60x30	30x80	40x30
1	70x30	40x80	40x30	30x60	40x30	30x60	70x30	40x80	40x30
Storey	Beams of the 3-storey frames								
All	30x60			30x60			30x60		

force. The details of the cross section of columns and the location of their reinforcement bars are reported in Appendix B.

The cross section of beams is the same at all levels of each frame. Longitudinal reinforcements of beams are supposed to be realized by bent-up bars, which reinforce the bottom side of the cross section at the mid-span and the top side of the end cross sections (Figure 20). This type of reinforcement optimized the use of steel required to sustain bending moments provided by gravity loads, and they were common in Italy during the Seventies.

4. Design of SR frames

The design of the seismic-resistant frames was performed according to the regulations for building structures and seismic resistance enforced in Italy in the nineties [60, 61, 62, 63]. The design assumptions, the adopted design procedure, and the results of the design are resumed in the following sections.

4.1. Loads, materials and design procedure

The lateral force method of analysis is adopted to evaluate the effect of seismic force. For building structures, the seismic code [62] determines the design seismic force F_h as a fraction of the total seismic weight W of the building:

$$F_h = C R I W \varepsilon \beta \quad (99)$$

The seismic coefficient C is related to the seismicity of the site and it is determined as follows:

$$C = (S - 2)/100 \quad (100)$$

Assuming that at the time of construction of the building the site was classified as low seismicity area, the level of seismicity S is assumed equal to 6. Thus, a seismic coefficient $C = 0.04$ is adopted. The response coefficient R is the ordinate of the design acceleration spectrum normalised to g , and it is function of the fundamental period T_1 :

$$R = \begin{cases} 1.0, & T_1 < 0.8s \\ \frac{0.862}{T_1^{2/3}}, & T_1 > 0.8s \end{cases} \quad (101)$$

A response coefficient $R = 1.0$ was usually used when the effect of seismic forces was determined by equivalent force method of analysis and the T_1 was unknown. The coefficient of seismic protection I was assumed 1 because the buildings are designed for residential use, the coefficient of foundations ε was assumed 1 because the soil was supposed to be regular, and the coefficient of structure β was assumed equal to 1 as suggested for framed structures. To evaluate W , the entire permanent dead load and the live load reduced by the factor s given in [62] are considered. Dead load, including self-weight of structural and non-structural elements, and live load are determined considering the nominal values provided in [63]. The value of gravity loads on beams and columns adopted for the design of frames SR are summarised in Ta-

Table 7 – Distributed gravity loads on beams for design of frames SR.

	Length (m)	G_k (kN/m)	Q_k (kN/m)	$G_k + sQ_k$
SR1				
Deck	5.50	30.3	12.1	
Beam	5.50	4.0		38.2
Infill	5.50			
SR2				
Deck	5.50	13.8	5.5	
Beam	5.50	4.0		26.6
Infill	5.50	7.0		
SR3				
Deck	5.50	2.5	1.0	
Beam	5.50	4.0		13.8
Infill	5.50	7.0		
Total floor seismic weight			4191.4 kN	
Seismic mass of single frame			106.8 t	

Table 8 – Total seismic weight and total seismic force for the design of frames SR.

N. of storeys	Total seismic weight W (kN)	Total design seismic force F_h (kN)
9	9429.4	377.2
6	6286.2	251.5
3	3143.1	125.7

ble 7. The seismic weight of a generic floor is equal to 4191.4 kN. Each SR frame is designed to sustain one fourth of the total seismic force. Thus, the seismic weight W_i of a generic level of a single frame SR is equal to 1047.9 kN (i.e. the seismic mass is 106.8 t). The total seismic weight W and the total design seismic force F_h are reported in Table 8 for each frame SR. The design seismic force F_h is distributed along the height according to an inverted triangular distribution. The seismic force F_i to be applied at each i -th level is:

$$F_i = K_{hi} W_i \quad (102)$$

$$K_{hi} = C \cdot R \cdot \varepsilon \cdot \beta \cdot \gamma_i \cdot I \quad (103)$$

where γ_i is the coefficient that determines the distribution of seismic forces along the height as function of the floor height h (height of the floor above the level of the foundation):

$$\gamma_i = h_i \frac{\sum_{j=1}^N W_j}{\sum_{j=1}^N W_j h_j} \quad (104)$$

Design internal forces of beams and columns are determined from the most unfavourable combination of gravity loads with seismic force. To determine the effect of gravity load on beams and columns the dead load and live load are entirely considered, as stipulated in [63]. For the evaluation of the design internal forces of columns, the capacity design is not explicitly applied. However, in order to promote yielding of beams

and prevent concentration of plastic hinges in columns of a single storey, cross sections of columns are generally assumed not smaller than those of beams. This is consistent with the common design practice of that time. Size of cross sections and rebars are designed to satisfy the safety verification of structural members according to the allowable stress method [61].

Consistently with GL frames, 9-storey frames were designed considering a characteristic compressive cubic strength R_{ck} for concrete equal to 30 MPa (C25/30), and 6- and 3-storey frames were designed with a characteristic compressive cubic strength R_{ck} for concrete equal to 25 MPa (C20/25). Steel grade Feb44k with a characteristic yield stress $f_{yk} = 430$ MPa is assumed for rebars. These design assumptions are consistent with the construction practice of that time, and lead to allowable stresses for concrete C20/25 and C25/30 equal to 8.5 MPa and 9.75 MPa, and for steel equal to 255 MPa, respectively. The homogenization coefficient for rebars is assumed equal to 15. The minimum tension reinforcement ratio of beams is 0.0015, while the adopted total longitudinal reinforcement ratio of columns is at least 0.006.

4.2. Geometrical characteristics of SR frames

The cross sections of columns and beams defined by the design procedure explained in Section 4.1 are summarised in Table 9. The size of the columns of frames SR does not significantly decrease along the height. In particular, the design procedure sets the cross section with dimensions 30x60 as minimum cross section for columns of 9- and 6-storey frames. In case of the three storey frames, the minimum cross section assumed was that with dimension 30x40. For the sake of simplicity, frames SR with the same number of storeys are supposed to have the same cross sections of columns. In particular, since frame SR1 sustains the largest gravity loads, the cross sections designed for frame SR1 were adopted also for frames SR2 and SR3 with the same number of storeys. Details of cross sections of columns can be found in Appendix B.

Generally, the cross section of beams has dimensions 30x60 at every storey of each frame, except from the six lower levels of the nine sto-

Table 9 – Cross section of SR frames members

9 storeys			6 storeys		3 storeys	
SR1 - SR2 - SR3			SR1 - SR2 - SR3		SR1 - SR2 - SR3	
Storey	Columns		Columns		Columns	
	1, 6	2-5	1, 6	2-5	1, 6	2,5
9	30x60	30x60	-	-	-	-
8	30x60	30x60	-	-	-	-
7	30x60	30x60	-	-	-	-
6	30x60	30x60	30x70	30x60	-	-
5	30x60	30x70	30x70	30x60	-	-
4	30x70	40x70	40x70	30x70	-	-
3	30x80	40x80	40x70	30x70	30x40	30x40
2	30x90	40x90	40x80	40x70	30x40	30x50
1	30x90	45x90	40x80	40x70	30x50	30x60
Storey	Beams		Beams		Beams	
1 - 3	30x70		30x60		30x60	
3 - 6	30x60		30x60		-	
6 - 9	30x60		-		-	

reys frames, where the cross section size of beams increases to 30x70. Longitudinal reinforcement of beams is supposed to be realized by longitudinal straight steel bars. Because of the different effect of seismic force at every storey, the distribution of reinforcement bars changes almost at each storey of each frame.

As an example, Figure 21 shows the details of rebars in beams at the ninth storey of the 9-storey SR1 frame (SR91). The distribution of rebars at each storey and for each span of frame SR91 is summarised in Table 10. For both the ends of each beam span, the rebars located in the upper and lower part of the cross section are specified. Since the frame is symmetrical with respect to y-axis, Table 10 shows only the rebars of the first two and a half beam spans. In Appendix A, similar tables show the cross sections and the reinforcement bars of beams at every storey for the other SR frames. Transverse reinforcement of columns and criti-

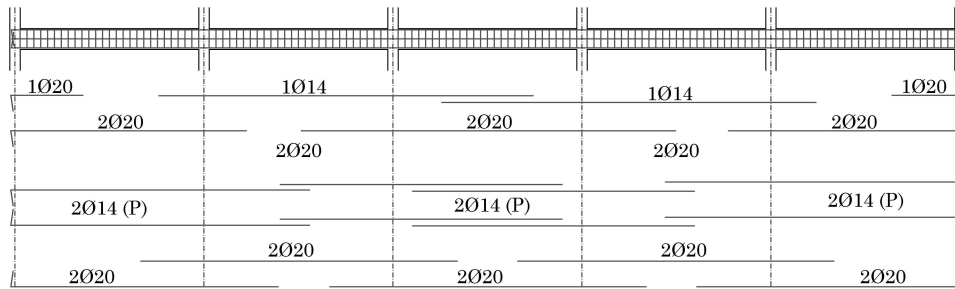


Figure 21 – Reinforcement bars of beams at the 9th storey of frame SR91

cal regions of beams is made of stirrups with 8 mm diameter and a spacing of 100 mm.

Table 10 – Cross section and rebars of beams of the 9-storey SR91 frame

Storey	Cross sect.	Rebar					
9	30x60	Upper	3φ20	3φ20+1φ14	3φ20+1φ14	3φ20+1φ14	3φ20+1φ14
		Lower	2φ20	2φ20	2φ20	2φ20	2φ20
8	30x60	Upper	4φ20	4φ20	4φ20	4φ20	4φ20
		Lower	2φ20	2φ20	2φ20	2φ20	2φ20
7	30x60	Upper	4φ20+1φ14	4φ20+1φ14	4φ20+1φ14	4φ20+1φ14	4φ20+1φ14
		Lower	2φ20+1φ14	2φ20+1φ14	2φ20+1φ14	2φ20+1φ14	2φ20+1φ14
6	30x70	Upper	4φ20	4φ20	4φ20	4φ20+1φ14	4φ20+1φ14
		Lower	2φ20	2φ20	2φ20	2φ20+1φ14	2φ20+1φ14
5	30x70	Upper	4φ20	4φ20+1φ14	4φ20+1φ14	4φ20+1φ14	4φ20+1φ14
		Lower	2φ20	2φ20+1φ14	2φ20+1φ14	2φ20+1φ14	2φ20+1φ14
4	30x70	Upper	4φ20+1φ14	5φ20	5φ20	5φ20	5φ20
		Lower	2φ20+1φ14	3φ20	3φ20	3φ20	3φ20
3	30x70	Upper	4φ20+1φ14	5φ20	5φ20	5φ20	5φ20
		Lower	2φ20+1φ14	3φ20	3φ20	3φ20	3φ20
2	30x70	Upper	4φ20+1φ14	5φ20	5φ20	5φ20	5φ20
		Lower	2φ20+1φ14	3φ20	3φ20	3φ20	3φ20
1	30x70	Upper	4φ20	4φ20+1φ14	4φ20+1φ14	4φ20+1φ14	4φ20+1φ14
		Lower	2φ20	2φ20+1φ14	2φ20+1φ14	2φ20+1φ14	2φ20+1φ14

Chapter 4

CALIBRATION OF THE D-DAP

1. Object and research methodology

The first part of the conducted numerical study aims at the calibration of the ruling parameters of the D-DAP. Because of the multimodal and incremental character of the D-DAP, the number of modes of vibration taken into account through the load vector and the increment of displacement applied at each step are the key parameters of the analysis. On one hand, taking into account the contribution of all modes of vibration is expected to lead to the most accurate results. On the other hand, it is well recognized that the higher the mode of vibration and the least its contribution to the total seismic response. Furthermore, enveloping the contribution of all modes of vibration complicates the calculation to update the load vector at each step, and increases the computational burden. As for the incremental step of the load vector, a very small load increment increases significantly the number of steps of the analysis and the computational time, without necessarily improving the level of accuracy.

In addition to the ruling parameters, the accuracy of the seismic prediction provided by the D-DAP depends on the law adopted for the estimation of the equivalent viscous damping at each step. Various authors [45,53-55] have proposed different equations for the evaluation of the equivalent damping (Equations 73-77). However, each of those equations led the D-DAP to predict the seismic behaviour of different

types of RC frames with a different level of accuracy. Indeed, among those equations it was not possible to find a single equation that could be adopted in the D-DAP to estimate with almost the same accuracy the seismic response of all different types of RC frames, i.e. seismic resistant frames, frames designed for gravity loads, with or without infills. Generally, when the damping laws in literature are adopted in the D-DAP, they led to an over/under estimation of the displacement demand and of the distribution of drifts along the height of the frame. This is probably due to the fact that those damping laws had been calibrated on SDOF systems [55], or were based on results of experimental tests conducted on single elements or one-storey frames [45,54]-.

Because of aforementioned reasons, the goals of the numerical calibration are (i) the selection of the ruling parameters to provide a good accuracy of the results without uselessly complicating the analysis, (ii) the development of a damping law to have an accurate prediction by the D-DAP of the seismic response of the different types of frames considered. The numerical calibration has required the conduction of several D-DAP analyses on the frames described in Chapter 3. To this end, a numerical model of the cases study has been built using the software OpenSees. Furthermore, to optimize the execution of the parametric analyses, a pre- and post-processor program, named ExeOS, was created in Visual Basic language. The features of this program are showed in Appendix F.

The numerical calibration developed into three steps. A first sensitivity analysis has been conducted on the number of modes of vibration. The seismic response of the case study frames has been determined by various D-DAPs, with an increasing number of enveloped modes. When a further increase of the number of the included modes did not change the seismic response anymore, it meant that the modes so far included were those actually significant. As a consequence, higher modes of vibration could be neglected. A second sensitivity analysis has been conducted on the value of the incremental step. The response of the cases study has been evaluated by different D-DAPs, with decreasing values of the displacement increment at the generic step (step size). When a further reduction of the displacement step size did not affect the seis-

mic response anymore, that step size was the optimal one. As third step, a new damping law has been developed. To this end, the response of the case study frames determined by nonlinear dynamic analysis has been assumed as benchmark. Hence, the new damping law has been defined through an optimization of the prediction of the nonlinear dynamic response provided by the D-DAP.

2. Modelling of reinforced concrete frames

The nonlinear response of the case study frames has been investigated by means of a two-dimensional numerical model, whereby the masses are concentrated at the floor levels. The numerical model has been built in OpenSees [67], the open source software developed at University of California at Berkeley. This software allows the use of a variety of numerical models for the analysis of structures including the fibre modelling technique. Although the computational costs are very high, this technique provides a refined numerical model and results that are more reliable and likely to be closer to the real behaviour of the structure. The following sections will explain the general assumptions adopted in the numerical model, the evaluation of the seismic masses and the loads applied, the modelling adopted to simulate structural and non-structural elements of the case study frames.

2.1. Set up of the numerical model

The numerical model adopts two reference systems (Figure 22). The global system is assigned by default by the software, and it presents the horizontal x -axis orientated towards the right direction, the vertical y -axis orientated towards the upper direction. The z -axis is perpendicular to the plane traced by the x - and y -axis and is orientated according to the right hand rule. The local system is assigned to the cross sections of the structural elements, and it presents the x -axis orientated along the longitudinal direction of the generic element, the z -axis with the same direction and orientation of the global z -axis, and the y -axis perpendicular to the plane traced by the x - and z -axis and orientated according to the right hand rule.

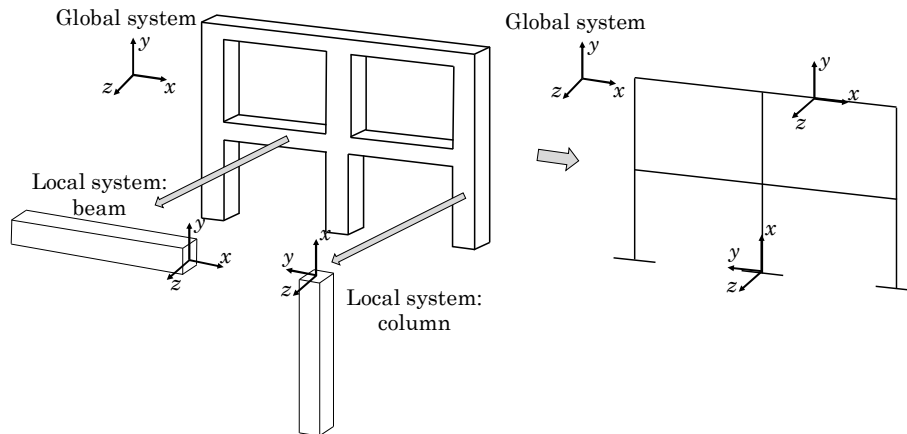


Figure 22 – Global and local reference system adopted in the numerical model

The columns of the first storey are fixed at the base. The concrete slab at each level is assumed to be rigid in its own plane. In order to simulate this, all the nodes belonging to the same floor are constrained to have the same horizontal displacement. To take into account the $P-\Delta$ effect, a leaning column is added to the numerical model. At each storey, the leaning column is modelled by an elastic member, and its lower and upper ends are connected to the lower and the upper nodes by springs with very low rotational stiffness (pins). The ends of the leaning column are connected to the relevant rigid diaphragm as well. For non-linear dynamic analysis, a Rayleigh viscous damping is used and set at 5% for the first and the third mode of vibration.

2.2. Loads and masses

The gravity loads assigned to beams and columns are those specified in EC8 for the seismic design situation. Indeed, the live loads are reduced by a factor ψ_2 equal to 30% and they are added to the dead loads assumed equal to their full characteristic value. The values of gravity loads ($G_k + \psi_2 Q_k$) are reported in Table 11.

Table 11- Loads in seismic combination, force concentrated on columns, seismic mass of a generic storey for frames GL and SR

	$G_k + \psi_2 Q_k$ (kN/m)	$P_{col1,col6}$ (kN)	$P_{col2,col5}$ (kN)	$P_{col3,col4}$ (kN)	Floor mass (t)	Floor weight (kN)
Frames GL						
GL1	37.9	66.5	-	-	99.3	974.6
GL2	26.4	30.2	-	-	99.3	974.6
GL3	13.8	64.9	87.2	80.3	202.7	1988.5
Frames SR						
SR1	37.9	72.6	26.4	26.4	106.1	1040.8
SR2	26.4	30.3	11.0	11.0	106.1	1040.8
SR3	13.8	64.9	109.6	109.6	106.1	1040.8

The floor masses are determined as a percentage of the total mass of the deck. In particular, in case of the building designed for gravity loads with the deck arranged along y -direction it is assumed that seismic force acting along x -direction is equally resisted by four frames. Being the storey seismic weight of this building equal to 3898.4 kN (397.4 t), the floor mass assigned to frames GL1 and GL2 is equal to 25% of the total one (99.3 t). In case of the building designed for gravity loads with the deck orientated along the x -direction, only the two outermost frames can be considered seismic resistant. Hence, seismic force is equally shared between those two frames, and the floor mass assigned to frame GL3 is equal to 50% of the total one. Since the seismic weight of the generic storey of this building is 3976.3 kN (405.3 t), the floor mass of frame GL3 is 202.7 t. In case of SR frames, seismic force acting along the longitudinal axis x is equally resisted by four frames, regardless of the direction of the deck. Thus, the floor mass assigned to frames SR1, SR2 and SR3 is equal to 25% of the total one (106.1 t). The gravity load applied at each level of the leaning column are equal to the seismic

weight of the storey of the frame. The $P-\Delta$ effect is considered only by this additional leaning column, while it is not considered for other structural elements.

2.3. Modelling of RC members

A member-by-member modelling with beam with hinges elements is adopted for beams and columns. In particular, the “Beam With Hinges Element” implemented in OpenSees is used, and beams and columns of the RC frame are modelled as members constituted by an elastic element with plastic hinges at their ends, as shown in Figure 23. The length of the plastic hinge Lp_i is equal to the depth of the cross section. A fibre cross section is assigned to each plastic hinge, where both concrete and steel components are considered. The concrete part of the cross section is subdivided into fibres having 5 mm depth and width equal to the width of the cross section. Single fibres enclosed in the cross section are used to model rebars.

The Mander constitutive law (“Concrete04” uniaxial material, showed in Figure 24) is assigned to concrete fibres. This material is derived from the constitutive law proposed by Popovics [68] and based on Mander’s constitutive law [69]. In order to define the properties of this material, the following parameters are required:

f_c is the maximum compression strength for concrete. It is assumed equal to the average value of compression strength evaluated as follows [13]:

$$f_{cm} = f_{ck} + 8[MPa] \quad (105)$$

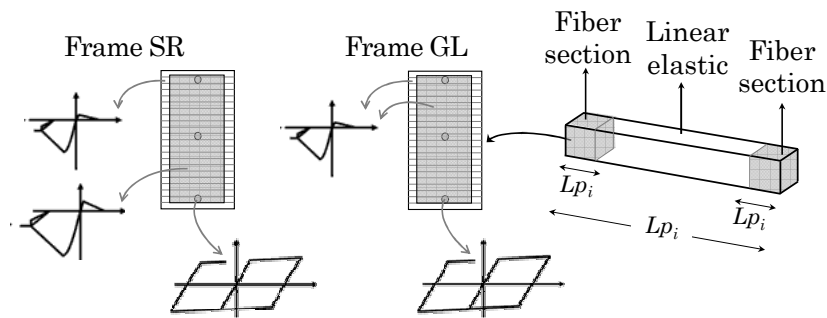


Figure 23 – Explanation of Beam With Hinges element

E_c is the concrete Young modulus that is calculated as suggested by the Italian building/seismic code (NTC08) [13]:

$$E_c = 22000 \left(\frac{f_{cm}}{10} \right)^{0.3} \quad (106)$$

ε_c is the concrete strain corresponding to the maximum compression strength.

ε_{cu} is the strain corresponding to the ultimate strength of concrete in compression.

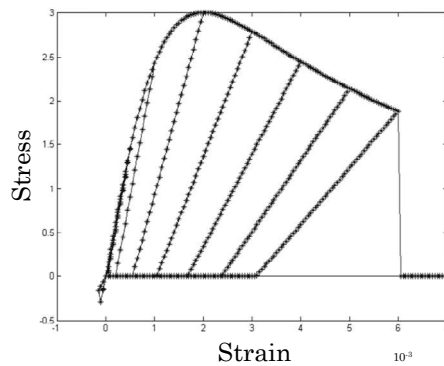
f_t is the maximum concrete tension strength. It is calculated as function of the concrete compressive strength, according to the equation suggested by NTC08 (11.2.10.2) [13]:

$$f_t = 0.3 \sqrt[3]{f_{ck}^2} \quad (107)$$

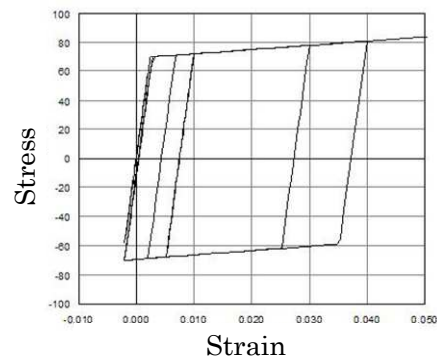
ε_t is the strain corresponding to the tension strength of concrete, and it is evaluated as:

$$\varepsilon_t = \frac{f_t}{E_c} \quad (108)$$

β_1 is the parameter ruling the tension behaviour and it is assumed equal to 0.1.



(a)



(b)

Figure 24 – Cyclic tension and compression response of (a) Concrete 04 and (b) Steel 01

The parameters used for concrete material are summarised in Table 12 for all the 3 and 6 storeys frames, and in Table 13 for the 9 storeys frames. Those values are representative of the mean value properties of the existing materials that could be obtained from in-situ tests and are derived from the characteristic values assumed in design.

For all the analysed frames, the concrete strain at crushing strength ϵ_{cu} is assumed large (5×10^{-2}) for the core region of the cross section (Table 12 and 13). Indeed, if the concrete fibres of the core reach the ultimate strain ϵ_{cu} numerical instabilities are likely to occur. Thus, a large ultimate concrete strain has been adopted as an expedient to avoid such numerical instabilities. In order to take into account a possible confinement effect on the concrete of the core due to the presence of stirrups, the value of maximum compression strength of concrete in the core region is distinguished from that of the cover region. Before seismic codes entered in force, the design and construction practice did

Table 12- Parameters adopted for Concrete C20/25 in SR and GL frames

Members of the 3- and 6-storey frames – Concrete C20/25					
	Type	Columns		Beams	
		Cover	Core	Cover	Core
f_{cm} (MPa)	GL	28.0	28.0	28.0	28.0
	SR	28.0	37.7	28.0	33.0
E_{cm} (MPa)	GL	29962	29962	29962	29962
	SR	29962	29962	29962	29962
ϵ_c	GL	0.002	0.002	0.002	0.002
	SR	0.002	0.005	0.002	0.005
ϵ_{cu}	GL				
	SR	0.0035	0.0500	0.0035	0.0500
f_t (MPa)	GL				
	SR	0.001	0.001	0.001	0.001
ϵ_t	GL				
	SR	0.0738×10^{-4}	0.0738×10^{-4}	0.0738×10^{-4}	0.0738×10^{-4}
β	GL				
	SR	0.1	0.1	0.1	0.1

not pay enough attention to the construction details. In particular, the diameter of stirrups was underestimated, and they were positioned with a large spacing. Because of this, the confinement effect on the core of the concrete section of these structures is likely to be negligible. Afterwards, when seismic codes entered in force, the use of stirrups in the RC cross sections became compulsory, and stirrups with larger diameter were employed with a tighter spacing. Based on this, since frames GL are representative of RC framed structures designed without seismic provisions, very few stirrups were endowed in the concrete members. Thus, the confinement effect on the core was neglected and the maximum compression strength of concrete of core was assumed equal to that of the cover. On the contrary, frames SR, which are representative of seismic-resistant structures, are endowed with dense and well detailed stirrups. As a consequence, the beneficial confinement effect of

Table 13 – Parameters adopted for Concrete 04 in SR and GL frames

Members of the 9-storey frames – Concrete C25/30					
	Type	Columns		Beams	
		Cover	Core	Cover	Core
f_{cm} (MPa)	GL	33.0	33.0	33.0	33.0
	SR	33.0	44.4	33.0	41.2
E_{cm} (MPa)	GL	31477	31477	31477	31477
	SR	31477	31477	31477	31477
ε_c	GL	0.002	0.002	0.002	0.002
	SR	0.002	0.005	0.002	0.005
ε_{cu}	GL	0.0035	0.0500	0.0035	0.0500
	SR				
f_t (MPa)	GL	0.001	0.001	0.001	0.001
	SR				
ε_t	GL	0.0738×10^{-4}	0.0738×10^{-4}	0.0738×10^{-4}	0.0738×10^{-4}
	SR				
β	GL	0.1	0.1	0.1	0.1
	SR				

stirrups in terms of resistance was considered, and the concrete compression strength of the core of the member cross section was assumed larger than that of the cover. Since the confinement effect on the concrete depends on the size of cross sections and the amount of steel bars and stirrups located in it, the value of f_{cm} in the core region should change from section to section. For the sake of simplicity, one value of maximum compression strength was estimated for the confined concrete of all columns. This value was obtained as a weighted average of the exact maximum compression strength of confined concrete of each cross section of columns, with respect to the total number of cross sections of columns. The same procedure was followed to determine one single value of maximum compression strength representative of confined concrete of all beams. The Young modulus E_c is calculated as function of the value f_{cm} of the cover region (Equation 106) [69].

An elasto-plastic with strain kinematic hardening constitutive law (“Steel01” uniaxial material) is assigned to steel fibres. The definition of this material required the following parameters:

- f_y is the steel yielding strength
- E_s is the steel Young modulus, equal to 210000 MPa
- b is the hardening ratio, defining the slope of the plastic branch as percentage of the slope of the stiffness of the elastic branch. It is evaluated according to the prescription of EC2 for steel type B. The average value of the yielding strength is increased by 1.15 times, and the ultimate strain of 5% is reduced by 0.9 times. The following equations are used:

$$\epsilon_{ym} = \frac{f_{ym}}{E_s} \quad (109)$$

$$E_{s,pl} = \frac{0.15 f_{ym}}{0.9 \epsilon_u - \epsilon_{ym}} \quad (110)$$

$$b = \frac{E_{s,pl}}{E_s} \quad (111)$$

Table 14 – Parameters adopted for Steel 01 in SR and GL frames

	Frames GL	Frames SR
f_{ym} (MPa)	450.0	400.0
E_s (MPa)	210000	210000
b	0.0049	0.0044

For all the analysed frames, the parameters adopted for Steel 01 are reported in Table 14.

The area, the moment of inertia of concrete cross section and the Young’s modulus of concrete are assigned to the elastic element.

A “ZeroLength Element” is added at one end of each beam. This element connects the end of the beam to the corresponding node restrained by the rigid deck and is characterized by a large axial deformability. This expedient allows the beams to deform axially and avoids arising of axial force, which typically leads RC beams modelled by fibre elements to an artificial stiffening and strengthening. Furthermore, large shear and flexural stiffnesses are assigned to the ZeroLength Element to transfer shear force and bending moment from the beam to the frame node

2.4. Modelling of infill panels

Infill panels are modelled by means of a pair of diagonal trusses without tension resistance. This model, although relatively simple, is widely used because it is numerically stable and computationally efficient. As proposed by Panagiotakos and Fardis [70] and Celarec et al. [71], the force-displacement relationship of the diagonal truss is calibrated to replicate the shear force-drift relationship of the infill panel. This relationship consists of four branches, as shown in Figure 25(a). The first branch corresponds to the linear elastic behaviour up to the first cracking of the infill. The stiffness K_{el} of the first branch and the shear cracking strength F_{cr} are calculated as follows:

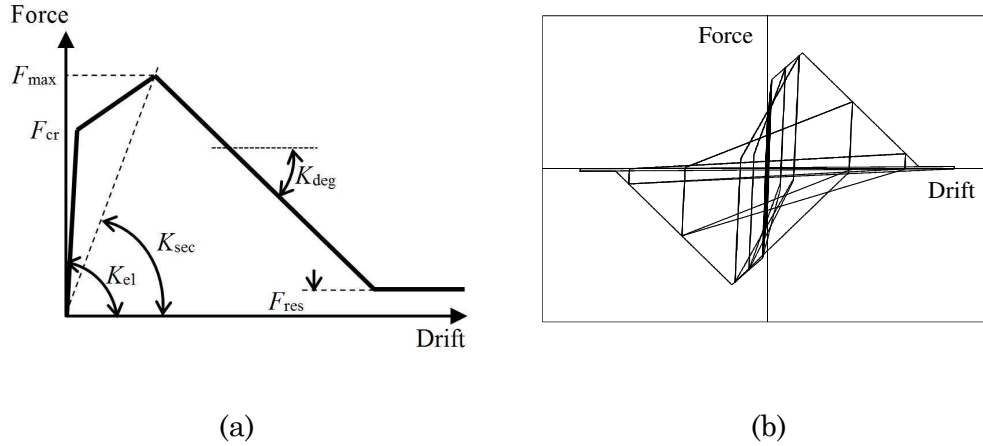


Figure 25 – Shear force-drift relationship of the infill panel (a) monotonic and (b) cyclic response

$$K_{el} = \frac{G_w A_w}{h_w}; \quad F_{cr} = \tau_{cr} A_w \quad (112)$$

where τ_{cr} is the shear cracking stress, G_w is the elastic shear modulus, A_w and h_w are the cross-sectional area and the clear height of the infill panel, respectively. The second branch of the envelope runs from the first cracking point up to the point of maximum strength F_{max}

$$F_{max} = 1.30 F_{cr} \quad (113)$$

The drift corresponding to the maximum strength is evaluated assuming a secant stiffness K_{sec} as follows:

$$K_{sec} = \frac{E_c b_w t_w}{\sqrt{L_w^2 + h_w^2}} \cos^2 \theta \quad (114)$$

where θ is with respect to the horizontal axis, L_w and t_w are the length and the thickness of the masonry infill, respectively, and b_w is the equivalent truss width evaluated by the following equation:

$$b_w = 0.175 (\lambda_h h_w)^{-0.4} d_w \quad \text{with} \quad \lambda_h = \sqrt[4]{\frac{E_w t_w \sin(2\theta)}{4 E_c I_c h_w}} \quad (115)$$

where d_w is the clear diagonal length of the infill panel. In the second expression above, λ_h is a coefficient defined as a function of Young's

moduli of the infills (E_w) and of the concrete (E_c), of the geometry of the infill (t_w , h_w , and θ), and of the moment of inertia I_c of the RC column.

The third branch of the envelope is the post-capping degrading branch, which runs from the maximum strength to the residual strength. The stiffness K_{deg} of this branch and the residual strength F_{res} are equal to:

$$K_{deg} = 0.10 K_{el}; F_{res} = 0.02 F_{max} \quad (116)$$

Finally, the fourth branch is horizontal and corresponds to the residual strength. The abovementioned multi-linear force-displacement relationship is then converted into an equivalent stress-strain relationship. The values of stress and strain corresponding to the three corners of the envelope both in the positive and negative direction are assigned to the truss member by means of the hysteretic uniaxial material implemented in Opensees. The obtained cyclic response is showed in Figure 25(b). Two types of infill panels have been considered in the present work. Both of them were supposed to be realized by ceramic bricks, with thickness equal to 20 cm, Young modulus and shear modulus equal to 4130 and 1240 MPa, respectively. However, the so called “stronger” infills were characterized by a stiffness and a cracking strength (0.28 MPa) that were double the stiffness and strength (0.14 MPa) of the “weaker” type of infills. The adopted mechanical properties were taken from the data provided in [71] according to the experimental tests conducted at University of Pavia [72].

3. Sensitivity analysis of the parameters ruling the D-DAP

The two following sections show the sensitivity analysis conducted to calibrate (1) the number of modes to be enveloped and (2) the value of the displacement step size. For the sake of simplicity, the obtained results will be showed for frame type SR1 and frame type GL1. For each type, the frames with 3, 6 and 9 storeys were considered. Each frame has been studied both in the bare and in the infilled configuration. The goal of this analysis is to select the values of the ruling parameters to ensure the best accuracy together with the best efficiency of the D-DAP for the case study frames.

3.1. Evaluation of the number of modes enveloped

The load vector applied in the D-DAP is evaluated from the envelope of the modal drifts at each storey. If all modes of vibration are taken into account for the determination of the load vector, the obtained structural

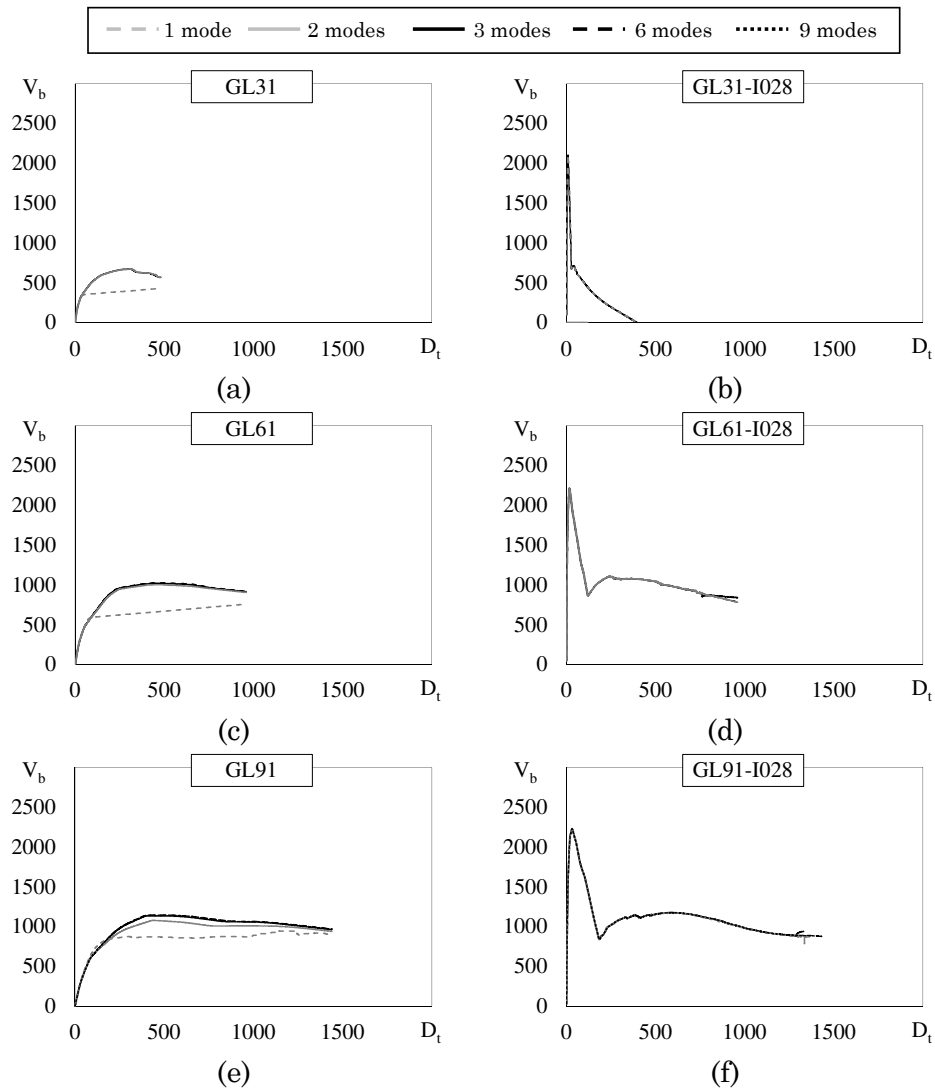


Figure 26 – Sensitivity analysis of significant modes of vibration for GL frames with 3, 6 and 9 storeys: (a, c, e) without infills and (b, d, f) with infills

response is expected to be more accurate. However, it is well recognized that the higher the mode of vibration, and the least its contribution to the total seismic response. It should be also considered that a larger number of included modes of vibration requires more data from the modal analysis, and complicates the envelope algorithm for the update

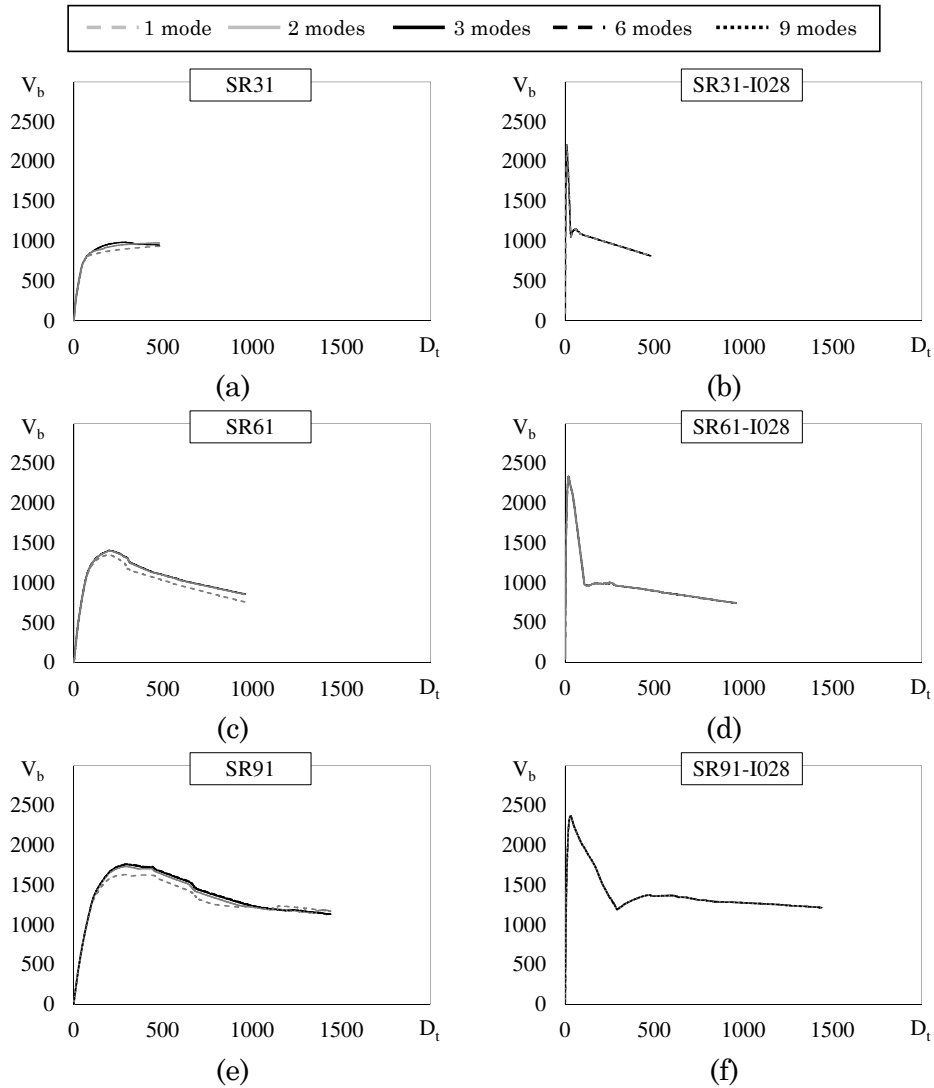


Figure 27 – Sensitivity analysis of significant modes of vibration for SR frames with 3, 6 and 9 storeys: (a, c, e) without infills and (b, d, f) with infills

of the load vector at each analysis step. In order to select the number of modes actually significant for the analysed frames, the seismic response of the case study frames has been evaluated by the D-DAP including an increasing number of modes. For each frame the number of modes of vibration ranged from 1 to the total number of participating modes, equal to the number of storeys.

The results of the sensitivity analysis are showed in Figure 26 and 27 for frame type GL-1 and SR-1, respectively. For both the frame types, frames with 3, 6 and 9 storeys were analysed, and the results are showed in the aforementioned figures in plots (a) and (b), (c) and (d), (e) and (f), respectively. For a fixed number of storeys, the seismic response of the frame without and with infills is evaluated. Figure 26 and 27 show the results of the D-DAP for bare frames and for frames with stiff infills (named in Chapter 3 by the suffix I028) in the plots on the left and right column, respectively. In each plot, each line represents the performance curve of the relevant frame evaluated by the D-DAP with a different number of included modes.

The seismic responses of the considered bare frames show that for a fixed value of top displacement the influence of higher modes of vibration leads to a larger base shear. In particular, this tendency becomes more significant when the number of storeys increases. Indeed, when the structure yields, the first mode of vibration becomes very flexible and its period increases. As a consequence, the contribution of the first mode to displacements becomes progressively more significant, while its contribution to the internal forces reduces and tends to be null. On the contrary, higher modes of vibration are less influenced by the yielding of the structure, and keep their stiffness almost equal. Thus, although the structure has already yielded, higher modes still contribute to the internal forces of the structure. This means that when the contribution of higher modes of vibration is taken into account, the base shear of the structure keeps increasing even after the yielding of the structure. In particular, for the presented bare frames, the contribution of the second and third modes of vibration is actually significant, while higher modes of vibration become negligible. If infill panels are included in the frame, the first mode of vibration is predominant regardless of

the number of storeys, and the contribution of higher modes of vibration becomes negligible. Based on the previous considerations, the D-DAP has been applied including the contribution of the first three modes of vibration for all cases study.

3.2. Evaluation of the displacement step size

Since the D-DAP is an incremental analysis, another crucial choice is the value adopted for the increment of displacement Δ_{step} applied at each step. When a larger displacement step size is adopted, the computational time of the analysis reduces. However, if the incremental step becomes too large, the analysis lacks of accuracy. In order to select the most appropriate value of step size, the same frames have been analysed using the D-DAP with gradually reduced displacement step sizes. The final step of each analyses has been set at a target top displacement equal to the 5% of the total height of the frame. Four values of displacement step size have been considered: 100, 10, 1 and 0.1 mm.

Figure 28 and 29 show the results of the sensitivity analysis conducted on frames GL-1 and SR-1, respectively. In both the figures, (a) and (b), (c) and (d), (e) and (f) refer to the frames with 3, 6 and 9 storeys, respectively. The plots in the left column of the pictures show the results for the bare frames, while the plots in the right column show the results for frames with infills. In each figure, each line represents the performance curve of the relevant frame obtained by the D-DAP with a different step size.

Although four incremental steps were considered, only the results of no more than three analyses are showed for each frame. This is because when the step $\Delta_{step} = 100$ mm was adopted, every analysis failed since the first step. Indeed, the step size corresponds to the increment imposed to the top displacement at each step. If the structure is forced to reach a very large top displacement all at once, many sections can suddenly yield, the structural damage spreads rapidly, and the unbalanced forces cannot be redistributed in the structure. This is even more likely to occur in infilled frames where the infill panels reach their maximum strength and suddenly collapse. Thus, the modal shape at the end of this step is significantly different from the previous step and

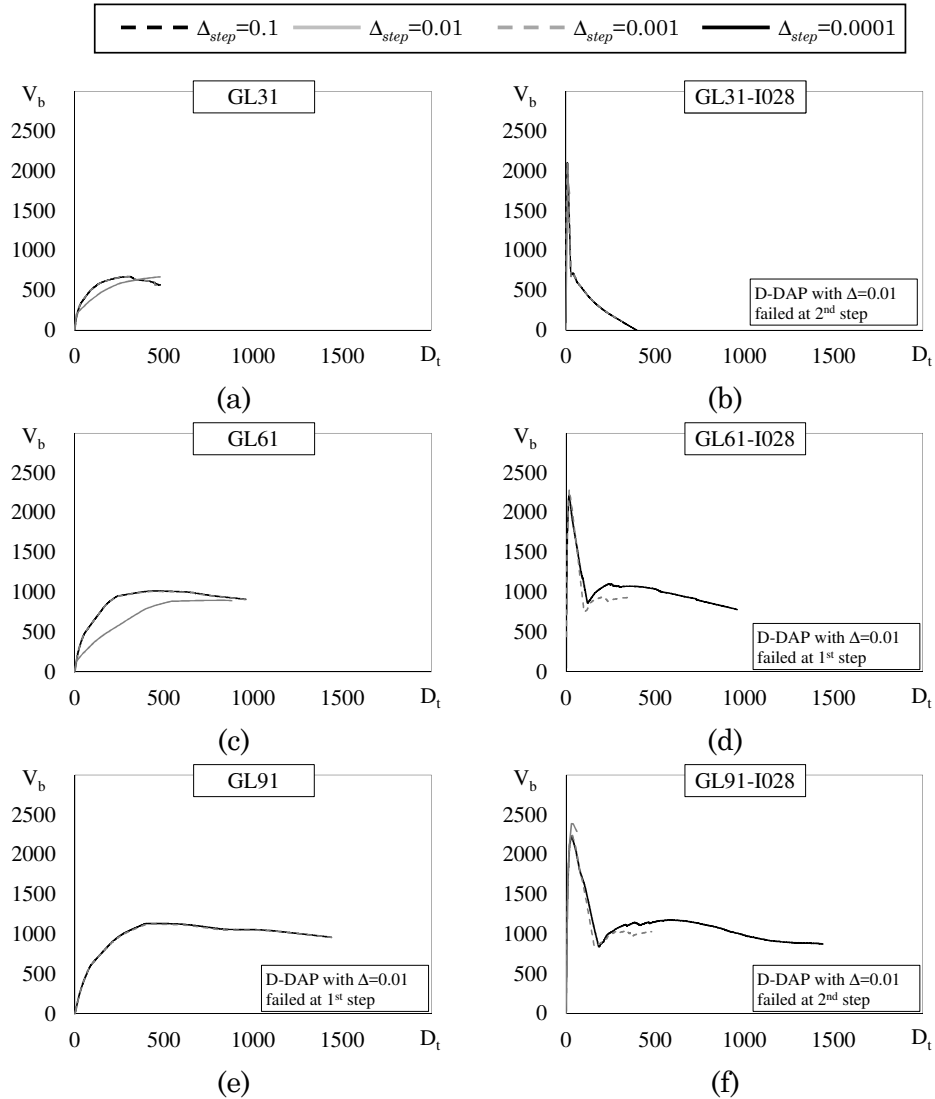


Figure 28 – Sensitivity analysis of incremental step size for GL frames with 3, 6 and 9 storeys: (a, c, e) without infills and (b, d, f) with infills

may present changes in direction along the height. Since the load vector is derived from the updated modal shape, in the following step the structure is subjected to a very different load vector, that is likely to push the structure to opposite directions simultaneously. Under such

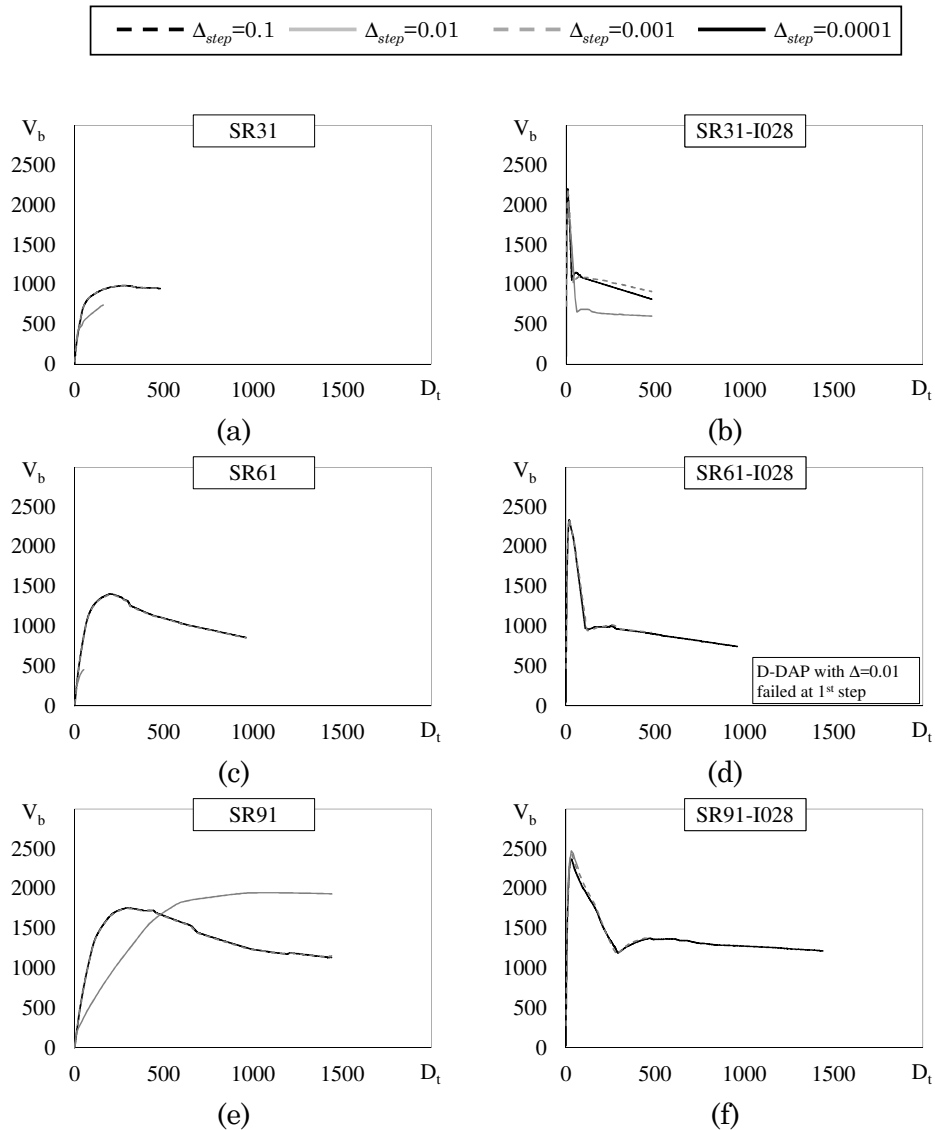


Figure 29 – Sensitivity analysis of incremental step size for SR frames with 3, 6 and 9 storeys: (a, c, e) without infills and (b, d, f) with infills

loading conditions, the analysis fails to find the convergence and does not provide solutions to the equations of equilibrium.

When the incremental step is reduced to 10 mm, the D-DAP is able to predict part of the seismic response of the structures. However,

sometimes the analysis stops before the target displacement is reached, or fails at the very beginning. A value of Δ_{step} equal to 1 mm avoids the untimely failure of the analysis, especially in case of infilled frames (Figure 28 and 29(b), (d), (f)) whereby the analysis with larger Δ_{step} stopped right after the attainment of the maximum strength of infills. Furthermore, the prediction of the seismic response provided by the D-DAP with $\Delta_{step} = 1$ mm is significantly different from that obtained with $\Delta_{step} = 10$ mm, as showed in Figure 28(a) and (c), or Figure 29(a), (c), (d). The step size has been further reduced to 0.1 mm. However, any significant change in the prediction of the seismic response were observed, and the obtained plots are basically the same as those obtained with $\Delta_{step} = 1$ mm.

Since the tendency noted in the showed frames has been essentially observed in all other analysed frames, a value of $\Delta_{step} = 1$ mm could be considered appropriate. However, since the D-DAP with $\Delta_{step} = 1$ mm in very few cases failed slightly before the target displacement was reached, for the sake of accuracy the displacement step size has been assumed equal to 0.1 mm for all the case study frames.

4. Calibration of the equivalent damping law

A new damping law has been developed through a numerical calibration on the case study frames. Firstly, the equations provided by the scientific literature were compared [45,53-55]. All those equations evaluate the total equivalent viscous damping ratio as the summation of the inherent viscous damping in the elastic range ξ_0 , and the viscous damping ξ_{hyst} due to the hysteretic behaviour:

$$\xi_{eq} = \xi_0 + \xi_{hyst} \quad (117)$$

Despite some differences among those equations, it was observed that the damping ratio due to the hysteretic behaviour ξ_{hyst} (hysteretic damping) is generally assumed as function of the ductility demand μ , according to the following form:

$$\xi_{hyst} = \xi_{\infty} \left(1 - \frac{1}{\mu^{\alpha_1}} \right) \quad (118)$$

whereby ξ_∞ represents the asymptotic limit value that the hysteretic damping can reach for infinite value of ductility demand, and α_1 is a constant usually assumed equal to 0.5 or 1.

Based on this background knowledge, the goal of the numerical calibration is the determination of the asymptotic damping ξ_∞ that is appropriate for the structural types under investigation. To this end, the average drift Δ_m , defined as the summation of drifts at all storeys of the considered structure divided by the total number of storeys, is assumed as the reference parameter of the numerical calibration. Given the ten accelerograms defined in Chapter 2, Incremental Dynamic Analyses (IDA) are conducted on every case study frame for peak ground acceleration from 0.02 g to 2 g, in step of 0.02 g. For every level of seismic excitation and for each of the 10 ground motions, the maximum values during the time history of the average drift Δ_m is calculated. Then, following the suggestion of EC8, the mean value of the average drift Δ_m over the values of the 10 ground motions is calculated for each peak ground acceleration. In the first step of the calibration, the value of Δ_m is calculated at each step of the D-DAP analysis. Thus, every average drift Δ_m corresponds to a value of ground acceleration a_g determined by the D-DAP with an elastic response spectrum with fixed 5% damping. For every fixed value of Δ_m in the D-DAP, the corresponding ground acceler-

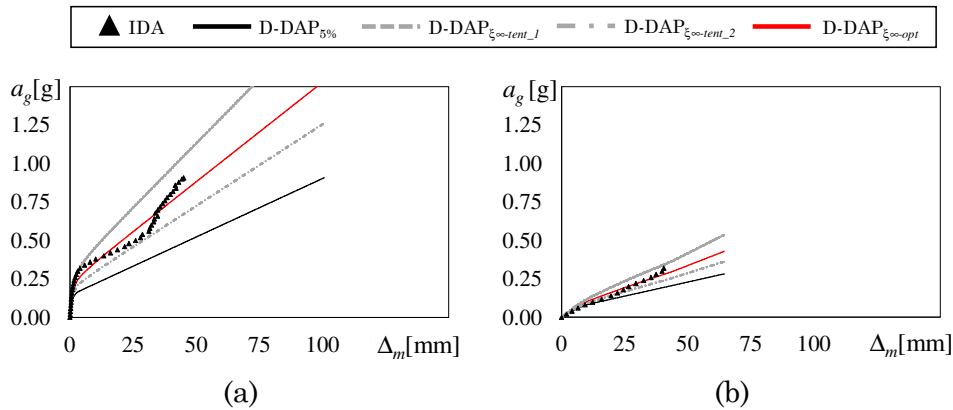


Figure 30 – Performance curve in terms of PGA and average drift Δ_m for frame (a) SR32-I014 and (b) GL91

ation in the IDA is determined. Figure 30(a) and (b) shows the performance curves in terms of a_g and Δ_m of frames SR32-I014 and GL91, respectively. The results of the IDA display that the average drift Δ_m increases with the peak ground acceleration, until the structure starts to yield and the stiffness of the structure reduces. However, in case of infilled frames, the decrease of the stiffness may be followed by a hardening behaviour, as showed by frame SR32-I014. Indeed, after the cracking of infill panels the stiffness of the structure drastically reduces. Nonetheless, seismic actions still can be supported by columns, which provide the structure with the additional stiffness showed in the hardening branch. Generally, for a fixed Δ_m , the D-DAP with 5% damping (black line) underestimates the values of a_g provided by the IDA (black triangles). Since the response provided by the IDA is the target, the ground acceleration evaluated by the D-DAP has to be corrected with an appropriate value of damping ratio. Indeed, if a too large or a too low hysteretic damping ξ_∞ is adopted, the D-DAP overestimates or underestimates the ground acceleration for a fixed value of Δ_m , as showed by the grey dashed line and the grey dashed-dotted line in Figure 30, respectively. Thus, for every relevant frame, the optimal hysteretic damping ξ_∞ is determined by an optimization process. In this process, for every fixed value of average drift Δ_m , the difference between the ground accel-

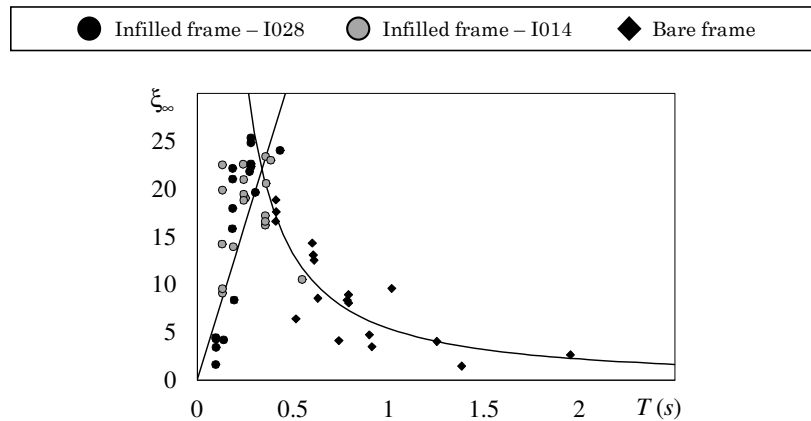


Figure 31 – Relation between the optimized ξ_∞ and the fundamental period T for every case study frame

eration associated by the D-DAP and the ground acceleration associated by the IDA is elevated to the square. Afterwards, the squares of those differences are summated all together. Finally, the optimal ξ_∞ is the value that minimizes the summation of the squares of the differences between the ground accelerations by D-DAP and that by IDA. This optimization is conducted for values of Δ_m lower than or equal to that corresponding to the structural collapse. Particularly, the collapse of the structure is identified with two alternative conditions: (1) the attainment of a maximum drift equal to the 4% of interstorey height or (2) a reduction of the 30% of the maximum base shear. The 4% drift is the limit value suggested by FEMA [7] for the collapse prevention limit state. The 30% reduction of the resistance has been assumed following the suggestion provided by NTC08 [13]. Actually, Italian code admits a maximum reduction of the seismic resistance equal to the 20%. Because of this, the maximum reduction of seismic resistance has been slightly extended to the value of 30%. This expedient allows the investigation of a larger range of behaviour, especially for infilled frames whereby the reduction of seismic resistance is abrupt and significant. The first of these two conditions that occurs determines the collapse of the structure, and the corresponding Δ_m is the maximum average drift to be considered in the optimization process. Figure 30 shows that when the hysteretic damping of the relevant frame is evaluated using the optimized ξ_∞ , the D-DAP (red line) approximates more accurately the values of a_g provided by the IDA. This result is found for all the case study frames. For every case study frame, the optimization process led to a different value of optimal ξ_∞ .

In the second step of the calibration, the optimized values of ξ_∞ obtained for every frame were analysed to find a ruling parameter. Different possible parameters were considered and the fundamental period T_1 showed the most significant influence on the value of ξ_∞ . Figure 31 shows the influence of T_1 on ξ_∞ . In particular, in case of very stiff structures the values of ξ_∞ tend to increase with T_1 . This tendency is demonstrated by almost all the infilled case study frames, whose fundamental periods range basically from 0.096 s to 0.384 s (grey and black dots). However, for fundamental periods larger than 0.40 s this tendency is

inverted, and the values of ξ_∞ tend to decrease for larger T_1 . This trend is exhibited by all the analysed bare frames (black diamonds). In fact, the lack of infill panels strongly reduces the stiffness of bare structures, which have larger fundamental periods, ranging from 0.40 to 1.95 s. Only two infilled frames fall in this region of the plot, and they are frame GL91-I028 and GL91-I014. Indeed, these frames are the most flexible among the set of infilled frames, and their fundamental period is equal to 0.433 and 0.548 s, respectively. Based on these results, the asymptotic damping ξ_∞ can be reasonably considered as a function of the fundamental period of the structure.

The third step of the calibration aimed at proposing an equation for the evaluation of the asymptotic damping ξ_∞ given a structure with a fundamental period T_1 . To this end, the domain $\xi_\infty - T_1$ has been divided into two regions: the first region includes the structures with larger stiffness, whilst the second region includes more flexible structures. Looking at those two regions, it was observed that for low fundamental periods the relation between ξ_∞ and T_1 could be approximated by a linear function, whilst for larger fundamental periods it could be approximated by an hyperbolic function. Based on these considerations, the linear equation has been calibrated by minimizing the sum of the square deviations of case study frames whose fundamental period was lower than 0.40 s. Instead, the hyperbolic function has been calibrated by minimizing the sum of the square deviations of frames with fundamental period higher than 0.40 s. Hence, given a period T_1 , the value of ξ_∞ to be assumed is the minimum between the values provided by the linear and the hyperbolic equations, as expressed in the following function:

$$\xi_\infty = \min\left(65T_1; \frac{5.4}{T_1^{1.3}}\right) \quad (119)$$

The intersection between the two functions is equal to a period of 0.34 s and indicates the shift from the first region to the second region of the $\xi_\infty - T_1$ domain. In Figure 31 Equation 119 is plotted with the continuous black line. It can be seen that the calibrated function approximates with a good accuracy the tendency of the values of ξ_∞ . Some approximations are present, but they are generally conservative.

In conclusion, the equation of the proposed equivalent damping law is obtained by substituting Equation 119 into 70:

$$\xi_{eq} = \xi_0 + \min\left(65T_1; \frac{5.4}{T_1^{1.3}}\right) \left(1 - \frac{1}{\mu}\right) \quad (120)$$

Thus, the equivalent damping is not only a function of the ductility demand μ , but also of the fundamental period of the structure T_1 . Figure 32(a) plots the proposed equation of ξ_{eq} as function of the ductility demand μ . Each curve displays the results obtained for a different value of T_1 . Note that Figure 32(a) shows the value of ξ_{eq} for ductility demand μ larger than unity. In fact, when the structure response is still elastic, i.e. μ is lower or equal to 1, the equivalent damping ξ_{eq} is always equal to $\xi_0=5\%$. Regardless of T_1 , the equivalent damping increases with the ductility demand μ . However, when the ductility demand becomes larger the rate of increase of ξ_{eq} becomes smaller, and the equivalent viscous damping tends towards the asymptotic value $\xi_0 + \xi_{\infty}(T_1)$. For fixed values of ductility demand μ , smaller ξ_{eq} are obtained when larger T_1 are considered. However, if fundamental periods lower than 0.34 are considered (dashed lines), the value of ξ_{eq} increases with the fundamental period. Figure 32(b) shows the dependency of the equivalent damping ξ_{eq} from the fundamental period T_1 . Each curve refers to a different ductility demand μ . The y-axis starts from 5% because this is the minimum value that ξ_{eq} can assume. Indeed, for $\mu=1$, no additional hysteretic damping is required, and ξ_{eq} keeps the constant value of 5%. When the

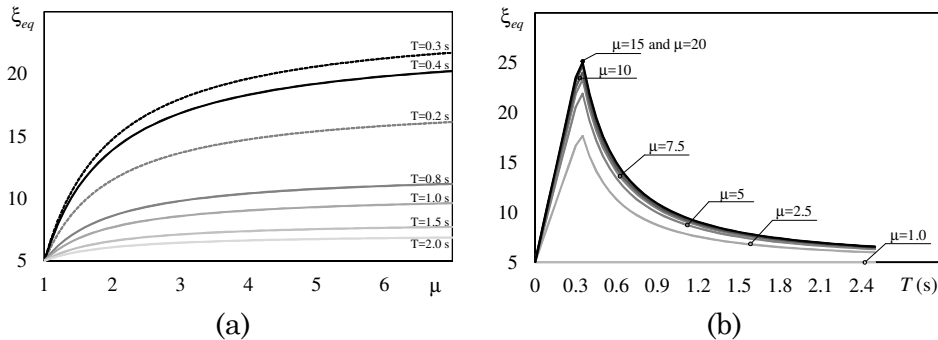


Figure 32 – Equivalent damping evaluated by the proposed law plotted (a) for fixed value of T_1 and (b) for fixed values of μ

ductility demand becomes larger than 1, the equivalent viscous damping increases as well. In particular, for fixed values of T_1 , larger values of μ lead to larger ξ_{eq} . However, when the ductility demand overcomes the value of 7.5, further increase of μ leads to almost negligible increase of ξ_{eq} .

Chapter 5

VALIDATION OF THE D-DAP

1. Object

The second part of the numerical study investigates the accuracy of the previously calibrated D-DAP in predicting the seismic response of RC frames. Since the D-DAP aims at being a method of analysis particularly indicated for the seismic assessment of existing RC buildings, its accuracy has been tested on a large set of RC frames representative of buildings with various geometrical and mechanical characteristics. The case study frames are those already described in Chapter 3. The goal of this study is (i) to verify if the D-DAP can provide a prediction of the seismic behaviour of RC buildings that is generally reliable regardless the features (presence of infills, number of storeys, collapse mechanism, material properties) of the analysed structures, (ii) to compare the level of accuracy of the D-DAP with that provided by other nonlinear static method of analysis.

For the first goal, the seismic response of the case study frames estimated by the D-DAP is compared to that obtained by the Incremental nonlinear Dynamic Analysis (IDA). Indeed, IDA is recognized as the most accurate method of analysis and its results are considered likely to predict the actual behaviour of structures. Because of this, the results obtained by IDA are assumed as benchmark.

For the second purpose, the seismic response of the considered RC buildings predicted by the D-DAP has been compared to that provided

by nonlinear static methods of analysis suggested in seismic codes and by other advanced nonlinear static methods available in literature.

2. Research methodology

In order to fulfil the goals described in the previous paragraph, the applied research methodology required the assessment of the case study frames by means of nonlinear dynamic analysis and nonlinear static analysis. To describe the seismic response provided by those analyses, both global parameters (base shear, top displacement, ground acceleration, average drift along the height) and local parameters (storey drift) were considered.

Firstly, the seismic response of the frames predicted by the D-DAP needs to be compared to that provided by nonlinear dynamic analysis. Thus, for each frame, an IDA was conducted considering the set of 10 ground motions already described in Chapter 2. For each step of the IDA, this reference suite of ground motions was scaled by the ratio of the relevant peak ground acceleration to the value 0.35 g. The value of the ground acceleration was increased in step of 0.02 g until the 5% of storey drift is attained at one of the storeys. For every level of seismic excitation and for each of the 10 ground motions, the maximum values during the time history of the following response parameters are evaluated:

- maximum top displacement D_t
- maximum base shear $V_{b,max}$
- maximum drift at each i -th storey Δ_i
- mean value of the maximum storey drifts along the height Δ_m .

Then, following the recommendation of EC8, the mean over the values of the 10 ground motions is calculated for each response parameter. In particular, the maximum drifts Δ_i and the mean drifts Δ_m are normalised with respect to the interstorey height, which is equal to 3200 mm for every frame. In order to estimate the dispersion of the results over the ten accelerograms, the standard deviation of the base shear σ_{vb} and the standard deviation of the peak ground acceleration σ_{ag} have been evaluated for every fixed value of top displacement. In case of the inter-

storey drifts, the standard deviation σ_{Δ} has been evaluated at the fixed peak ground acceleration corresponding to the considered limit state (1%, 2% or 4% of maximum storey drift). For each of the aforementioned response parameter (RP), the standard deviation σ_{RP} has been added and subtracted to the mean value RP . The red dashed lines in the following figures (from Figure 33 to 37) represent the values of $RP+\sigma_{RP}$ and $RP-\sigma_{RP}$ and they are plotted alongside the mean values (represented by the red continuous line with triangles) of the response parameters. They show that the dispersion of the results is modest and confirm that, in this case, it is reasonable to assume the mean value as representative of the response, as suggested by EC8.

Afterwards, the seismic response of the case study frames evaluated by the proposed D-DAP and the IDA has been compared to that obtained by other nonlinear static method of analysis. For each frame, the results provided by the D-DAP and the IDA are plotted alongside those determined by nonlinear static analysis suggested by codes, i.e. the N2 method and the Capacity Spectrum Method (CSM). Both those methods considered two load patterns: forces with constant distribution along the height and forces proportional to the first mode of vibration. In addition, advanced methods of analysis were also considered, and the results provided the Multimodal Pushover Analysis (MPA) by Chopra and the Displacement Adaptive Procedure (DAP) by Pinho were included in this comparison as well. To ensure a fair comparison among the considered methods, all the nonlinear static analyses were conducted with a displacement step size of 0.1 mm, and the multimodal methods enveloped 3 modes of vibrations. At each step of the nonlinear static analysis, the top displacement D_i , the base shear V_b , the i -th storey drift Δ_i and the mean storey drift Δ_m were evaluated.

3. Analysis of the results

The seismic prediction obtained by the D-DAP is compared in detail to that provided by the other nonlinear static methods, assuming the response estimated by the IDA as target. The investigation is conducted for all the 54 frames but, for the sake of simplicity, the results are here

presented for four significant frames, that were chosen to be representative of the sets of analysed frames. Two frames were selected from the set of frames designed for gravity loads only, and the other two frames were drawn from the set of seismic resistant frames. In each pair of frames, one was infilled while the other one was a bare frame. To cover the widest possible range of behaviour, the four selected frames included frames with 3 storeys and frames with 9 storeys, with large, medium and low gravity loads resting on beams. The frames thus picked are:

- GL32: frame designed for gravity loads, 3 storey high and with medium gravity loads on beams;
- GL91-014: frame designed for gravity loads, 9 storey high, with large gravity loads on beams, and with weak infills;
- SR31-028: frame designed for seismic actions, 3 storey high, with large gravity loads on beams and stiff and strong infills;
- SR91 frame designed for gravity loads, 9 storey high and with low gravity loads on beams;

The results obtained for all the other cases study are reported in Appendix C, D, and E.

3.1. Global response

The global response of the four case study frames is illustrated in terms of base shear V_b and top displacement D_t (Figure 33), and in terms of ground acceleration a_g and top displacement D_t (Figure 34). The top displacement D_t at every step is evaluated as the summation of storey drifts at the current step. In each figure, every plot refers to one of the selected case study frames. In every plot, the target response predicted by the IDA (red line with triangles) is compared to the response predicted by the proposed D-DAP (black continuous line), the methods proposed by seismic codes (i.e. the N2 method and the CSM, represented by the dark and light grey lines, respectively) and the advanced non-linear static methods (i.e. the DAP and the MPA, represented by the dashed and the dotted black lines, respectively). The N2 method and the CSM are applied considering a distribution of forces proportional to the first elastic mode of vibration (dashed line) and a distribution of

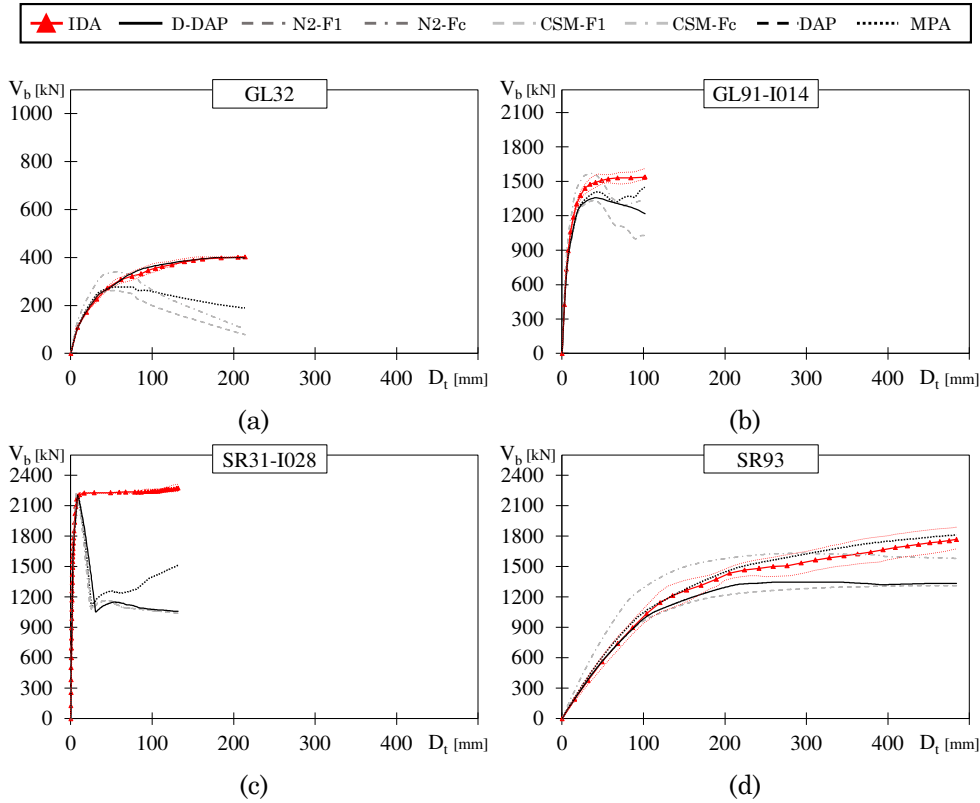


Figure 33 – Performance curve in terms of V_b - D_t of frames (a) GL32, (b) GL91-I014, (c) SR31-I028, (d) SR93

forces proportional to seismic masses (dashed dotted line), as suggested by EC8. In case of the V_b - D_t curve, the D-DAP and the DAP provide the same results. For every frame, the seismic response provided by the IDA and by nonlinear static methods is reported until the attainment of the structural collapse, which is identified with the attainment of a maximum storey drift equal to 4%, or a 30% reduction of the maximum base shear of columns. In particular, all curves are stopped at the top displacement that corresponds to the attainment of the structural collapse in the IDA.

Figure 33 shows that the D-DAP provides an accurate estimation of the seismic behaviour of the considered bare frames (Figure 33(a) and

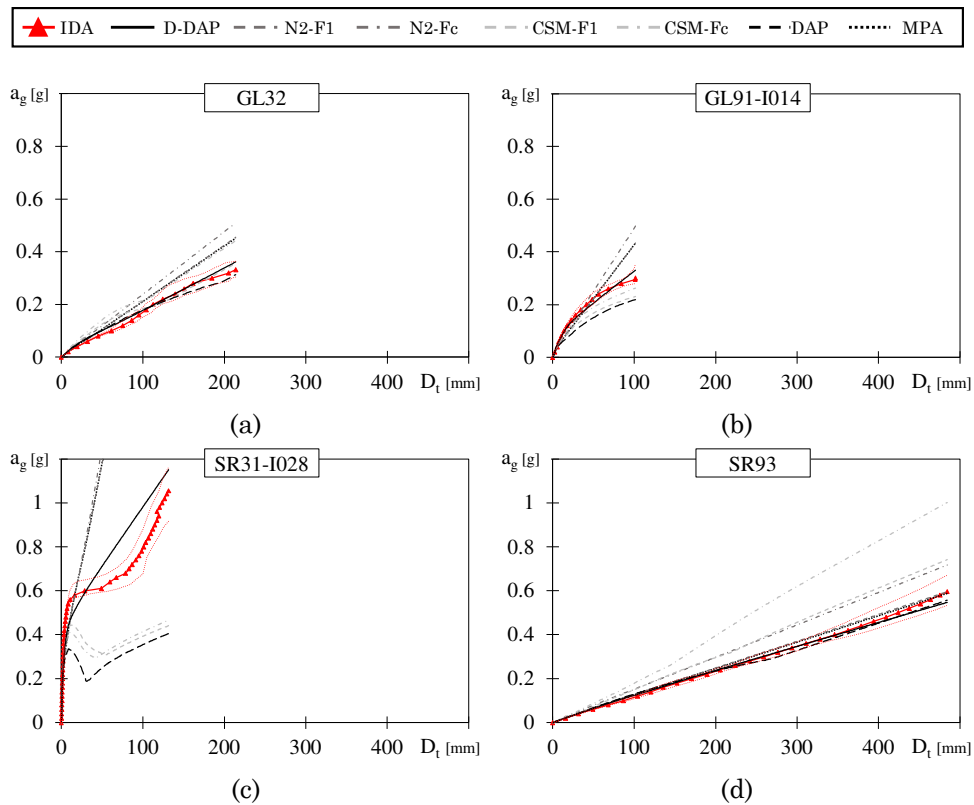


Figure 34 – Performance curve in terms of a_g - D_t of frames (a) GL32, (b) GL91-I014, (c) SR31-I028, (d) SR93

(d)), with an error lower than 18%. In those cases, the maximum base shear increases with the top displacement, and the D-DAP follows the trend of the IDA with a level of accuracy that is at least comparable to that of other methods of analysis (such as for frame SR93), or higher than them (such as for frame GL32). In case of infilled frames, an almost constant branch is observed in the V_b - D_t curve determined by the IDA. This upper value of the base shear is due to the fact that for every peak ground acceleration the maximum base shear is recorded in the IDA. Thus, once the structure has reached the collapse, the displacements keep increasing while the maximum base shear maintains almost the same value. This constant branch represents an upper limit

for the base shear, and is here interpreted as the ultimate lateral strength of the frame. The nonlinear static methods of analysis estimate accurately the elastic behaviour predicted by the IDA, and provides an abrupt reduction of the base shear force right after the cracking of the infills. The maximum shear force of this V_b-D_i curve represents the prediction of the ultimate lateral strength of the frame. Indeed, for such degrading structures, the peak value of the nonlinear static methods estimates with reasonable accuracy the maximum value of the IDA. In particular, the D-DAP evaluates the maximum resistance with an error lower than 15%.

In Figure 34 the ground accelerations associated to the displacement demands by the considered methods are compared to the values predicted by the IDA. For a fixed value of ground acceleration, the displacement demand of bare frames (Figure 34 (a) and (d)) is generally overestimated by the MPA and the CSM with respect to the DAP and the N2 method. Instead, in case of infilled frames (Figure 34 (b) and (c)) the displacement demand is generally underestimated by the DAP and the CSM, whilst it is overestimated by the N2 method and the MPA. On the contrary, given a value of ground acceleration, the D-DAP leads to the most accurate prediction of the displacement demand among the considered nonlinear static methods, regardless of the presence of infill panels.

3.2. Local response

The local seismic response of the case study frames has been evaluated considering the distribution of storey drifts along the height (Figure 35, 36 and 37). To this end, three limit states were considered in the IDA (red lines with triangles), i.e. the attainment of a maximum storey drift equal to 1%, 2% and 4%. These maximum storey drifts correspond to different levels of structural damage and are indicated by seismic codes, such as FEMA [7], as the limit values to satisfy the Immediate Occupancy (IO) limit state, the Life Safety (LS) limit state and the Near Collapse (NC) limit state, respectively. Each limit state was reached in every frame for a different value of peak ground acceleration. Fixing the ground acceleration at the value corresponding to the considered limit

state in the IDA, the corresponding distribution of storey drift in every frame has been evaluated by the D-DAP (continuous black line), the DAP (dashed black line), the MPA (dotted black line), the N2 method (continuous dark grey line) and the CSM (continuous light grey line). In these two latter methods, the drift at each storey is obtained from the envelope of the drifts obtained with the distribution of forces proportional to the first mode and proportional to storey masses. The distribution of storey drifts thus evaluated are reported in Figure 35, 36 and 37 for the limit state corresponding to 1%, 2% and 4% storey drift provided by IDA, respectively. In those figures, every plot refers to one of the four selected frames. At the top of each figure the V_b - D_t curve obtained by IDA is reported for each of the considered frame. On this curve, the black diamond represents the value of base shear and top displacement corresponding to the attainment of the relevant limit state (1%, 2% and 4% storey drift) and allows to visualize the level of inelastic behaviour reached by the structure at the considered limit state.

At 1% limit state, the considered nonlinear static methods estimate accurately the value and the shape of distribution of storey drifts of bare frames (Figure 35 (a) and (d)). In case of infilled frames, all methods localize the maximum concentration of damage at the correct storeys, however the effectiveness of each method is different. Indeed, the DAP and the CSM significantly overestimate the drifts, while the MPA and the N2 method underestimate them. The most accurate prediction is provided by the proposed D-DAP, which estimates the maximum storey drift with an error lower than 5% for GL91-I014 and 35% for SR31-I028.

For medium and large storey drifts (i.e. 2% and 4% limit state), the difference in the level of accuracy showed by the considered nonlinear static methods becomes more significant. Generally, the DAP and the CSM tends to overestimate the maximum drift with a larger error than the other methods, whilst the MPA and the N2 method lead to a larger error in underestimating the lowest drifts. The estimation of drifts obtained by the proposed D-DAP leads to an average error along the height that is usually lower than the other methods of analysis. Furthermore, it is noteworthy that in case of infilled frames not all the

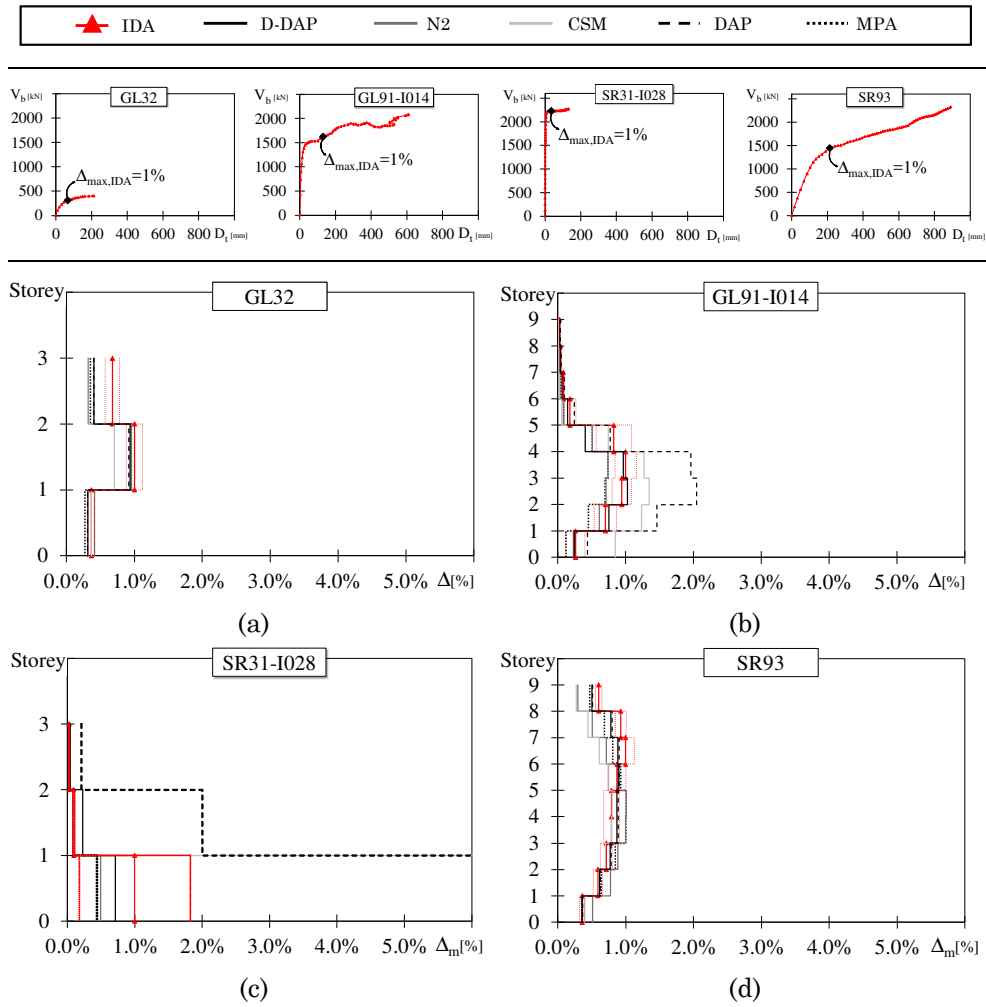


Figure 35 – Distribution of drift corresponding to the ground acceleration leading 1% of maximum drift in the IDA along the height of frames (a) GL32, (b) GL91-I014, (c) SR31-I028, (d) SR93

considered nonlinear static methods are able to attain the distribution of storey drifts corresponding to the 4% limit state. This is due to the fact those frames are very strong and stiff, thus such a large value of storey drift is obtained for ground accelerations larger than 1.0 g (1.06 g and 1.023 g for SR31-I028 and GL91-I014, respectively). Because of the approach adopted for the association of the displacement demand to the

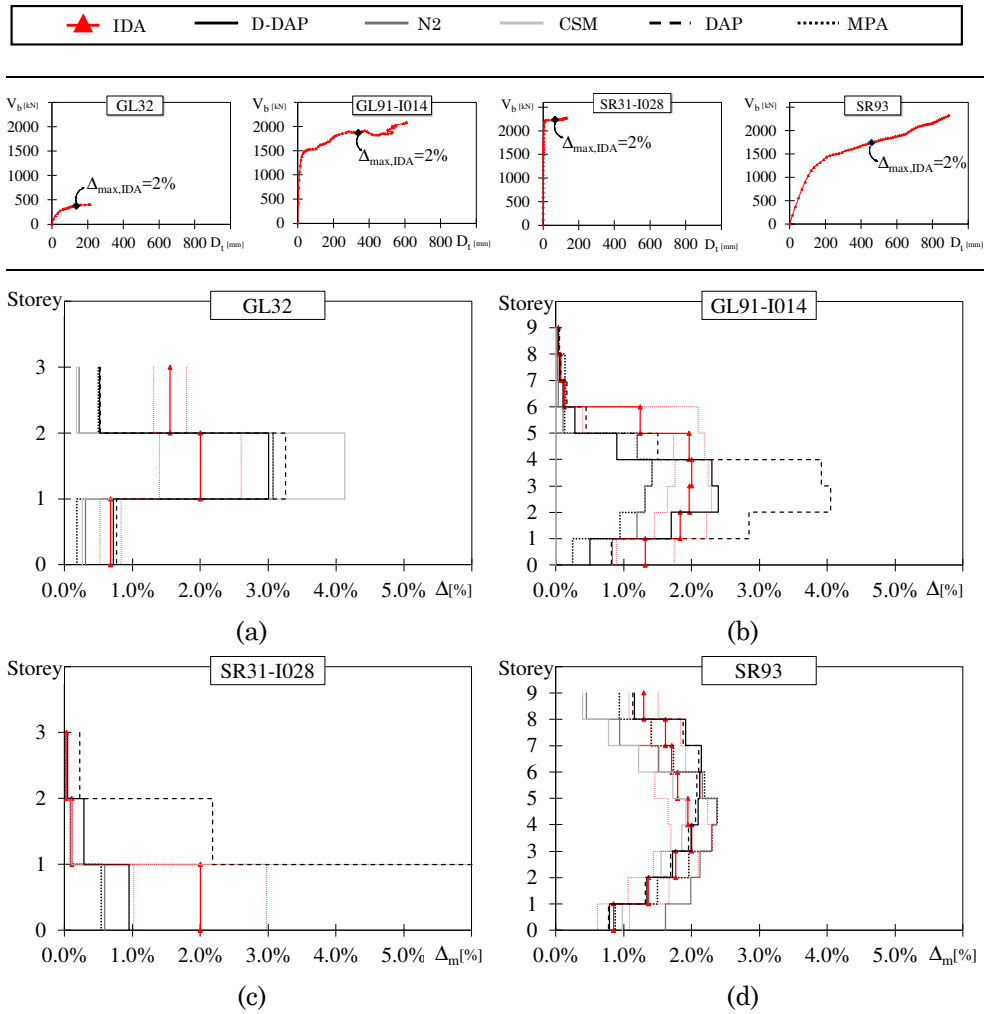


Figure 36 – Distribution of drift corresponding to the ground acceleration leading 2% of maximum drift in the IDA along the height of frames (a) GL32, (b) GL91-I014, (c) SR31-I028, (d) SR93

ground acceleration, the maximum displacement reached in the push-over analysis by the DAP and the CSM is associated to a ground acceleration smaller than that corresponding to 4% limit state in the IDA. This may be due to the fact that the equivalent viscous damping law adopted in those methods does not take into account properly the energy dissipation, and larger displacements are associated to a given ground ac-

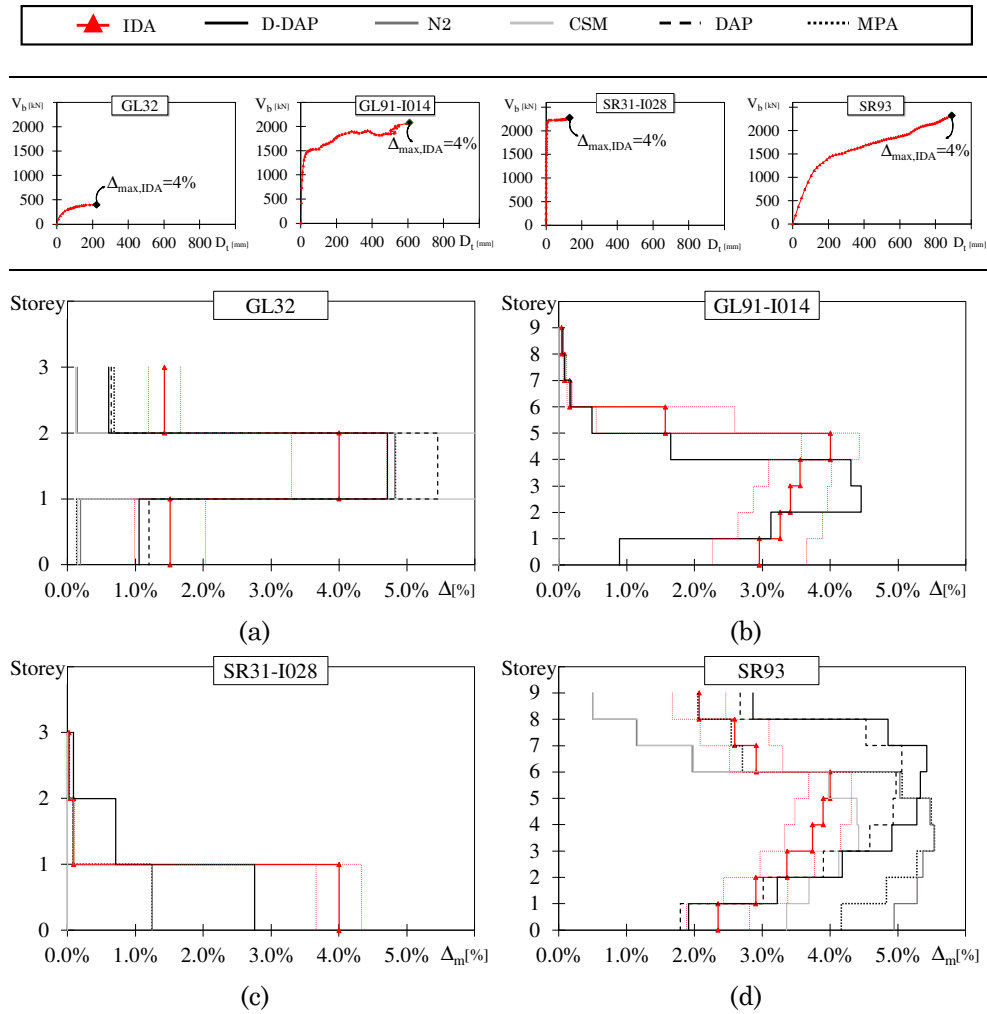


Figure 37 – Distribution of drift corresponding to the ground acceleration leading 4% of maximum drift in the IDA along the height of frames (a) GL32, (b) GL91-I014, (c) SR31-I028, (d) SR93

celeration. Thus, the distribution of drifts at that large limit state cannot be evaluated by those methods. For such large displacements, both the MPA and the N2 method fail before the attainment of the ground acceleration corresponding to the 4% limit state of frame GL91-I014, while they significantly underestimate the drift of frame SR31-I028. On the contrary, the proposed D-DAP allowed the evaluation of the distri-

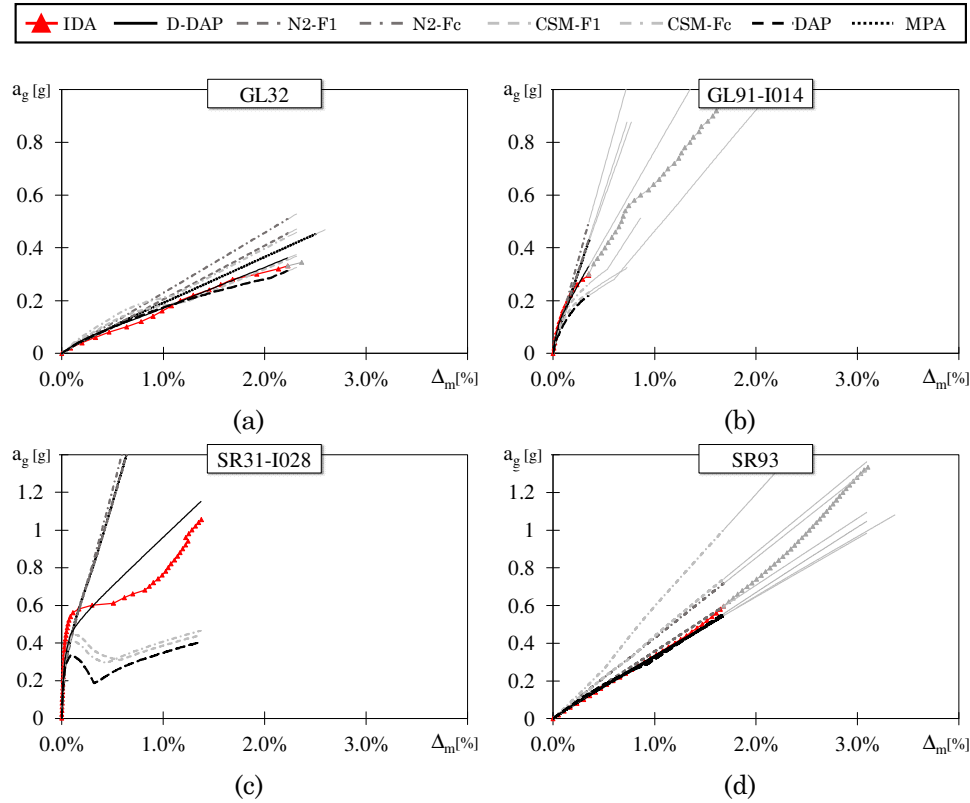


Figure 38 – Performance curve in terms of a_g - Δ_m of frames (a) GL32, (b) GL91-I014, (c) SR31-I028, (d) SR93

bution of drift corresponding to the 4% limit state for both the selected infilled frames, and for more than the 90% of the 54 analysed frames. The error committed by the D-DAP in evaluating the maximum drift is lower than 12% and 31% for frame GL91-I014 and SR31-I028, respectively.

In order to have a more comprehensive parameter to compare the accuracy of the considered methods, the average drift Δ_m is calculated as the summation of drifts along the height, divided by the number of storeys. Figure 38 displays for every peak ground acceleration the corresponding average drift as percentage of the interstorey height, which is equal to 3200 mm at every storey of every frame. All plots are reported up to the value of average drift corresponding to the top displace-

ment determined by the IDA at the structural collapse. Until this point, the plots are identified by the coloured lines presented in the legend. For frame SR31-I028 the structural collapse occurred because the maximum storey drift reached the 4%, and the last point of the coloured plots reports the average drift corresponding to this maximum storey drift. Instead, all other frames collapsed because of a reduction of the base shear larger than 30%, and the last point of the coloured plots represents the average drift corresponding to this collapse condition. In order to compare the effectiveness of the nonlinear static methods at the maximum inelastic behaviour experienced by the frames, the average drift of frame GL32, GL91-I014 and SR93 has been also evaluated up to the attainment of 4% limit state in the IDA. However, since this behaviour goes beyond the limit assumed as structural collapse, it is reported as a “ghost” grey line, that continues the previous coloured plots. Although all plots are stopped at the same value of top displacement, the value of the average drift evaluated by the IDA and that determined by the nonlinear static methods of analysis is different, and this explains why the plots do not stop at the same point. In addition to this, some nonlinear static analysis in some cases, such as N2 method and CSM in frame GL91-I014, crashed before the attainment of the 4% limit state, thus stopping earlier. For bare frames (SR93 and GL32), the D-DAP provides an accurate estimation of the average drift of IDA, with an error lower than 10% at the peak ground accelerations corresponding to the 30% reduction of shear resistance. Given the peak ground acceleration corresponding to the 4% limit state in the IDA, the D-DAP predicted the average drift with less than 10% of error for frame GL32. For frame SR93 the error reached a value around 35%, but however it was comparable to that committed by the other nonlinear static methods. Also the DAP and the MPA predict accurately the average drift corresponding to the reduction of 30% of the base shear evaluated in the IDA, but with an error slightly larger than that of the proposed D-DAP. Furthermore, their error increased when the average drift was evaluated at the peak ground acceleration corresponding to the 4% limit state. The prediction of the N2 method, obtained by the envelope of the two distribution of forces, overestimated the average drifts of frame SR93

and underestimated those of frame GL32, respectively, with an error larger than 16% at the ground acceleration corresponding to the 30% reduction of base shear, and larger than 25% at the attainment of 4% drift in the IDA. The CSM method with distribution of forces proportional to seismic masses overestimated the average drifts of frames, with an error larger than 35% at the ground acceleration corresponding to the 30% reduction of base shear. The error decreases if the average drift corresponding to the 4% limit state is considered. In case of infilled frames, the most accurate evaluation of the average drift is provided by the D-DAP. Indeed, for the acceleration corresponding to the 4% limit state in the IDA, the error committed by the D-DAP is lower than 14% and 20% for frame SR31-I028 and GL91-I014, respectively. In case of frame GL91-I014, the D-DAP predicted with accuracy also the average drift at the ground acceleration corresponding to the 30% reduction of base shear, with an error of 11%. Since for frame SR31-I028 the degrading of infill panels is less abrupt, the 30% reduction of the base shear occurs for a peak ground acceleration larger than that corresponding to the 4% limit state, thus it is not taken into account here. On the contrary, none of the other methods of analysis predicted the average drift corresponding to the 4% limit state of frame GL91-I014, and led to error larger than 35% also at the peak ground acceleration corresponding to the 30% reduction of base shear. As for frame SR31-I028, only the MPA and the N2 predicted the average drift corresponding to the 4% limit state, but led to errors larger than 60%. The poor accuracy of those methods of analysis was probably due to the fact that the equal displacement rule is less appropriate for infilled frames, and led to over/underestimated values of displacements for fixed accelerations. Moreover, the other methods of analysis, particularly the DAP and the CSM, often crashed untimely, because they could not follow the brittle behaviour of infills. The tendency showed in those plots can be found generally in all the other case study frames, and confirms the good performance provided by the proposed D-DAP method applied with the calibrated damping law in predicting the seismic behaviour of RC frames. In particular, the D-DAP with the calibrated damping law led to an improvement, compared to other existing methods, especially

in the evaluation of the seismic response of RC frames with infill panels.

4. Global evaluation of the D-DAP effectiveness

In order to have a more comprehensive evaluation of the accuracy of the D-DAP, the following section summarises the error committed in each frame by the D-DAP (with various damping laws) and by other nonlinear static analysis available in literature in predicting the target response provided by the IDA.

This comparison was conducted in terms of average drift along the height, because it was considered representative of the average damage cumulated by the structure. For each limit state considered in the IDA, i.e. the attainment of a maximum storey drift equal to 1%, 2% and 4%, the average drift corresponding to that limit state has been calculated by summing the drifts provided by the IDA at each storey, and dividing the sum by the number of storeys. Each of this limit state corresponds to a peak ground acceleration provided by the IDA. Thus, fixing the ground acceleration equal to the value corresponding in the IDA to the relevant limit state, the corresponding average drift is evaluated by the considered nonlinear static method. In this comparison, for each limit state it was considered the average drifts evaluated by the calibrated D-DAP with (i) the proposed damping law, (ii) Priestley's damping law for concrete elements, (iii) Freeman's damping law and (iv) Gulkan and Sozen damping law. When one of the first three equations was adopted, the coefficient η was evaluated by the proposed equation (Equation 95). Instead, when the equation by Gulkan and Sozen was considered, the response spectra was corrected by the coefficients a and b proposed by Lin and Chang [47]. This latter approach was the same suggested by Pinho et al [33], and allowed a fair comparison between the D-DAP and the DAP. Moreover, the average drifts corresponding to each limit state were evaluated also by Pinho's DAP according to [33], Chopra's MPA, the N2 method and the CSM. The accuracy of the prediction provided by the relevant nonlinear static method was expressed in terms of error, which was calculated as the difference between the

average drift provided by the IDA and that provided by the D-DAP, divided by the average drift obtained by the IDA.

To sum up, the average drifts corresponding to three limit states were evaluated for each of the 54 frames by the eight nonlinear static methods and the corresponding errors with respect to the IDA results were calculated. The results for all the case study frames are presented in Figure 39, 40 and 41, which report the error between the nonlinear static methods of analysis and the IDA in evaluating the average drift corresponding to the limit states of 1%, 2% and 4%, respectively. Those figures are composed by eight “radar” plots, each referred to a different nonlinear static method of analysis. In particular, plots (a), (b), (c) and (d) show the error between the average drift of IDA and that predicted by the D-DAP applied with the proposed damping law, Priestley’s damping law, Freeman’s damping law and Gulkan-Sozen damping law, respectively. Plots (e), (f), (g) and (h) display the error committed by Pinho’s DAP, Chopra’s MPA, the N2 method and the CSM. The radar plot is represented by a triangle. Each vertex of the triangle refers to a particular group of the 54 case study frames: the lower right vertex refers to the infilled frames with stiff and strong infill panels (named I028), the lower left vertex is referred to the frames with weak infills (named I014) and the upper vertex is referred to the bare frames (named I000). Since each of those groups is composed by 18 frames, the maximum number at the external corner is 18. The radar plot aims at indicating for how many frames the considered nonlinear static method estimates the average drift of the IDA at the relevant limit state with an error lower than 20%, 40% and 60%. In particular, the vertexes of the grey surface indicate the number of frames for which the error is not larger than 20%. Similarly, the orange and blue surfaces specify in how many cases the error is not larger than 40 and 60%, respectively. If for all the frames of the three groups the committed error was lower than 60%, the blue area should cover the entire area of the triangle. If for all frames the error was lower than the 40% the orange area should cover the triangle, while if the error of each frame was lower than 20% the area of the triangle should become entirely grey.

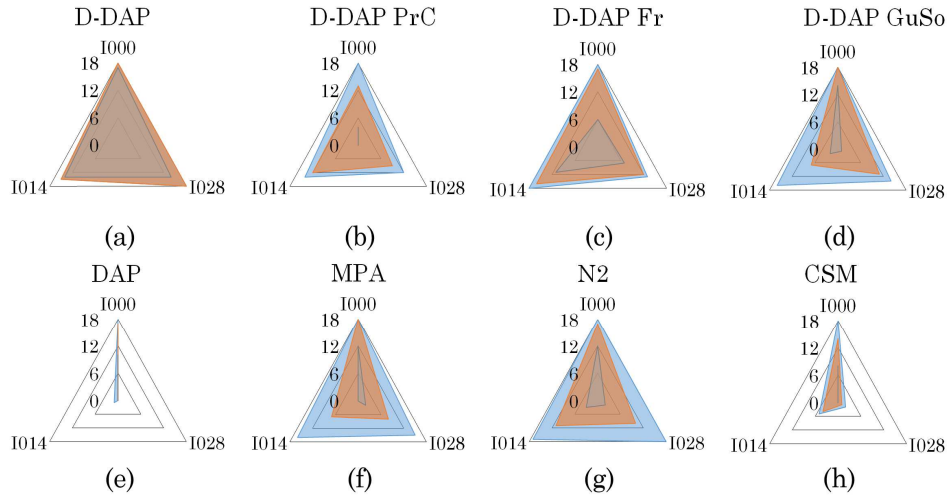


Figure 39 – Error in the average drift for the ground acceleration that leads to a maximum drift of 1% in the IDA obtained by: the D-DAP with several damping laws (a) proposed law, (b) Priestley for concrete, (c) Freeman, (d) Gulkan and Sozen’s, and by (e) the DAP by Pinho, (f) the MPA by Chopra, (g) the N2 method, (h) the Capacity Spectrum Method

This type of plot allows a straightforward evaluation of the accuracy of each nonlinear static method. Indeed, the larger the coloured areas, the larger the number of frames for which the error is lower than the admitted benchmarks (20%, 40%, 60%). In particular, the very final goal is to have the largest *grey* area possible, meaning that the error is lower than 20% for the majority of frames, and the accuracy is higher.

From Figure 39, 40 and 41 it was observed that when the D-DAP is applied to predict the average drift along the height, the blue hatch, as well as the orange and the grey hatches, in the radar plot cover a larger area of the triangle compared to all the other considered methods. Considering the bare frames grouped in I000 (upper vertex), the D-DAP applied with the proposed damping law (Figure 39 (a), 40 (a) and 41 (a)) commits an error lower than the 40% in estimating the average drift of all the bare frames (18/18) at each limit state. In fact, the upper vertex of the orange (and also blue) triangle corresponds to the maximum val-

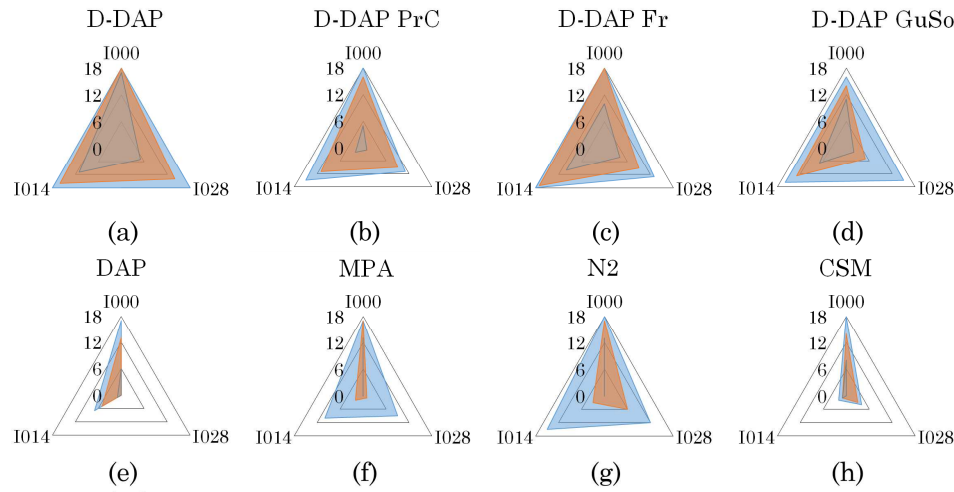


Figure 40 – Error in the average drift for the ground acceleration that leads to a maximum drift of 2% in the IDA obtained by: the D-DAP with several damping laws (a) proposed law, (b) Priestley for concrete, (c) Freeman, (d) Gulkan and Sozen’s, and by (e) the DAP by Pinho, (f) the MPA by Chopra, (g) the N2 method, (h) the Capacity Spectrum Method

ue of 18 in each of the three plots. The error in estimating the average drift was lower than 20% for almost all the bare frames at 1% and 2% limit state, and for the majority of bare frames (11/18) at 4% limit state. Indeed, the upper vertex of the grey triangle corresponds exactly to the black external vertexes in Figure 39 (a), 40 (a), while it is behind the black corner in Figure 41 (a). With regards to frames with strong infills, grouped in I028, and weak infills, grouped in I014, (lower right corner and lower left corner, respectively), the D-DAP estimated the drift of IDA with an error lower than 20% or 40% for the majority of the frames both at lower storey drifts (1% limit state) and large storey drifts (4% limit state). However, for more than the 90% of frames grouped in I028 and I014, the D-DAP applied with the calibrated damping law estimated the average drift with an error lower than 60%.

The accuracy of the D-DAP decreases when the damping laws from literature, showed in plots (b) (c) and (d) of Figure 39, 40 and 41, are

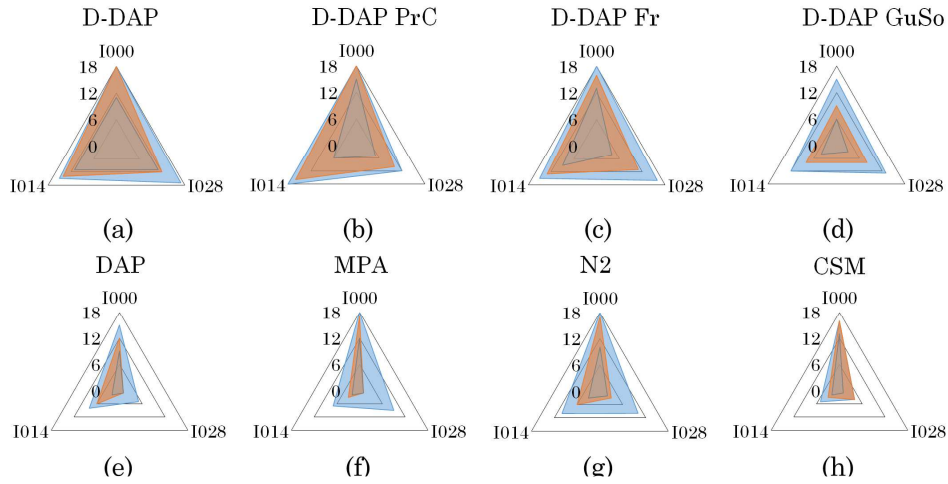


Figure 41 – Error in the average drift for the ground acceleration that leads to a maximum drift of 4% in the IDA obtained by: the D-DAP with several damping laws (a) proposed law, (b) Priestley for concrete, (c) Freeman, (d) Gulkan and Sozen's, and by (e) the DAP by Pinho, (f) the MPA by Chopra, (g) the N2 method, (h) the Capacity Spectrum Method

used instead of the proposed one. For most of the frames with and without infills the error in the evaluation of the average drift was lower than 40% at all limit states, almost regardless of the damping law. However, at limit state of 1% and 2% of drift, the D-DAP with those damping laws led to an error lower than 20% only for few frames (mainly infilled frames belonging to group I014), and the most and the least accurate results (corresponding to the largest and the smallest grey triangles, respectively) were obtained by applying the D-DAP with Freeman's damping law and Priestley's damping law, respectively. Indeed, at 1% limit state, the D-DAP with Priestley's damping law led to an error lower than 20% only for 4 bare frames, whilst the D-DAP with Freeman's equation led to an error lower than 20% for 6 bare frames, 11 frames belonging to I014 group and 7 frames belonging to group I028. On the contrary, the D-DAP with the proposed damping law led to

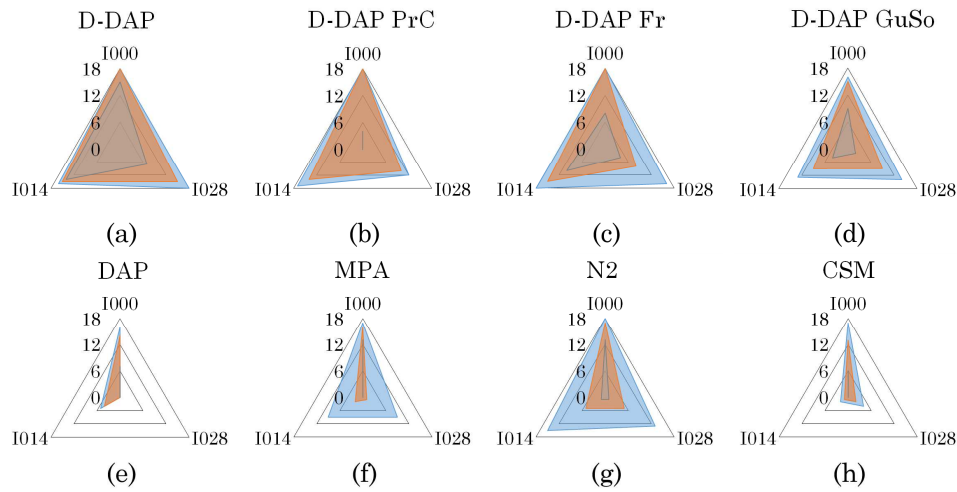


Figure 42 – Error in the average drift along the height committed by the D-DAP with (a) the proposed damping law, (b) Priestley’s damping law for concrete, (c) Freeman’s damping law, (d) Gulkan and Sozen’s damping law, and by (e) the DAP by Pinho, (f) the MPA by Chopra, (g) the N2 method, (h) the Capacity Spectrum Method

an error lower than 20% in 17 bare frames, 14 frames of group I014 and 14 frames of group I028. A similar trend is observed at 2% limit state. When the 4% limit state was considered, the D-DAP with Priestley’s damping equation led to a more accurate average drift prediction, with an error lower than 20% in 15 bare frames, 6 frames of I014 group and 5 frames of I028 group. However, better results for infilled frames (both I014 and I028) were obtained by the proposed D-DAP with the calibrated damping law, which led to an error lower than 20% for 11 frames I014 and 11 frames I028. On the contrary, if the damping law by Gulkan and Sozen was adopted the least accurate results were obtained, and the error was lower than 20% for 6 bare frames, 4 frames I014 and 3 frames I028. damping equation.

The error committed by the DAP, the MPA, the N2 method and the CSM are reported in plots (e), (f), (g) and (h) of Figure 39, 40 and 41, respectively. It can be noted at all limit states, the error committed by

those methods in estimating the average drift of IDA is larger than that obtained by the D-DAP, especially if the D-DAP applies the proposed damping law (Figure (a)). Although for bare frames those methods lead to a good estimation of the average drift (the upper vertex of the coloured hatches is generally between 12 and 18), significantly less accurate results are obtained for infilled frames, regardless of stiffness and strength of panels.

To further summarise the results, for each frame it was calculated the average error committed by every nonlinear static method in evaluating the average drift over the three limit states. For a given frame and a fixed nonlinear static method, the average error was evaluated summing the errors committed by that method in estimating the average drifts corresponding to the three limit values of 1%, 2% and 4% of storey drift, and the sum was divided by 3. With the same approach followed before, the results are represented for all the cases study frames in eight radar plots, each referred to a nonlinear static method, in Figure 42. Plot (a) shows that the D-DAP applied with the proposed damping law leads to an error in predicting the average drift lower than 40% for all the bare frames and for more than 85% of the infilled frames. The error was kept lower than 20% for more than 80% of the bare frames and of the infilled frames with weak infill panels. An error lower than the 20% was also committed by the proposed D-DAP in the majority of frames with strong infills. A lower global accuracy was reached by the D-DAP applied with the damping laws from literature, or by the other methods of analysis considered. In conclusion, the D-DAP applied with the proposed damping law revealed itself the most accurate approach among the investigated nonlinear methods of analysis and the improvement it can provide is remarkable in the prediction of the response of frames with infill panels.

Chapter 6

APPLICATION OF D-DAP IN SEISMIC UPGRADING: AN EXAMPLE

1. Object

Nowadays, after the tragic seismic events that have occurred in the Mediterranean area, and in particular in the Italian territory, the new seismic codes strongly encourage the seismic upgrading of existing buildings. However, the seismic retrofit of existing structures is quite an elaborate process, which develops into two main steps. The first step requires the seismic assessment of the structure, to compare the structural capacity to the demand required by the code. Based on this evaluation, in the second step the most appropriate seismic upgrading technique is selected to compensate for the structural deficiencies of the building. The evaluation of the strengths and weaknesses of the structure is fundamental for the success of the retrofit intervention. However, engineers need straightforward tools that allow the analysis of structures within reasonable time. The object of this section of the thesis is to show an illustrative practical application of the D-DAP in a seismic upgrading process of an existing RC building, as a tool to evaluate the capacity of the existing structure and the structural benefit provided by the seismic retrofit.

The structure to be updated is the three-storey RC building designed for gravity loads only (Section 3.3). Firstly, the capacity of the existing structure is estimated by the D-DAP. Afterwards, a seismic

upgrading technique is selected to retrofit the structure. To this end, among the available seismic upgrading techniques, an innovative approach, named base shear capping building, is selected.

The technology of the base shear capping building has been recently developed [73-76]. The authors proposed a simple approach to prevent structural collapse by separating the superstructure from its foundation to let the superstructure slide during extreme ground shaking. Thanks to the controlled friction force at the base, the proposed structural system realizes a sliding mechanism, which acts as a structural fuse. The sliding mechanism contributes to cap the horizontal force exerted on the superstructure. In such approach, the friction coefficient of the sliding surface is the main parameter and the key is to maintain the friction force between the superstructure and the foundation sufficiently low and stable. Indeed, a too large friction coefficient may refrain the structural displacement and force the system to behave as a fixed base system; a too small friction coefficient may cause untimely displacements of the structure. Based on previous experimental tests, carbon powder has been used to lubricate the bases of the structure's columns, in order to reduce the friction coefficient between steel and mortar to a stable value.

In order to determine the fundamental behaviour of the proposed system, various experimental and numerical studies have been conducted at Kyoto University. Former studies investigated the sliding behaviour between steel and mortar and the influence of steel conditions on the friction coefficient [73]. The following research evaluated the fundamental dynamic behaviour of the proposed system through a short rigid specimen with two masses [74, 75]. The last shaking table test investigated the application of the base shear capping system to a one storey one bay steel frame [76]. This latter was a joined research work between University of Catania and Kyoto University. In particular, the shaking table test was directly followed at the laboratory of the Disaster Prevention Research Institute of Kyoto University, and the elaboration of the results obtained from both the experimental and numerical studies was part of the present Ph.D. project.

This technique has been chosen because it is particularly suitable for a rapid verification by means of nonlinear static analysis. In fact, this technique has a sort of “boolean” character: if the base shear developed by the upgraded structure is lower than the base shear capacity of the original structure the seismic upgrading is successful, otherwise it is not applicable. Thus, to show an illustrative example, its effectiveness in preventing the structural collapse has been verified by means of the D-DAP.

The results that will be presented show that the base shear capping system can be a promising retrofitting technique for RC buildings. However, the presented example aims at being just an application of the D-DAP in a more practical environment, and further studies on the base shear capping upgrading are still in progress.

2. The base shear capping building: fundamental characteristics and experimental results

Analytical and numerical studies dealing with sliding objects investigated the nonlinear behaviour of such systems and provided the nonlinear equations of motion in cases of harmonic input [77,78] or earthquake motion [79]. Since the studies on sliding objects are closely related to the proposed approach, the fundamental dynamic behaviour of the base shear capping system could be explained. More recently, the friction between steel and mortar, the effect of carbon powder lubrication and the properties of the base shear capping system applied to structures have been investigated by shaking table tests and numerical simulations.

2.1. Basic behaviour of the base shear capping building

The base shear capping building requires the separation of the superstructure from its foundation. Due to this disconnection, the sliding system can be simplified with a two degree of freedom (2DOF) system, where the superstructure and the lower structure are modelled by two masses, m_t and m_b respectively, connected by two springs of stiffness $k/2$ and a dashpot of damping c (Figure 43(a)). The friction force develops

between the sliding base and the rigid horizontal support (foundation). The static friction force f is equal to $\mu_f N$, where μ_f is the friction coefficient of the sliding surface, and N is the total normal force equal to $(m_t + m_b)g$.

The fundamental dynamic behaviour of a sliding system is characterized by two phases [77-79]: the *stick state* and the *sliding state*. The transition from the *stick* to *sliding state* is governed by the friction force. When the base force transmitted by the foundation is lower than the friction force, the sliding does not occur, and the system behaves as a fixed base structure, with natural frequency ω_n and damping ratio ξ . When the base force attains the value f , the structure slides, and the base mass is subjected to a horizontal force that equals the friction force. For the 2DOF system, as represented in Figure 43(a), the governing equations for the *stick state* can be written as follows:

$$m_t(\ddot{u}_g + \ddot{u}_s + \ddot{u}_r) + c\dot{u}_r + ku_r = 0 \quad (121)$$

$$m_b(\ddot{u}_g + \ddot{u}_s) + m_t(\ddot{u}_g + \ddot{u}_s + \ddot{u}_r) = f \quad (122)$$

where u_g is the ground displacement, u_s is the sliding displacement, and u_r is the relative displacement between the top mass and the sliding base; \dot{u}_g , \dot{u}_s and \dot{u}_r are the corresponding velocities; \ddot{u}_g , \ddot{u}_s and \ddot{u}_r are the corresponding accelerations; c is the viscous damping coefficient; k

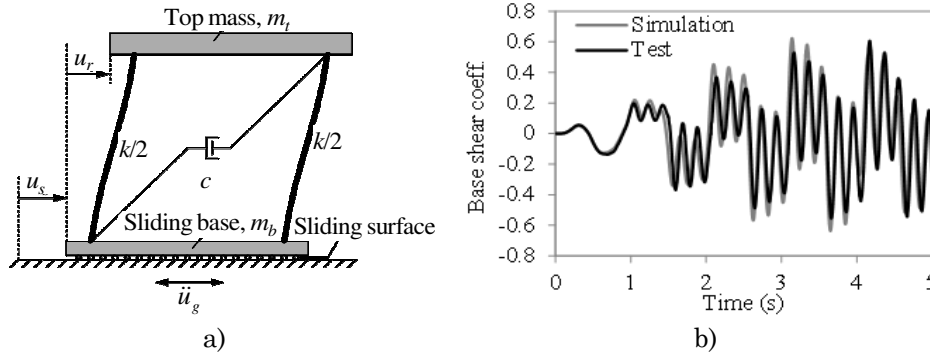


Figure 43 – (a) Basic features of sliding model; (b) Base shear coefficient time history under sinewave 1.5 Hz 4.0 m/s²

is the lateral stiffness of the superstructure. Equation 121 represents the dynamic equilibrium of the top mass, while Equation 122 represents the dynamic equilibrium of the entire system. Substituting the condition of the occurrence of sliding ($f = (m_t + m_b)\mu_f g$) into Equation 122, the sliding acceleration is obtained as:

$$\ddot{u}_s = \mu_f g - \alpha \ddot{u}_r - \ddot{u}_g \quad (123)$$

where g is the gravitational constant, and α is the mass ratio defined as the ratio of the upper mass over the total mass. Substituting Equation 123 into Equation 121 and dividing by $(1-\alpha)$, the equation of motion for the sliding phase is written in terms of the relative displacement u_r :

$$\ddot{u}_r + 2\omega' \xi' \dot{u}_r + \omega'^2 u_r = \frac{-\mu_f g}{1-\alpha} \quad (124)$$

$$\omega' = \frac{\omega_n}{\sqrt{1-\alpha}} \quad \xi' = \frac{\xi}{\sqrt{1-\alpha}} \quad \alpha = \frac{m_t}{m_t + m_b} \quad (125)$$

Equation 125 demonstrates that the response characteristics of the sliding structure change with respect to those of the fixed base structure. Due to the slippage, the structure exhibits a new “internal” sliding frequency ω' , which is larger than the natural frequency ω_n . This higher frequency is evidenced by the smaller oscillations showed in the base shear coefficient time history obtained both from experimental test and numerical analysis conducted with a sinusoidal input (Figure 43(b)). Furthermore, the structure shows a new damping ratio ξ' , larger than ξ . Both the sliding frequency ω' and the damping ratio ξ' are related to the frequency and the damping of the structure in the *stick* state by means of the mass ratio α .

From previous studies [78,79], this parameter is found to play a fundamental role in the dynamic response of the sliding system. In fact, larger mass ratios lead to lower levels of acceleration response. For values of mass ratio α reasonable for realistic structures, such as 0.80-0.90, the maximum shear in the sliding structure over its weight would reach 2.0 to 2.5 times the friction coefficient. It is notable that the degree of amplification is not specifically related to the type of superstructure, i.e. RC, masonry, or steel structure, but depends primarily on the flexi-

bility of the superstructure as well as the ratio of the superstructure's mass to the total mass. Looking at the existing structures, it is notable that the majority of RC buildings are characterized by a significant presence of infill panels. Several experimental and numerical studies [71,80-82] have demonstrated that the contribution of infill panels to the base shear coefficient of the structure can increase it up to values of 0.4. However, even with such an additional strength, those structures would still suffer severe damage or collapse when subjected to large ground motion. Considering the background noted above, a friction coefficient of around 0.20, half of the base shear coefficient of about 0.40, was chosen as a target friction coefficient in this study.

2.2. Experimental studies on the base shear capping system

In a preliminary experimental study, McCormick et al. [73] explored the possible sliding behaviour between steel and mortar, and showed that their friction coefficient was approximately equal to 0.8. However, different steel surface conditions, such as the presence of carbon, may significantly change the value of friction coefficient. Following those results, Enokida et al. [74, 75] carried out shaking table tests on a flexible specimen to study the friction of steel column, steel column with graphite lubrication, cast-iron column and iron column.

Between 2014 and 2015, the effectiveness of the lubricated base shear capping system has been examined by two series of shaking table tests conducted on specimens with two types of superstructures. The experimental test on the first type of specimen, referred to here as the "short specimen", aimed at the investigation of the fundamental dynamic behaviour of the system, with particular attention to the performance of graphite lubrication. The experimental test on the second type of specimen, referred to as the "tall specimen", aimed at considering the effect of overturning moment on the response of the separated system. The shaking table test on the tall specimen, and the elaboration of the test results of both the short and the tall specimen were part of the present Ph.D. work. In the following sections, the two types of specimen used in the two last shaking table tests and the experimental results will be presented.

2.2.1. Description of the specimens

Two series of shaking table tests were conducted with two types of superstructures assembled by steel elements. The first type of specimen, referred to as the “short specimen” (*SF*), was designed to investigate the fundamental dynamic behaviour of the system. The short specimens consisted of two rigid steel frames connected by ten rubber bearings (Figure 44(a) and (b)). As the mass ratio α affects the degree of amplification [78,79], the mass plates attached to the upper and lower frames were adjusted to achieve various mass ratios. The adopted mass ratios were 0.79, 0.65 and 0.49, keeping the total mass of the specimen at 5,015 kg. The natural frequencies of the superstructures equalled 2.8 Hz, 3.0 Hz and 3.5 Hz (i.e. a fundamental period equal to 0.357 s, 0.333 s and 0.286 s, respectively) for the mass ratios of 0.79, 0.65 and 0.49, respectively. These specimens were referred to as “short *flexible* speci-

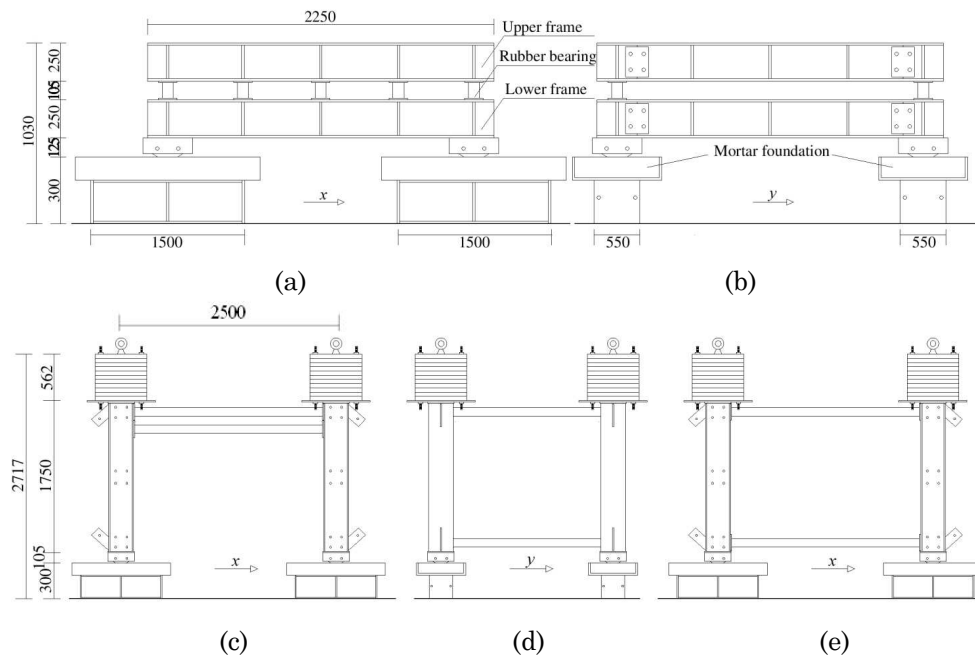


Figure 44 – Details of the test specimen (units in mm): (a) front view of short specimen; (b) lateral view of short specimen; (c) front view of TTB specimen; (d) lateral view of TTB and TBB specimens; (e) front view of TBB specimen

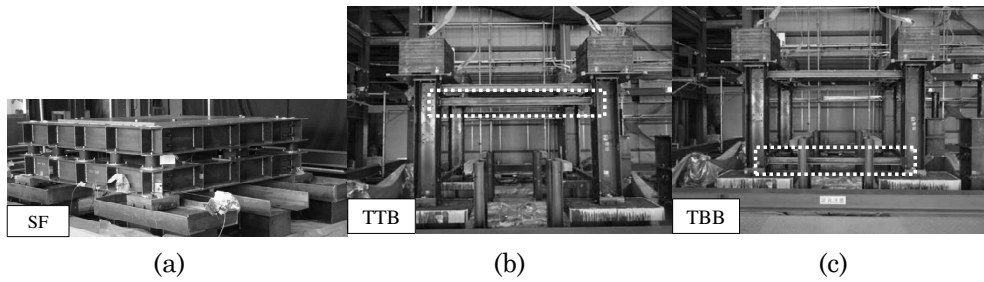


Figure 45– Pictures of (a) short specimen, (b) *TTB* specimen and (c) *TBB* specimen

mens”, named *SF-3*, *SF-2* and *SF-1*, respectively. Additionally, a “short rigid specimen”, named *SRig*, was prepared. In the rigid specimen, the upper frame and lower frame were rigidly connected each other by stiff I-shaped fixers. This treatment enabled that the upper and lower frames moved together as a single mass with natural frequency of 17.7 Hz (i.e. a fundamental period of 0.057 s).

The second type of specimen, referred to as the “tall specimen”, was designed to consider the effect of overturning moment on the response of the separated system. The tall specimens were a one-storey high, one-bay steel frame, as shown in Figure 44(c), (d) and (e). The superstructure consisted of four I-shaped relatively rigid columns, connected by flexible I-shaped beams. Since the major target of this study was low rise buildings, the target natural frequency was set at around 3.0 Hz. Two types of geometric configuration, with emphasis on the location of the lower beams, were considered for the tall specimens. The first type of specimen, named Top–Top Beam (*TTB*), aimed at the application of the separation at the base of the columns, so that the columns could dislocate individually. However, this may result in relative displacement among the respective columns. To look into such behaviour, the specimen named Top–Bottom Beam (*TBB*) was also constructed. In the *TBB* specimen the lower parts of the four columns were joined by beams (Figure 44(e)), and the four columns always moved together. The mass ratios α of the *TTB* and *TBB* specimens were 0.91 and 0.89, respectively. The aspect ratio of the frame, i.e. the ratio of the height over the

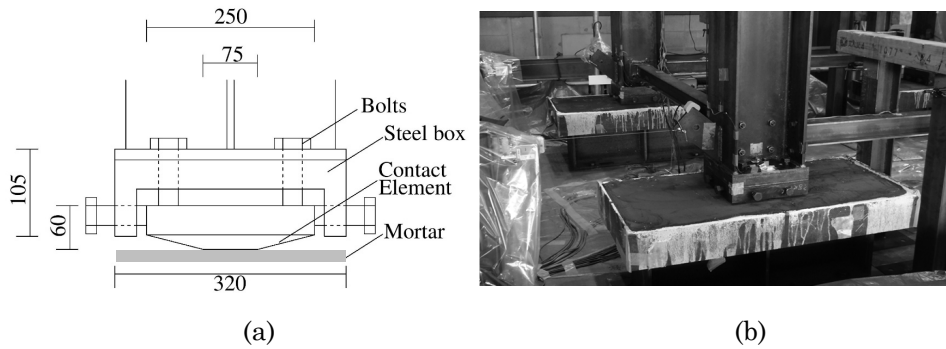


Figure 46 – Sliding base: (a) slider installation at column base (units in mm);
(b) graphite lubricated foundations

span length, was designed to prevent uplifts. The natural frequencies equalled 3.2 Hz and 3.3 Hz for the *TTB* and *TBB* specimen, respectively (meaning a fundamental period of 0.312 and 0.303 s, respectively). Pictures of both specimens are showed in Figure 45

In all the test specimens, the steel contact elements encased in steel boxes were firmly attached underneath each column (Figure 46(a)). The bottom surface of the contact element was polished and in order to achieve the target friction coefficient of about 0.20 the contact surface was lubricated with graphite powder (Figure 46(b)).

2.2.2. Evaluation of friction coefficient with graphite lubrication

The most fundamental parameter that governs the sliding response is the friction coefficient of the sliding surface. For each test specimen, which was regarded as a 2DOF system with upper and lower masses, the friction coefficient μ was estimated as

$$\mu_f = \frac{m_t a_t + m_b a_b}{(m_t + m_b)g} \quad (126)$$

where m_t , m_b , a_t and a_b are the masses and acceleration responses of the superstructure and lower structure, respectively.

Two friction coefficients, the static friction coefficient μ_s and dynamic friction coefficient μ_d , were estimated. The static friction coefficient μ_s was determined for the state when the superstructure does not slide (stick state) and the sliding velocity is close to zero. For the state

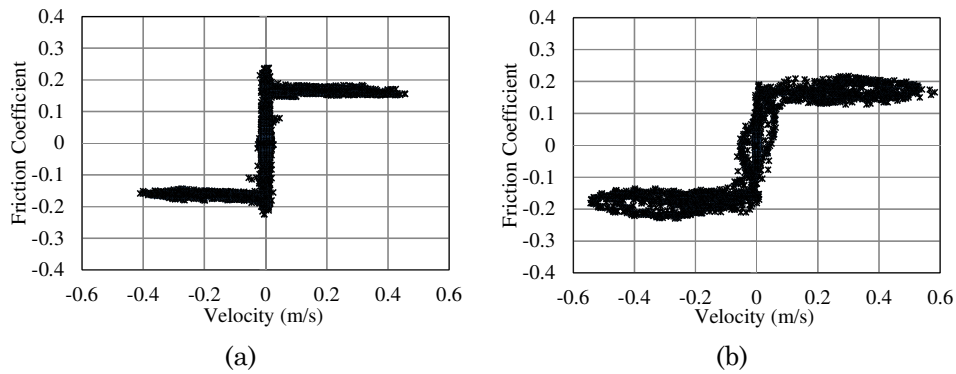


Figure 47 – Friction coefficient vs. sliding velocity relationship: (a) *SF-3* under sinusoidal loading 1.0 Hz 2 m/s²; (b) *TBB* under sinusoidal wave 1.5 Hz 4.0 m/s²

when the structure starts to slide (sliding state) and the velocity is non-zero, the dynamic friction coefficient μ_d was evaluated. Figure 47 shows an example of the relationships between the friction coefficient thus estimated and the sliding velocity (a) for the *SF-3* specimen (short specimen) subjected to the sinusoidal wave of 1.0 Hz and 2.0 m/s², and (b) for the *TBB* specimen (tall specimen) subjected to the sinusoidal wave of 1.5 Hz and 4.0 m/s². Both the short and tall specimens show a similar trend in the friction coefficient–velocity relationship. Once the sliding occurs, the friction coefficient decreases to the dynamic friction coefficient. This transition is clearer in the short specimen (Figure 47 (a)). In the tall specimen (Figure 47 (b)) this trend is less evident because of a larger variation of the dynamic friction coefficient. This variation is due primarily to a phase difference in the acceleration record of the distributed masses. As Equation 126, used to estimate the dynamic friction coefficient, assumes a concentrated mass for the upper structure, the phase difference arising from the actual distributed masses in the superstructure leads to somewhat larger variation. In summary, the static friction coefficient μ_s reached a value around 0.20 in both specimens, and the dynamic friction coefficients μ_d seemed weakly dependent on the velocity. The mean value and the coefficient of variation (COV) of μ_d are 0.16 and 0.05 for the *SF-3* specimen (Figure 47 (a)), and 0.17 and 0.13 for the *TBB* specimen (Figure 47 (b)), respectively.

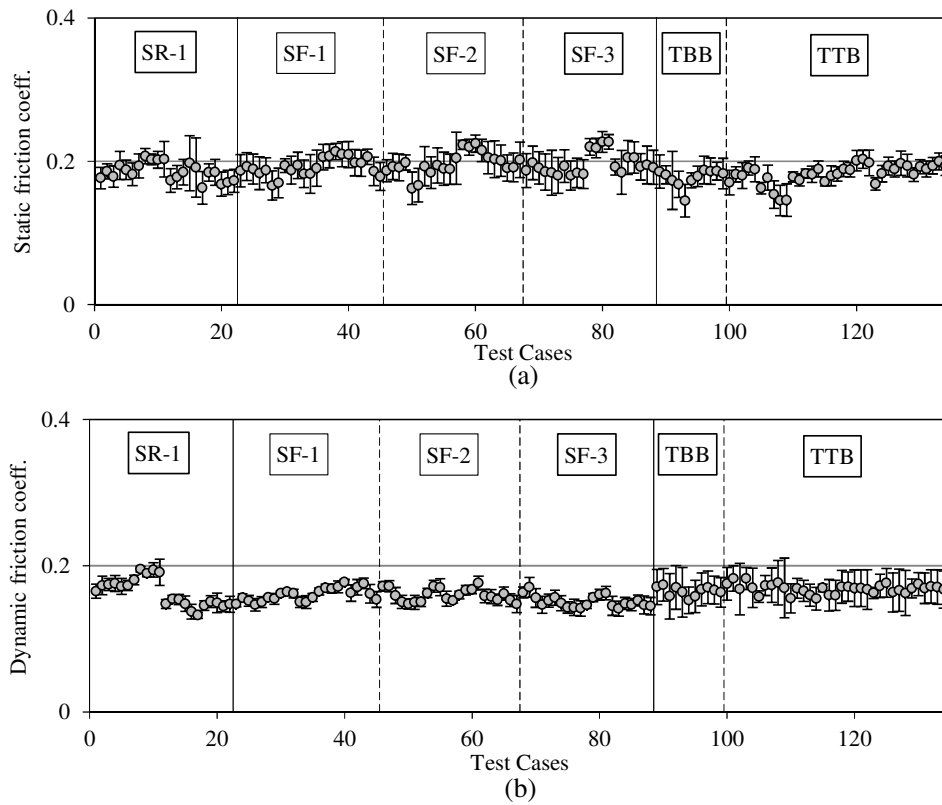


Figure 48 – Evaluation on dispersion of static and dynamic friction coefficients:
 (a) static friction coefficient; (b) dynamic friction coefficient

To investigate the stability of friction coefficient and the durability of graphite lubrication, the absolute values of mean and dispersion of static and dynamic friction coefficients were examined for all 134 loading cases. Figure 48 shows the results, with the loading case for the abscissa and the absolute value of the mean (circle) and standard deviation (bar) for the ordinate. The first 88 loading cases correspond to the tests of the short specimens, and the subsequent 46 loading cases correspond to the tests of the tall specimens. The main properties of the superstructure, such as the fundamental period, mass ratio and geometrical configuration, did not significantly influence the values of the friction coefficient. The results indicate that the graphite lubrication was very stable in both the stick (static friction coefficient) and sliding state

(dynamic friction coefficient), and its properties remained nearly the same for repeated loadings. Indeed, even after 1068 loading cycles imposed on the short specimens and 546 loading cycles on the tall specimens, the graphite powder remained effective. For the short and tall specimens, the static friction coefficients μ_s were close and on average equal to 0.19 and 0.18, respectively. The maximum COV of μ_s was 0.21 among the short specimens and 0.22 among the tall specimens. Moreover, the dynamic friction coefficients of the short and tall specimens were on average equal to 0.16 and 0.17, respectively. The maximum COV of μ_d was 0.11 among the short specimens and 0.24 among the tall specimens. Thus, the influence of overturning moment in the tall specimens did not affect the static and dynamic friction coefficients. The conditions of the mortar surface did not affect the friction characteristics either. While the surface of the mortar foundations used for the tall specimens had nearly no imperfections, the surface of the mortar bases used for the short specimens presented some indents of depth around 1.0–2.0 mm. However, the graphite powder filled the indents, forming a smooth sliding surface.

2.2.3. Dynamic characteristics of tall specimens

Figure 49(a) presents the experimental time history responses in terms of base shear coefficient of the *TTB* and *TBB* specimens subjected to the sinusoidal wave with a magnitude of 8.0 m/s^2 and frequency of 1.5 Hz. The numerical analysis results were included as well. Two main frequency components can be observed: the main frequency, which is represented by the larger wave oscillating around the origin, is the natural frequency of the superstructure; the smaller frequency, which is represented by the smaller oscillations of base shear coefficient, is the sliding frequency evaluated by Equation 125. This tendency is found to be consistent both with the theoretical studies and the dynamic response of the short specimen in the first test.

To investigate a possible influence on the sliding response of the lower beams, the time histories of the base shear coefficients of the *TTB* and *TBB* specimens were compared each other. The difference between the maximum base shear of the two specimens was 9%, which means

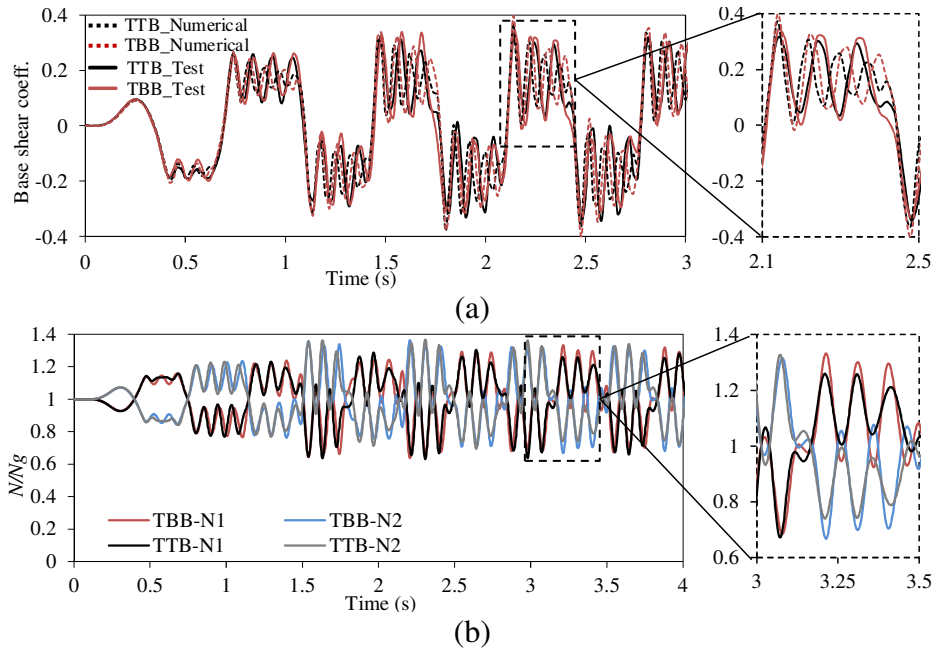


Figure 49 – Experimental and numerical time histories responses of TTB and TBB specimens undergoing sinusoidal loading with magnitude of 8.0 m/s^2 and frequency of 1.5 Hz : (a) base shear coefficient time histories; (b) of axial force of the front columns

that despite the lack of the lower tie (the bottom beams), the overall behaviour was not significantly affected. The difference in the maximum displacement amplitude was also small, with a discrepancy not greater than 3%. The agreement between the results of the experimental and numerical analyses was also notable.

Figure 49(b) shows the experimental time history of the axial force N in columns belonging to the same plane, normalised by the gravity load N_g . Because of the overturning moment, the ratio N/N_g oscillates around the value of unity. The observed maximum variation of the axial force was 35% relative to the axial force exerted by gravity. However, since the axial force never decreased to zero, the columns were always in touch with the foundation, and no uplift occurred.

2.2.4. Dynamic response of the base shear capping building under earthquake and maximum base shear coefficient

The sliding response against earthquake ground motions was investigated. Figure 50(a) and (b) show the time history of the base shear coefficients derived from the experimental results and the numerical analysis for the specimen *SF-1* with mass ratio 0.5 and the *TTB* specimen, respectively, subjected to the N–S component of the JMA Kobe earthquake (PGA = 8.26 m/s², PGD = 117.4 mm). The base shear coefficient of *SF-1* and *TTB* specimens reached a maximum value of 0.68 and 0.31 respectively. According to the numerical analysis, if the *SF-1* and the *TTB* specimens were fixed at the column base and responded elastically, the maximum base shear coefficients would be 2.38 and 0.91, respectively. This indicates that the application of graphite lubrication allowed the reduction of the maximum base shear coefficient by 71% for the *SF-1* specimen and by 66% for the *TTB* specimen.

An extensive parametric study on the value of the maximum base shear coefficient has been conducted for all the test specimens. To this end, incremental dynamic analyses were run considering various natural accelerograms and sinusoidal input motions. Figure 51 shows the results in terms of the maximum base shear coefficient versus peak ground acceleration for the short and tall specimens subjected to the Kobe N–S earthquake motion (Figure 51(a)) and the sinusoidal input

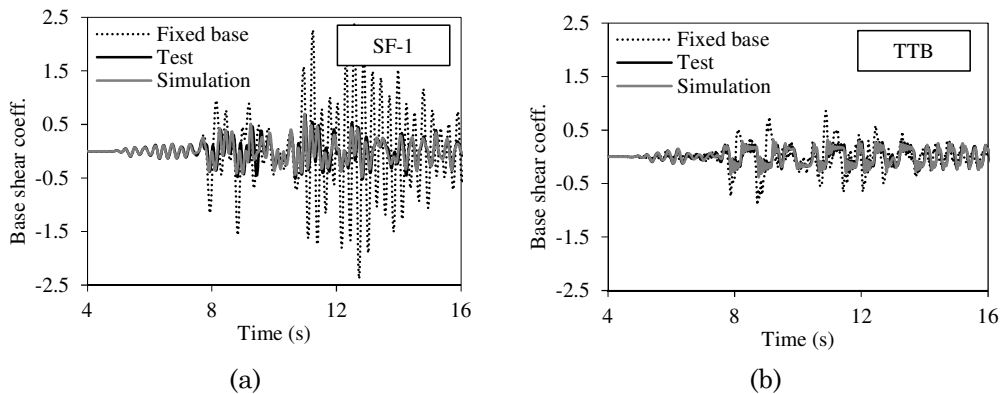


Figure 50 – Base shear coefficient time history under Kobe NS: (a) *SF-1* specimen; (b) *TTB* specimen

motion at the frequency of 0.50 Hz (Figure 51(b)). In both the tests and the numerical analyses, the increase of input magnitude led to higher values of the base shear coefficient, but the rate of increase progressively lessened for larger magnitudes. Unlike in the fixed-base elastic structures, in the separated system severe loading levels did not lead to indefinite increase in the base shear coefficient. Rather, the experimental results and the numerical analyses confirmed that the base shear of the separated system has an asymptotic tendency towards an upper limit. For comparison, if an ideal rigid mass slides on a surface with a specific friction coefficient, the maximum base shear coefficient would be equal to the dynamic friction coefficient, regardless of the amplitude of the input motion. Unlike the rigid mass, the inertia forces developed in the flexible superstructures are actually larger than the sliding friction forces between the sliders and the mortar surfaces because of the internal dynamic amplifications during the sliding. This leads to a maximum base shear coefficient larger than the static friction coefficient. According to Figure 51, when PGA exceeds 2.0 to 3.0 m/s^2 , the rate of increase in the maximum base shear coefficient becomes minimal, particularly for larger mass ratios. This asymptotic nature in the maximum base shear is also evident in the associate numerical simulation. However, comparison of the various specimens shows that the uppermost base shear coefficients are strongly dependent on the mass ratio α . In particular, higher values of α led to lower maximum

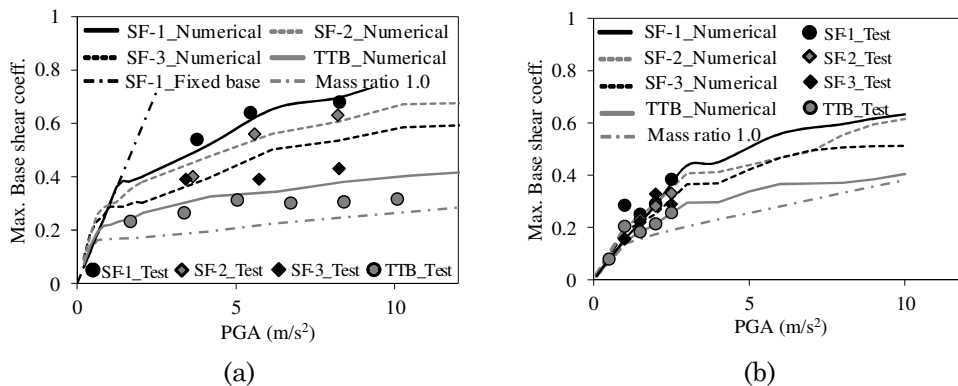


Figure 51 – Relationship between the maximum base shear coefficient and PGA for all specimens subjected to: (a) KobeNS; (b) sinusoidal loading of frequency 0.50 Hz

base shear coefficients. For instance, the maximum base shear coefficients recorded in the test were 0.68 for $\alpha = 0.50$, 0.63 for $\alpha = 0.68$, 0.40 for $\alpha = 0.80$ and 0.31 for $\alpha = 0.90$ for the Kobe NS ground motion (Figure 51(a)). Similar values of maximum base shear coefficients were obtained from the numerical analyses run for the sinusoidal input at 0.50 Hz frequency (Figure 51(b)). Previous parametrical studies available in the literature [e.g. 79] also indicated that the acceleration response is a function of the mass ratio and decreases for larger values of α . The influence of the mass ratio can be interpreted in relation to Equation 125, during the sliding phase, the system responds with damping ratio ξ_1 , which is higher than the originally assigned damping ratio ξ . As the higher damping ratio ξ_1 is a function of the mass ratio α , an increase in α increases the damping ratio ξ_1 , which becomes in turn a source to reduce the maximum acceleration response.

As the *TTB* specimen is the closest to real structures with regard to the geometrical configuration and mass ratio, the response of this frame is discussed in further detail. Figure 52 shows the maximum base shear coefficient of the *TTB* specimen subjected to increasing earthquake motions (Figure 52(a)) and sinusoidal inputs (Figure 52(b)). Both the numerical and experimental results are presented and they are in good agreement. For all the inputs applied, larger peak ground accelerations led the maximum base shear coefficient towards an up-

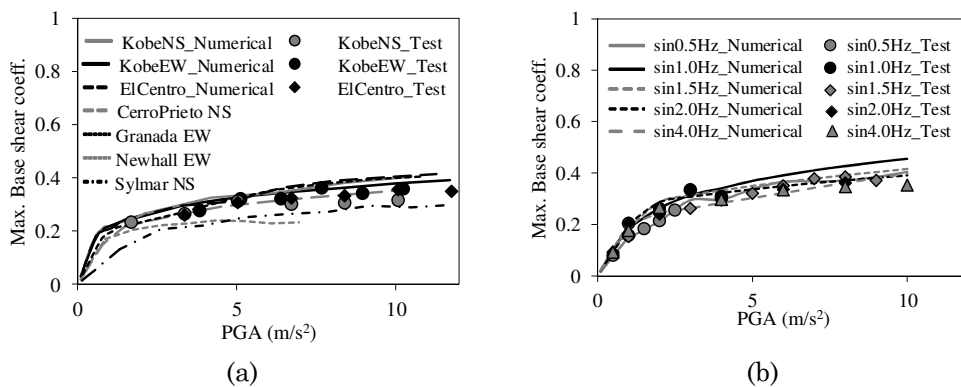


Figure 52 – Relationship between maximum base shear coefficient and input magnitude for *TTB* specimen subjected to: (a) earthquakes input; (b) sinusoidal loadings

permost value, which conformed to the aforementioned asymptotic tendency. Although various ground motions with different frequency contents and peak ground accelerations were applied, this upper limit kept values of around 0.40 and did not show an obvious dependency on the input features, as displayed in Figure 52(a). Similar results can be observed also for the sinusoidal inputs, as shown in Figure 52(b). Based on these results, in case of large mass ratios, such as in real buildings, the input characteristics do not have a major influence on the evaluation of the maximum base shear coefficient.

3. Seismic assessment and upgrading of an existing RC frame

An illustrative application of the base shear capping system has been conducted to upgrade the 3-storey RC infilled building designed (Chapter 3) for gravity loads only, with the deck orientated along the y-axis. Before the seismic upgrading, the columns of the building are fixed at the base. To apply the base shear capping system, the column bases have to be disconnected from the ground, to let them free to slide. Furthermore, a concrete slab is made at the ground level of the building to connect the column bases above the sliding surface.

Preliminarily, it should be evaluated if the upgrading of the existing building by the base shear capping system has a positive effect, and eventually this effect should be quantified. In particular, the seismic assessment of the existing (fixed base) building is required firstly to estimate the capacity of the building before the seismic upgrading. Secondly, it should be evaluated how much the seismic upgrading can improve the seismic performance of the structure, thus reducing the seismic risk. Based on this considerations, the methodology described in the following sections evaluates the ground acceleration (PGA capacities) corresponding to the attainment of the maximum resistance of (i) the fixed base building and (ii) the retrofitted building. If the PGA capacity of the base shear capping building is larger than that of the fixed base building, it means that the retrofitting system has improved the seismic response of the considered building. The increase of the PGA capacity quantifies the effect achieved by the seismic upgrading. To this

end, the developed D-DAP is here proposed as a useful and practical tool that can easily fulfil those goals. Indeed, both the two PGA capacities can be evaluated running the D-DAP on the numerical models that simulate the building before and after the application of the seismic upgrading.

3.1. Assessment of the existing RC building

Thanks to the in-plan symmetry of the structure with respect to the x -axis, the response of the entire building subjected to the seismic action along the x -axis could be obtained considering a two dimensional model of one half of the building. This plane model connects in series one of the two outermost frames of the building (GL32-I028), i.e. the infilled frame, and one of the inner frames (GL31). This is the so called “train-of-frame” model, showed in Figure 53, whereby all nodes of each frame belonging to the same storey are constrained to have the same horizontal displacement. The numerical model of the train-of-frame has been built in OpenSees to run the D-DAP analyses. All the modelling assumptions adopted for structural and nonstructural elements are equal to those already described in Section 4.2. In the numerical model of the building before the application of the base shear capping system all the three degrees of freedom (displacements and rotation) of the base col-

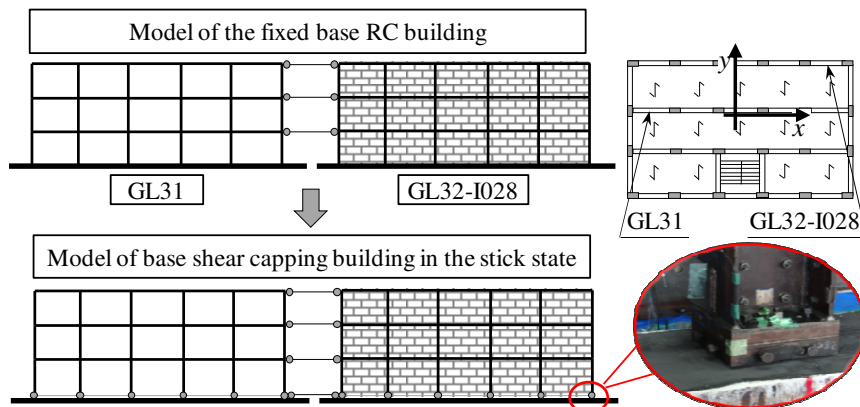


Figure 53 – Train of frames GL31 – GL32-I028, from the fix base configuration to the introduction of the sliding at column base

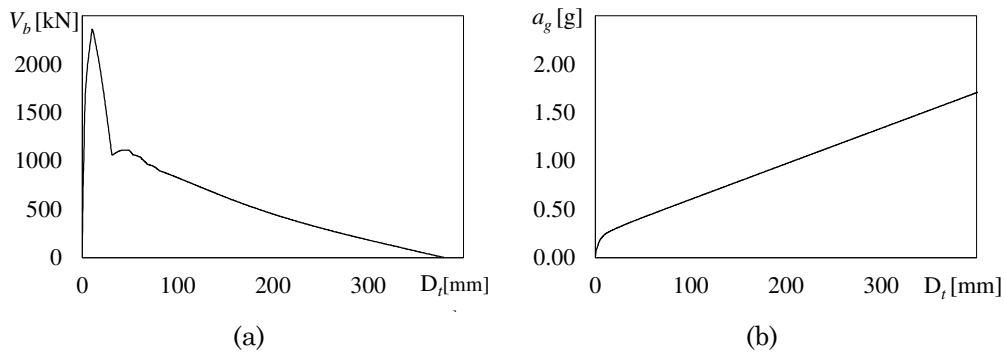


Figure 54 – Performance curve of the building designed for gravity loads only in the fixed base configuration, in terms of (a) V_b - D_t and (b) a_g - D_t

umns are restrained. Instead, when the disconnection is introduced, but the structure is still in the stick state, the column bases can be constrained by pins. Figure 53 shows the fixed base model (Figure 53(a)), and the seismic upgraded model in the stick state with pinned column bases (Figure 53(b)).

The calibrated D-DAP analysis is run to evaluate the maximum resistance of the existing building. For this purpose, the train-of-frames model with fixed base columns is analysed. The seismic response of the existing RC building thus evaluated is plotted in Figure 54. The base shear-top displacement curve is reported in Figure 54(a) and it is obtained by the D-DAP enveloping three modes of vibration, with a displacement step size equal to 0.1 mm. The maximum base shear is equal to 2360.4 kN and it corresponds to the crushing of infills. This value is assumed as the maximum resistance of the building, and its attainment is identified with the collapse of the building. Indeed, because of the brittle behaviour of infills, the attainment of the maximum shear resistance is followed by an abrupt reduction of the base shear. In order to evaluate the PGA capacity of the analysed building, Figure 54(b) plots the ground acceleration associated by the D-DAP at each top displacement demand, taking into account the dissipation of energy of the structure by means of the proposed damping law (Equation 120). The maximum resistance is attained for a ground acceleration equal to 0.243 g, which represents the PGA capacity of the base fixed building.

3.2. Effect of the seismic upgrading of RC building by the base shear capping system

The study of the design of the base shear capping system as retrofitting technique of RC infilled buildings is being developed in a separated research line by the student Roberto Barone for his master degree thesis, under the supervision of Prof. Marino. Being this topic beyond the scope of the present thesis, only the details necessary for the explicative application are here reported. Further information may be found in the master thesis by Barone [83].

Results obtained from former numerical analysis and experimental tests on the base shear capping system demonstrated that the maximum base shear $V_{b,max}$ attained by this system is not equal to the friction force at the column base, but it reaches larger values:

$$V_{b,max} = v \times F_{\mu} \quad (127)$$

This amplification v is due to the fact that the lower mass of the separated structure experiences the friction force as pulse like force. Depending on the instant when this force acts on the base mass during the sliding state, it can significantly increase the base shear transmitted to the superstructure. Although the maximum friction force can be easily calculated by multiplying the friction coefficient of the sliding surface by the total weight W of the structure ($F_{\mu} = \mu_f W g$), however the amplification of the friction force is not known a priori.

The prediction of the maximum base shear is fundamental to decide whether or not the base shear capping system is applicable to the considered structure. To overcome this limit, the current research on the base shear capping building and former analysis conducted by Prof. Marino focused on the evaluation of the amplification of the friction force. In particular, an extensive parametric analysis has been conducted by Barone [83] on simplified numerical models representative of RC frames with various geometrical and dynamic characteristics, endowed with infills with different stiffness and strength. This study led to the calibration of the following equation for the evaluation of the amplification factor v of the friction force:

$$v = \left(\frac{a_g}{a_{g,s}} \right)^{0.6-0.4\alpha} \quad (128)$$

where a_g is the value of the peak ground acceleration corresponding to the limit state to be verified, $a_{g,s}$ is the ground acceleration corresponding to the first sliding, α is the mass ratio. The value of $a_{g,s}$ is evaluated by equating the base shear determined by a modal response spectrum analysis to the friction force, and is equal to 0.0914 g for the analysed building. The value of the friction coefficient μ_f is assumed equal to 0.16, according to the results of the experimental tests. The total mass of the building is calculated by summing the floor mass (198.7 t) of the three storeys of the superstructure, plus the mass of the deck arranged at the base of the separated system. The total weight is 7797.0 kN and the friction force F_μ at the base is 1247.1 kN. Since the floor masses, included the one at the foundation level, are the same, α is equal to 0.75.

In order to evaluate the maximum resistance of the base shear capping building, the D-DAP analysis is run on the train-of-frame model with the pinned column bases. The performance curve of the base shear capping building thus evaluated is plotted in Figure 55, in terms of base shear and top displacement. The maximum resistance of the retrofitted building is equal to 2025.2 kN. In order to estimate the ground acceleration corresponding to the maximum resistance of the

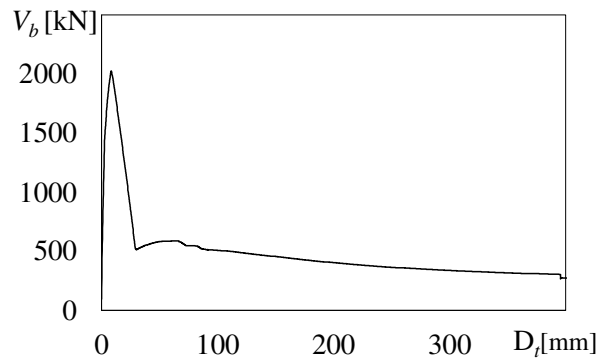


Figure 55 – Performance curve (V_b - D_t) of the building with pinned base column

base shear capping building, Equation 128 is placed in Equation 127, and this latter is equated to the maximum base shear obtained by the D-DAP (2025.2 kN). Given the values of $V_{b,max}$ and F_{μ} , the maximum amplification ν of the friction force that the base shear capping building could reach is 1.62. Given $a_{g,s}$ and α , the peak ground acceleration leading to the maximum amplification, and thus to the maximum resistance, of the base shear capping building is 0.46 g. In conclusion, the D-DAP takes into account that the introduction of the base shear capping system in the considered RC frame delays the attainment of the maximum resistance of the structure, and quantifies the reduction of the seismic risk predicting the new (increased) value of the maximum sustainable peak ground acceleration.

Conclusions and future developments

It is well recognised that nonlinear dynamic analysis is the most accurate tool to predict the seismic behaviour of structures. However, despite the technological progress and the potentialities of new computer programs, it is not an approach that can be extensively applied for professional purposes yet. To overcome this limitation, nonlinear static methods of analysis have been developed as simpler alternative tool for the evaluation of seismic response of structures, and they are still object of interest in the scientific community. The main purpose of the present thesis is to provide a further contribution in this field of research by the development of a novel nonlinear static method of analysis, named D-DAP. This method is properly calibrated for the assessment of RC frames, which represent an important part of the building stock in Italy and other European countries. However, differently from other nonlinear static methods proposed in literature or seismic codes, the peculiarity of the proposed method is that it has been developed by taking into account specifically the contribution of infill panels to the structural response. The final goal of this research is to provide a method of analysis that can estimate with good accuracy the seismic response of RC frames, with and without infills, keeping reasonable computational costs, so that it could be a tool suitable for professional purposes.

The proposed D-DAP combines the adaptive and multimodal character of the DAP by Antoniou and Pinho [28], with the direct approach of the Advanced N1 method by Ghersi et al. and Lenza et al. [34,35], which allows the evaluation of the displacement demand of the MDOF

system without the approximation to the equivalent SDOF system. In addition to this, an over damped response spectrum is used to take into account the energy dissipation due to the cumulated damage in the structure, including not only the plastic deformations occurred in columns and beams but also in the infill panels. Indeed, a new damping law is properly calibrated for RC frames with and without infill panels.

Since the goal of the study is the assessment of existing RC framed buildings, a set of 54 RC frames has been designed to be representative of existing buildings that may need seismic upgrading. Half of those frames were designed for gravity loads only, while the other were designed according to old seismic prescriptions. The designed frames are five spans wide and have 3, 6 or 9 storeys. Infill panels with negligible, medium or large stiffness and strength were considered alternatively in each frame. The research can be divided in three main parts. In the first part, the parameters that control the operation of the D-DAP were calibrated. In the second part, the D-DAP is equipped with a new equivalent damping law specifically calibrated to predict the response of infilled RC frames. In the third part, the effectiveness of the D-DAP with the proposed damping law is assessed by comparison with other nonlinear static methods well-established in scientific literature. In the following, the main results achieved in each part of the research are separately summarised.

The parameters ruling the operations of the D-DAP, i.e. the number of modes to be enveloped in the loading vector and the size of the displacement step, were calibrated on the designed RC frames. To this end, two sensitivity analyses were conducted. In the first sensitivity analysis the seismic response of the case study frames has been determined by various D-DAPs, with an increasing number of enveloped modes. It was found that, for the considered frames, the contribution of the modes of vibration higher than the third one is negligible. The second sensitivity analysis allowed the evaluation of the size of the displacement incremental step. To this end, the response of the cases study has been evaluated by different D-DAPs, with decreasing values of the displacement increment at the generic step (step size). It was found that a displacement increment of 0.1 mm has to be assigned at

each step to obtain accurate results for all the considered frames at reasonable computational cost.

The second part of the numerical investigation was devoted to the formulation and calibration of the new damping law to be used by D-DAP. The proposed damping law is formally similar to those of other studies available in scientific literature. The total equivalent viscous damping ratio has been assumed as the summation of the inherent viscous damping in the elastic range ξ_0 , and the viscous damping ξ_{hyst} due to the hysteretic behaviour. Generally, the hysteretic damping ξ_{hyst} is function of the ductility demand μ , and for infinite value of ductility demand it tends towards an asymptotic value ξ_∞ . The numerical calibration led to the determination of the asymptotic damping ξ_∞ that is appropriate for the structural types under investigation. To this end, the response of the case study frames determined by nonlinear dynamic analysis has been assumed as benchmark, and the average drift Δ_m is assumed as the reference parameter of the numerical calibration. For every case study frame, the value of ξ_∞ is determined by an optimization process that minimizes the differences between the results provided by the D-DAP and those obtained by the IDA. For each frame, the process led to a different value of optimal ξ_∞ , and those values were related to the fundamental period T_1 of the structure. In case of very stiff structures, it was found that the values of ξ_∞ tend to increase with T_1 up to periods of 0.40 s. Indeed, this tendency is demonstrated by almost all the infilled case study frames. For fundamental periods larger than 0.40 s this trend is inverted, and the values of ξ_∞ tend to decrease for larger T_1 . This tendency is exhibited by all the analysed bare frames. Based on these results, the following function of ξ_∞ was proposed:

$$\xi_\infty = \min\left(65T_1; \frac{5.4}{T_1^{1.3}}\right)$$

According to this equation, for very stiff structures, the value of ξ_∞ is linearly dependent from T_1 . Instead, for more flexible structures, the relation between ξ_∞ and T_1 is hyperbolic. Finally, the proposed equivalent damping law is the following:

$$\xi_{eq} = \xi_0 + \min\left(65T_1, \frac{5.4}{T_1^{1.3}}\right) \left(1 - \frac{1}{\mu}\right)$$

According to this equation, the equivalent damping increases with the ductility demand μ . However, when the ductility demand becomes larger the rate of increase of ξ_{eq} becomes smaller, and the equivalent viscous damping tends towards the asymptotic value $\xi_0 + \xi_{\infty}(T_1)$. For fixed values of T_1 , larger values of μ lead to larger ξ_{eq} . When the ductility demand overcomes 7.5, further increase of μ leads to negligible increase of ξ_{eq} .

In particular, the proposed equivalent damping law has been developed based on the new equation of the parameter η (the reduction factor of the spectral displacement due to larger damping ratios), that has been developed within this study. Both the NTC08 [13] and the EC8-Part 1 [56], suggest to calculate η as function of the damping ratio ξ_{eq} , as expressed by Equation 94. However, from the study of the displacement average response spectrum of the ten adopted accelerograms, reduced by various damping ratios, it was found that equation suggested by codes significantly underestimates the value of η compared to that obtained by the ratio spectral displacements, and neglects the dependence of the parameter η from the fundamental period T . In particular, when Equation 94 leads to overestimated values of η , the contribution of the damping ratio to the evaluation of the seismic demand of the structure is underestimated. In summary, NTC08 and EC8 conservatively take into account the energy dissipation due to the progressive yielding of the structure. The new equation of the parameter η has been proposed to overcome this limit. In order to simplify the approach, two assumptions were considered: (1) for a given damping ratio the minimum value of η has to be evaluated, (2) and the dependence from the fundamental period T_l is not introduced into the equation of η because it is already accounted for through the new equivalent viscous damping ξ_{eq} law. Thus, the following equation is proposed for the evaluation of η :

$$\eta = \sqrt{\frac{5}{\xi_{eq}}}$$

The effectiveness of the proposed D-DAP with the proposed damping law was investigated by (i) assuming the response of the case study

frames provided by the Incremental Dynamic Analyses as target and (ii) comparing the accuracy of the D-DAP to that of the DAP by Pinho and the MPA by Chopra, the N2 method (EC8) and the CSM (FEMA 440). These comparisons were conducted for each frame in terms of global (V_b - D_b , a_g - D_t) and local response parameters (average storey Δ_m drift and storey drift Δ). Furthermore, in order to estimate the effectiveness of the proposed equation of the equivalent damping ratio, the accuracy of the D-DAP applied with the proposed equation was compared to that of the D-DAP applied with the damping laws proposed by Priestley for concrete elements, Freeman, and Gulkan and Sozen. This further comparison was conducted considering the average storey Δ_m drift and storey drift Δ .

As for the seismic response in terms of V_b - D_b , the D-DAP with the proposed damping law predicted the maximum value of base shear with an error on average equal to 20% for bare frames, and 15% for infilled frames. The seismic response in terms of a_g - D_t was predicted more accurately by the proposed D-DAP, whilst the MPA and the DAP generally overestimated and underestimated the displacement demand, respectively. The CSM generally overestimated the displacement demand of bare frames and underestimated that of infilled frames. On the contrary, the N2 method tended to underestimate the displacement demand of bare frames and underestimate that of infilled frames.

With regards to the local response, the distribution of storey drifts along the height has been evaluated for three limit states, corresponding to the attainment of 1%, 2% and 4% storey drift in the IDA. For lower values of storey drifts, the prediction provided by all the nonlinear static methods of analysis was comparable. On the contrary, for larger storey drifts the displacements were overestimated by the DAP and the CSM, while the MPA and the N2 method generally led to underestimated displacements. The lowest error was committed by the proposed D-DAP. In particular, the average drift along the height corresponding to the 4% limit state was generally better predicted in bare frames by the advanced nonlinear static methods, i.e. D-DAP, DAP and MPA. However, the proposed D-DAP predicted the average drift at 4% limit state of infilled frames with an error lower than 20%, whilst the

other methods of analysis led to significantly larger errors. Looking at the average error over the three limit states committed by the nonlinear static methods of analysis in predicting the average drift, it was found that the D-DAP with the proposed damping law led to the lowest error (lower than 20%) in the largest number of considered frames. In particular, the average error committed by the D-DAP with the proposed damping law was lower than 20% for more than 80% of bare frames, for more than the 80% of frames with weak infills and for more than 50% of frames with strong infills.

Based on the presented results, the D-DAP applied with the proposed damping law showed a level of accuracy in predicting the seismic response of RC frames, with and without infills, generally higher than the other nonlinear static methods of analysis. The advantage achieved over the other existing methods is remarkable especially in the prediction of the response of RC frames with infill panels.

Following the conclusions reached in the present work, some steps ahead still can be done, to extend the results beyond the adopted assumptions. For the sake of simplicity, in this work infill panels have been considered uniformly distributed inside the frame, and only the variability related to the mechanic characteristics of infills has been considered. However, in real structures the distribution of infill panels may be quite irregular, because of the presence of windows or doors, or because of the lack of entire infill panels (such as in case of shop windows). This feature may lead to a different nonlinear response of the structure, and in turn to a different capability of dissipating energy. Based on this, the methodology adopted to develop the presented damping law could be extended also to account for the irregular distribution of infills and, in case it is needed, to update the proposed damping law. Furthermore, it would be worth evaluating the efficiency of the D-DAP in predicting the seismic response of such structures, which are more irregular along the height.

Another fundamental assumption at the base of the D-DAP has been that the considered buildings are regular in plan. This means that they do not rotate under seismic forces, and their seismic response can be simulated by plane frames. However, real structures may present

some irregularities in plan and could develop significant torsional response, which cannot be investigated by plane frames. The scientific research dedicated much effort to propose variants of the existing nonlinear static methods properly for the seismic assessment of tridimensional buildings that are irregular in plan. However, the tridimensional nonlinear static methods currently proposed generally are not adaptive. Based on this consideration, it could be worth investigating the possibility of extending the D-DAP to predict the seismic response of tridimensional structures. It could widen the range of application of the D-DAP and provide an advanced tool for the seismic assessment of real buildings.

References

- [1] CEN. Eurocode 8: Design of structures for earthquake resistance - Part 3: Assessment and retrofitting of buildings, EN 1998-3. European Committee for Standardization: Bruxelles, Belgium, 2005.
- [2] Christovasilis P, Cimellaro GP, Barani S, Foti S, 2014. On the selection and scaling of ground motions for fragility analysis of structures, proceedings of *Second European Conference of Earthquake Engineering and Seismology*, 2014.
- [3] Naeim F, Alimoradi A, Pezeshk S, 2004. Selection and scaling of ground motion time histories for structural design using genetic algorithms, *Earthquake Spectra*, **20**: 413-426.
- [4] Grigoriu, M, 2011. To Scale or Not to Scale Seismic Ground-Acceleration Records, *Journal of Engineering Mechanics*, ASCE, **137**: 284-293.
- [5] Jayaram N, Lin T, Baker JW, 2011. A computationally efficient ground-motion selection algorithm for matching a target response spectrum mean and variance, *Earthquake Spectra*, **27**:797-815.
- [6] Vamvatsikos D, Cornell A, 2002. Incremental dynamic analysis, *Earthquake Engineering and Structural Dynamics*, **31**: 491-514.
- [7] FEMA 356. Prestandard and Commentary for the Seismic Rehabilitation of Buildings. Federal Emergency Management Agency: Washington, D.C., U.S.A., 2000.

- [8] FEMA 368. NEHRP Recommended Provisions for Seismic Regulations for New Buildings and Other Structures, Part 1: Provisions. Federal Emergency Management Agency: Washington, D.C., U.S.A., 2001.
- [9] FEMA 369. NEHRP Recommended Provisions for Seismic Regulations for New Buildings and Other Structures, Part 2: Commentary. Federal Emergency Management Agency: Washington, D.C., U.S.A., 2001.
- [10] FEMA 450. NEHRP Recommended Provisions for Seismic Regulations for New Buildings and Other Structures. Federal Emergency Management Agency: Washington, D.C., U.S.A., 2003.
- [11] FEMA 440. NEHRP Improvement of nonlinear static seismic analysis procedure. Federal Emergency Management Agency: Washington, D.C., U.S.A., 2005.
- [12] ATC (1996). "Seismic Evaluation and Retrofit of Concrete Buildings (Report SSC 96-01 of California Seismic Safety Commission)", Report ATC-40, Applied Technology Council, Redwood City, California, U.S.A.
- [13] D.M. 14/01/2008. Norme Tecniche per le costruzioni (Provisions for constructions). Rome, 2008. (in Italian)
- [14] Freeman SA, Nicoletti JP, Tyrell JV, 1975. Evaluations of existing buildings for seismic risk – A case study of Puget Sound Naval Shipyard, Bremerton, Washington, in proceedings of *1st U.S. National Conf. on Earthquake Engineering*, Earthquake Engineering Research Institute, Berkeley, 113-122.
- [15] Freeman S.A., 1998. The capacity spectrum method as a tool for seismic design, *11th European Conf. on Earthquake Engineering*, Paris, France.
- [16] Fajfar P, Gaspersic P, 1996. The N2 method for the seismic damage analysis of RC buildings, *Earthquake Engineering and Structural Dynamics*, **25**: 31-46.

- [17] Fajfar P., 1999. Capacity spectrum method based on inelastic demand spectra, *Earthquake Engineering and Structural Dynamics*, **28**: 979-993.
- [18] Paret TF, Sasaki KK, Eilbeck DH, Freeman SA, 1996. Approximate inelastic procedures to identify failure mechanism from higher mode effects, proceedings of *11th WCEE*, Acapulco, Mexico.
- [19] Sasaki KK, Freeman SA, Paret TF, 1998. Multi-mode pushover procedure (MMP) – A method to identify the effects of higher modes in a pushover analysis. 6th U.S. *National Conf. on Earthquake Engineering*, Seattle, USA.
- [20] Moghadam AS, Tso WK, 2002. A pushover procedure for tall buildings, proceedings of *12th European Conference of Earthquake Engineering*, London, UK.
- [21] Chopra AK, Goel RK, 2002. A Modal Pushover Analysis Procedure for Estimating Seismic Demands of Buildings, *Earthquake Engineering and Structural Dynamics*, **31**: 561-582
- [22] Sucuoglu H, Gunay MS, 2010. Generalized force vectors for multi-mode pushover analysis, *Earthquake Engineering and Structural Dynamics*, **40**: 55-74.
- [23] Bracci JM, Kunnath SK, Reinhorn AM, 1997. Seismic performance and retrofit evaluation of reinforced concrete structures, *Journal of structural engineering*, **123**: 3-10.
- [24] Gupta B, Kunnath SK, 2000. Adaptive spectra-based pushover procedure for seismic evaluation of structures, *Earthquake Spectra*, **16**: 367-391
- [25] Requena M, Ayala G, 2000. Evaluation of a simplified method for the determination of the nonlinear seismic response of RC frames, proceedings of *12th WCEE*, Auckland, New Zealand.
- [26] Shakeri K, Shayanfar M, Kabeyasawa T, 2010. A story shear-based adaptive pushover procedure for estimating seismic demands of buildings, *Engineering Structures*, **32**:174-183

- [27] Antoniou S, Pinho R, 2004. Advantages and limitations of adaptive and non-adaptive force-based pushover procedures, *Journal of Earthquake Engineering*, **8**: 497-522
- [28] Antoniou S, Pinho R, 2004. Development and verification of a displacement – based adaptive pushover procedures, *Journal of Earthquake Engineering*, **8**: 643 – 661
- [29] Bosco M., Gherzi A., Marino E.M., 2009. On the evaluation of seismic response of structures by nonlinear static methods, *Earthquake Engineering and Structural Dynamics*, **38** , pp. 1465-1482.
- [30] Ferraioli M, Lavino A, Avossa AM and Mandara A, 2008. Displacement-based seismic assessment of steel moment resisting framestructures, in proceedings of the *14th World Conference on Earthquake Engineering*, Beijing, China.
- [31] Ferraioli M, Lavino A, Mandara A, 2015. An adaptive capacity spectrum method for estimation seismic response of steel moment resisting frames, *International Journal of Earthquake Engineering*, Anno XXXIII, Speciale CTA 2015, Num. 1-2.
- [32] Pinho R, Casarotti C, 2007. An adaptive capacity spectrum method for assessment of bridges subjected to earthquake action, *Bulletin of Earthquake Engineering*, **5**: 377-390
- [33] Pinho R, Monteiro R, Casarotti C, 2008. Using the adaptive capacity spectrum method for seismic assessment of irregular frames, In proceedings of the *5th European workshop on the seismic behaviour of irregular and complex structures*, Catania, Italy
- [34] Gherzi A., Lenza P., Pellecchia M., 2013. Uno sviluppo Multimodale ed adattivo del metodo N1 per la verifica ed il progetto delle strutture intelaiate in c.a. *15th ANIDIS Conference*, Padova, Italy.
- [35] Lenza P, Gherzi A, Marino EM, Pellecchia M, 2017. A multimodal adaptive evolution of the N1 method for assessment and design of RC framed structures, *Earthquake and Structures*, **12**.

- [36] Bhatt C, Bento R, 2014. A 3D Pushover methodology for seismic assessment of plan irregular buildings, *Earthquake Spectra*, **2**:683-703
- [37] Bhatt C, Bento R, 2011. Assessing the seismic response of existing RC buildings using the extended N2 Method, *Bulletin of Earthquake Engineering*, **9**:1183-1201
- [38] Fajfar P, Marusic D, Perus I, 2005. Torsional effects in the pushover-based seismic analysis of buildings. *Journal of Earthquake Engineering*, **9**:831–854
- [39] Bosco M, Ghersi A, Marino EM, 2012. Corrective eccentricities for assessment by the nonlinear static method of 3D structures subjected to bidirectional ground motions, *Earthquake Engineering and Structural Dynamics*, **41**:1751–1773
- [40] Marino EM., Muratore M, Rossi PP, 2003. Pushover analysis in the evaluation of the seismic response of steel frames, in proceedings of *StESSA Conference*, Napoli, Italia
- [41] Yang P, Wang Y, 2000. A study on improvement of pushover analysis, in proceedings of *12th World Conference on Earthquake Engineering*, Auckland, New Zealand.
- [42] Vidic T, Fajfar P, Fishinger M, 1994. Consistent inelastic design spectra: strength and displacement”, *Earthquake Engineering and Structural Dynamics*, **23**: 502-521.
- [43] Freeman SA, 2004. Review of the development of the capacity spectrum method, *ISET Journal of Earthquake Technology*, **41**: 1-13.
- [44] Albanesi T, Biondi S, Petrangeli M, 2002. Pushover analysis: An energy based approach, in proceedings of the *12th European Conference on Earthquake Engineering*, Elsevier Science Ltd.
- [45] Gulkan P, Sozen M, 1974. Inelastic response of reinforced concrete structures to earthquakes motions. *ACI Journal*, **71**:604–610.

- [46] Takeda T, Sozen MA, Nielson NN, 1970. Reinforced concrete response to simulated earthquakes, *Journal of Structural Division ASCE*; **96**:2557–2573.
- [47] Lin YY, Chang KC, 2003. A study on damping reduction factors for buildings under earthquakes motions, *ASCE Journal of Earthquake Engineering*; **129**:206-214.
- [48] Miranda E, Ruiz-Garcia J, 2002. Evaluation of approximate methods to estimate maximum inelastic displacement demands, *Earthquake Engineering and Structural Dynamics*, **31**: 539-560
- [49] Miranda E, 2000. Inelastic displacement ratios for structures on firm sites, *Journal of Structural Engineering*, **126**: 1150-1159
- [50] Martinelli E, Faella C, 2015. Nonlinear static analyses based on either inelastic or elastic spectra with equivalent viscous damping: A parametric comparison, *Engineering Structures*, **88**: 241-250
- [51] Jacobsen LS, 1930. Steady forced vibration as influenced by damping. *Trans ASMEAPM-* 52-15; 169–181.
- [52] Chopra AK, “Dynamics of structures: Theory and application to earthquake engineering”, Prentice Hall, 1995, USA.
- [53] Rosenblueth E, Herrera I, 1964. On a kind of hysteretic damping. *Journal of Engineering Mechanics Division ASCE*, **90**:37– 48.
- [54] Priestley MJN, 2003, Myths and fallacies in earthquake engineering, Revisited, The Mallet Milne Lecture, IUSS Press, Pavia, Italy.
- [55] Blandon CA, Priestley MJN, 2005. Equivalent viscous damping equations for direct displacement based design, *Journal of earthquake engineering*, **9**: 257-278.
- [56] CEN. Eurocode 8: Design of structures for earthquake resistance - Part 1: Design of seismic resisting buildings, EN 1998–1. European Committee for Standardization: Bruxelles, Belgium, 2005.

- [57] Amara F, Bosco M Marino EM, Rossi PP, 2014. An accurate strength amplification factor for the design of SDOF system with P- Δ effects, *Earthquake Engineering and Structural Dynamics*, **43**, 589-611
- [58] SIMQKE. A program for artificial motion generation, User's manual and documentation, Department of Civil Engineering MIT, 1976.
- [59] Braga F, Manfredi V, Masi A, Salvatori A, Vona M, 2010. Performance of nonstructural elements in RC buildings during the L'Aquila, 2009, earthquake. *Bulletin of earthquake engineering*, **5**: 1-12.
- [60] Italian Ministry of Public Works: Law n. 1086, 5/11/1971, Norme per la disciplina delle opere in conglomerato cementizio normale e precompresso ed a struttura metallica (Regulations for constructions of normal and pre-stressed reinforced concrete and with steel structure), *Gazzetta Ufficiale Serie generale n. 321*, 21/12/1971, Rome. (in Italian)
- [61] Italian Ministry of Public Works: Ministry Decree, 14/02/1992, Norme tecniche per l'esecuzione delle opere in cemento armato normale e precompresso e per le strutture metalliche (Technical regulations for constructions with reinforced concrete, prestressed concrete and steel structure), *Suppl. Ord. Gazzetta Ufficiale*, 18/03/1992, Rome. (in Italian)
- [62] Italian Ministry of Public Works: Ministry Decree, 16/01/1996, Norme tecniche per le costruzioni in zone sismiche (Regulations for constructions in seismic areas), *Gazzetta Ufficiale Serie generale*, 5/02/1996, Rome. (in Italian)
- [63] Italian Ministry of Public Works: Ministry Decree, 16/01/1996, Norme tecniche relative ai criteri generali per la verifica di sicurezza delle costruzioni e dei carichi e sovraccarichi (Regulations for permanent and variable loads for safety verification of constructions), *Gazzetta Ufficiale Serie generale*, 5/02/1996, Rome. (in Italian)

- [64] Italian Ministry of Public Works: Ministry Decree, 30/05/1974, Norme tecniche per la esecuzione delle opere in cemento armato normale e precompresso e per le strutture metalliche (Technical regulations for constructions with reinforced concrete, prestressed concrete and steel structure), *Gazzetta Ufficiale Serie generale*, 29/07/1974, Rome. (in Italian)
- [65] Royal Decree n. 2229, 16/11/1939, Norme per l'esecuzione delle opere in conglomerato cementizio semplice ed armato (Regulations for constructions of concrete and reinforced concrete). *Supplemento Gazzetta Ufficiale n. 92*, 18/04/1940, Rome. (in Italian)
- [66] O.P.C.M. 3431. Norme tecniche per il progetto la valutazione e l'adeguamento sismico degli edifici (Provisions for seismic design, assessment and rehabilitation of buildings). Rome, 2005. (in Italian)
- [67] Mazzoni S, McKenna F, Scott MH, Fenves GL, Jeremic B, OpenSees command Language Manual, Pacific Earthquake Engineering Research Center, University of California at Berkely, USA,2003.
- [68] Popovics S, 1973. A numerical approach to the complete stress strain curve for concrete, *Cement and concrete research*, **3**: 583-599.
- [69] Mander JB, Priestley MJN, Park R, 1988, Theoretical stress strain model for confined concrete *Journal of Structural Engineering ASCE*; **114**:1804–1825.
- [70] Panagiotakos TB, Fardis MN,1996. Seismic response of infilled RC frame structures, in proceedings of *the 11th world conference on earthquake engineering*.
- [71] Celarec D, Ricci P, Dolšek M, 2012. The sensitivity of seismic response parameters to the uncertain modelling variables of masonry-infilled reinforced concrete frames, *Engineering Structures* **35**, 165–177.

- [72] Calvi M, Santini S, 1994. Preliminary tests in infill masonry, PREC8 Progress Report, University of Pavia, Department of structural mechanics, Pavia.
- [73] McCormick J, Nagae T, Ikenaga M, Zhang PC, Katsuo M, and Nakashima M, 2009. Investigation of the Sliding Behavior between Steel and Mortar for Seismic Applications in Structures, *Earthquake Engineering & Structural Dynamics*, **38**, 1401-1419.
- [74] Enokida R, Nagae T, Ikenaga M, Inami M, and Nakashima M 2013. Application of Graphite Lubrication for Column Base in Free Standing Steel Structure, *Journal of Structural and Construction Engineering* (Transactions of AIJ), **78**, 435-444.
- [75] Enokida R, Nagae T, Ikenaga M, Inami M, and Nakashima M, 2012. Development of free standing steel structure using kinematic friction of steel-mortar, in proceedings of *the 15th world conference on earthquake engineering*, Lisboa.
- [76] Barbagallo F, Hamashima I, Hu H, Kurata M, Nakashima M, 2016, Base shear capping buildings with graphite-lubricated bases for collapse prevention in extreme earthquakes, *Earthquake Engineering & Structural Dynamics*, **46**, 1003-1021.
- [77] Westermo B, Udawadia F, 1983. Periodic response of a sliding oscillator system to harmonic excitation, *Earthquake Engineering & Structural Dynamics*, **11**, 135-146.
- [78] Mostaghel N, Hejazi M, Tanbakuchi J, 1983. Response of sliding structure to harmonic support motion, *Earthquake Engineering & Structural Dynamics*, **11**, 355-366.
- [79] Mostaghel N, Hejazi M, Tanbakuchi J, 1983. Response of sliding structure to earthquake support motion, *Earthquake Engineering & Structural Dynamics*, **11**, 729-748.
- [80] Manfredi G, Ricci P, Verderame GM, 2012. Influence of infill panels and their distribution on seismic behaviour of existing reinforced concrete buildings. *The Open Construction and Building Technology Journal* **6**: 236-253.

- [81] Pujol S, Fick D, 2010. The test of a full-scale three-storey RC structure with masonry infill walls. *Engineering Structures* **32**: 3112-3121.
- [82] Dolsek M, Fajfar P, 2008. The effect of masonry infill on the seismic response of a four-storey reinforced concrete frame – a deterministic assessment. *Engineering Structures* **30**: 1991-2001.
- [83] Barone R, 2017. Adeguamento sismico di edifici in c.a. tamponati mediante sistemi a scorrimento lubrificati (Seismic upgrading of RC framed buildings with infills by lubricated sliding base systems), *Thesis for Master Degree in Structural and geotechnical engineering*, (in Italian) University of Catania.

Appendix A

This Appendix shows in details the results of the design of beam cross sections of SR frames and GL frames. Since the frames are symmetrical with respect to y-axis, only the rebars of the first two and a half spans are described. Particularly, the following results are reported:

- the longitudinal rebars of beams at every storey of the SR frames
- the longitudinal rebars of beams at every storey of the GL frames

At each storey of every frame and for both the ends of each beam span, the rebars located in the upper and lower part of the cross section are specified.

Table A.1 – Cross section of beams of SR frame, type 1, with 3 and 6 storeys

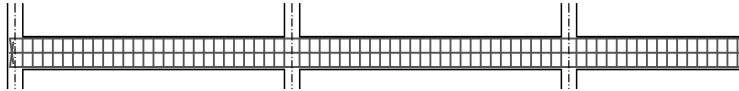
Frame SR31, SR31-I014, SR31-I028								
Storey	Cross sect.	Rebar						
3	30x60	Upper	2φ20	4φ20	4φ20	3φ20+1φ14	3φ20+1φ14	
		Lower	2φ20+1φ14	2φ20+1φ14	2φ20+1φ14	2φ20	2φ20	
2	30x60	Upper	3φ20	4φ20	4φ20	4φ20	4φ20	
		Lower	2φ20	2φ20+1φ14	2φ20+1φ14	2φ20	2φ20	
1	30x60	Upper	3φ20	4φ20+1φ14	4φ20+1φ14	4φ20	4φ20	
		Lower	2φ20	2φ20+1φ14	2φ20+1φ14	2φ20	2φ20	
Frame SR61, SR61-I014, SR61-I028								
6	30x60	Upper	3φ20	3φ20+1φ14	3φ20+1φ14	3φ20+1φ14	3φ20+1φ14	
		Lower	2φ20	2φ20	2φ20	2φ20	2φ20	
5	30x60	Upper	4φ20	4φ20	4φ20	4φ20	4φ20	
		Lower	2φ20	2φ20	2φ20	2φ20	2φ20	
4	30x60	Upper	4φ20	4φ20+1φ14	4φ20+1φ14	4φ20+1φ14	4φ20+1φ14	
		Lower	2φ20	2φ20+1φ14	2φ20+1φ14	2φ20+1φ14	2φ20+1φ14	
3	30x60	Upper	4φ20+1φ14	4φ20+1φ14	4φ20+1φ14	4φ20+1φ14	4φ20+1φ14	
		Lower	2φ20+1φ14	2φ20+1φ14	2φ20+1φ14	2φ20+1φ14	2φ20+1φ14	
2	30x60	Upper	4φ20+1φ14	3φ20	3φ20	3φ20	3φ20	
		Lower	2φ20+1φ14	2φ20	2φ20	2φ20	2φ20	
1	30x60	Upper	4φ20+1φ14	4φ20+1φ14	4φ20+1φ14	4φ20+1φ14	4φ20+1φ14	
		Lower	2φ20+1φ14	2φ20+1φ14	2φ20+1φ14	2φ20+1φ14	2φ20+1φ14	

Table A.2 – Cross section of beams of SR frame, type 1, with 9 storeys

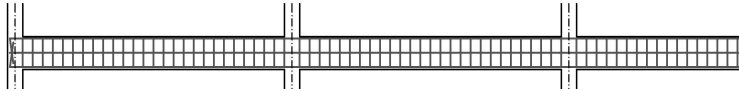
Frame SR91, SR91-I014, SR91-I028								
Storey	Cross sect.	Rebar						
9	30x60	Upper	3φ20	3φ20+1φ14	3φ20+1φ14	3φ20+1φ14	3φ20+1φ14	
		Lower	2φ20	2φ20	2φ20	2φ20	2φ20	
8	30x60	Upper	4φ20	4φ20	4φ20	4φ20	4φ20	
		Lower	2φ20	2φ20	2φ20	2φ20	2φ20	
7	30x60	Upper	4φ20+1φ14	4φ20+1φ14	4φ20+1φ14	4φ20+1φ14	4φ20+1φ14	
		Lower	2φ20+1φ14	2φ20+1φ14	2φ20+1φ14	2φ20+1φ14	2φ20+1φ14	
6	30x70	Upper	4φ20	4φ20	4φ20	4φ20+1φ14	4φ20+1φ14	
		Lower	2φ20	2φ20	2φ20	2φ20+1φ14	2φ20+1φ14	
5	30x70	Upper	4φ20	4φ20+1φ14	4φ20+1φ14	4φ20+1φ14	4φ20+1φ14	
		Lower	2φ20	2φ20+1φ14	2φ20+1φ14	2φ20+1φ14	2φ20+1φ14	
4	30x70	Upper	4φ20+1φ14	5φ20	5φ20	5φ20	5φ20	
		Lower	2φ20+1φ14	3φ20	3φ20	3φ20	3φ20	
3	30x70	Upper	4φ20+1φ14	5φ20	5φ20	5φ20	5φ20	
		Lower	2φ20+1φ14	3φ20	3φ20	3φ20	3φ20	
2	30x70	Upper	4φ20+1φ14	5φ20	5φ20	5φ20	5φ20	
		Lower	2φ20+1φ14	3φ20	3φ20	3φ20	3φ20	
1	30x70	Upper	4φ20	4φ20+1φ14	4φ20+1φ14	4φ20+1φ14	4φ20+1φ14	
		Lower	2φ20	2φ20+1φ14	2φ20+1φ14	2φ20+1φ14	2φ20+1φ14	

Table A.3 – Cross section of beams of SR frame, type 2, with 3 and 6 storeys

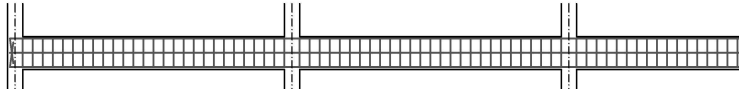
Frame SR32, SR32-I014, SR32-I028								
Storey	Cross sect.	Rebar						
3	30x60	Upper	1 ϕ 20+1 ϕ 14	2 ϕ 20+1 ϕ 14	2 ϕ 20+1 ϕ 14	2 ϕ 20+1 ϕ 14	2 ϕ 20+1 ϕ 14	
		Lower	1 ϕ 20+1 ϕ 14	1 ϕ 20+1 ϕ 14	1 ϕ 20+1 ϕ 14	1 ϕ 20+1 ϕ 14	1 ϕ 20+1 ϕ 14	
2	30x60	Upper	2 ϕ 20+1 ϕ 14	3 ϕ 20	3 ϕ 20	3 ϕ 20	3 ϕ 20	
		Lower	1 ϕ 20+1 ϕ 14	2 ϕ 20	2 ϕ 20	2 ϕ 20	2 ϕ 20	
1	30x60	Upper	2 ϕ 20+1 ϕ 14	3 ϕ 20	3 ϕ 20	3 ϕ 20	3 ϕ 20	
		Lower	1 ϕ 20+1 ϕ 14	2 ϕ 20	2 ϕ 20	2 ϕ 20	2 ϕ 20	
Frame SR62, SR62-I014, SR62-I028								
6	30x60	Upper	2 ϕ 20	2 ϕ 20+1 ϕ 14	2 ϕ 20+1 ϕ 14	2 ϕ 20+1 ϕ 14	2 ϕ 20+1 ϕ 14	
		Lower	1 ϕ 20+1 ϕ 14	1 ϕ 20+1 ϕ 14	1 ϕ 20+1 ϕ 14	1 ϕ 20+1 ϕ 14	1 ϕ 20+1 ϕ 14	
5	30x60	Upper	3 ϕ 20	3 ϕ 20	3 ϕ 20	3 ϕ 20	3 ϕ 20	
		Lower	2 ϕ 20	2 ϕ 20	2 ϕ 20	2 ϕ 20	2 ϕ 20	
4	30x60	Upper	3 ϕ 20+1 ϕ 14	3 ϕ 20+1 ϕ 14	3 ϕ 20+1 ϕ 14	3 ϕ 20+1 ϕ 14	3 ϕ 20+1 ϕ 14	
		Lower	2 ϕ 20	2 ϕ 20	2 ϕ 20	2 ϕ 20	2 ϕ 20	
3	30x60	Upper	3 ϕ 20+1 ϕ 14	3 ϕ 20+1 ϕ 14	3 ϕ 20+1 ϕ 14	3 ϕ 20+1 ϕ 14	3 ϕ 20+1 ϕ 14	
		Lower	2 ϕ 20	2 ϕ 20	2 ϕ 20	2 ϕ 20	2 ϕ 20	
2	30x60	Upper	4 ϕ 20	4 ϕ 20	4 ϕ 20	4 ϕ 20	4 ϕ 20	
		Lower	2 ϕ 20	2 ϕ 20	2 ϕ 20	2 ϕ 20	2 ϕ 20	
1	30x60	Upper	3 ϕ 20+1 ϕ 14	3 ϕ 20+1 ϕ 14	3 ϕ 20+1 ϕ 14	3 ϕ 20+1 ϕ 14	3 ϕ 20+1 ϕ 14	
		Lower	2 ϕ 20	2 ϕ 20	2 ϕ 20	2 ϕ 20	2 ϕ 20	

Table A.5 – Cross section of beams of SR frame, type 3, with 3 and 6 storeys

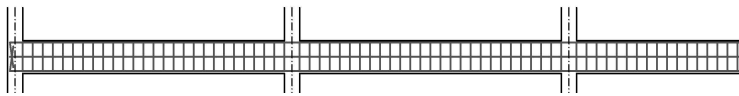
Frame SR33, SR33-I014, SR33-I028								
Storey	Cross sect.	Rebar						
3	30x60	Upper	3φ14	1φ20+1φ14	1φ20+1φ14	1φ20+1φ14	1φ20+1φ14	
		Lower	3φ14	3φ14	1φ20+1φ14	3φ14	1φ20+1φ14	
2	30x60	Upper	1φ20+1φ14	2φ20	2φ20	2φ20	2φ20	
		Lower	3φ14	1φ20+1φ14	1φ20+1φ14	1φ20+1φ14	1φ20+1φ14	
1	30x60	Upper	1φ20+1φ14	2φ20	2φ20	2φ20	2φ20	
		Lower	3φ14	1φ20+1φ14	1φ20+1φ14	1φ20+1φ14	1φ20+1φ14	
Frame SR63, SR63-I014, SR63-I028								
6	30x60	Upper	3φ14	3φ14	3φ14	3φ14	3φ14	
		Lower	1φ20+1φ14	1φ20+1φ14	1φ20+1φ14	1φ20+1φ14	1φ20+1φ14	
5	30x60	Upper	1φ20+1φ14	1φ20+1φ14	1φ20+1φ14	1φ20+1φ14	1φ20+1φ14	
		Lower	2φ20	2φ20	2φ20	2φ20	2φ20	
4	30x60	Upper	1φ20+1φ14	1φ20+1φ14	1φ20+1φ14	1φ20+1φ14	1φ20+1φ14	
		Lower	2φ20+1φ14	2φ20+1φ14	2φ20+1φ14	2φ20+1φ14	2φ20+1φ14	
3	30x60	Upper	2φ20	1φ20+1φ14	1φ20+1φ14	1φ20+1φ14	1φ20+1φ14	
		Lower	3φ20	2φ20+1φ14	2φ20+1φ14	2φ20+1φ14	2φ20+1φ14	
2	30x60	Upper	2φ20	2φ20	2φ20	2φ20	2φ20	
		Lower	3φ20	3φ20	3φ20	3φ20	3φ20	
1	30x60	Upper	1φ20+1φ14	1φ20+1φ14	1φ20+1φ14	1φ20+1φ14	1φ20+1φ14	
		Lower	2φ20+1φ14	2φ20+1φ14	2φ20+1φ14	2φ20+1φ14	2φ20+1φ14	

Table A.6 – Cross section of beams of SR frame, type 3, with 9 storeys

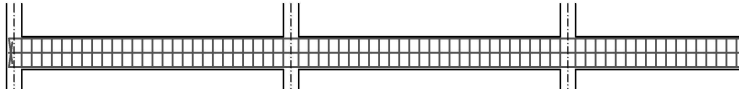
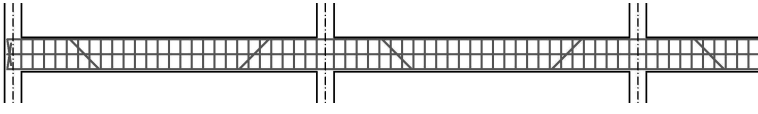
Frame SR93, SR93-I014, SR93-I028								
Storey	Cross sect.	Rebar						
9	30x60	Upper	1 ϕ 20+1 ϕ 14	1 ϕ 20+1 ϕ 14	1 ϕ 20+1 ϕ 14	1 ϕ 20+1 ϕ 14	1 ϕ 20+1 ϕ 14	
		Lower	1 ϕ 20+1 ϕ 14	1 ϕ 20+1 ϕ 14	1 ϕ 20+1 ϕ 14	1 ϕ 20+1 ϕ 14	1 ϕ 20+1 ϕ 14	
8	30x60	Upper	2 ϕ 20+1 ϕ 14	2 ϕ 20	2 ϕ 20	2 ϕ 20	2 ϕ 20	
		Lower	1 ϕ 20+1 ϕ 14	1 ϕ 20+1 ϕ 14	1 ϕ 20+1 ϕ 14	1 ϕ 20+1 ϕ 14	1 ϕ 20+1 ϕ 14	
7	30x60	Upper	3 ϕ 20	2 ϕ 20+1 ϕ 14	2 ϕ 20+1 ϕ 14	2 ϕ 20+1 ϕ 14	2 ϕ 20+1 ϕ 14	
		Lower	2 ϕ 20	1 ϕ 20+1 ϕ 14	1 ϕ 20+1 ϕ 14	1 ϕ 20+1 ϕ 14	1 ϕ 20+1 ϕ 14	
6	30x70	Upper	3 ϕ 20	2 ϕ 20+1 ϕ 14	2 ϕ 20+1 ϕ 14	2 ϕ 20+1 ϕ 14	2 ϕ 20+1 ϕ 14	
		Lower	2 ϕ 20	1 ϕ 20+1 ϕ 14	1 ϕ 20+1 ϕ 14	1 ϕ 20+1 ϕ 14	1 ϕ 20+1 ϕ 14	
5	30x70	Upper	3 ϕ 20	3 ϕ 20	3 ϕ 20	3 ϕ 20	3 ϕ 20	
		Lower	2 ϕ 20	2 ϕ 20	2 ϕ 20	2 ϕ 20	2 ϕ 20	
4	30x70	Upper	3 ϕ 20	3 ϕ 20	3 ϕ 20	3 ϕ 20	3 ϕ 20	
		Lower	2 ϕ 20	2 ϕ 20	2 ϕ 20	2 ϕ 20	2 ϕ 20	
3	30x70	Upper	3 ϕ 20+1 ϕ 14	3 ϕ 20+1 ϕ 14	3 ϕ 20+1 ϕ 14	3 ϕ 20+1 ϕ 14	3 ϕ 20+1 ϕ 14	
		Lower	2 ϕ 20	2 ϕ 20	2 ϕ 20	2 ϕ 20	2 ϕ 20	
2	30x70	Upper	3 ϕ 20+1 ϕ 14	3 ϕ 20+1 ϕ 14	3 ϕ 20+1 ϕ 14	3 ϕ 20+1 ϕ 14	3 ϕ 20+1 ϕ 14	
		Lower	2 ϕ 20	2 ϕ 20	2 ϕ 20	2 ϕ 20	2 ϕ 20	
1	30x70	Upper	3 ϕ 20	3 ϕ 20	3 ϕ 20	3 ϕ 20	3 ϕ 20	
		Lower	2 ϕ 20	2 ϕ 20	2 ϕ 20	2 ϕ 20	2 ϕ 20	

Table A.7 – Cross section of beams of GL frame, type 1, 2 and 3, with 3 and 6 storeys

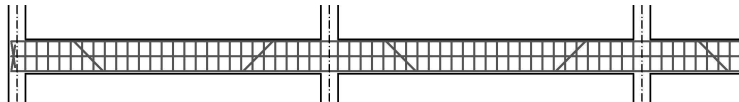
GL31, GL31-I014, GL31-I028, GL32, GL32-I014, GL32-I028, GL33, GL33-I014, GL33-I028

Storey	Cross sect.	Rebar						
3	30x60	Upper	3φ20+1φ14	4φ20+1φ14	4φ20+1φ14	2φ20+2φ14	2φ20+2φ14	
		Lower	2φ14	2φ14	2φ14	2φ14	2φ14	
2	30x60	Upper	3φ20+1φ14	4φ20+1φ14	4φ20+1φ14	2φ20+2φ14	2φ20+2φ14	
		Lower	2φ14	2φ14	2φ14	2φ14	2φ14	
1	30x60	Upper	3φ20+1φ14	4φ20+1φ14	4φ20+1φ14	2φ20+2φ14	2φ20+2φ14	
		Lower	2φ14	2φ14	2φ14	2φ14	2φ14	

GL61, GL61-I014, GL61-I028, GL62, GL62-I014, GL62-I028, GL63, GL63-I014, GL63-I028

6	30x60	Upper	3φ20+1φ14	4φ20+1φ14	4φ20+1φ14	2φ20+2φ14	2φ20+2φ14
		Lower	2φ14	2φ14	2φ14	2φ14	2φ14
5	30x60	Upper	3φ20+1φ14	4φ20+1φ14	4φ20+1φ14	2φ20+2φ14	2φ20+2φ14
		Lower	2φ14	2φ14	2φ14	2φ14	2φ14
4	30x60	Upper	3φ20+1φ14	4φ20+1φ14	4φ20+1φ14	2φ20+2φ14	2φ20+2φ14
		Lower	2φ14	2φ14	2φ14	2φ14	2φ14
3	30x60	Upper	3φ20+1φ14	4φ20+1φ14	4φ20+1φ14	2φ20+2φ14	2φ20+2φ14
		Lower	2φ14	2φ14	2φ14	2φ14	2φ14
2	30x60	Upper	3φ20+1φ14	4φ20+1φ14	4φ20+1φ14	2φ20+2φ14	2φ20+2φ14
		Lower	2φ14	2φ14	2φ14	2φ14	2φ14
1	30x60	Upper	3φ20+1φ14	4φ20+1φ14	4φ20+1φ14	2φ20+2φ14	2φ20+2φ14
		Lower	2φ14	2φ14	2φ14	2φ14	2φ14

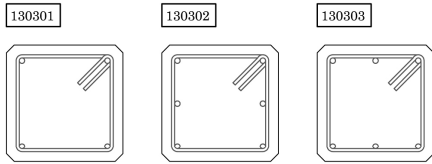
Table A.8 – Cross section of beams of GL frame, type 1, 2 and 3, with 9 storeys

GL91, GL91-I014, GL91-I028, GL92, GL92-I014, GL92-I028, GL93, GL93-I014, GL93-I028								
Storey	Cross sect.	Rebar						
9	30x60	Upper	3φ20+1φ14	4φ20+1φ14	4φ20+1φ14	2φ20+2φ14	2φ20+2φ14	
		Lower	3φ14	3φ14	3φ14	3φ14	3φ14	
8	30x60	Upper	3φ20+1φ14	4φ20+1φ14	4φ20+1φ14	2φ20+2φ14	2φ20+2φ14	
		Lower	3φ14	3φ14	3φ14	3φ14	3φ14	
7	30x60	Upper	3φ20+1φ14	4φ20+1φ14	4φ20+1φ14	2φ20+2φ14	2φ20+2φ14	
		Lower	3φ14	3φ14	3φ14	3φ14	3φ14	
6	30x60	Upper	3φ20+1φ14	4φ20+1φ14	4φ20+1φ14	2φ20+2φ14	2φ20+2φ14	
		Lower	3φ14	3φ14	3φ14	3φ14	3φ14	
5	30x60	Upper	3φ20+1φ14	4φ20+1φ14	4φ20+1φ14	2φ20+2φ14	2φ20+2φ14	
		Lower	3φ14	3φ14	3φ14	3φ14	3φ14	
4	30x60	Upper	3φ20+1φ14	4φ20+1φ14	4φ20+1φ14	2φ20+2φ14	2φ20+2φ14	
		Lower	3φ14	3φ14	3φ14	3φ14	3φ14	
3	30x60	Upper	3φ20+1φ14	4φ20+1φ14	4φ20+1φ14	2φ20+2φ14	2φ20+2φ14	
		Lower	3φ14	3φ14	3φ14	3φ14	3φ14	
2	30x60	Upper	3φ20+1φ14	4φ20+1φ14	4φ20+1φ14	2φ20+2φ14	2φ20+2φ14	
		Lower	3φ14	3φ14	3φ14	3φ14	3φ14	
1	30x60	Upper	3φ20+1φ14	4φ20+1φ14	4φ20+1φ14	2φ20+2φ14	2φ20+2φ14	
		Lower	3φ14	3φ14	3φ14	3φ14	3φ14	

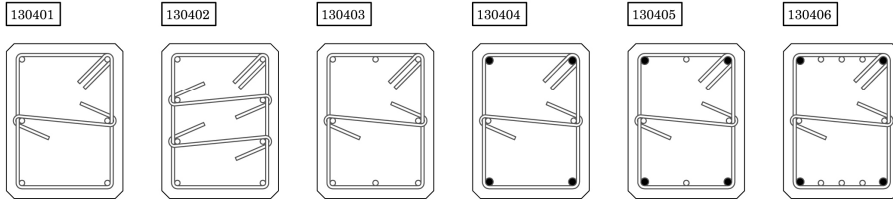
Appendix B

This appendix shows the size and the rebars of the cross sections of columns designed for frames GL and frames SR. The drawings of all the cross sections used in the relevant frame are reported in the initial index. Then, for each frame, the cross section of each column at every storey is indicated in a table. In particular, two cross sections are listed for every column, one for the lower end and the other for the upper end of the column. The rebars used for columns of both GL and SR frames have diameter equal to 14 mm ($\phi 14$) and 20 mm ($\phi 20$), and they are indicated by white and black dots, respectively.

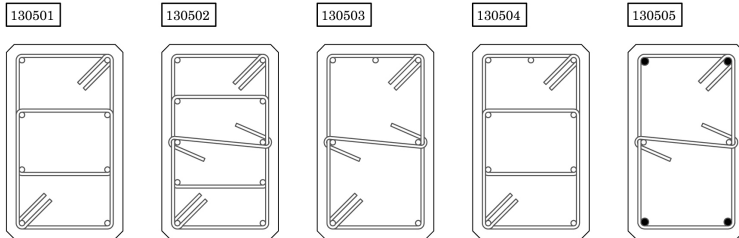
Cross sections: 30x30



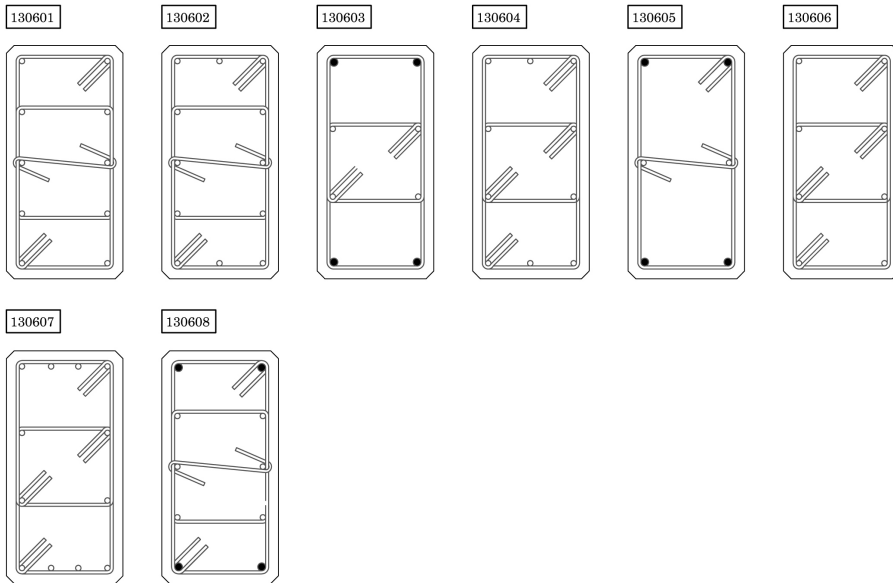
Cross sections: 30x40



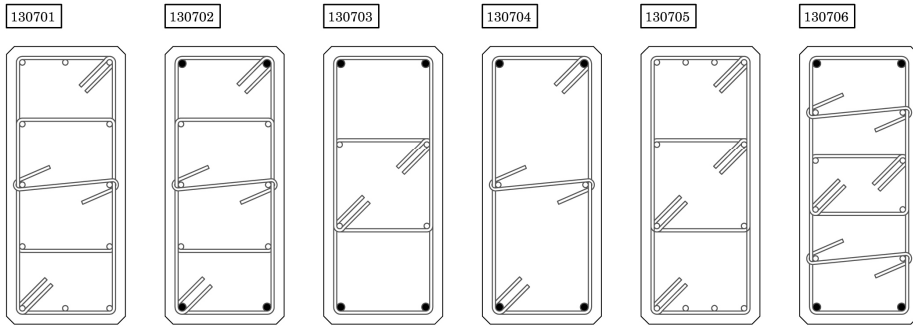
Cross sections: 30x50



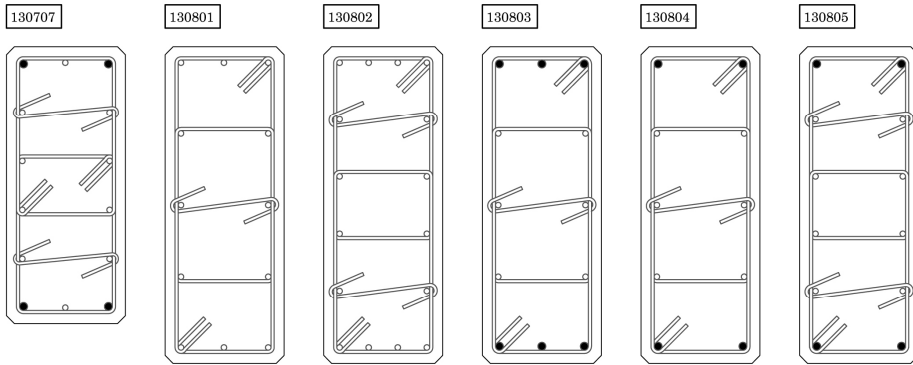
Cross sections: 30x60



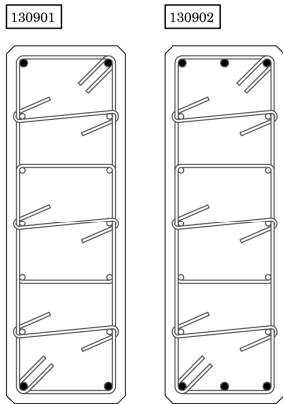
Cross sections: 30x70



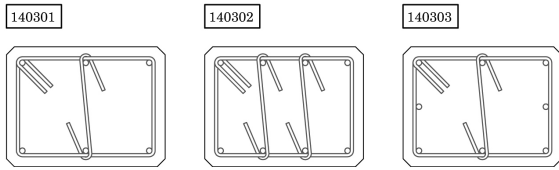
Cross sections: 30x80



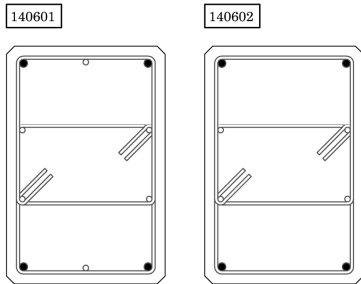
Cross sections: 30x90



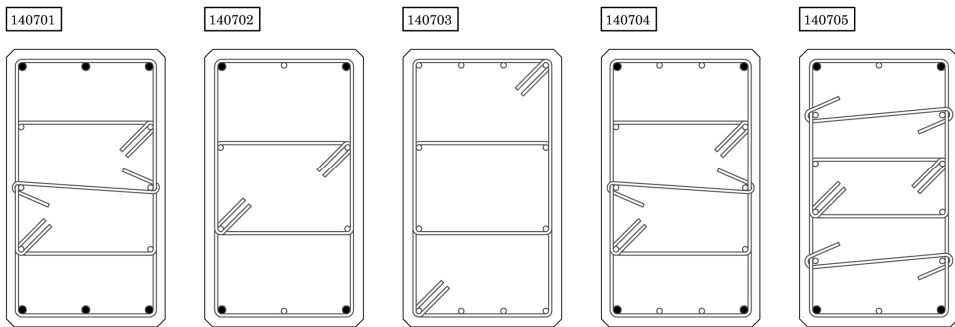
Cross sections: 40x30



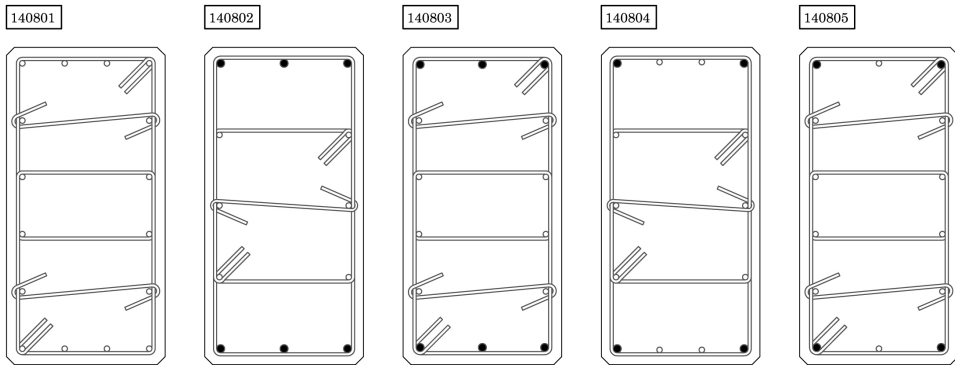
Cross sections: 40x60



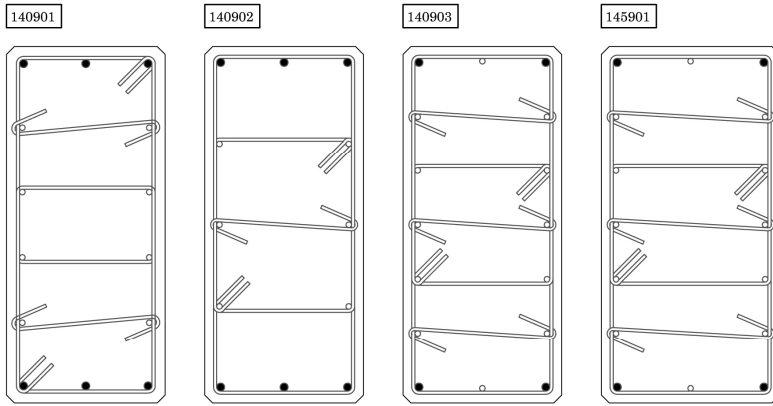
Cross sections: 40x70



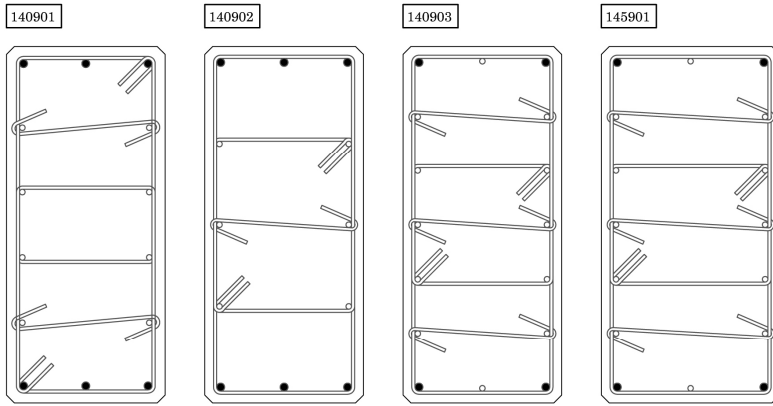
Cross sections: 40x80



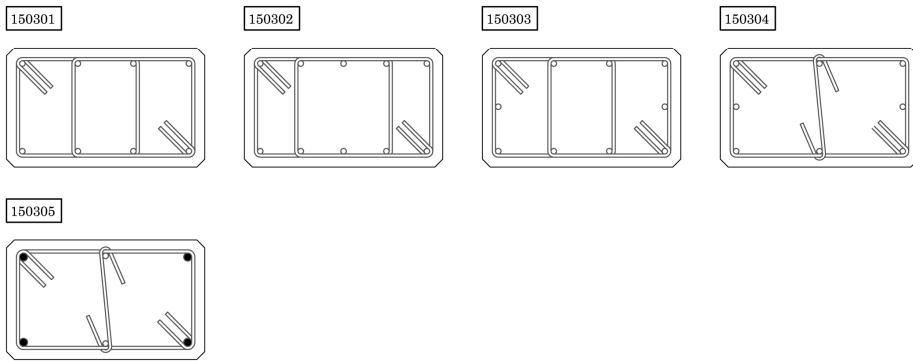
Cross sections: 40x90



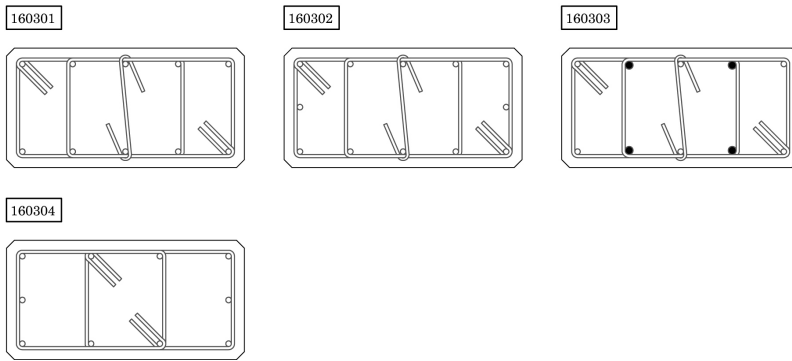
Cross sections: 45x90



Cross sections: 50x30

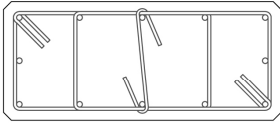


Cross sections: 60x30

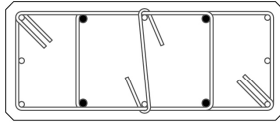


Cross sections: 70x30

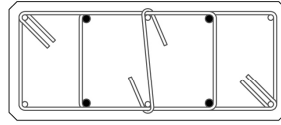
170301



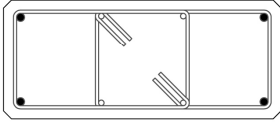
170302



170303

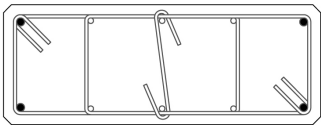


170304



Cross sections: 80x30

180301



Cross sections: 90x30

190301

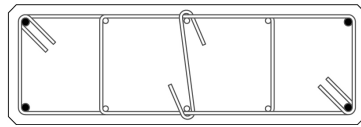


Table B.1- Cross section of columns of GL31, GL31-I014 and GL31-I028

Column												
Storey	1		2		3		4		5		6	
	Lower end	Upper end	Lower end	Upper end	Lower end	Upper end	Lower end	Upper end	Lower end	Upper end	Lower end	Upper end
3	130301	130301	130302	130301	130302	130301	130302	130301	130302	130301	130302	130301
2	130303	130301	130402	130401	130402	130401	130402	130401	130402	130401	130402	130401
1	140302	140301	130502	130501	130502	130501	130502	130501	130502	130501	130502	130501

Table B.2 Cross section of columns of GL61, GL61-I014 and GL61-I028

Column												
Storey	1		2		3		4		5		6	
	Lower end	Upper end	Lower end	Upper end	Lower end	Upper end	Lower end	Upper end	Lower end	Upper end	Lower end	Upper end
6	130301	130301	130302	130301	130302	130301	130302	130301	130302	130301	130302	130301
5	130303	130301	130402	130401	130402	130401	130402	130401	130402	130401	130402	130401
4	140302	140301	130502	130501	130502	130501	130502	130501	130502	130501	130502	130501
3	150302	150301	130602	130601	130602	130601	130602	130601	130602	130601	130602	130601
2	160302	160301	130802	130801	130802	130801	130802	130801	130802	130801	130802	130801
1	170301	170301	140801	140801	140801	140801	140801	140801	140801	140801	140801	140801

Table B.3- Cross section of columns of GL91, GL91-I014 and GL91-I028

Column												
Storey	1		2		3		4		5		6	
	Lower end	Upper end	Lower end	Upper end	Lower end	Upper end	Lower end	Upper end	Lower end	Upper end	Lower end	Upper end
9	130301	130301	130302	130301	130301	130301	130301	130301	130301	130302	130301	130301
8	130302	130301	130403	130401	130302	130301	130301	130302	130401	130403	130301	130302
7	130302	130302	130504	130503	130403	130401	130401	130403	130503	130504	130302	130302
6	140303	140301	130603	130604	130504	130503	130503	130504	130604	130603	140301	140303
5	150303	150304	130702	130703	130603	130604	130604	130603	130703	130702	150304	150303
4	160303	160304	130803	130804	140601	140602	140602	140601	130804	130803	160304	160303
3	170302	170303	140802	140802	140701	140702	140702	140701	140802	140802	170303	170302
2	180301	180301	140803	140802	140802	140802	140802	140802	140802	140803	180301	180301
1	190301	190301	140901	140901	140902	140902	140902	140902	140901	140901	190301	190301

Table B.4- Cross section of columns of GL32, GL32-I014 and GL32-I028

Column												
Storey	1		2		3		4		5		6	
	Lower end	Upper end	Lower end	Upper end	Lower end	Upper end	Lower end	Upper end	Lower end	Upper end	Lower end	Upper end
3	130301	130301	130301	130301	130301	130301	130301	130301	130301	130301	130301	130301
2	130301	130301	130302	130301	130302	130301	130302	130301	130302	130301	130302	130301
1	130301	130301	130402	130401	130402	130401	130402	130401	130402	130401	130402	130401

Table B.5- Cross section of columns of GL62, GL62-I014 and GL62-I028

Column												
Storey	1		2		3		4		5		6	
	Lower end	Upper end	Lower end	Upper end	Lower end	Upper end	Lower end	Upper end	Lower end	Upper end	Lower end	Upper end
6	130301	130301	130301	130301	130301	130301	130301	130301	130301	130301	130301	130301
5	130301	130301	130302	130301	130302	130301	130302	130301	130302	130301	130302	130301
4	130301	130301	130402	130401	130402	130401	130402	130401	130402	130401	130402	130401
3	130303	130301	130501	130501	130501	130501	130501	130501	130501	130501	130501	130501
2	140301	140301	130502	130501	130502	130501	130502	130501	130502	130501	130502	130501
1	140301	140301	130601	130601	130601	130601	130601	130601	130601	130601	130601	130601

Table B.6- Cross section of columns of GL92, GL92-I014 and GL92-I028

Column												
Storey	1		2		3		4		5		6	
	Lower end	Upper end	Lower end	Upper end	Lower end	Upper end	Lower end	Upper end	Lower end	Upper end	Lower end	Upper end
9	130301	130301	130301	130301	130301	130301	130301	130301	130301	130301	130301	130301
8	130301	130301	130301	130301	130301	130301	130301	130301	130301	130301	130301	130301
7	130301	130301	130302	130301	130301	130301	130301	130301	130301	130302	130301	130301
6	130302	130301	130302	130302	130302	130301	130301	130302	130302	130302	130301	130302
5	130302	130302	130401	130403	130403	130403	130403	130403	130403	130401	130302	130302
4	140301	140301	130501	130501	130401	130403	130403	130401	130501	130501	140301	140301
3	140303	140301	130505	130501	130501	130501	130501	130501	130501	130505	140301	140303
2	150305	150305	130605	130605	130505	130501	130501	130505	130605	130605	150305	150305
1	150305	150305	130704	130704	130605	130605	130605	130605	130704	130704	150305	150305

Table B.7- Cross section of columns of GL33, GL33-I014 and GL33-I028

Column												
Storey	1		2		3		4		5		6	
	Lower end	Upper end	Lower end	Upper end	Lower end	Upper end	Lower end	Upper end	Lower end	Upper end	Lower end	Upper end
3	130301	130301	130301	130301	130301	130301	130301	130301	130301	130301	130301	130301
2	130301	130301	130302	130301	130302	130301	130302	130301	130302	130301	130302	130301
1	130301	130301	130402	130401	130402	130401	130402	130401	130402	130401	130402	130401

Table B.8- Cross section of columns of GL63, GL63-I014 and GL63-I028

Column												
Storey	1		2		3		4		5		6	
	Lower end	Upper end	Lower end	Upper end	Lower end	Upper end	Lower end	Upper end	Lower end	Upper end	Lower end	Upper end
6	130301	130301	130301	130301	130301	130301	130301	130301	130301	130301	130301	130301
5	130301	130301	130302	130301	130302	130301	130302	130301	130302	130301	130301	130301
4	130301	130301	130402	130401	130402	130401	130402	130401	130402	130401	130301	130301
3	130303	130301	130502	130501	130502	130501	130502	130501	130502	130501	130303	130301
2	140301	140301	130602	130601	130602	130601	130602	130601	130602	130601	140301	140301
1	140301	140301	130701	130701	130701	130701	130701	130701	130701	130701	140301	140301

Table B.9- Cross section of columns of GL93, GL93-I014 and GL93-I028

Column												
Storey	1		2		3		4		5		6	
	Lower end	Upper end	Lower end	Upper end	Lower end	Upper end	Lower end	Upper end	Lower end	Upper end	Lower end	Upper end
9	130301	130301	130301	130301	130301	130301	130301	130301	130301	130301	130301	130301
8	130301	130301	130301	130301	130301	130301	130301	130301	130301	130301	130301	130301
7	130301	130301	130302	130301	130302	130301	130301	130302	130301	130302	130301	130301
6	130302	130301	130302	130302	130302	130302	130302	130302	130302	130302	130301	130302
5	130302	130302	130402	130401	130402	130401	130401	130402	130401	130402	130302	130302
4	140301	140301	130501	130501	130402	130402	130402	130402	130501	130501	140301	140301
3	140302	140301	130604	130606	130504	130501	130501	130504	130606	130604	140301	140302
2	150304	150304	130603	130604	130604	130604	130604	130604	130604	130603	150304	150304
1	150304	150304	130703	130703	130604	130604	130604	130604	130703	130703	150304	150304

Table B.10- Cross section of columns of AS31, AS31-I014, AS31-I028, AS32, AS32-I014, AS32-I028, AS33, AS33-I014 and AS33-I028

Column												
Storey	1		2		3		4		5		6	
	Lower end	Upper end	Lower end	Upper end	Lower end	Upper end	Lower end	Upper end	Lower end	Upper end	Lower end	Upper end
3	130405	130406	130403	130403	130403	130403	130403	130403	130403	130403	130403	130406
2	130403	130405	130503	130503	130503	130503	130503	130503	130503	130503	130503	130405
1	130503	130505	130604	130604	130604	130604	130604	130604	130604	130604	130604	130505

Table B.11- Cross section of columns of AS61, AS61-I014, AS61-I028, AS62, AS62-I014, AS62-I028, AS63, AS63-I014 and AS63-I028

Column												
Storey	1		2		3		4		5		6	
	Lower end	Upper end	Lower end	Upper end	Lower end	Upper end	Lower end	Upper end	Lower end	Upper end	Lower end	Upper end
6	130607	130607	130705	130705	130705	130705	130705	130705	130705	130705	130607	130607
5	130607	130607	130705	130705	130705	130705	130705	130705	130705	130705	130607	130607
4	130705	130705	140703	140703	140703	140703	140703	140703	140703	140703	130705	130705
3	130705	130705	140704	140703	140704	140703	140704	140703	140704	140703	130705	130705
2	140703	140703	140804	140804	140804	140804	140804	140804	140804	140804	140703	140703
1	140703	140703	140804	140804	140804	140804	140804	140804	140804	140804	140703	140703

Table B.12- Cross section of columns of AS91, AS91-I014, AS91-I028, AS92, AS92-I014, AS92-I028, AS93, AS93-I014 and AS93-I028

Column												
Storey	1		2		3		4		5		6	
	Lower end	Upper end	Lower end	Upper end	Lower end	Upper end	Lower end	Upper end	Lower end	Upper end	Lower end	Upper end
9	130608	130608	130608	130608	130608	130608	130608	130608	130608	130608	130608	130608
8	130608	130608	130608	130608	130608	130608	130608	130608	130608	130608	130608	130608
7	130608	130608	130608	130608	130608	130608	130608	130608	130608	130608	130608	130608
6	130608	130608	130608	130608	130608	130608	130608	130608	130608	130608	130608	130608
5	130608	130608	130707	130706	130707	130706	130707	130706	130707	130706	130608	130608
4	130706	130706	140705	140705	140705	140705	140705	140705	140705	140705	130706	130706
3	130805	130805	140805	140805	140805	140805	140805	140805	140805	140805	130805	130805
2	130901	130901	140903	140903	140903	140903	140903	140903	140903	140903	130901	130901
1	130902	130901	145901	145901	145901	145901	145901	145901	145901	145901	130902	130901

Appendix C

In this appendix the seismic response of the case study frames without infill panels is presented. The seismic behaviour of each case study frame is evaluated by the Incremental Dynamic Analysis (IDA), which is assumed as reference target (red lines with triangles). The seismic response of every frame is also predicted by:

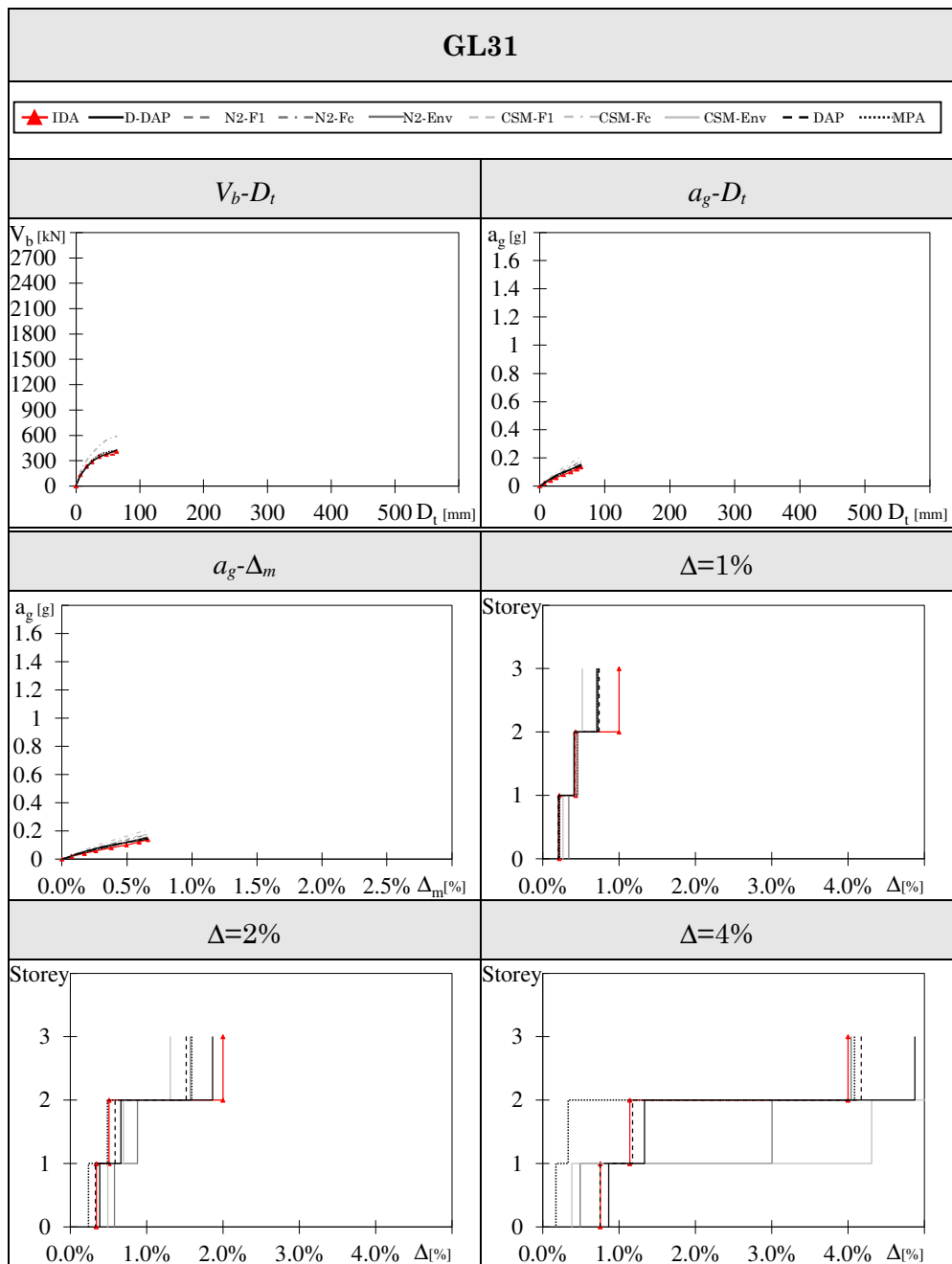
- the proposed D-DAP (black continuous line)
- the N2 method (dark grey line)
- the CSM (light grey line)
- the DAP by Pinho (black dashed line)
- the MPA (black dotted line)

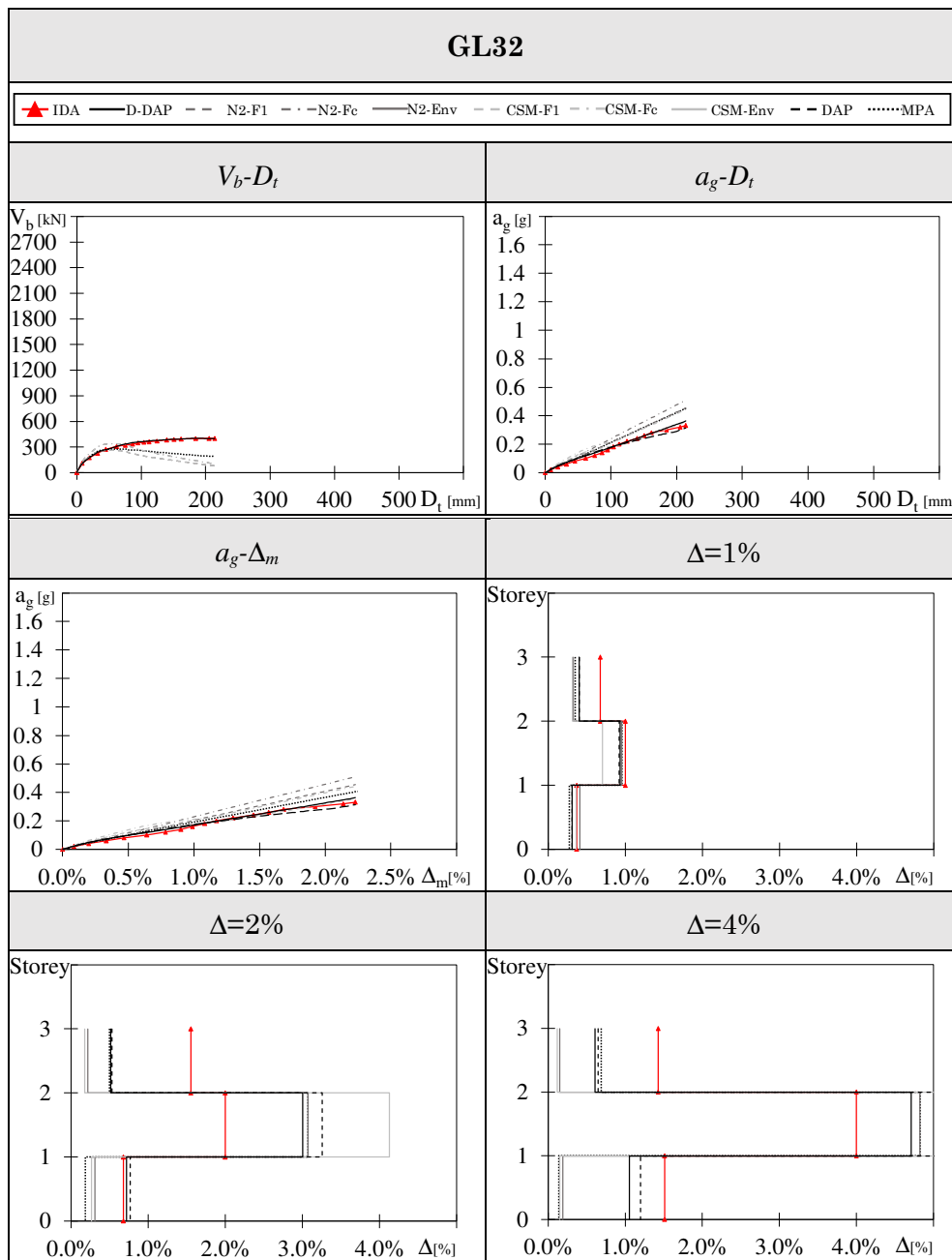
The N2 method and the CSM are applied considering a distribution of forces proportional to the first elastic mode of vibration (dashed line) and a distribution of forces proportional to seismic masses (dashed dotted line), as suggested by EC8. The seismic response provided by the nonlinear static methods of analysis is compared to that predicted by the IDA, to evaluate the accuracy of the considered nonlinear static methods of analysis.

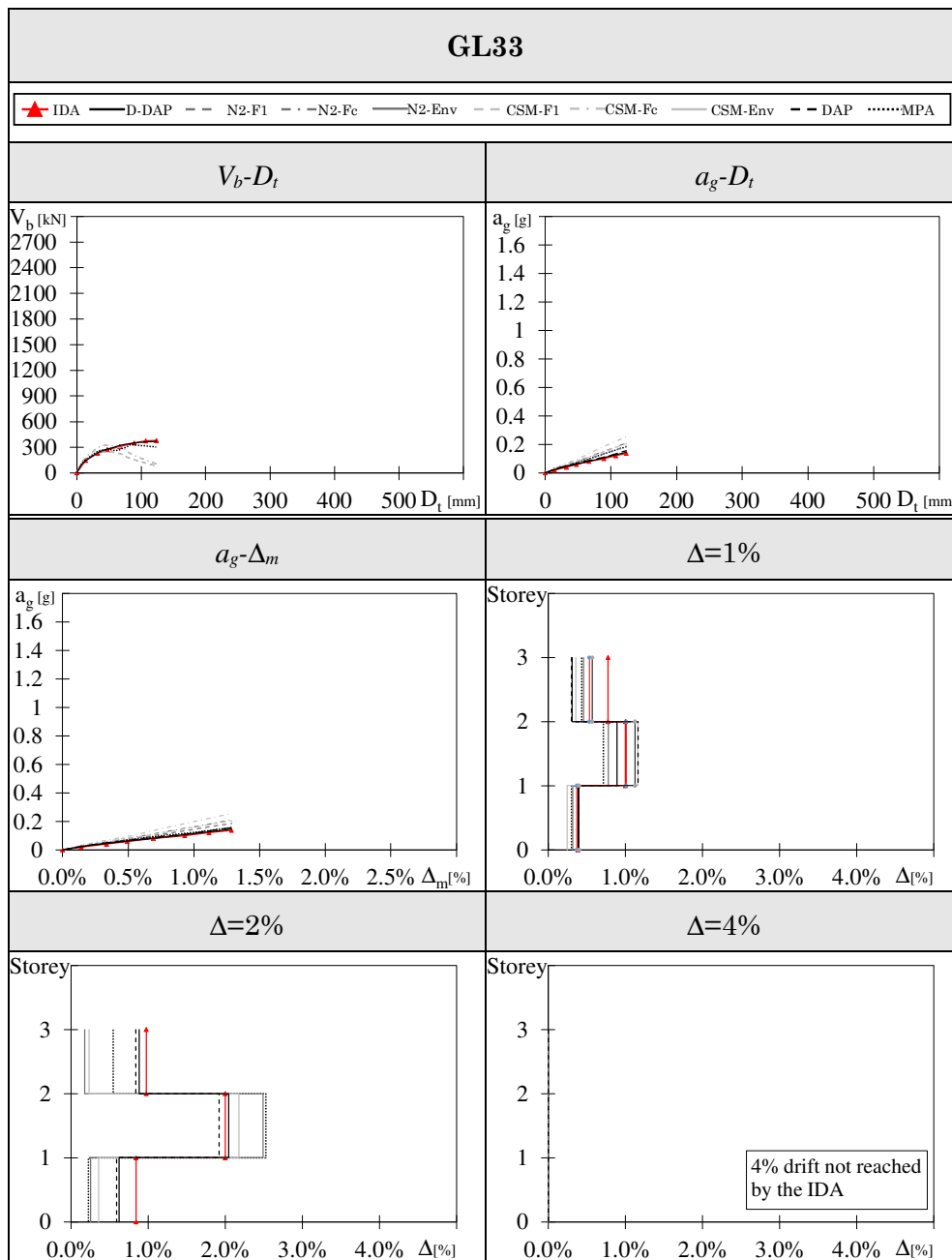
For each frame, the seismic response evaluated by all those nonlinear methods of analysis is reported in six plots. In the first two plots, the performance curve of the relevant frame is showed in terms of global response parameters, i.e. base shear and top displacement (V_b-D_t), and peak ground acceleration and top displacement (a_g-D_t). For every frame, the seismic response provided by the IDA is reported until the attainment of the structural collapse, which is identified with the attainment of a maximum storey drift equal to 4%, or a 30% reduction of

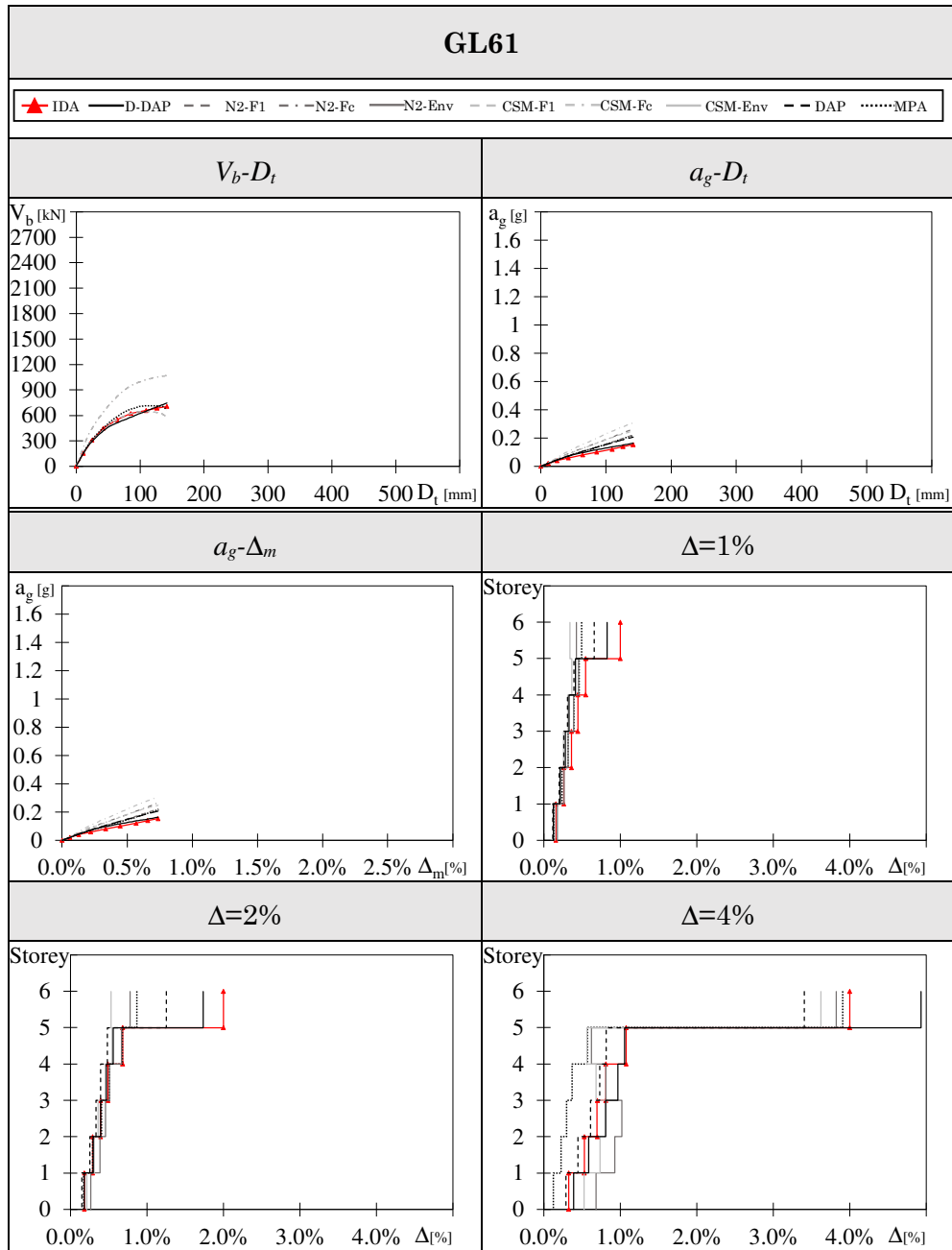
the maximum base shear of columns. The seismic response obtained by nonlinear static methods of analysis is reported until the top displacement equals the top displacement that in the IDA corresponds to the structural collapse. In case of the V_b-D_t curve, the D-DAP and the DAP provide the same results. It is specified that in case of nine storey frames belonging to SR set, the maximum value of the x -axis is extended compared to that adopted for all other frames. This allowed to show the entire seismic response of those frames up to the collapse.

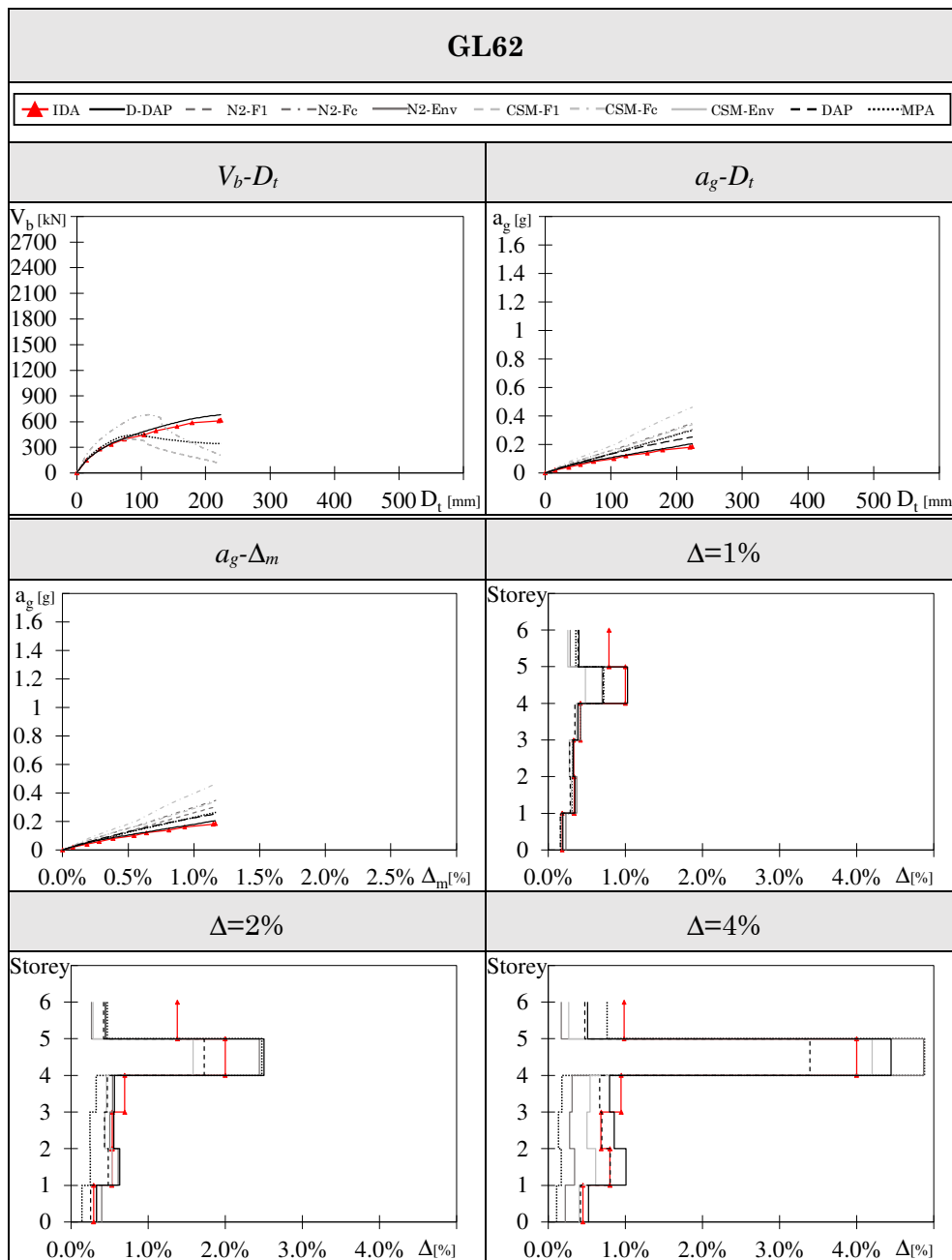
In the following four plots, the seismic response of the frame is presented in terms of local parameters. In particular, in the third plot the average drift Δ_m is calculated at each step as the summation of the drifts at all the storeys, divided by the total number of storeys. Each value of Δ_m is associated to the value of ground acceleration and this relationship is reported in the third plot. All curves stop when the average drift equals the average drift corresponding to the structural collapse in the IDA. The last three figures show the distribution of storey drifts along the height of the considered frame, for three limit states. Three limit states were considered in the IDA (red lines with triangles), i.e. the attainment of a maximum storey drift equal to 1%, 2% and 4%. In each frame, each limit state was reached for a different value of ground acceleration. Fixing the ground acceleration at the value corresponding to the considered limit state in the IDA, the corresponding distribution of storey drift in every frame has been evaluated by the abovementioned nonlinear static methods of analysis. In case of the N2 method or the CSM, the drift at each storey is obtained from the envelope of the drifts obtained with the distribution of forces proportional to the first mode and proportional to storey masses.

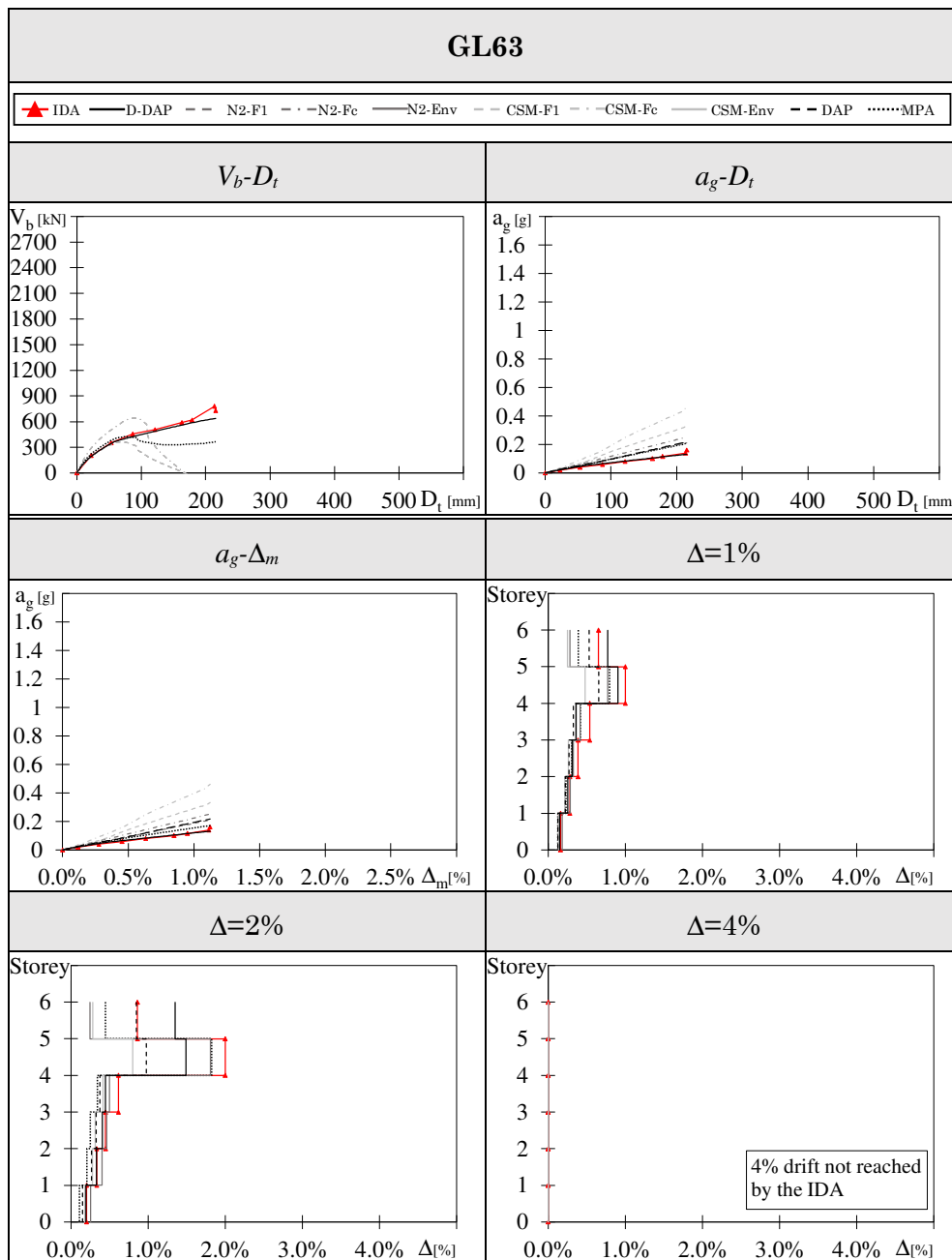


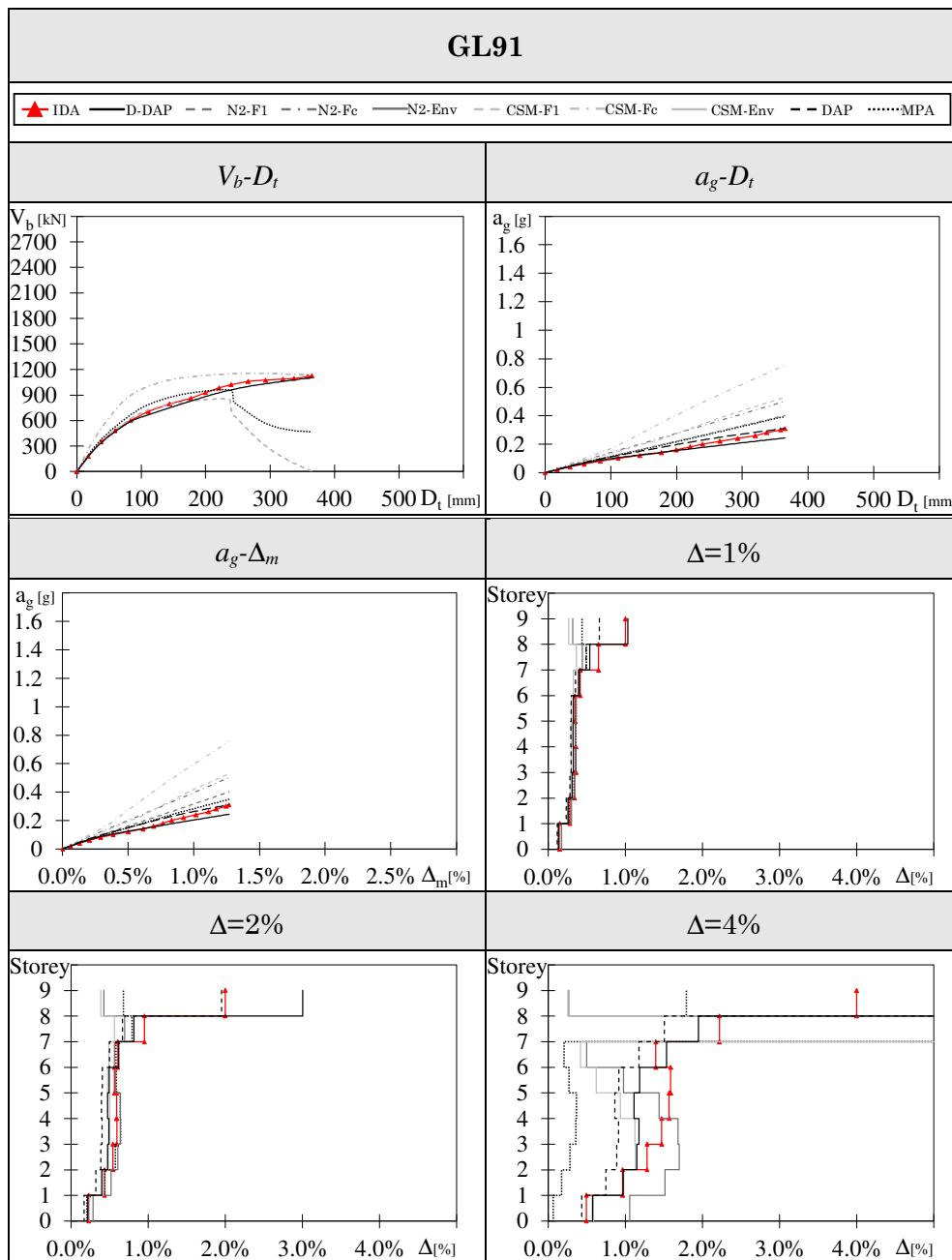


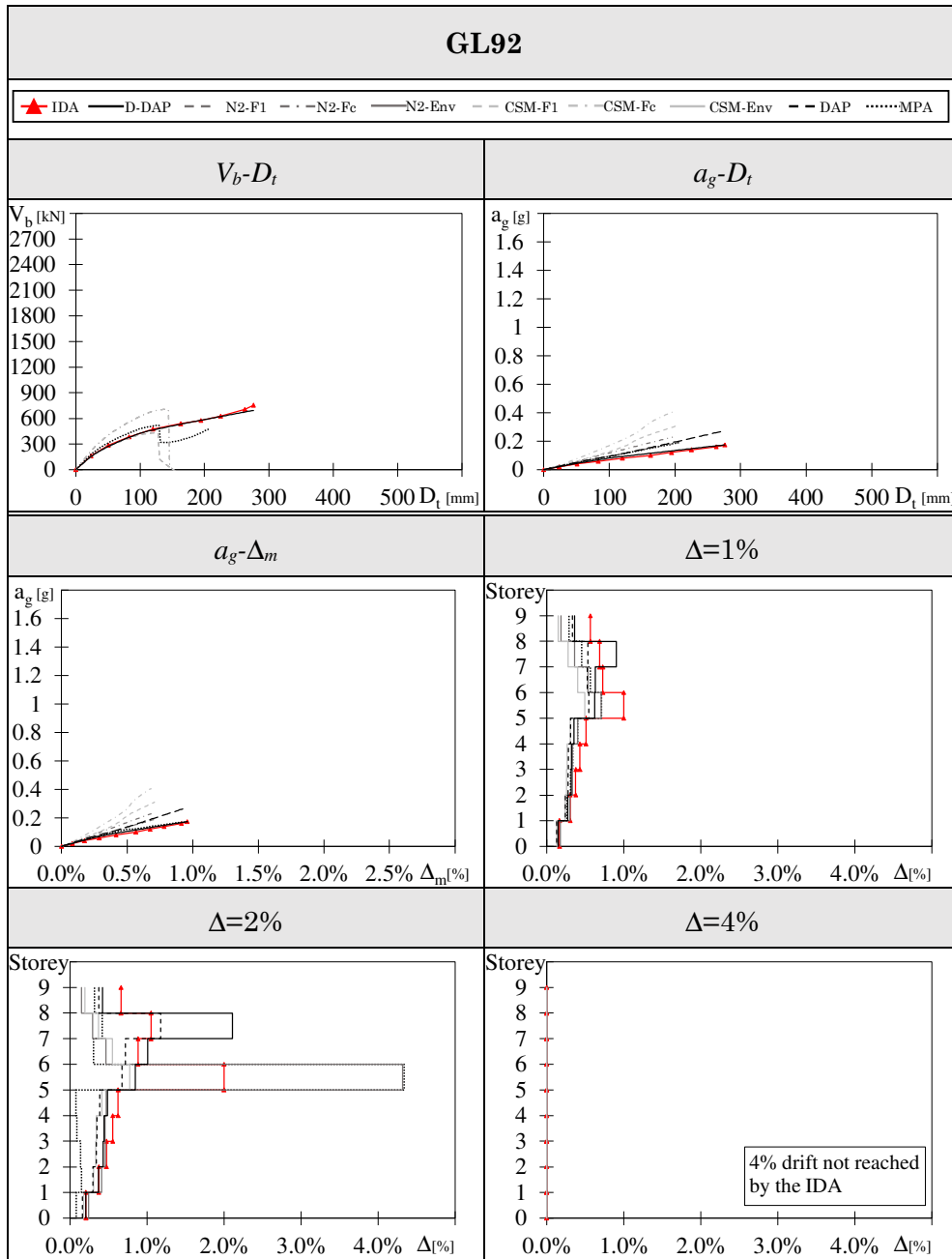


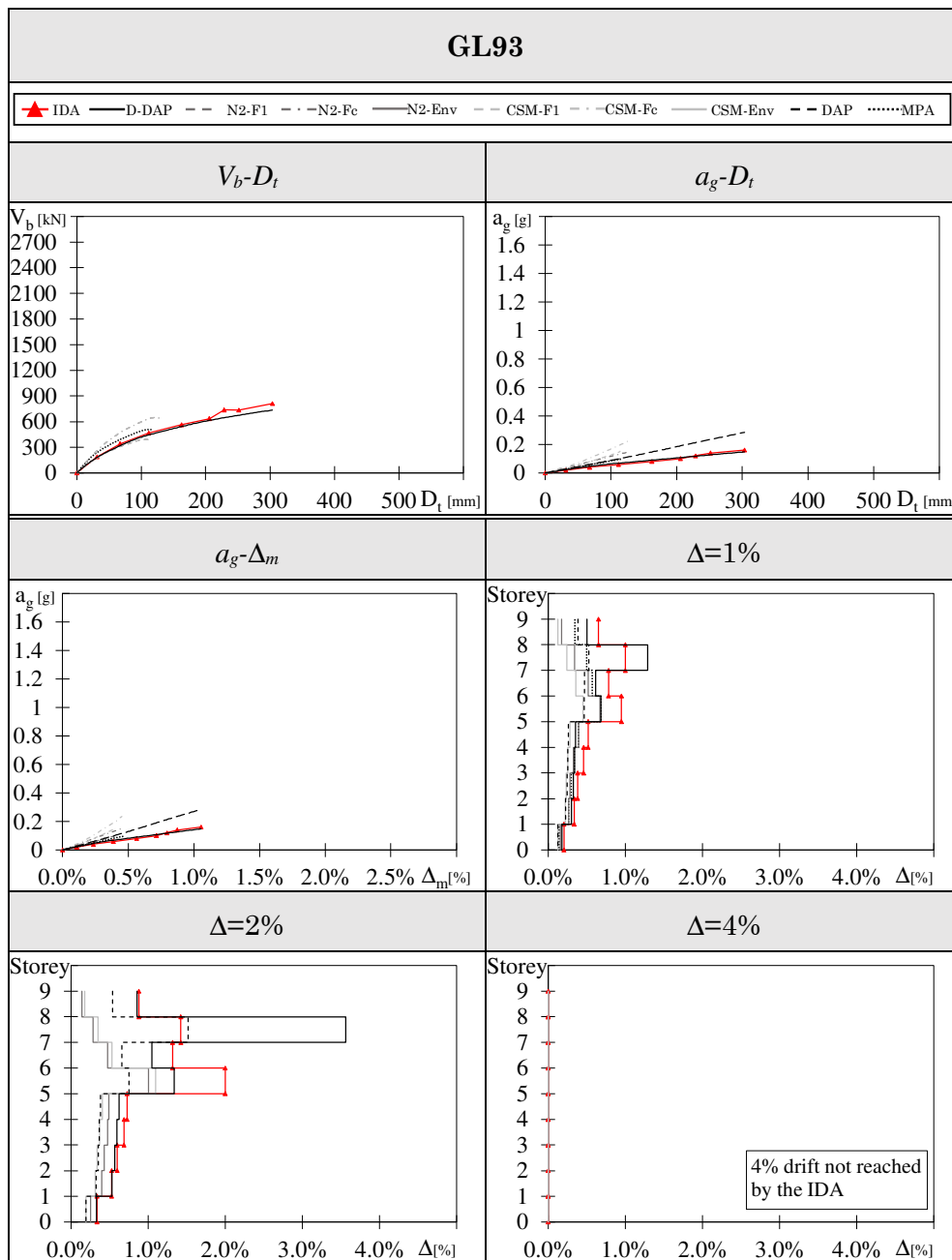


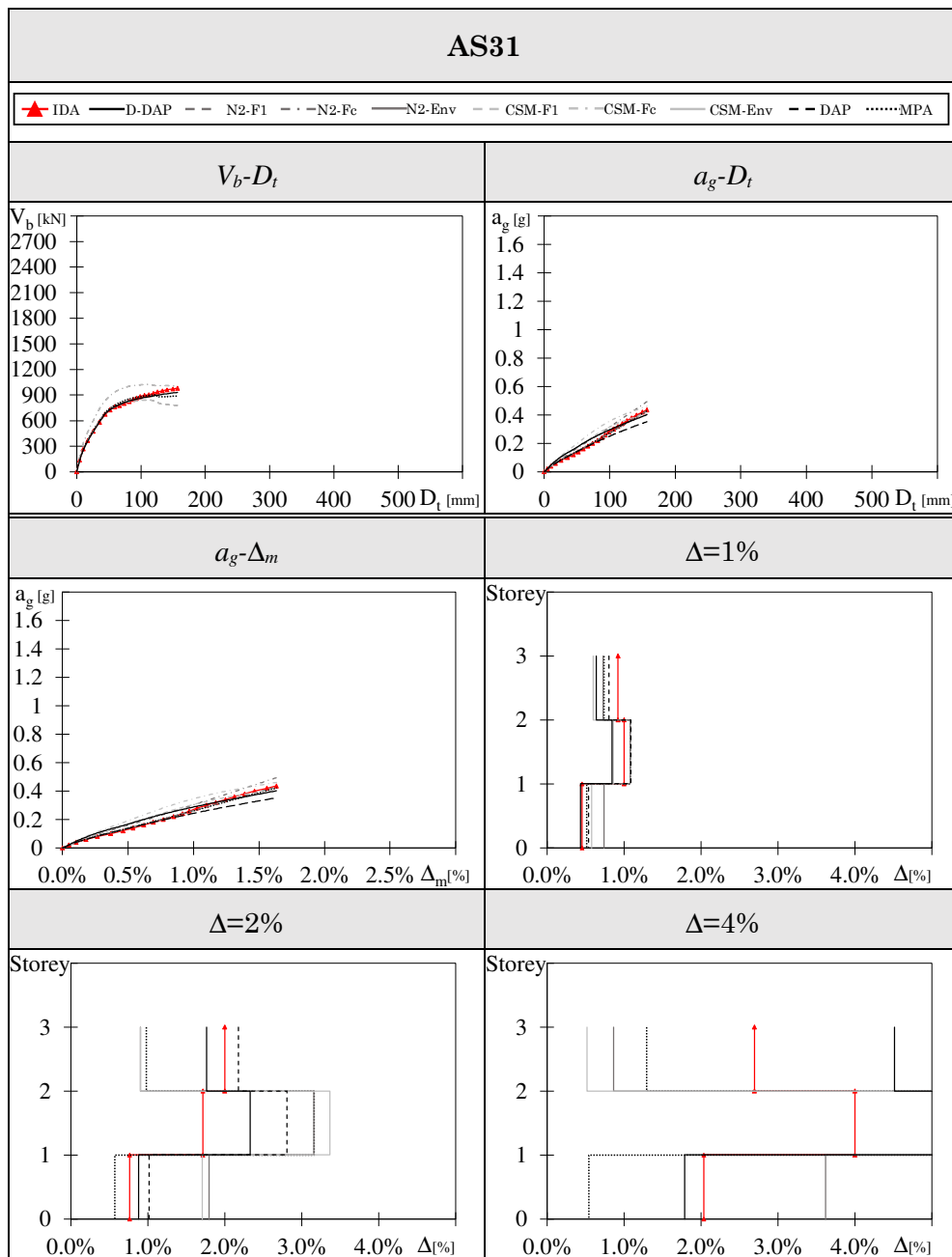


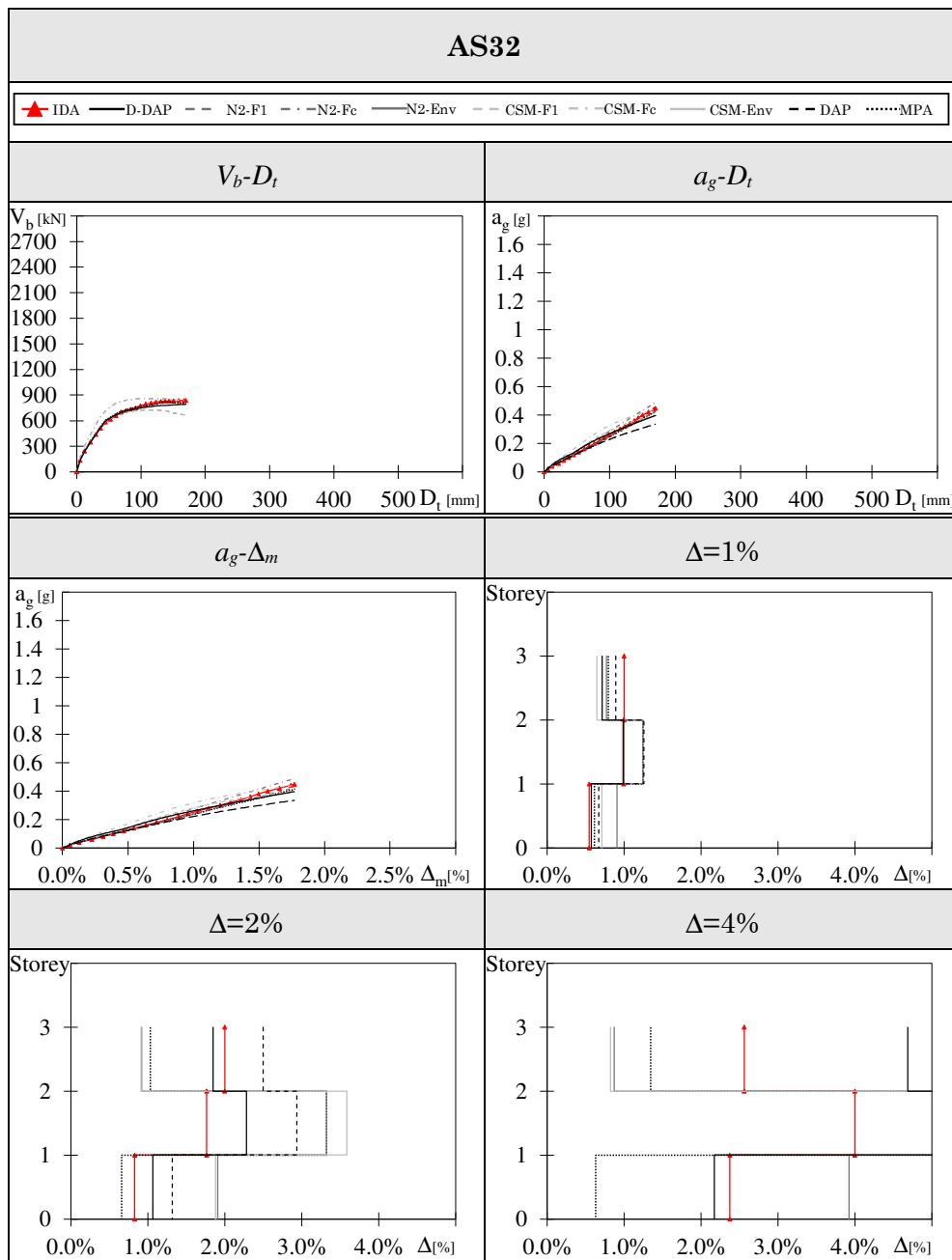


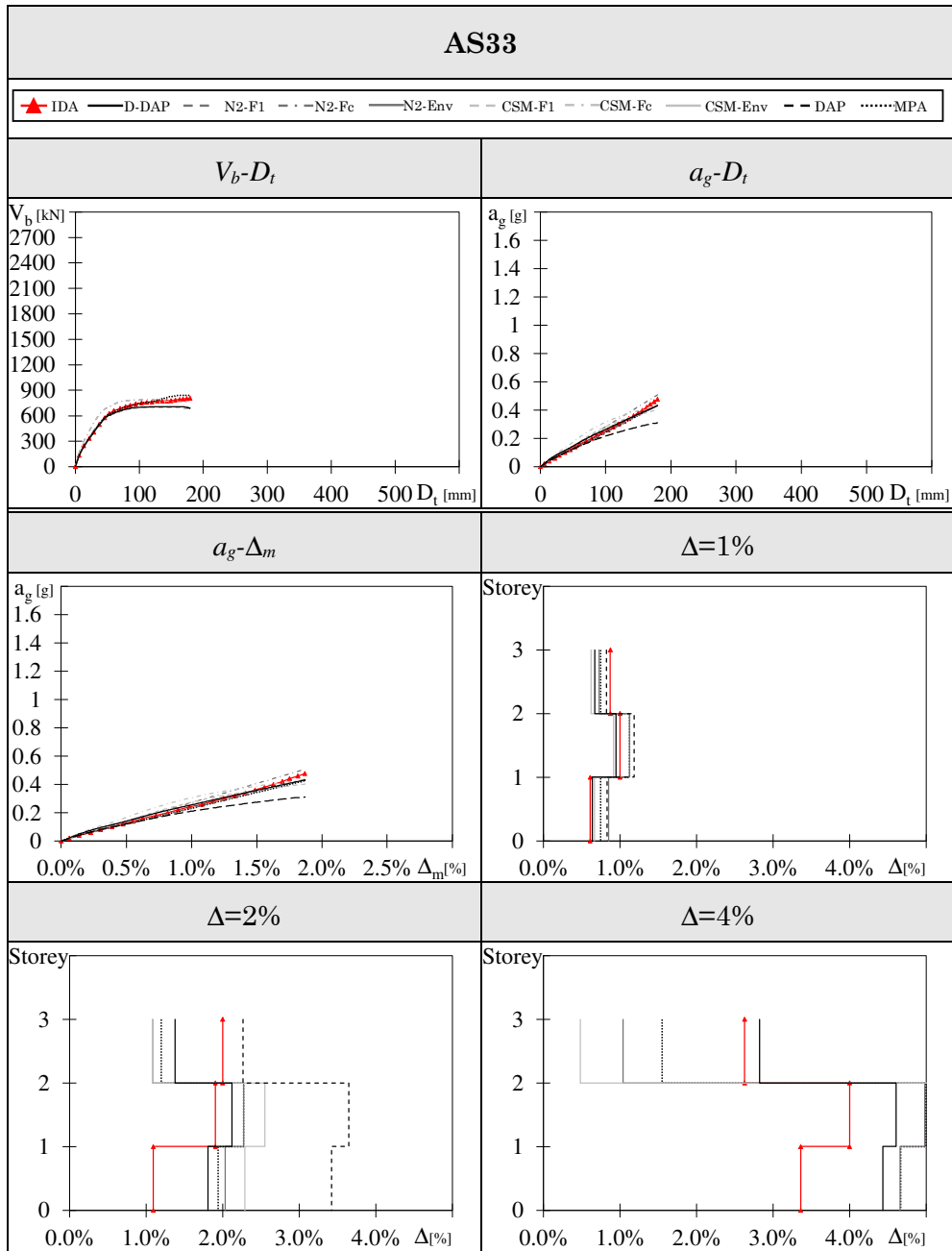


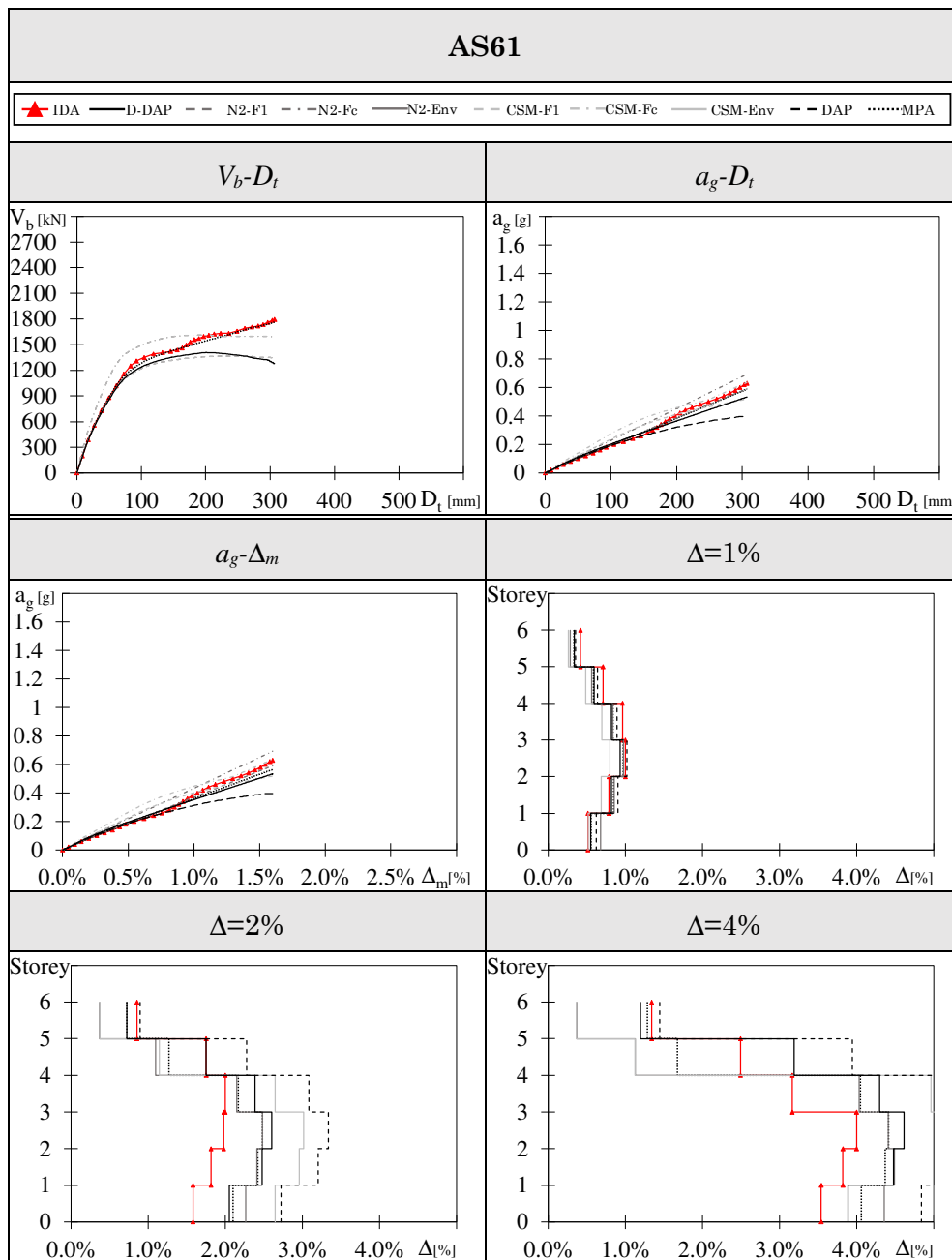


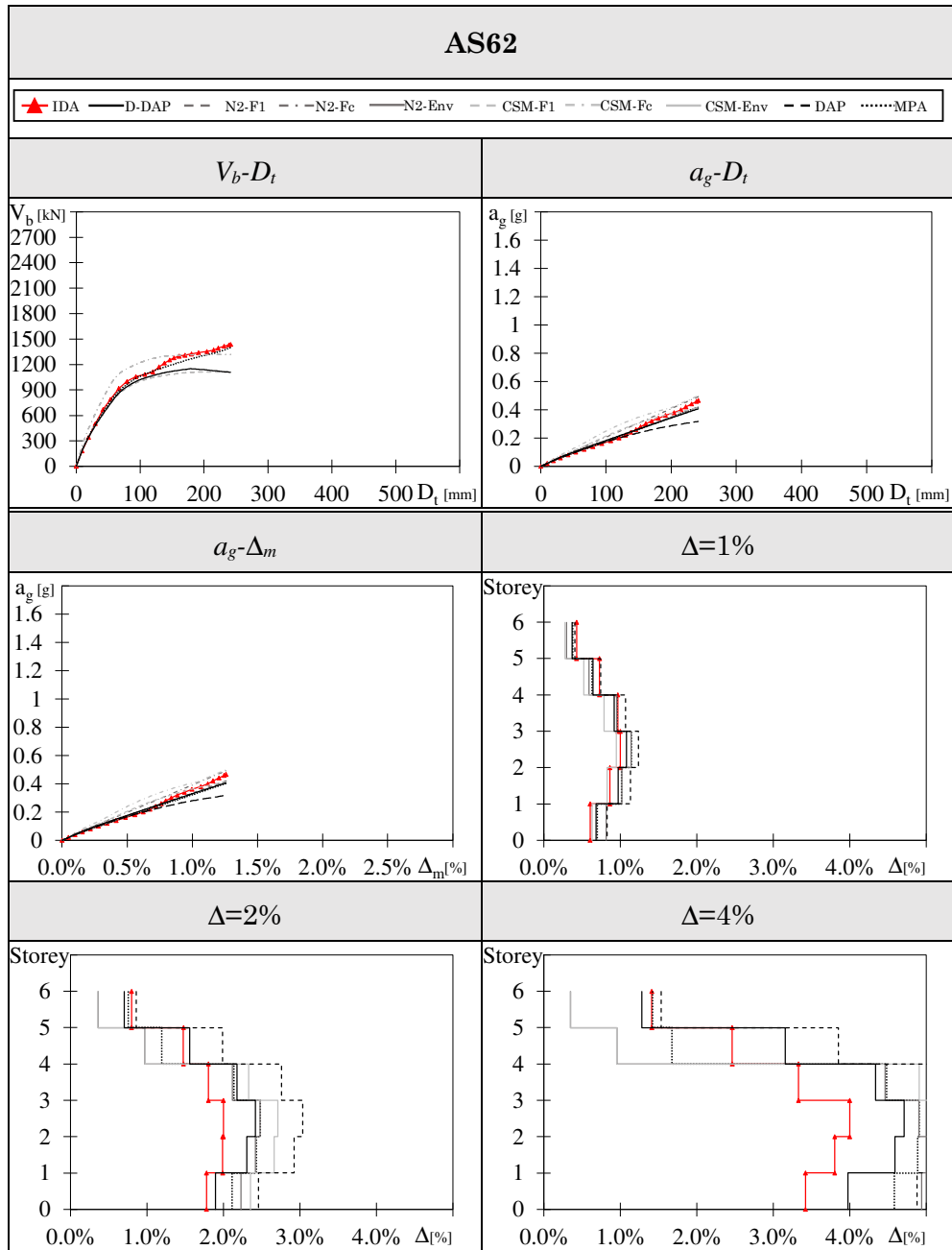


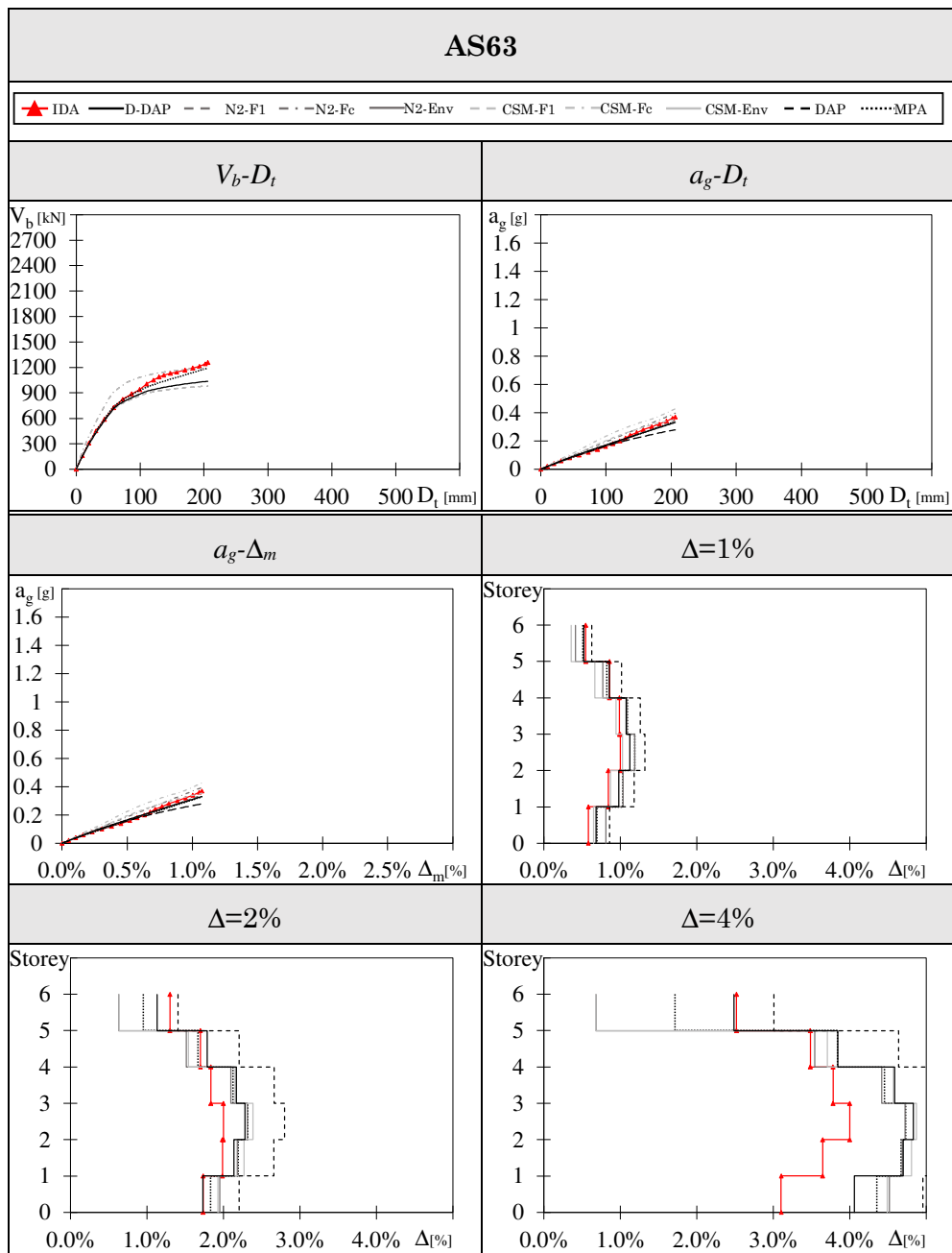


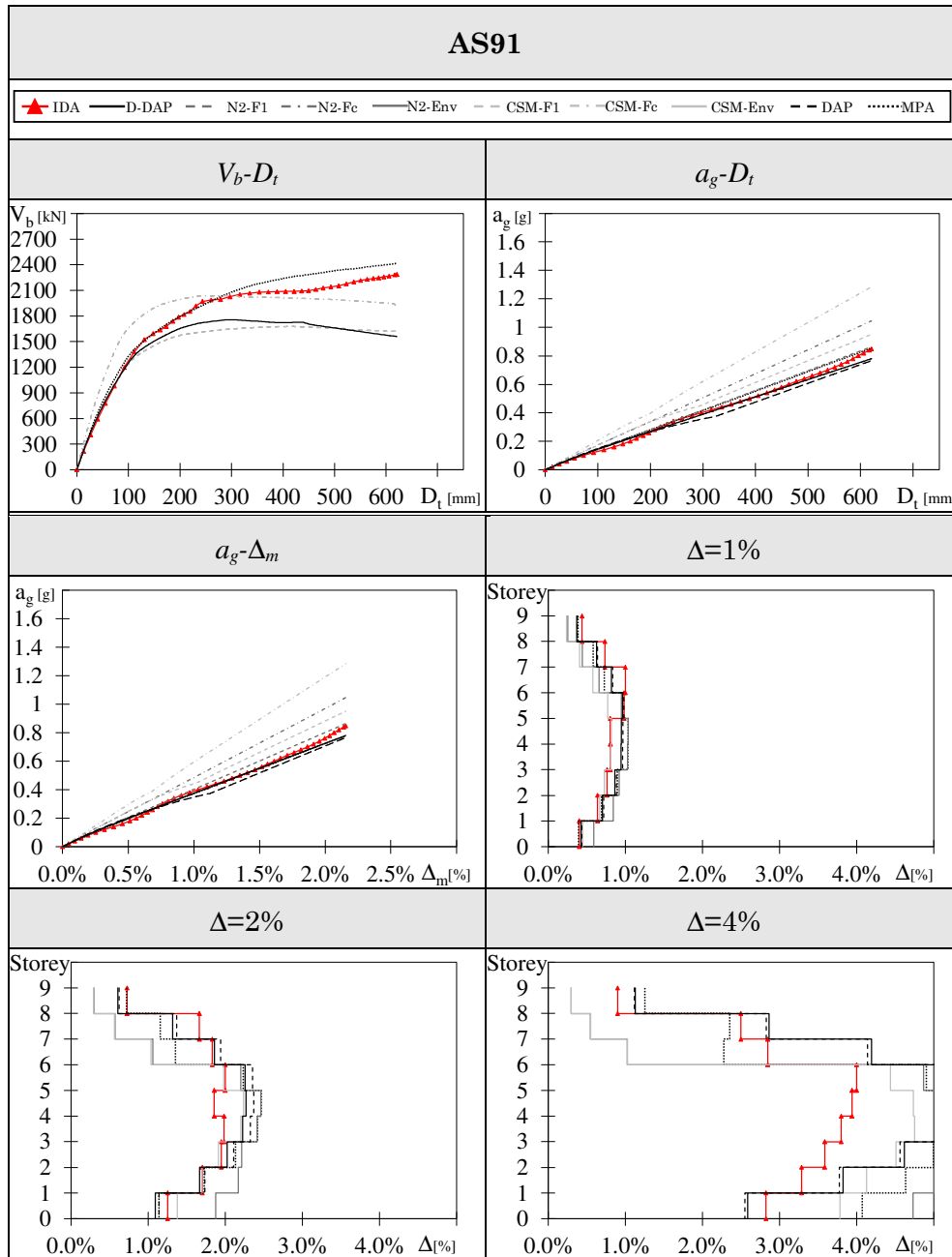


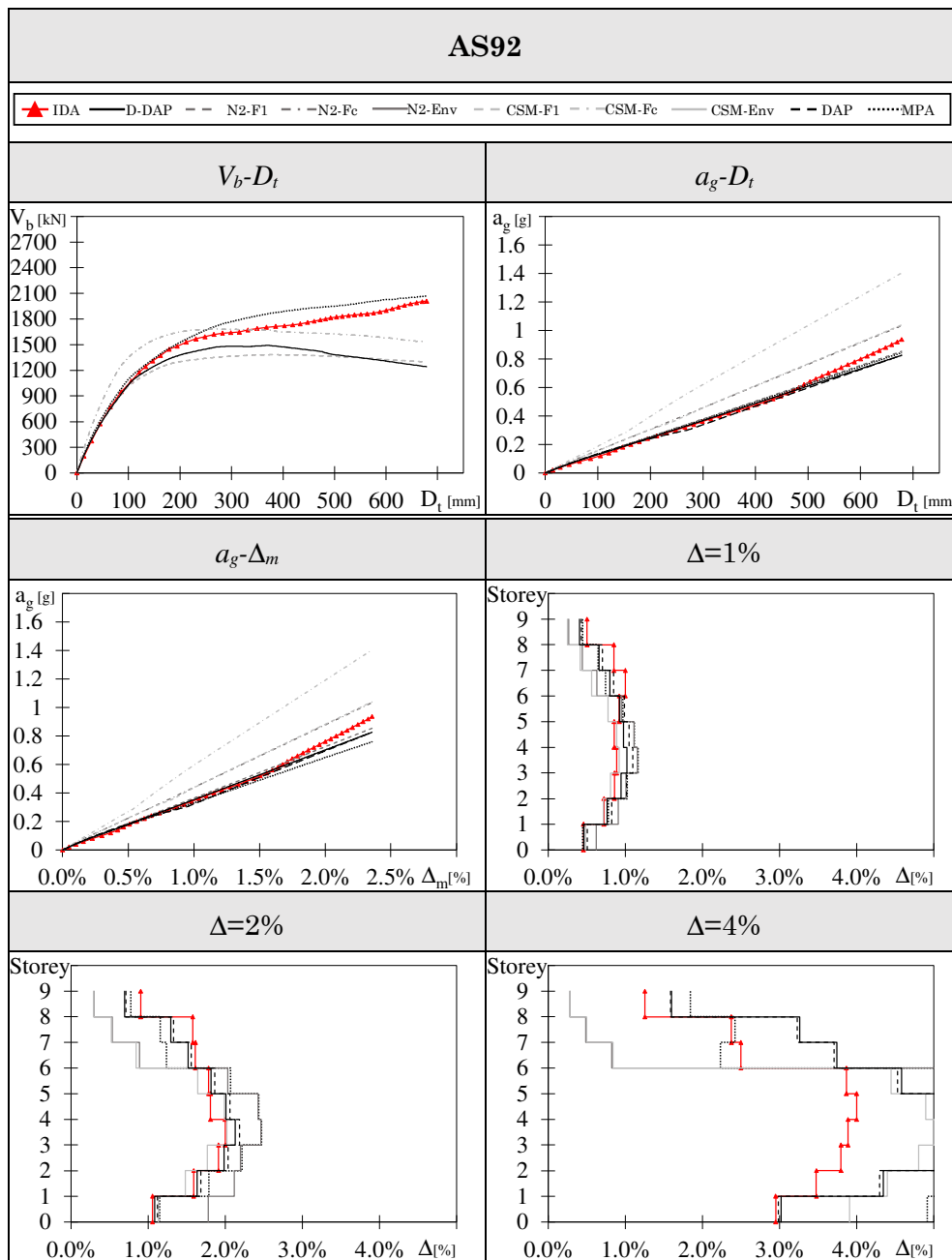


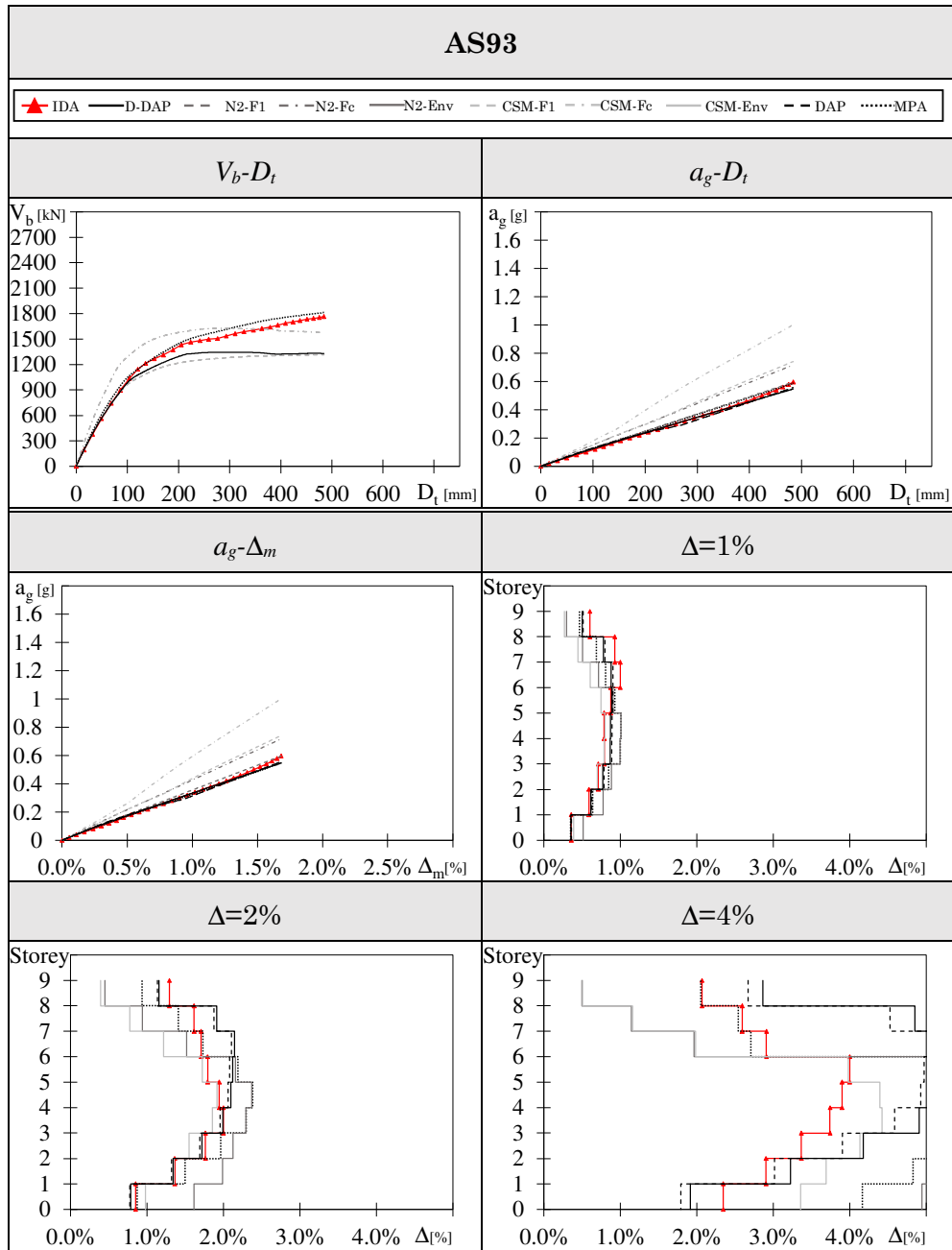












Appendix D

This appendix shows the seismic response of the case study frames with infill panels with medium stiffness and strength (indicated by the suffix I014). The seismic behaviour of each case study frame is evaluated by the Incremental Dynamic Analysis (IDA), which is assumed as reference target (red lines with triangles). The seismic response of every frame is also predicted by:

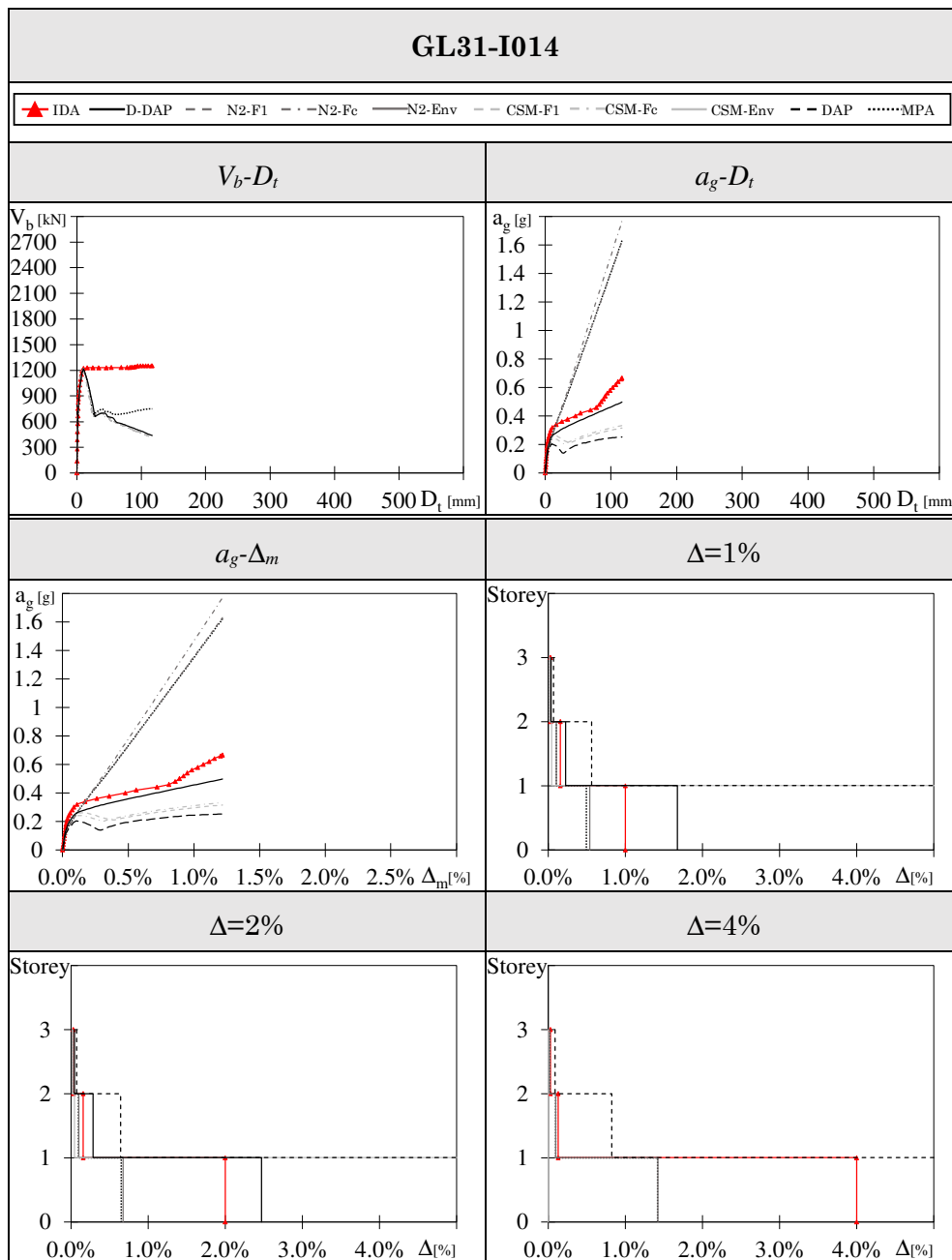
- the proposed D-DAP (black continuous line)
- the N2 method (dark grey line)
- the CSM (light grey line)
- the DAP by Pinho (black dashed line)
- the MPA (black dotted line)

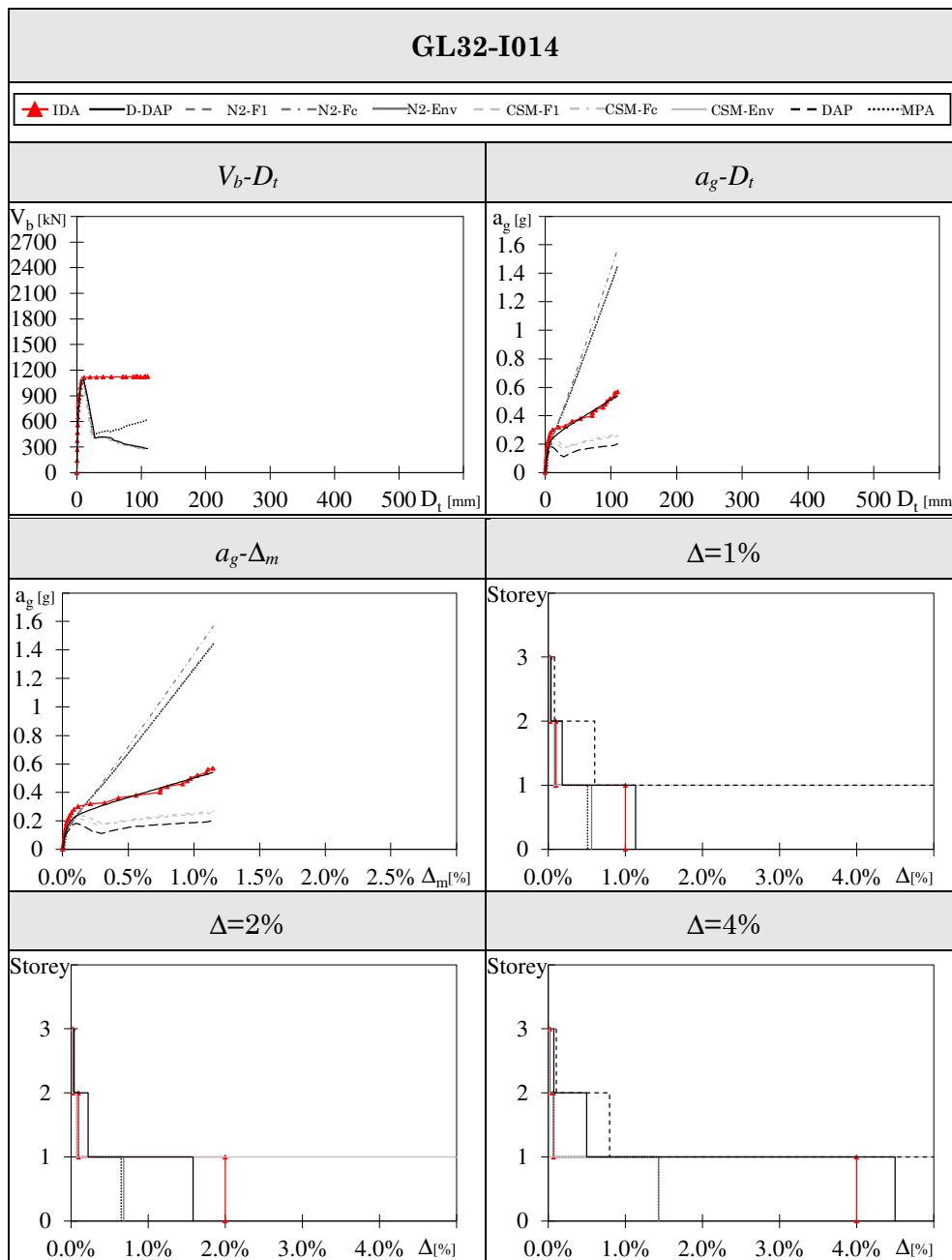
The N2 method and the CSM are applied considering a distribution of forces proportional to the first elastic mode of vibration (dashed line) and a distribution of forces proportional to seismic masses (dashed dotted line), as suggested by EC8. The seismic response provided by the nonlinear static methods of analysis is compared to that predicted by the IDA, to evaluate the accuracy of the considered nonlinear static methods of analysis.

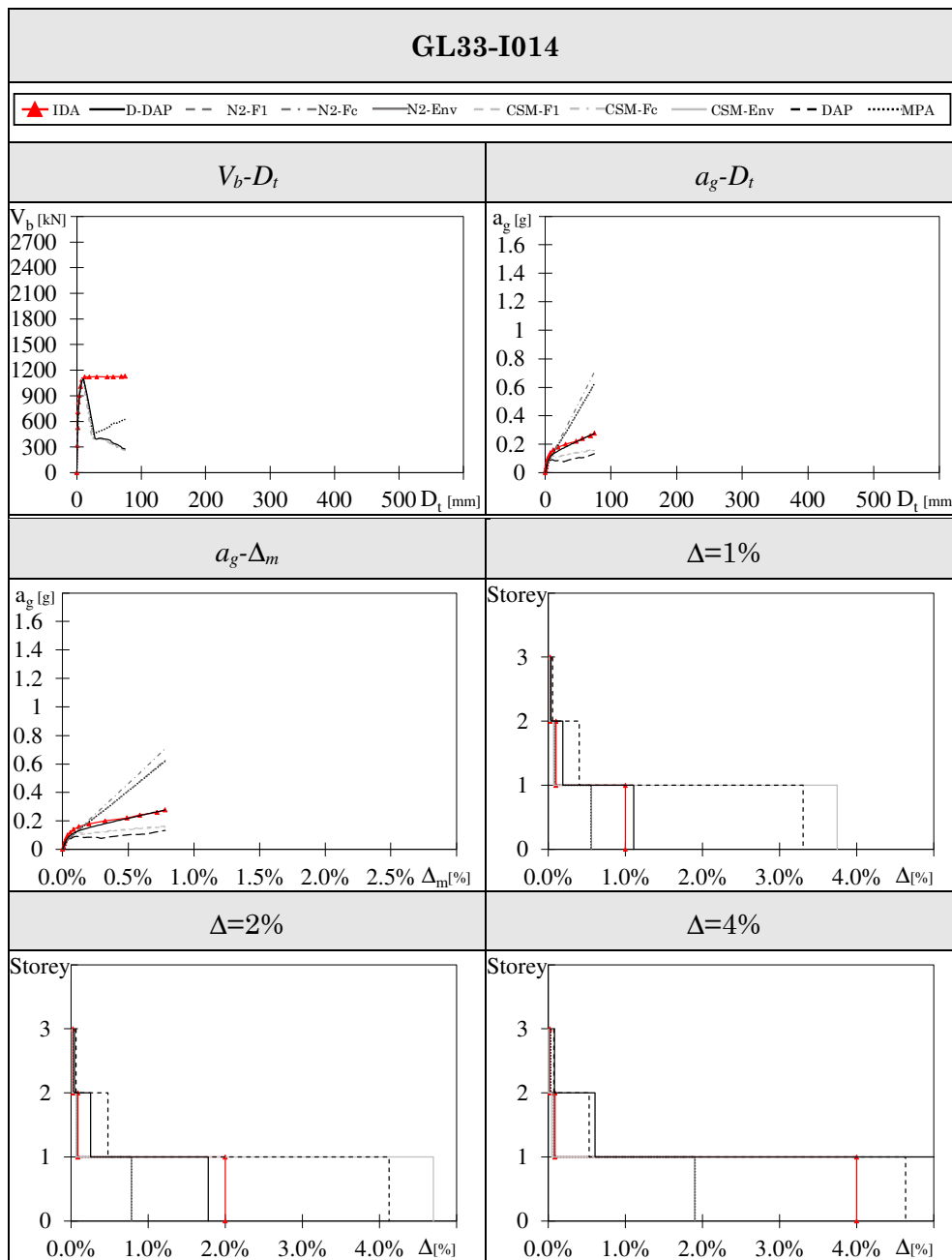
For each frame, the seismic response evaluated by all those nonlinear methods of analysis is reported in six plots. In the first two plots, the performance curve of the relevant frame is showed in terms of global response parameters, i.e. base shear and top displacement (V_b-D_t), and peak ground acceleration and top displacement (a_g-D_t). For every frame, the seismic response provided by the IDA is reported until the attainment of the structural collapse, which is identified with the at-

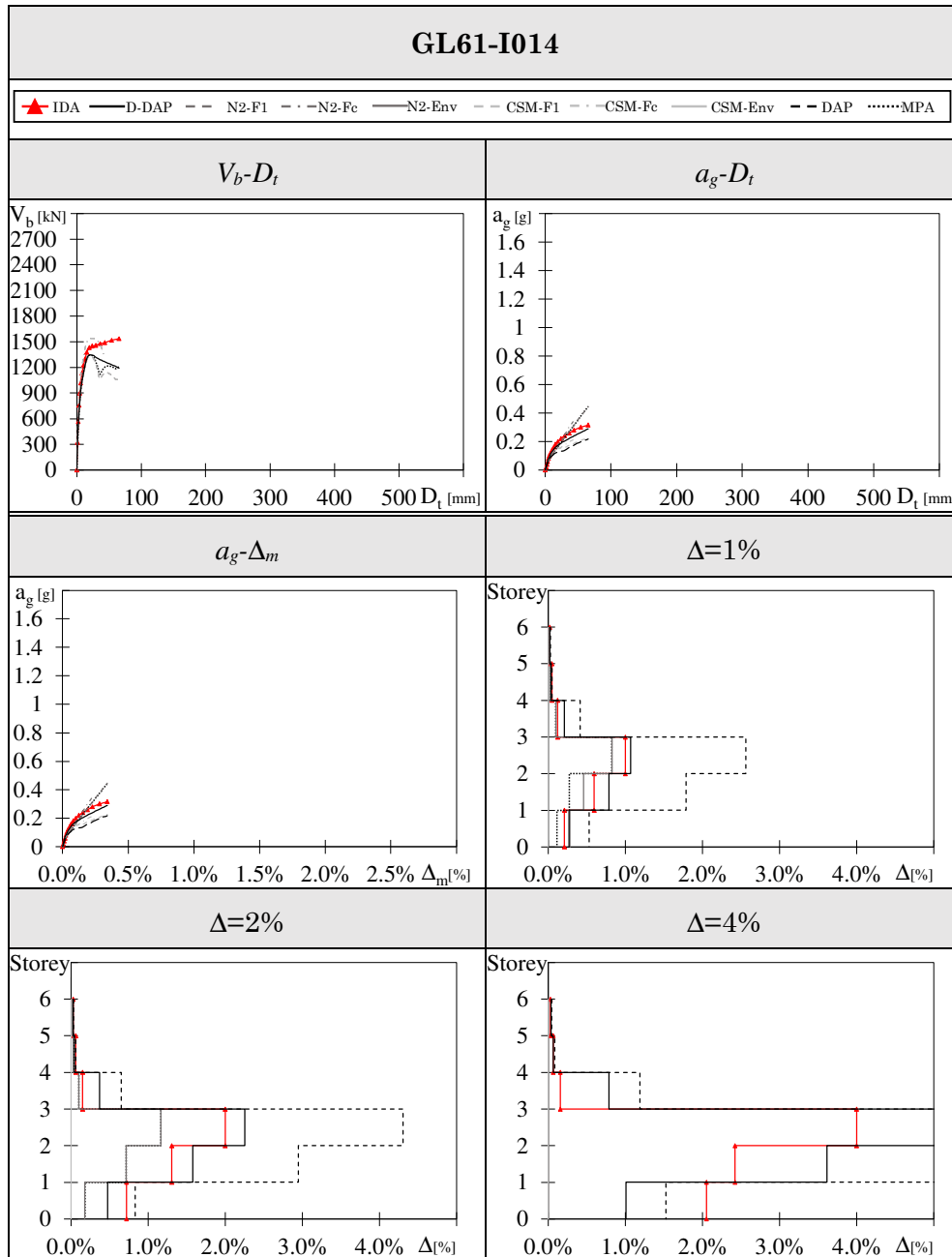
tainment of a maximum storey drift equal to 4%, or a 30% reduction of the maximum base shear of columns. The seismic response obtained by nonlinear static methods of analysis is reported until the top displacement equals the top displacement that in the IDA corresponds to the structural collapse. In case of the V_b - D_t curve, the D-DAP and the DAP provide the same results.

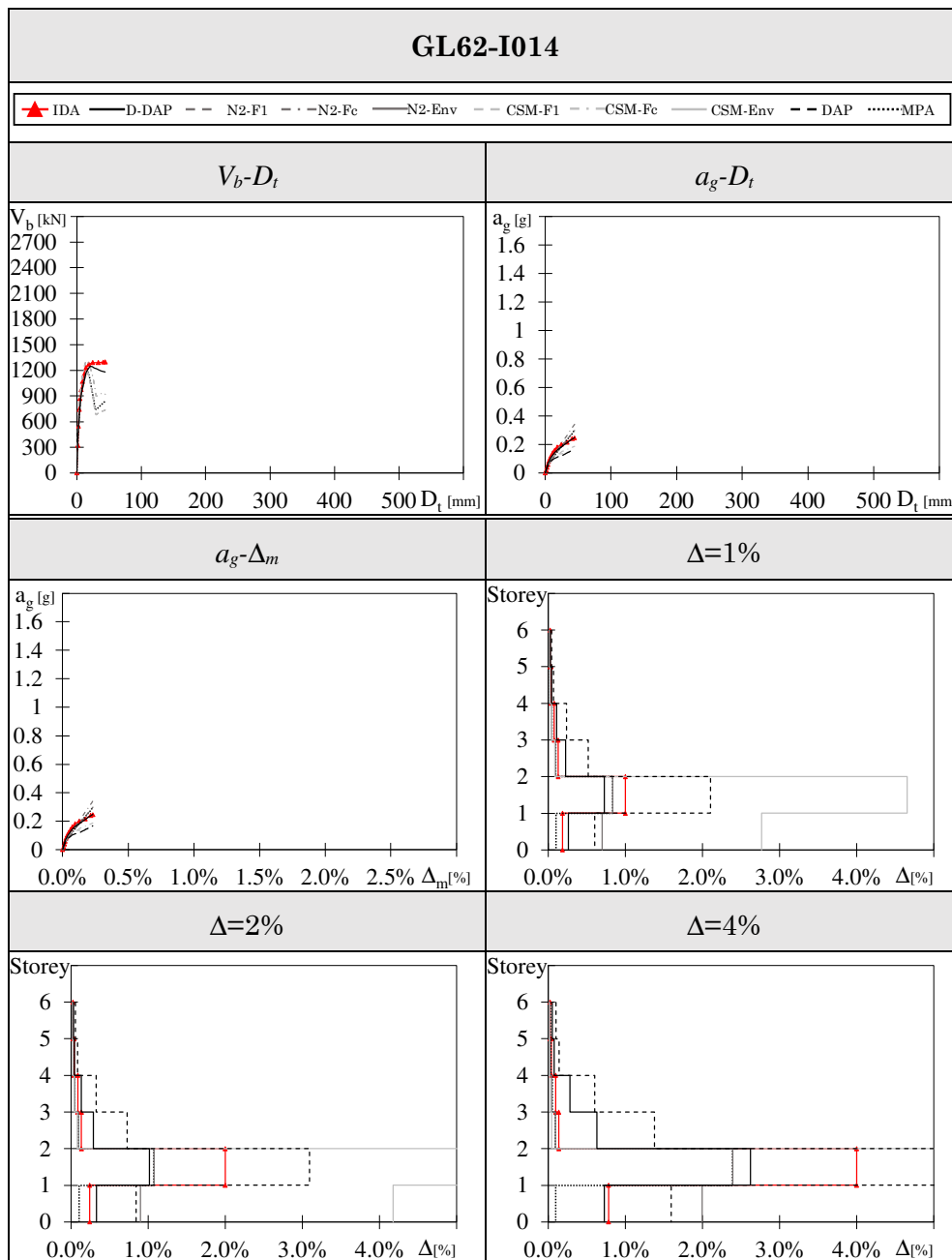
In the following four plots, the seismic response of the frame is presented in terms of local parameters. In particular, in the third plot the average drift Δ_m is calculated at each step as the summation of the drifts at all the storeys, divided by the total number of storeys. Each value of Δ_m is associated to the value of ground acceleration and this relationship is reported in the third plot. All curves stop when the average drift equals the average drift corresponding to the structural collapse in the IDA. The last three figures show the distribution of storey drifts along the height of the considered frame, for three limit states. Three limit states were considered in the IDA (red lines with triangles), i.e. the attainment of a maximum storey drift equal to 1%, 2% and 4%. In each frame, each limit state was reached for a different value of ground acceleration. Fixing the ground acceleration at the value corresponding to the considered limit state in the IDA, the corresponding distribution of storey drift in every frame has been evaluated by the abovementioned nonlinear static methods of analysis. In case of the N2 method or the CSM, the drift at each storey is obtained from the envelope of the drifts obtained with the distribution of forces proportional to the first mode and proportional to storey masses.

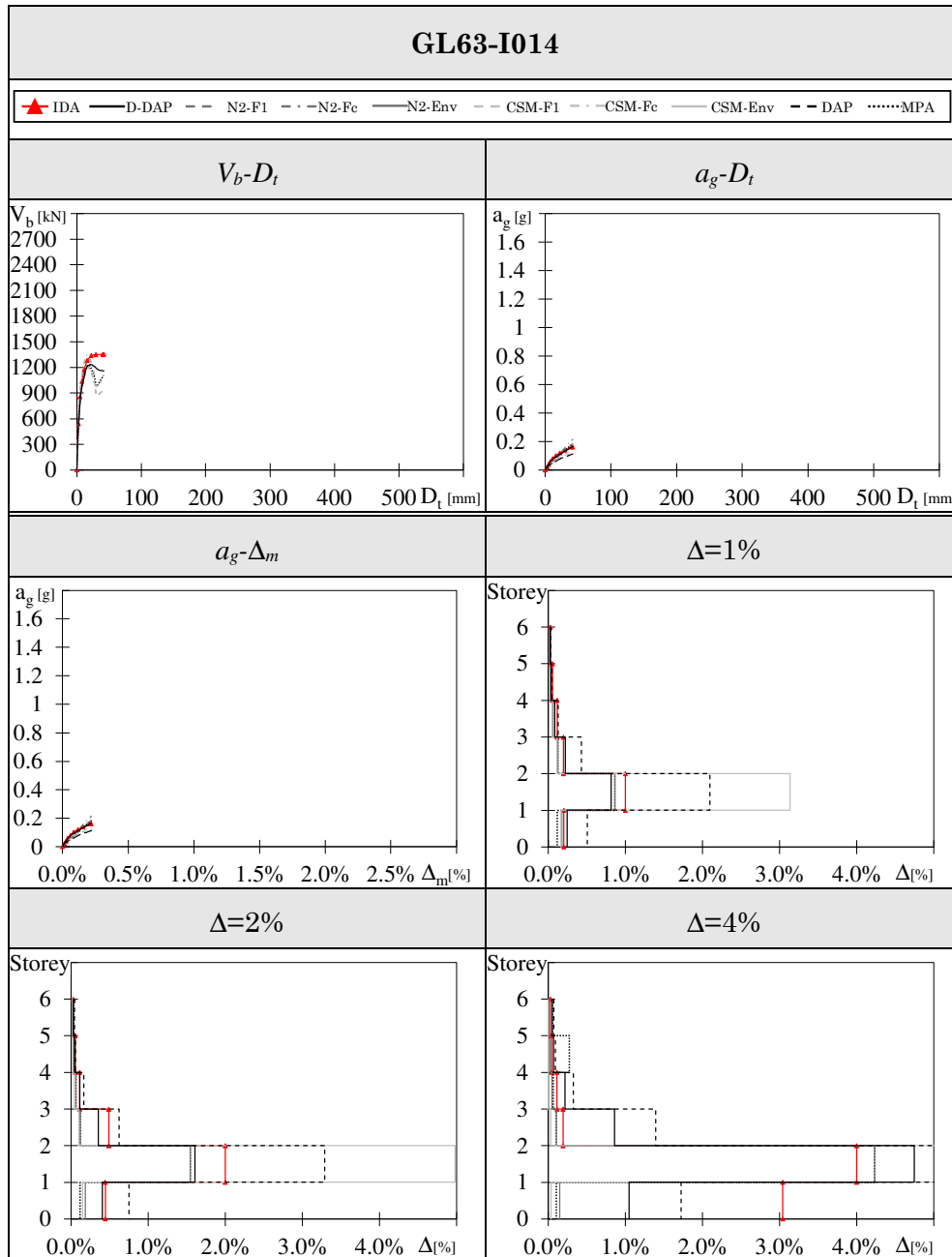


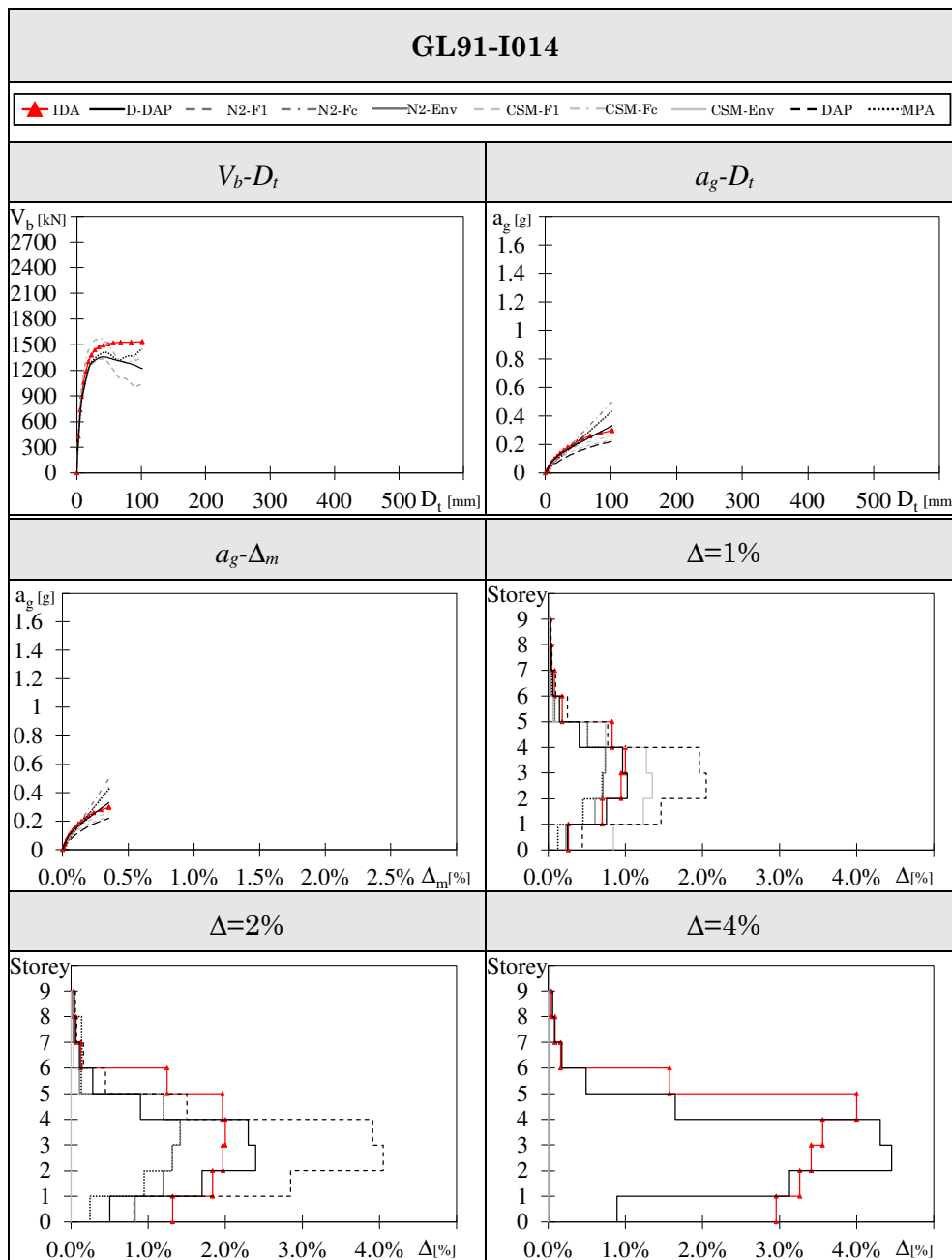


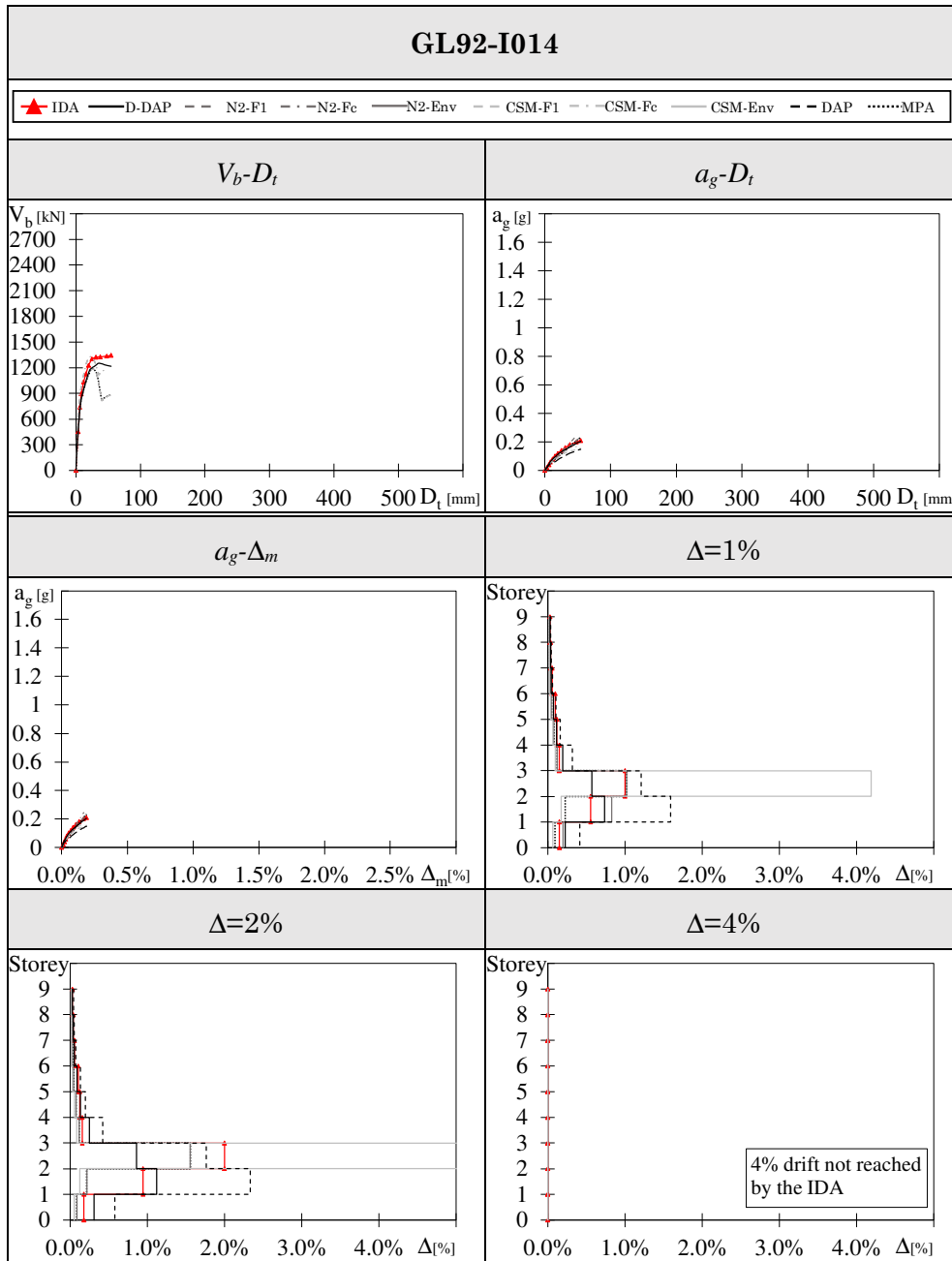


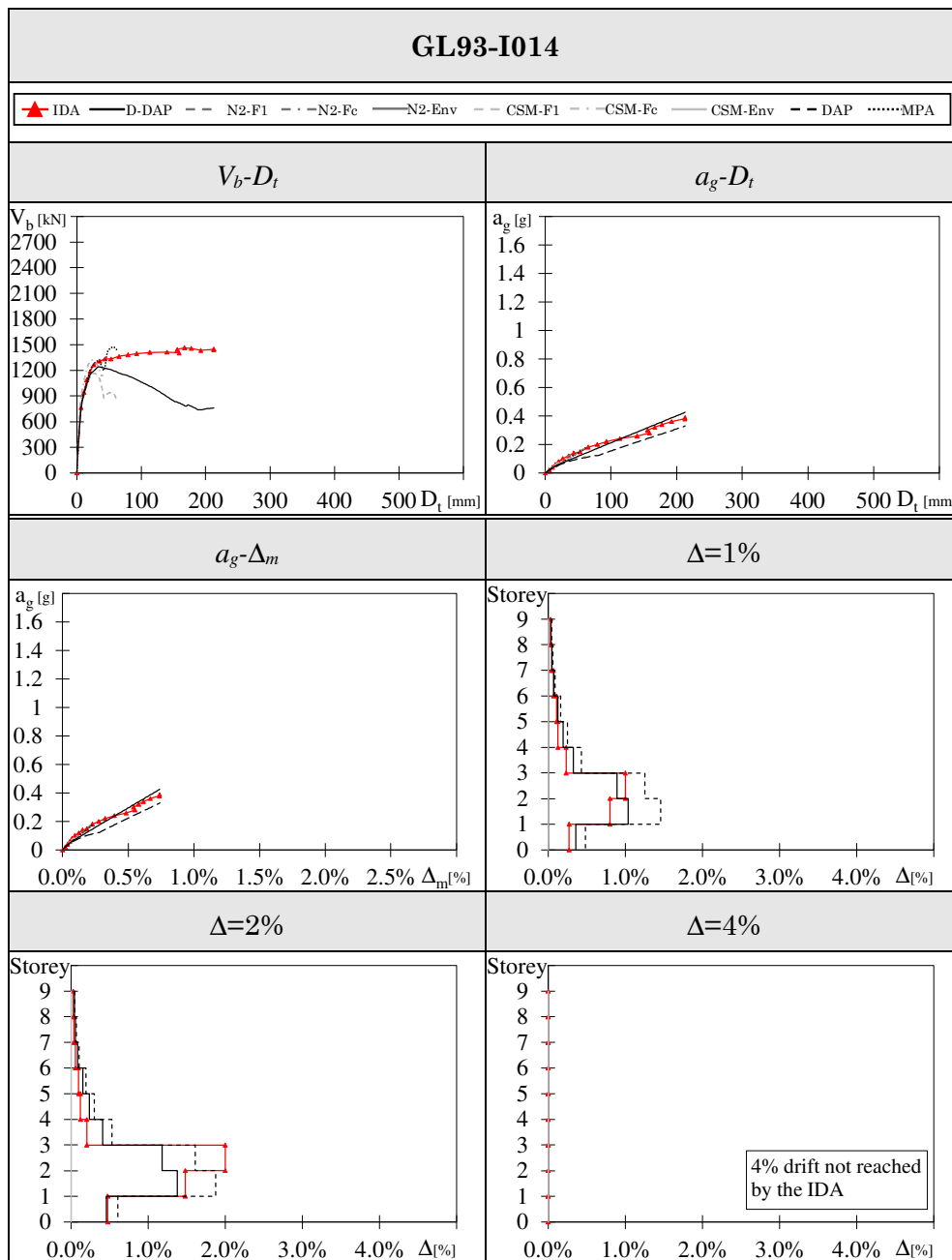


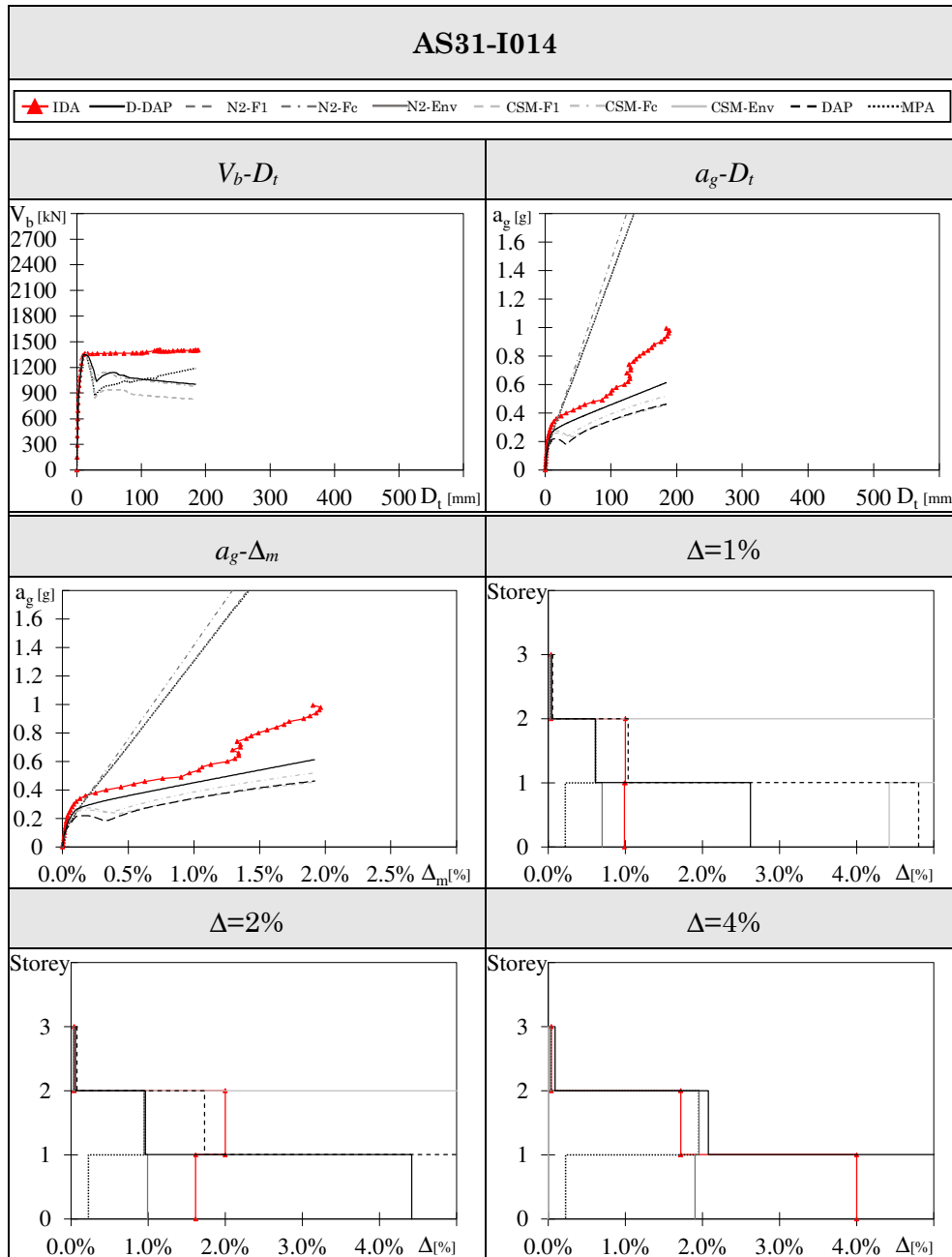


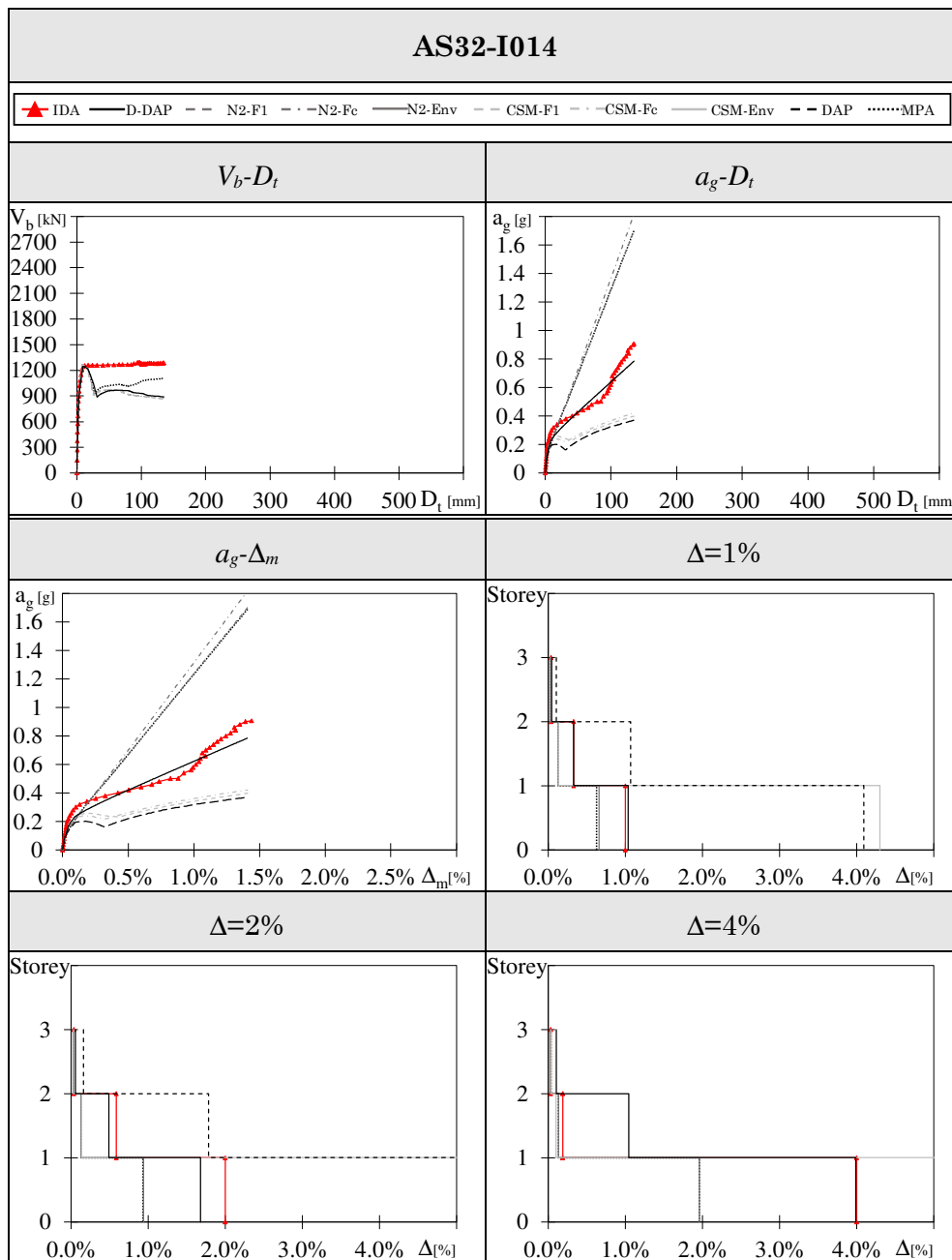


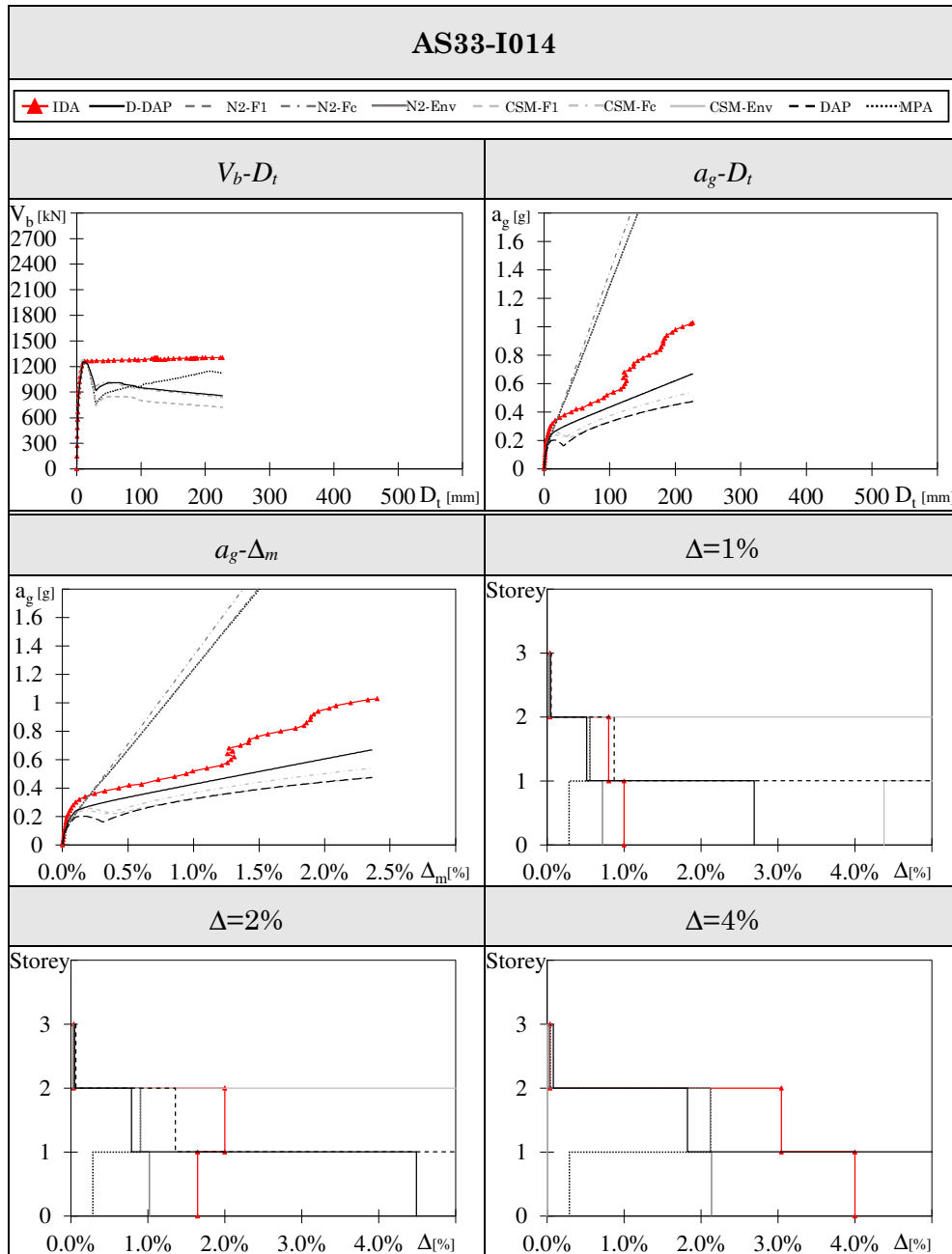


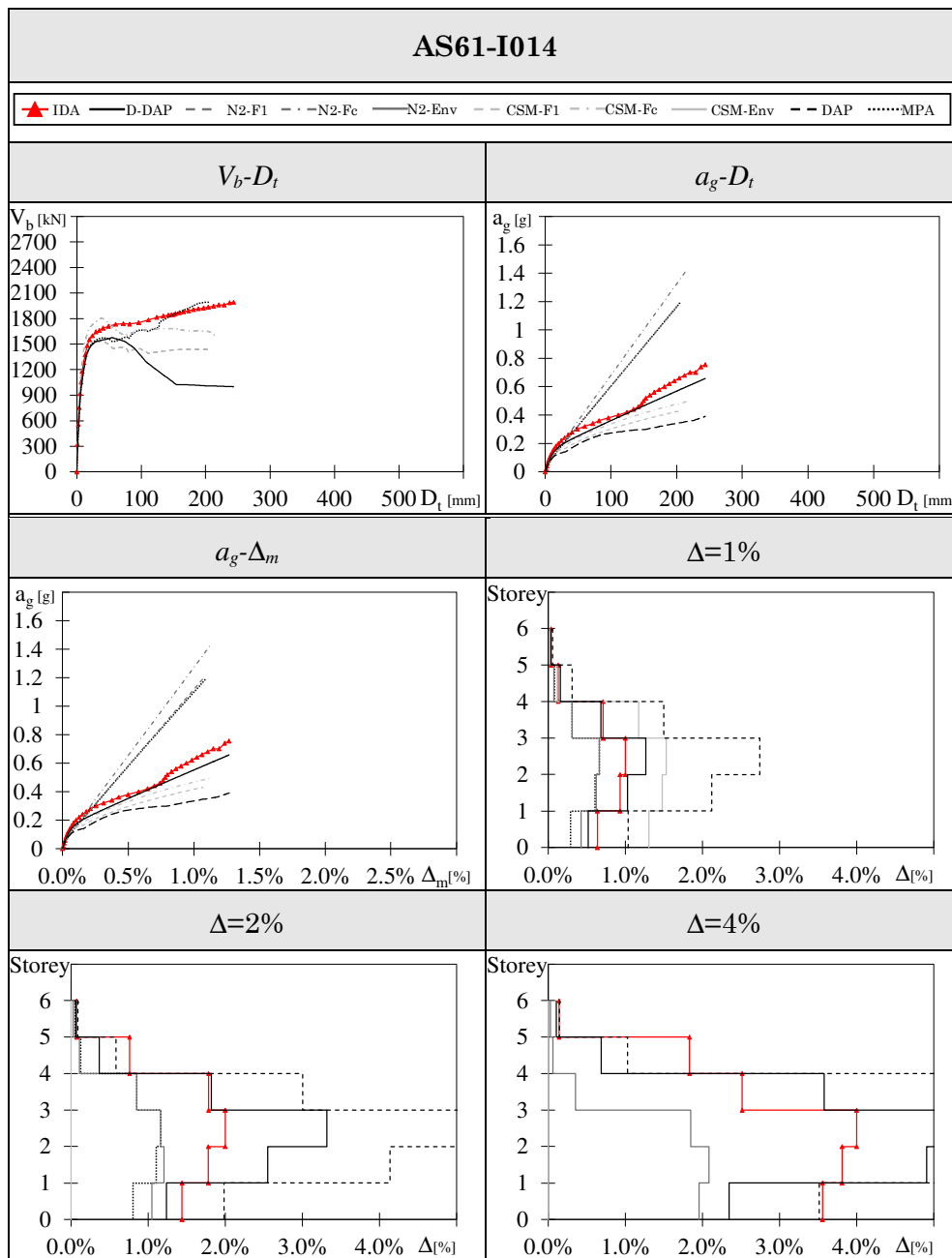


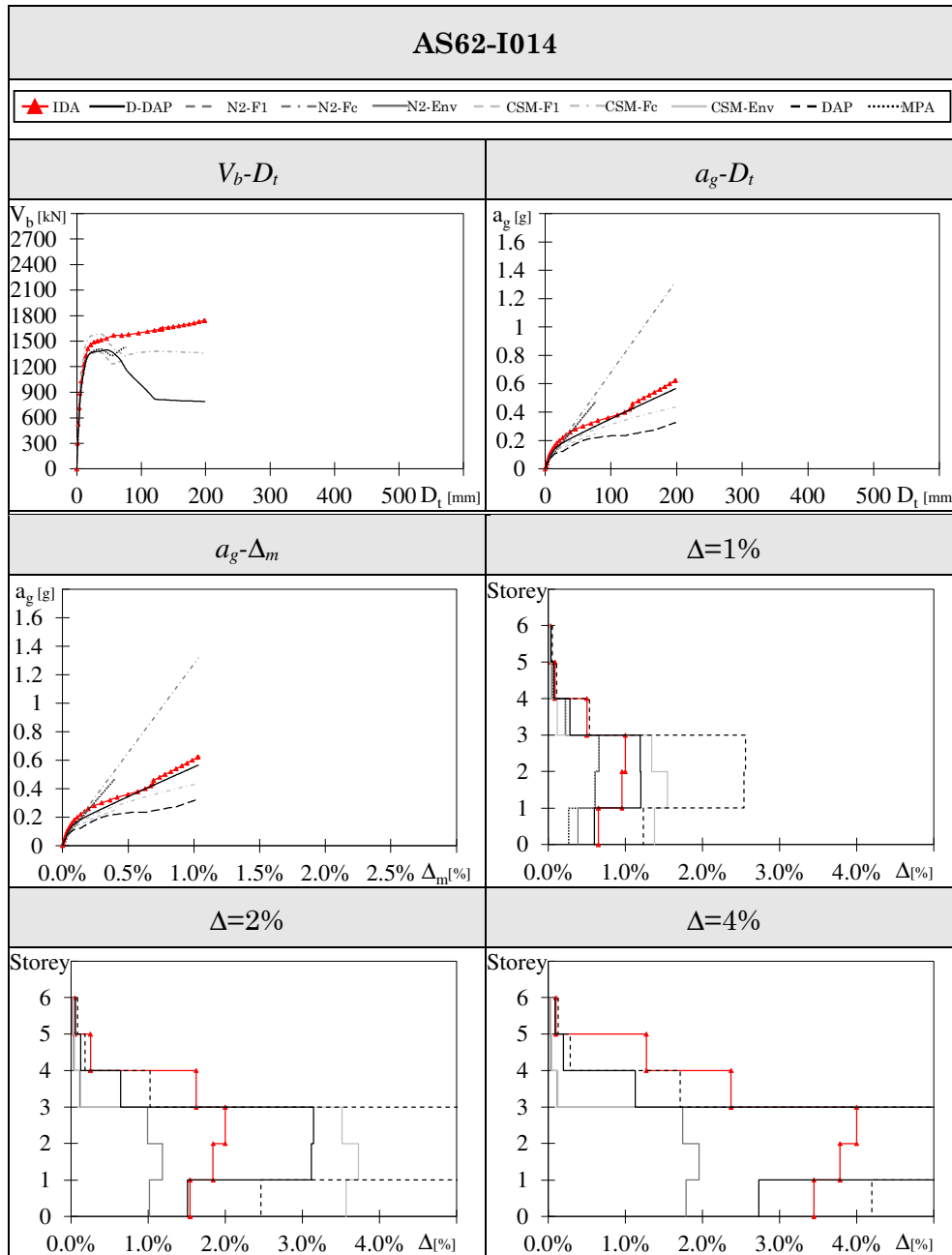


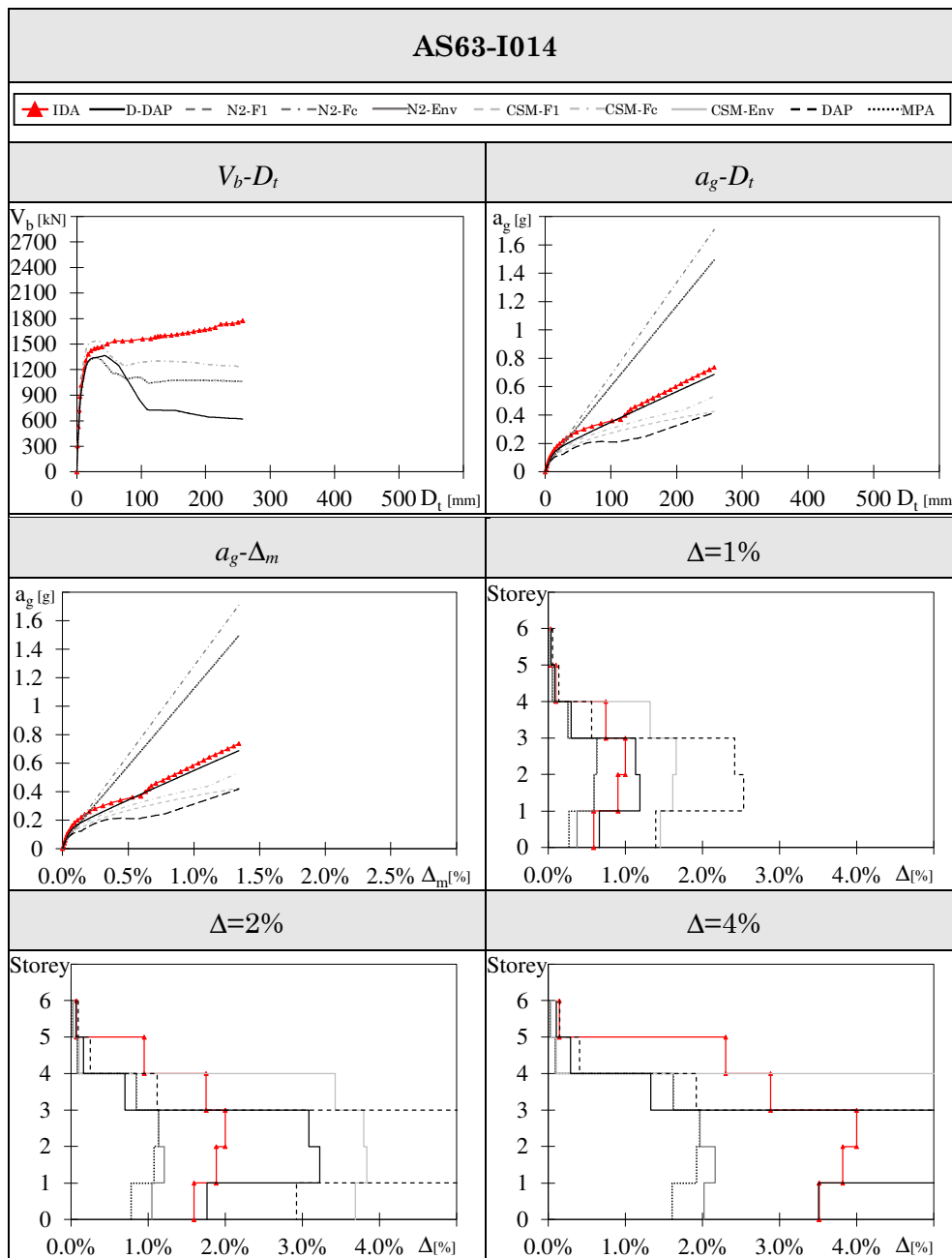


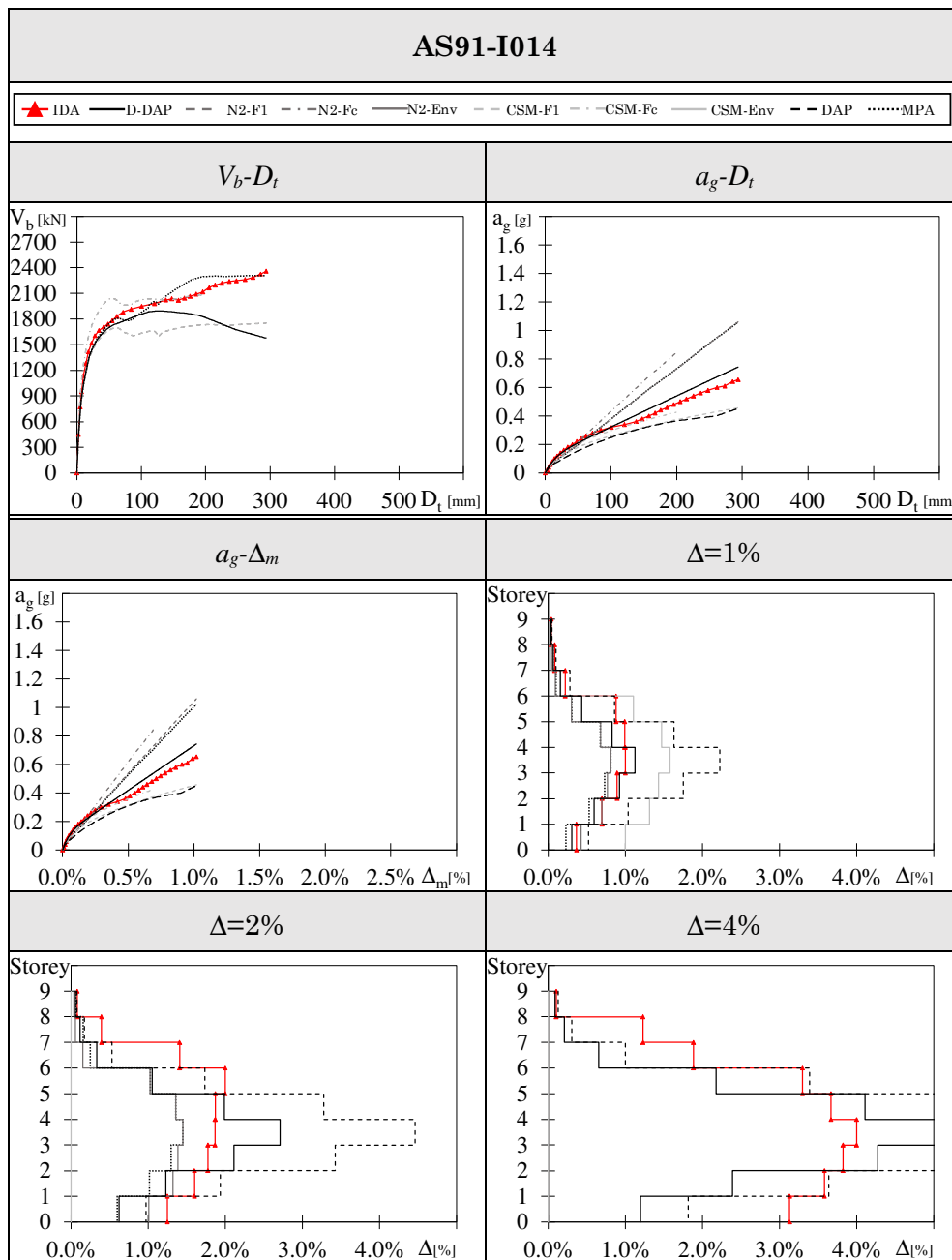


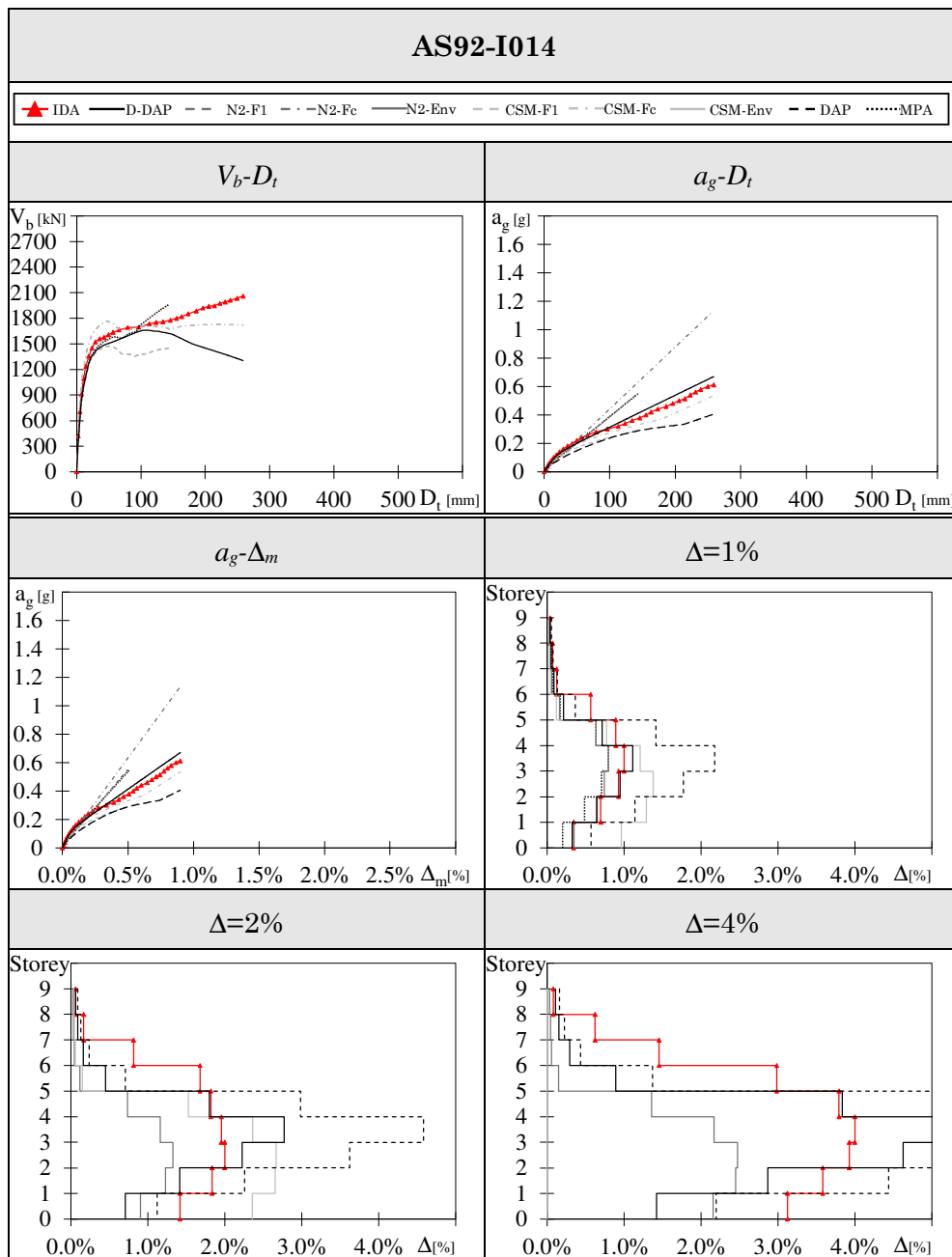


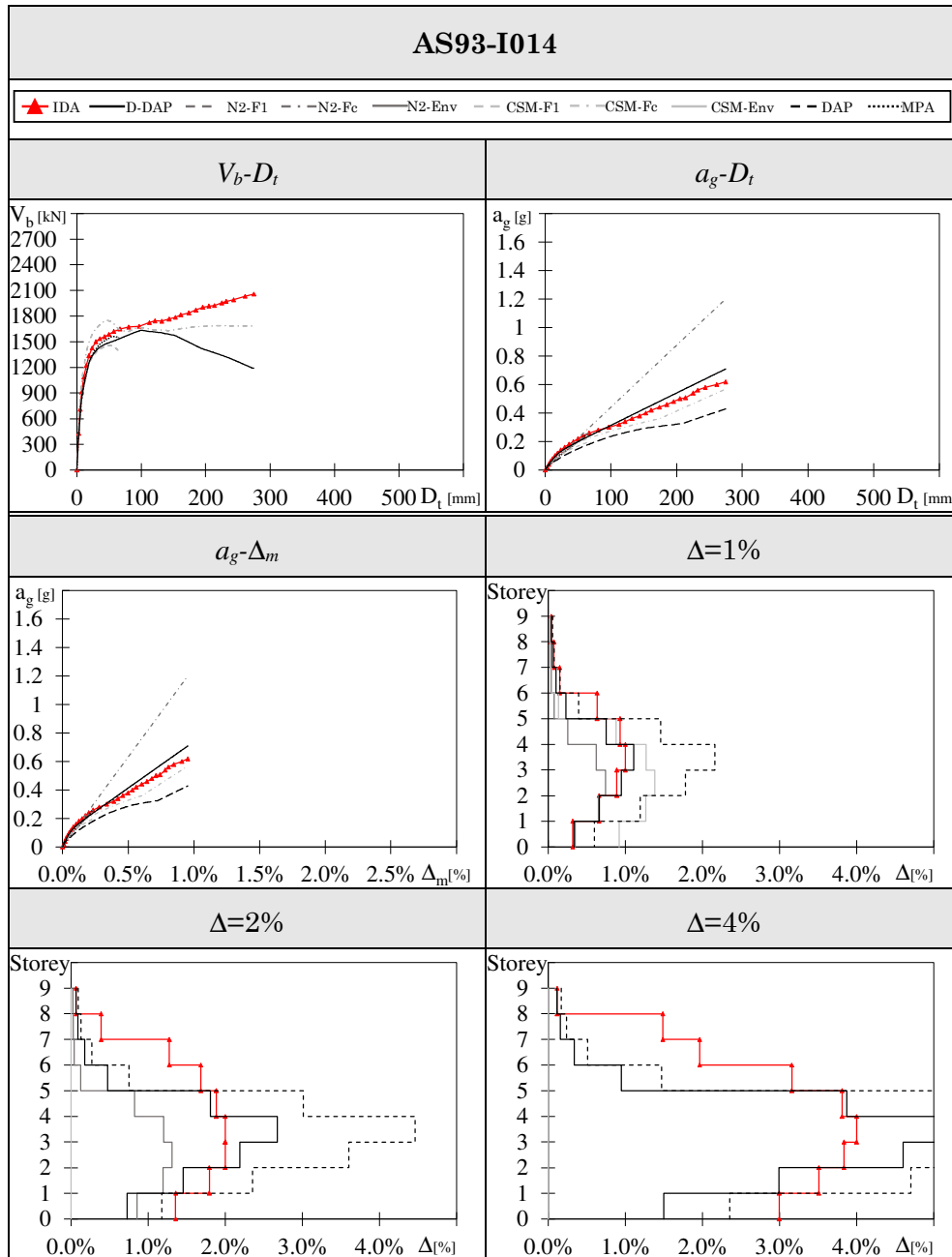












Appendix E

This appendix shows the seismic response of the case study frames with infill panels with large stiffness and strength (indicated by the suffix I028). The seismic behaviour of each case study frame is evaluated by the Incremental Dynamic Analysis (IDA), which is assumed as reference target (red lines with triangles). The seismic response of every frame is also predicted by:

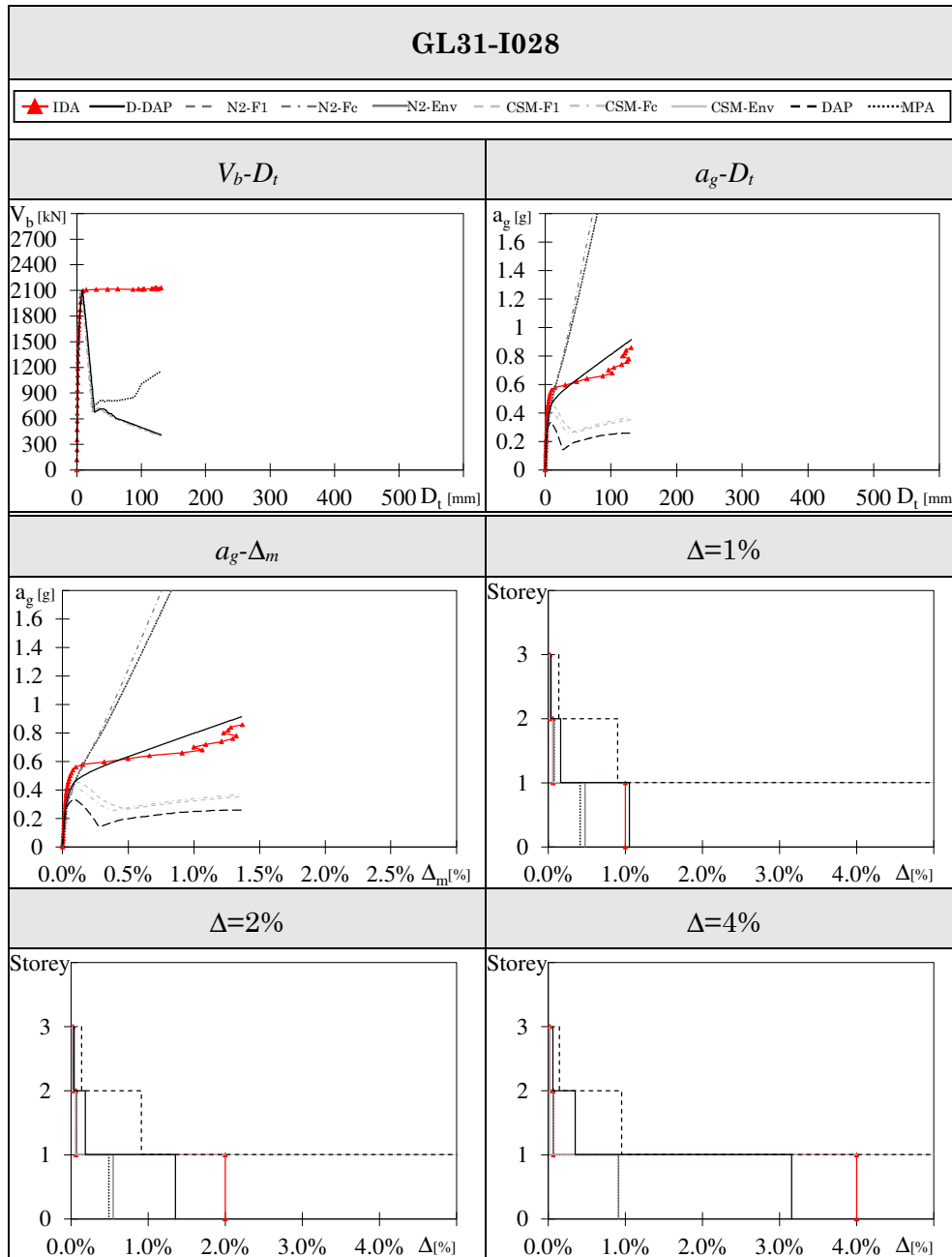
- the proposed D-DAP (black continuous line)
- the N2 method (dark grey line)
- the CSM (light grey line)
- the DAP by Pinho (black dashed line)
- the MPA (black dotted line)

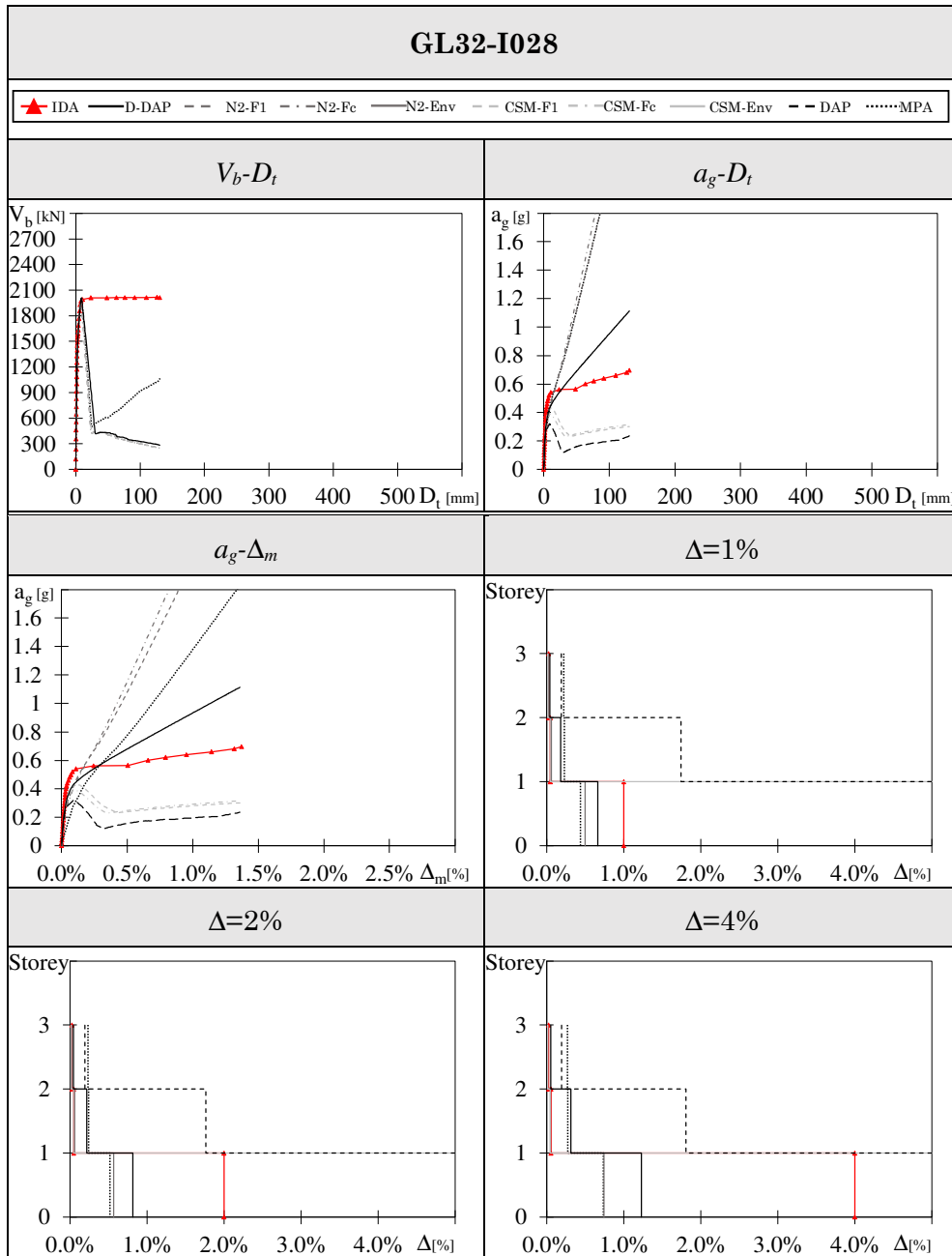
The N2 method and the CSM are applied considering a distribution of forces proportional to the first elastic mode of vibration (dashed line) and a distribution of forces proportional to seismic masses (dashed dotted line), as suggested by EC8. The seismic response provided by the nonlinear static methods of analysis is compared to that predicted by the IDA, to evaluate the accuracy of the considered nonlinear static methods of analysis.

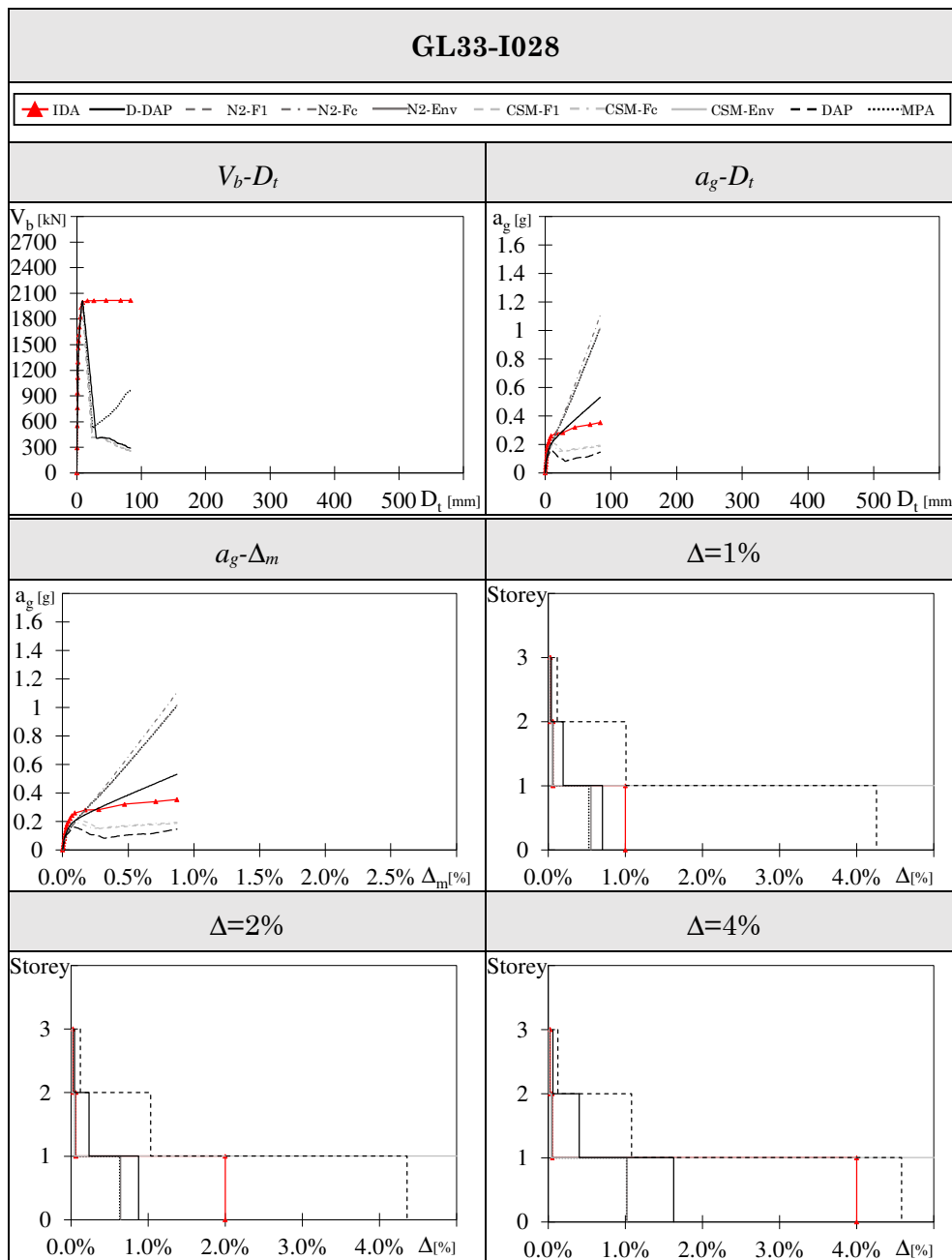
For each frame, the seismic response evaluated by all those nonlinear methods of analysis is reported in six plots. In the first two plots, the performance curve of the relevant frame is showed in terms of global response parameters, i.e. base shear and top displacement (V_b-D_t), and peak ground acceleration and top displacement (a_g-D_t). For every frame, the seismic response provided by the IDA is reported until the attainment of the structural collapse, which is identified with the at-

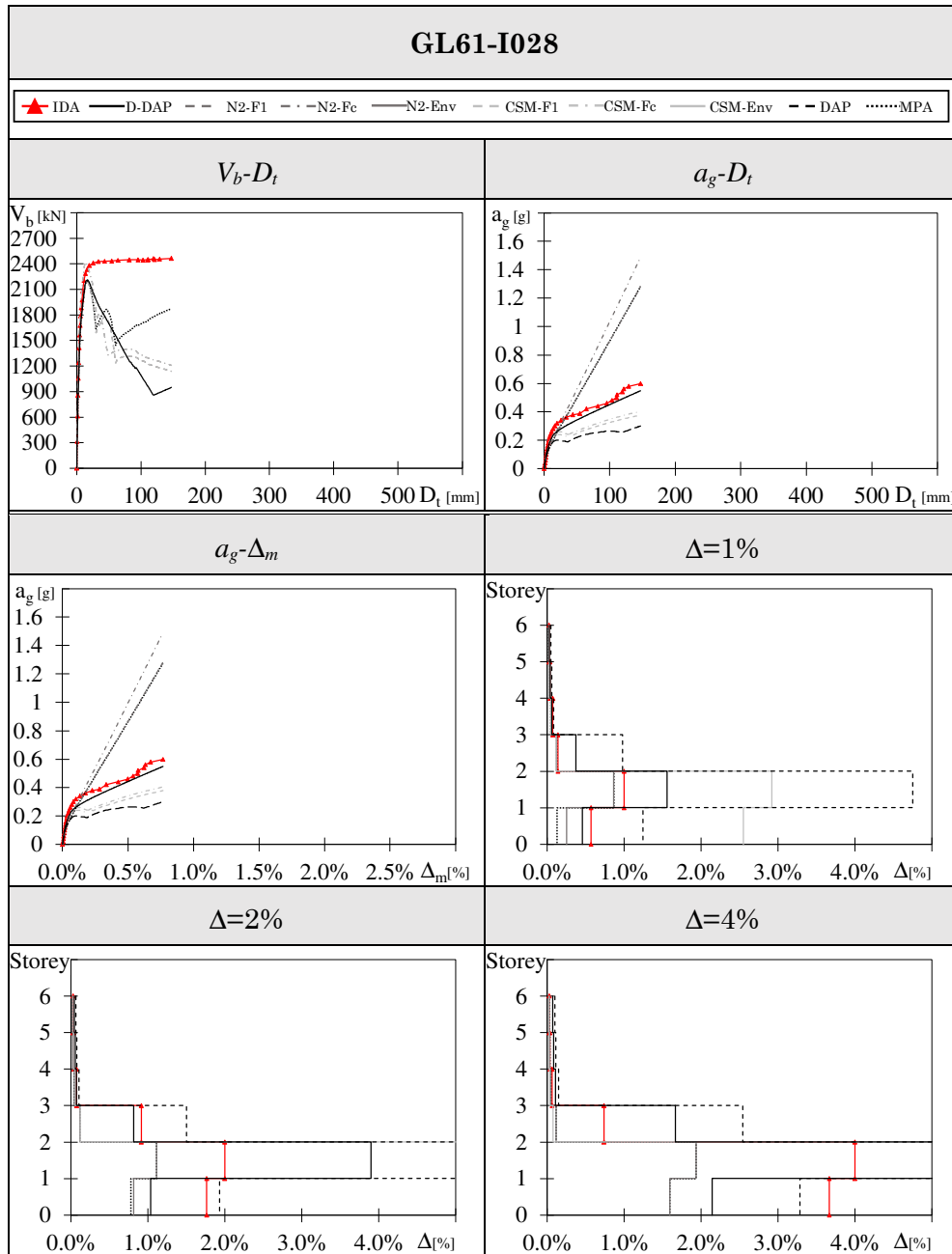
tainment of a maximum storey drift equal to 4%, or a 30% reduction of the maximum base shear of columns. The seismic response obtained by nonlinear static methods of analysis is reported until the top displacement equals the top displacement that in the IDA corresponds to the structural collapse. In case of the V_b - D_t curve, the D-DAP and the DAP provide the same results.

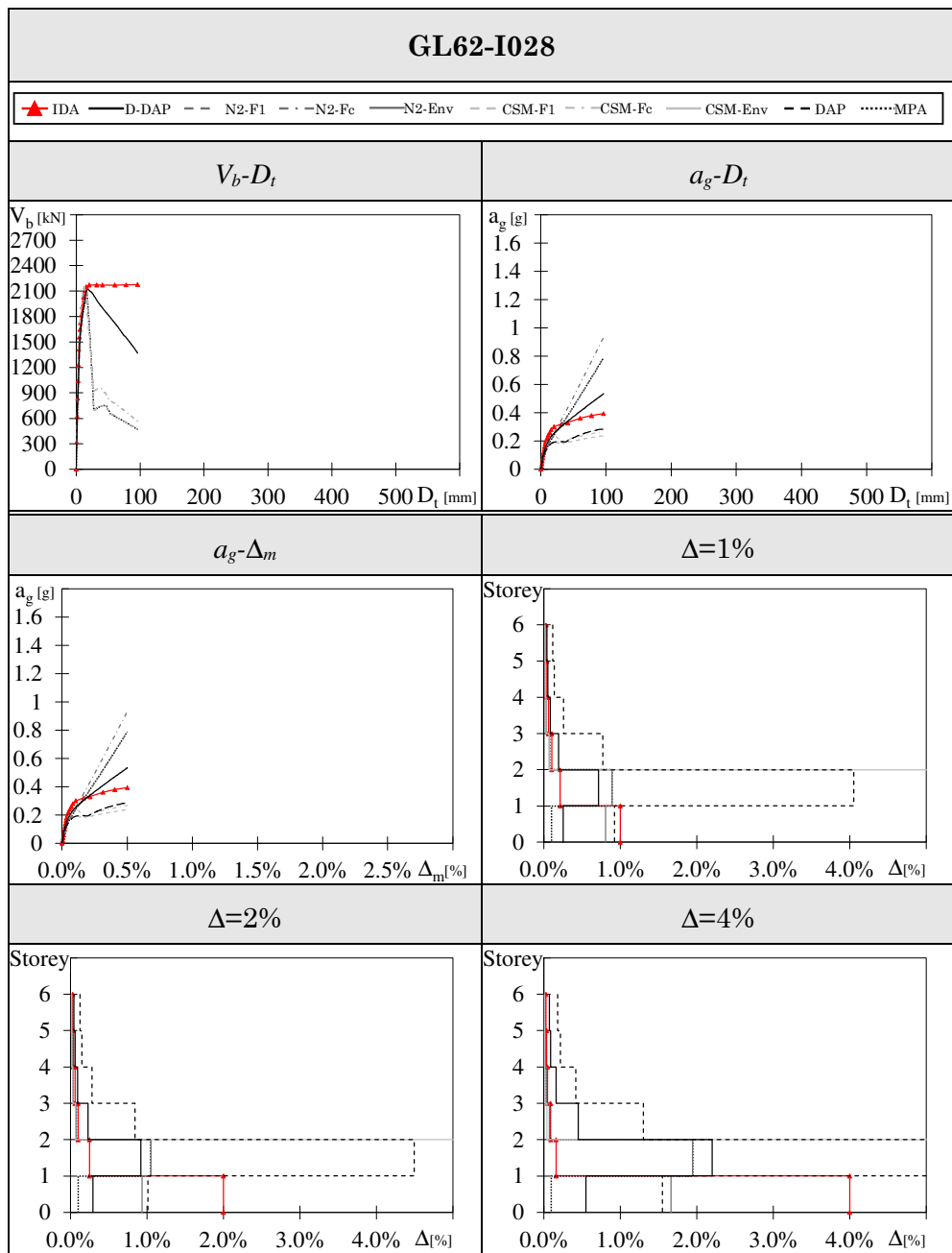
In the following four plots, the seismic response of the frame is presented in terms of local parameters. In particular, in the third plot the average drift Δ_m is calculated at each step as the summation of the drifts at all the storeys, divided by the total number of storeys. Each value of Δ_m is associated to the value of ground acceleration and this relationship is reported in the third plot. All curves stop when the average drift equals the average drift corresponding to the structural collapse in the IDA. The last three figures show the distribution of storey drifts along the height of the considered frame, for three limit states. Three limit states were considered in the IDA (red lines with triangles), i.e. the attainment of a maximum storey drift equal to 1%, 2% and 4%. In each frame, each limit state was reached for a different value of ground acceleration. Fixing the ground acceleration at the value corresponding to the considered limit state in the IDA, the corresponding distribution of storey drift in every frame has been evaluated by the abovementioned nonlinear static methods of analysis. In case of the N2 method or the CSM, the drift at each storey is obtained from the envelope of the drifts obtained with the distribution of forces proportional to the first mode and proportional to storey masses.

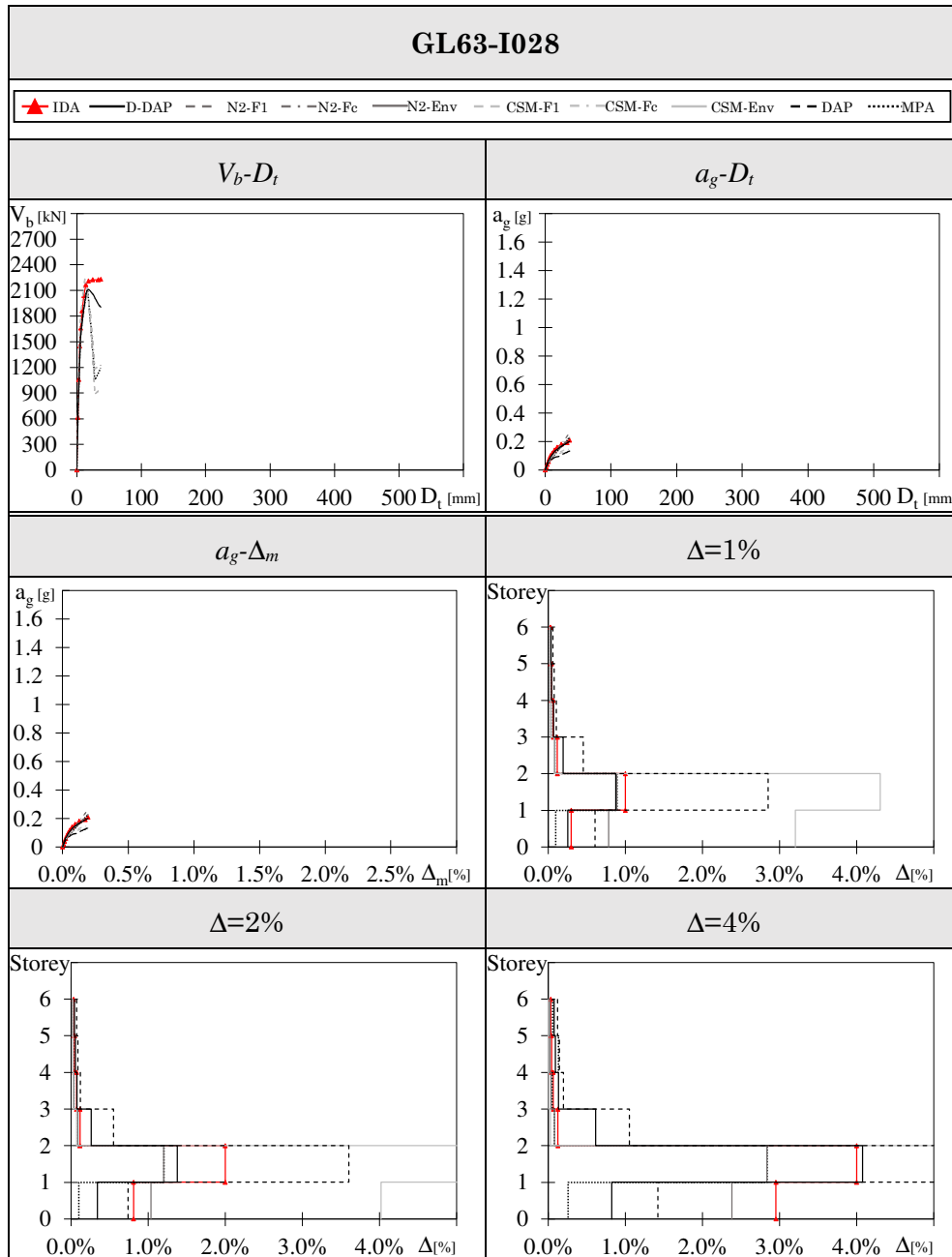


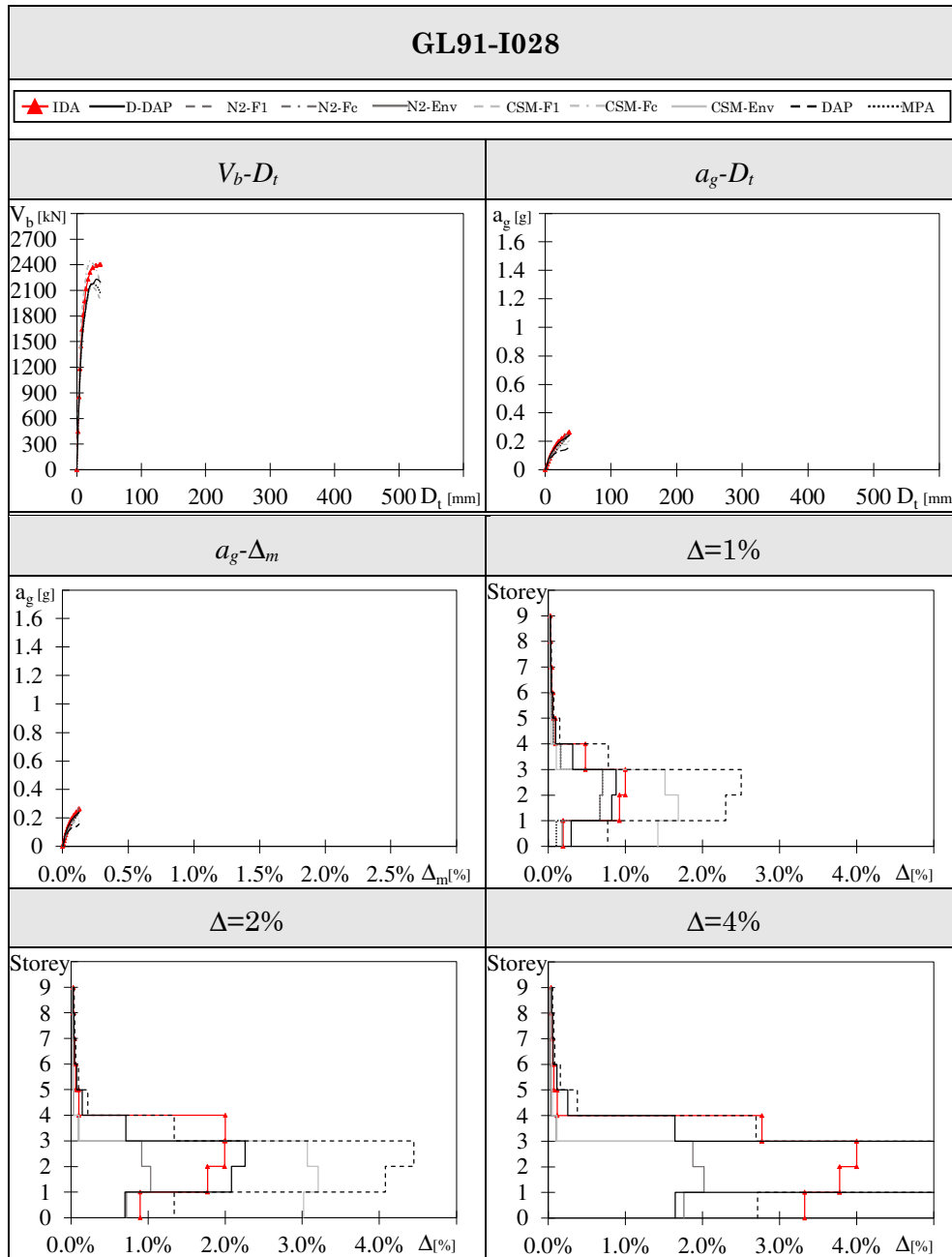


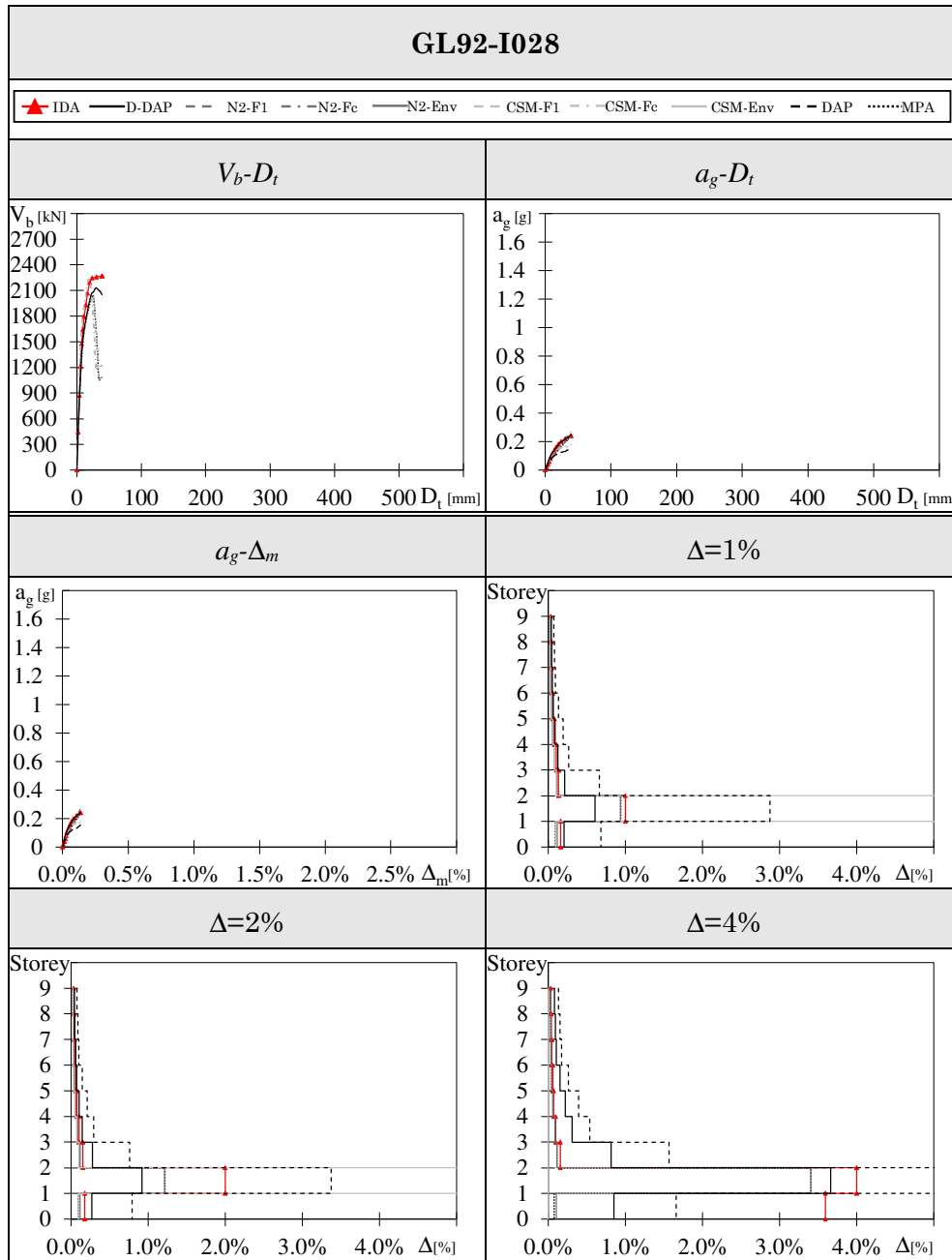


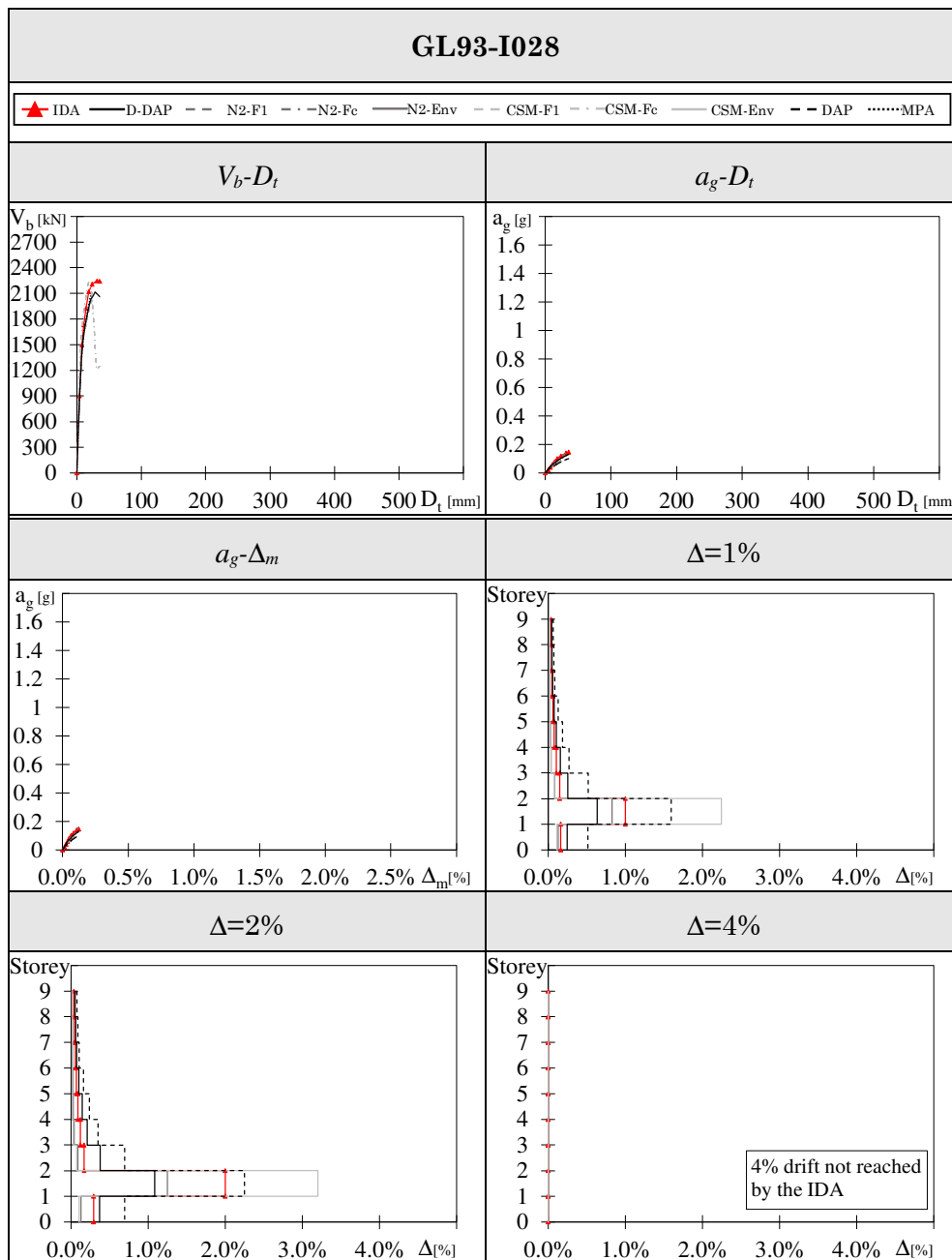


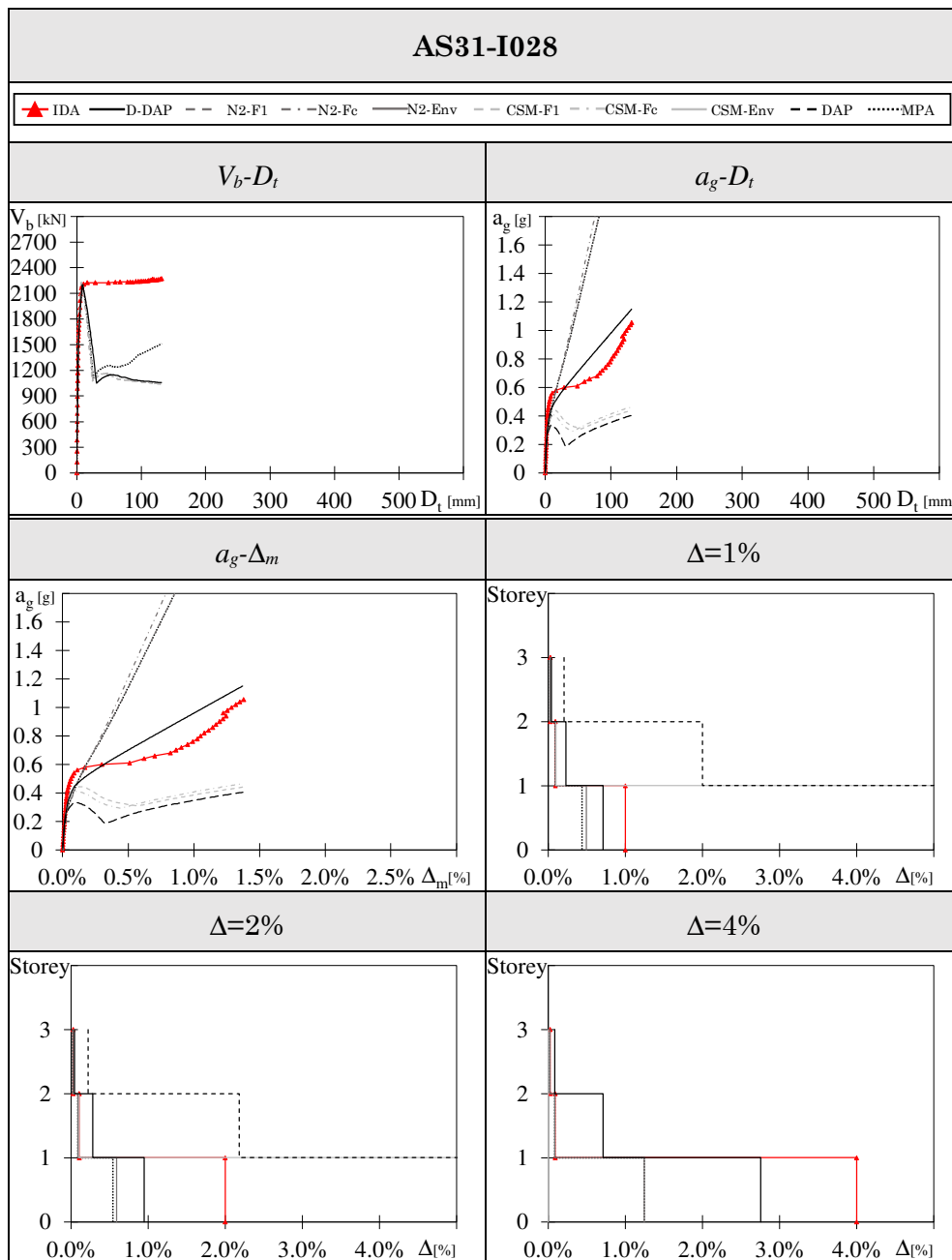


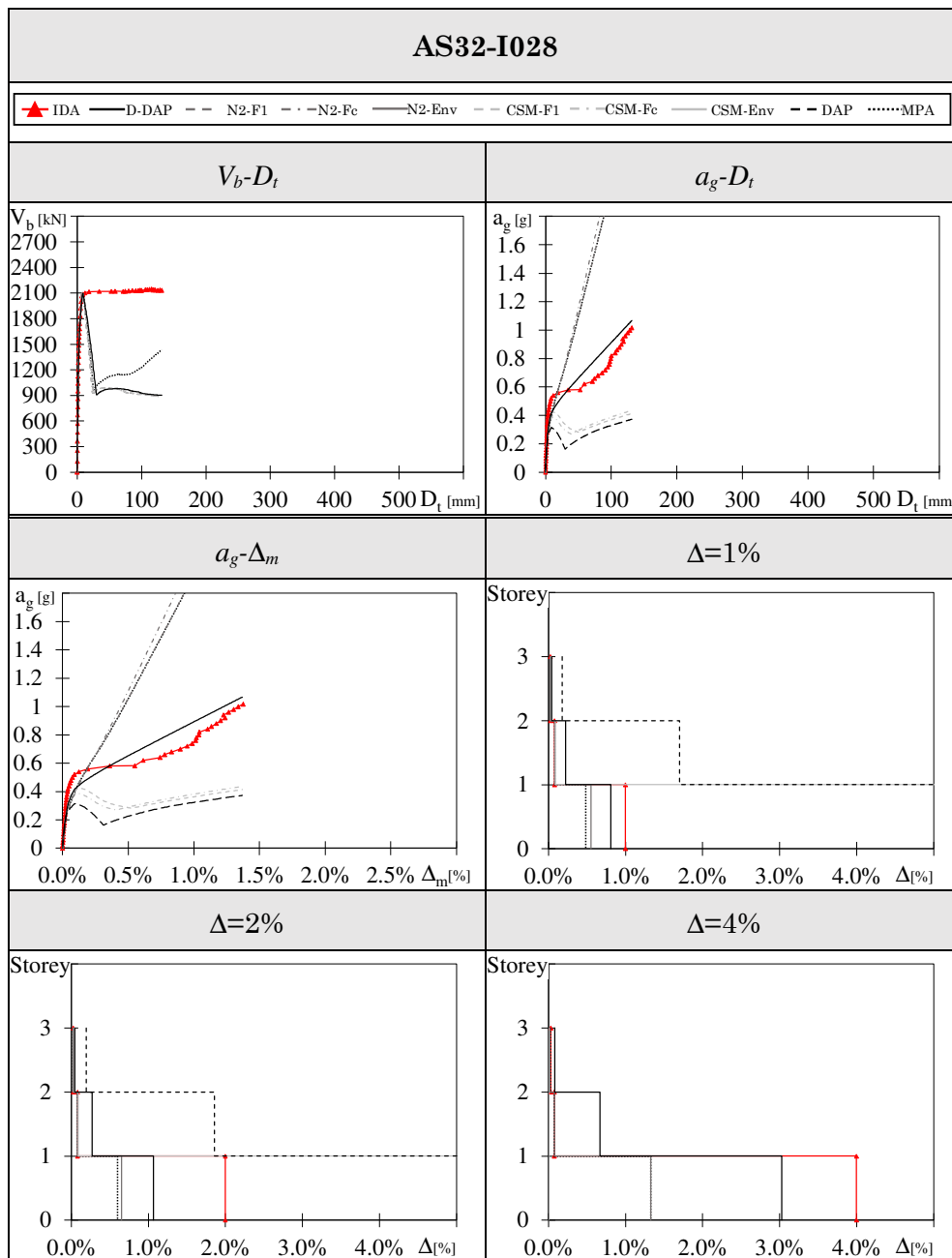


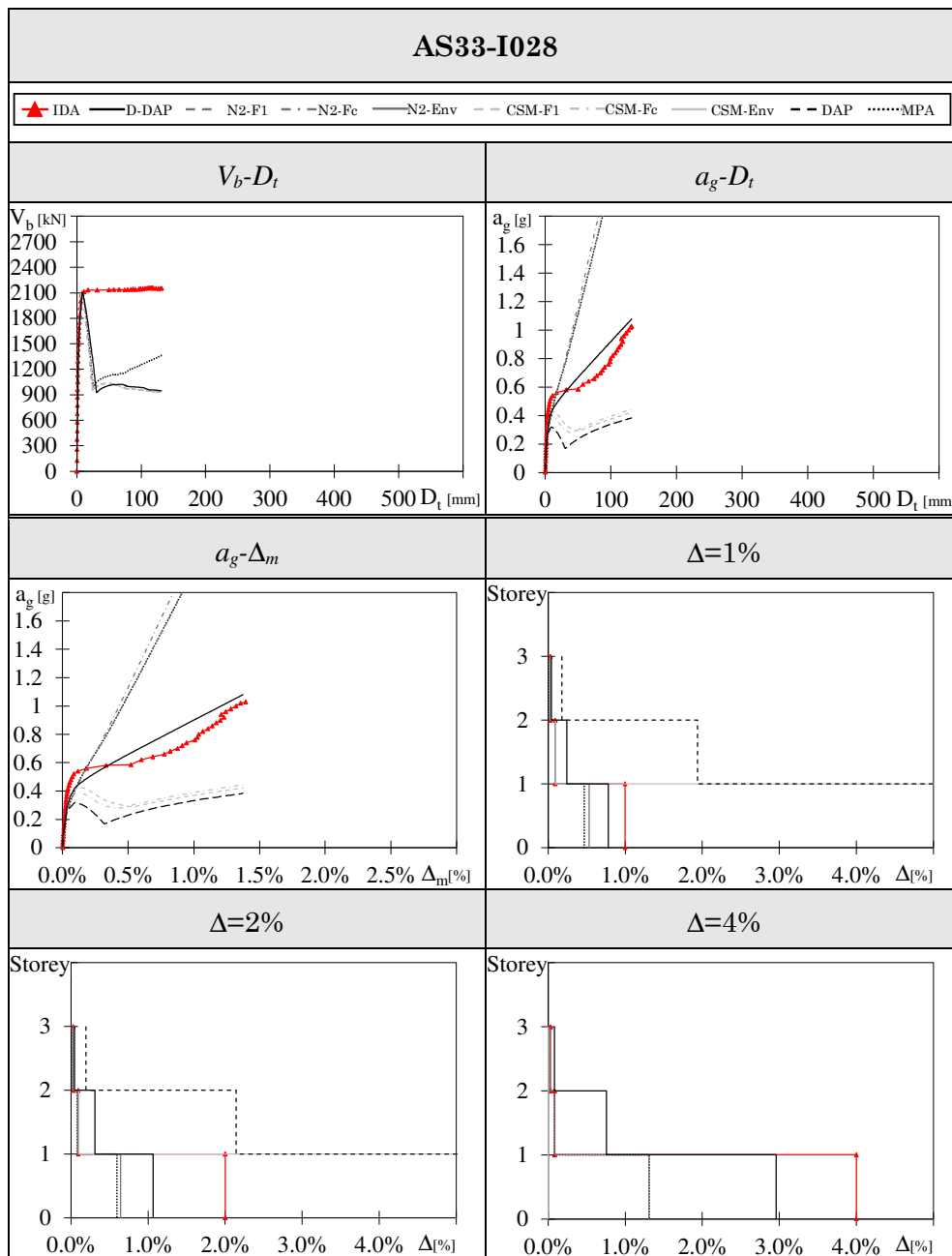


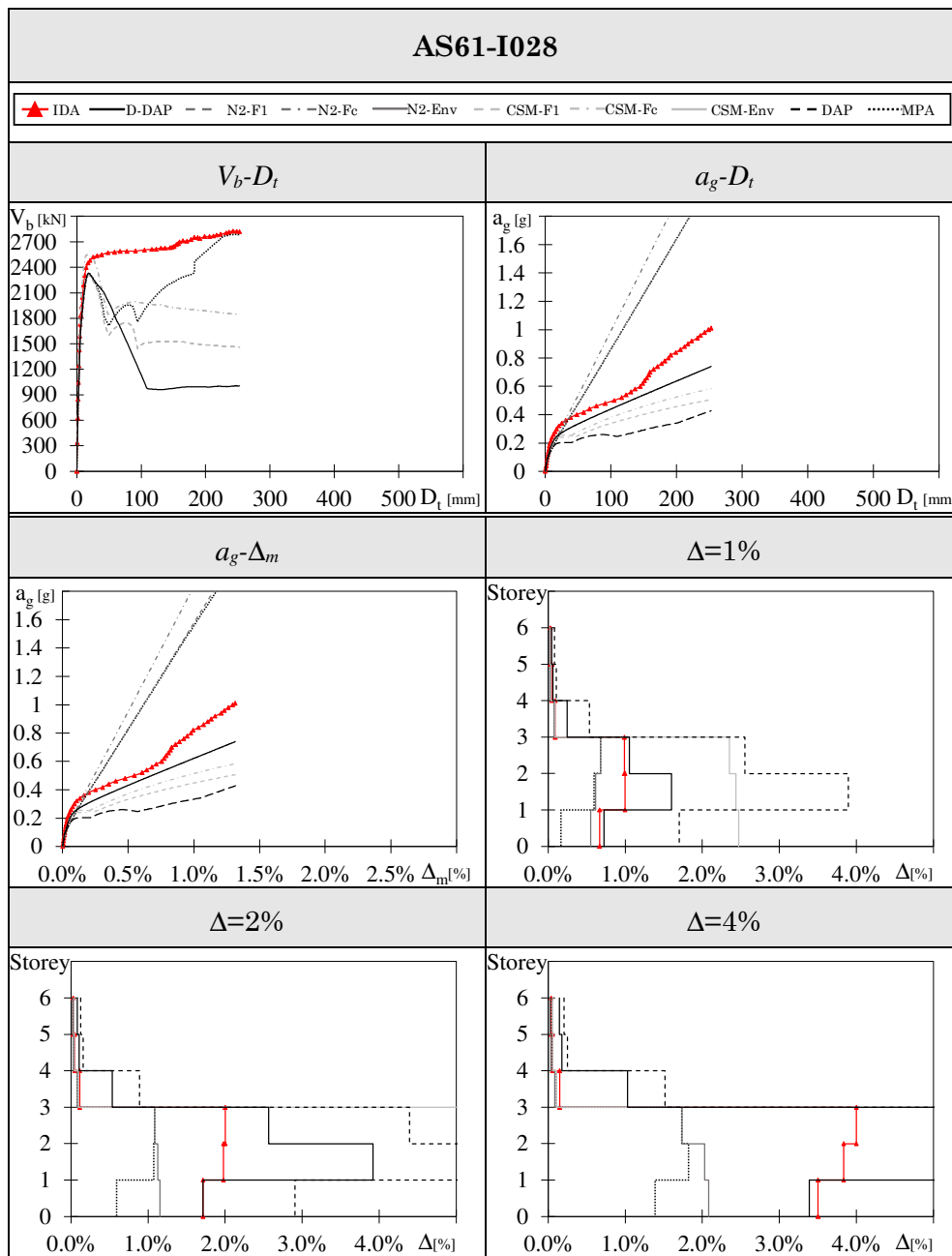


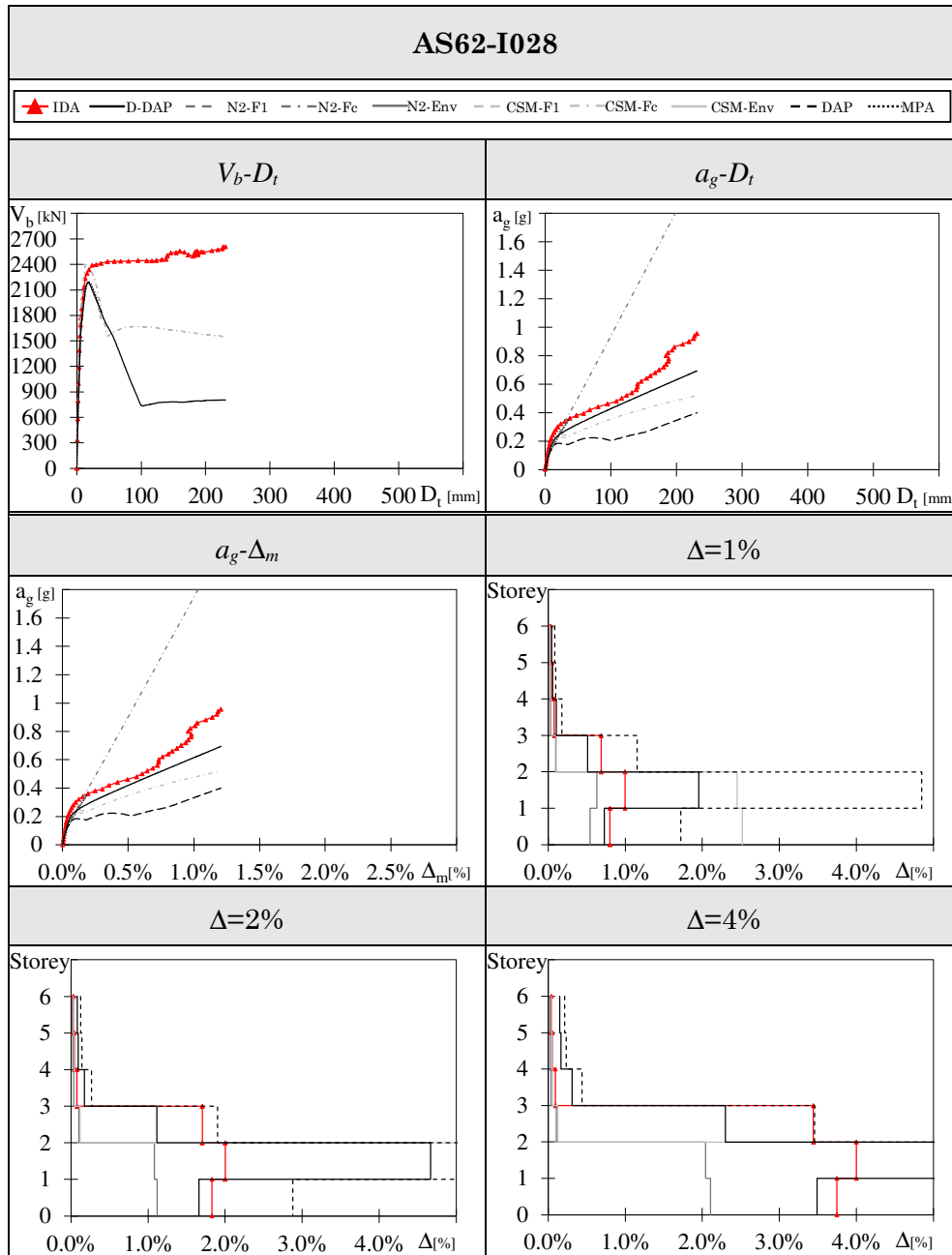


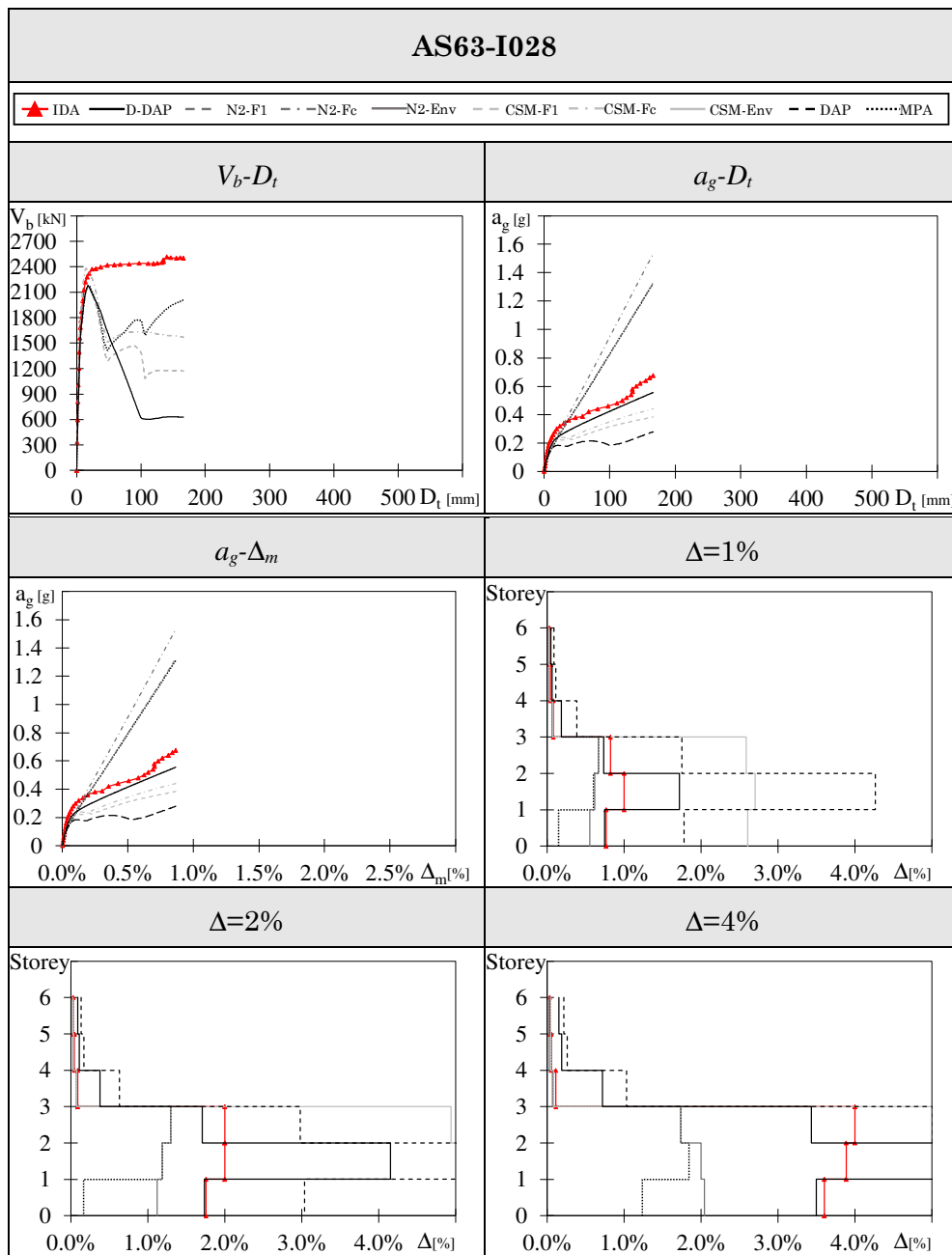


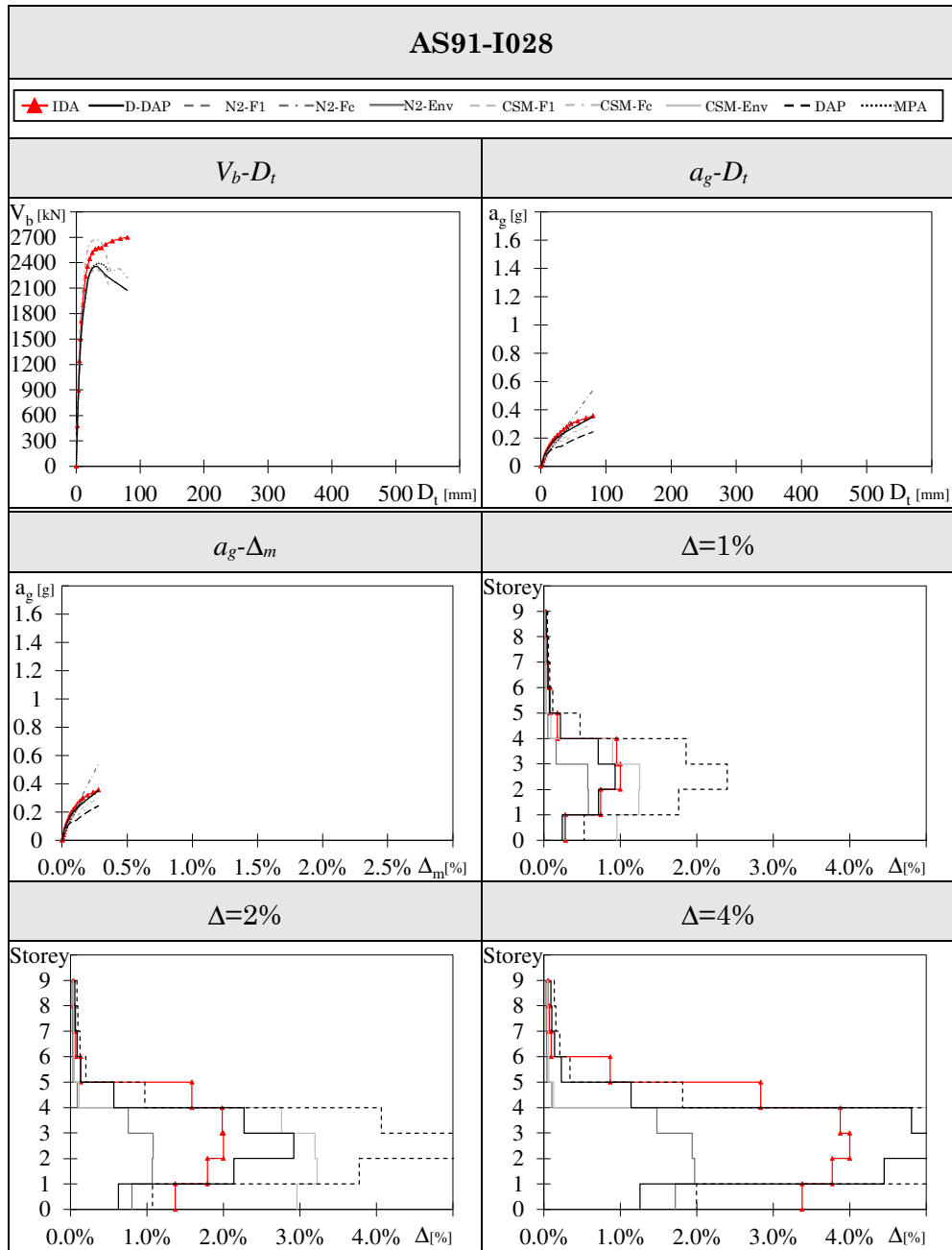


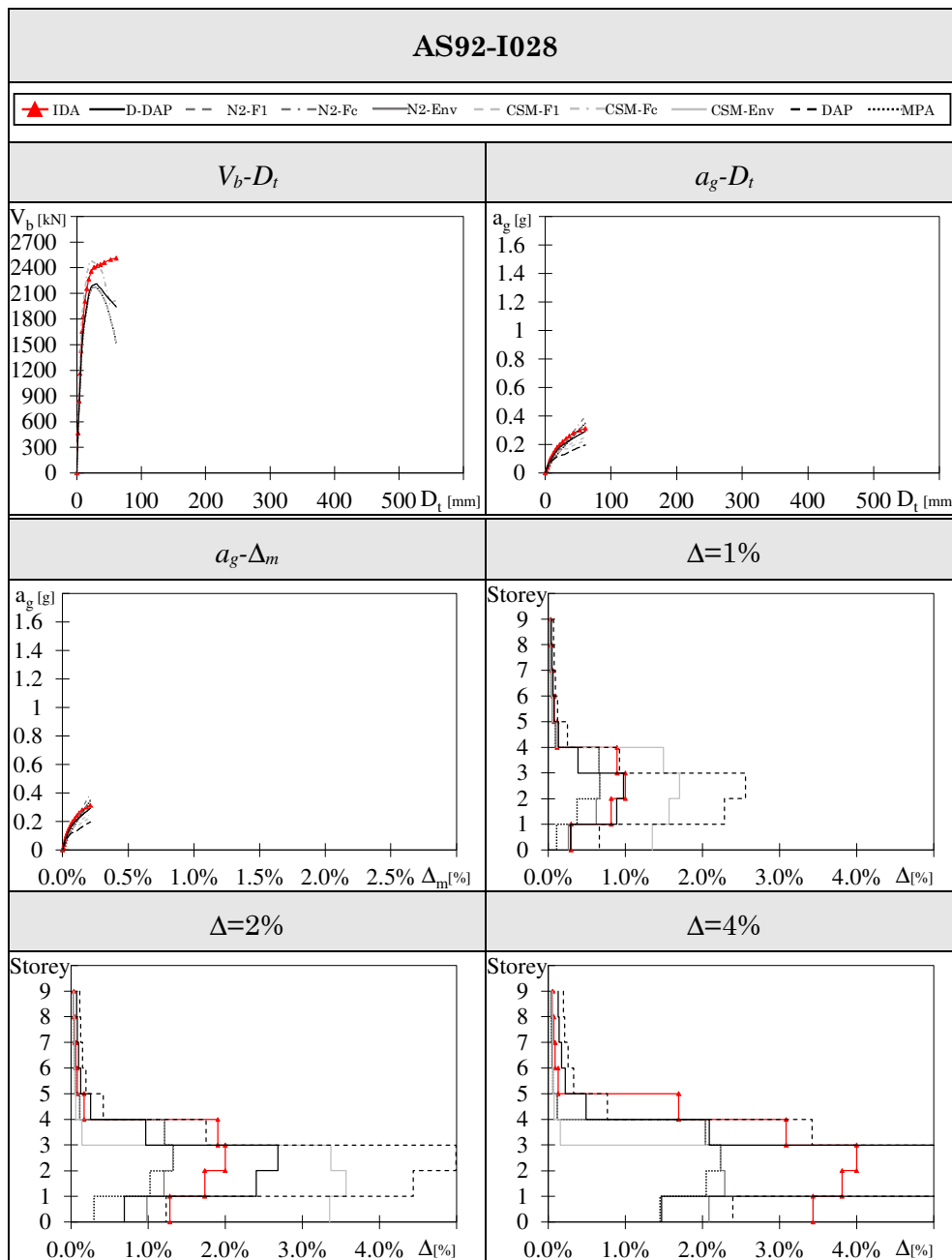


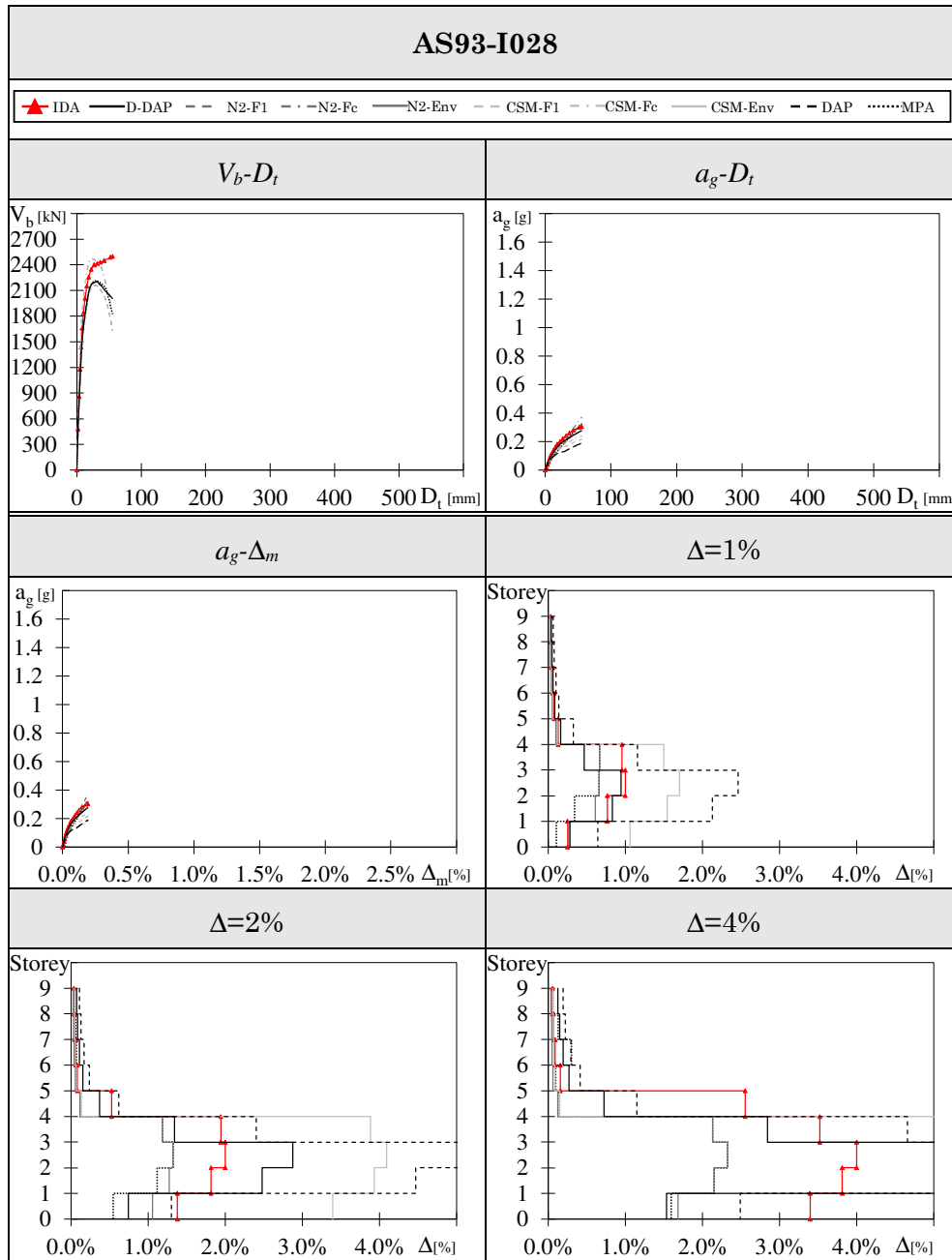












Appendix F

This appendix shows the main feature of the software ExeOS, which has been used to conduct the numerical analyses of the case study frames. ExeOS is a user friendly pre- and post-processor program that comes from the combination and the development of two previous programs, called “ExeDRAIN” and “RC-BRBs”, written by Prof. Marino and his co-workers using Visual Basic language. The program ExeOS allows the automatic execution of linear and nonlinear static and dynamic analysis of plane RC frames modelled with fibres in OpenSees. The program requires a very basic data file with the fundamental geometrical and mechanical features of the analysed frame. The user can easily manage the analysis by the program main frame (Figure 56), which allows the selection of all the analysis parameters.

The functions available in ExeOS and the operating modes will be briefly explained in the following sections.

1.1. Set up of numerical analysis in the pre-processor phase

In order to run numerical analysis by means of ExeOS two steps are required:

- Step 1: describing the frame to be analysed in a data text file;
- Step 2: setting the numerical analysis in the main frame.

A brief part of the data file is shown in Figure 57. This file contains all the essential information that are necessary for the description of the frame. In particular, it requires (i) the geometrical features of the

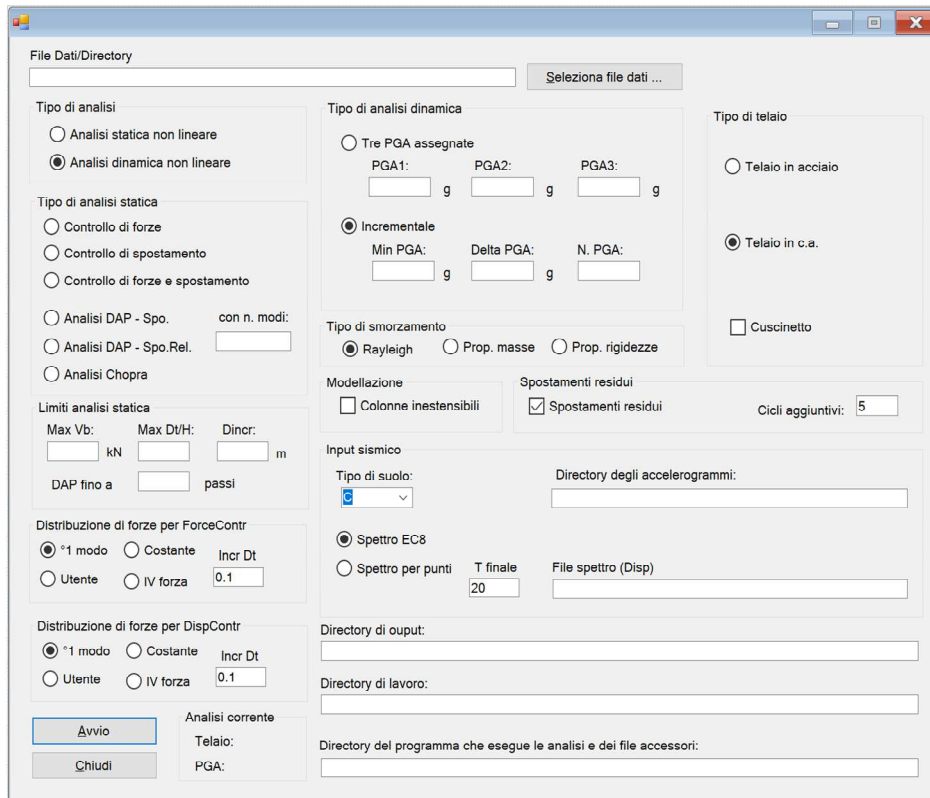
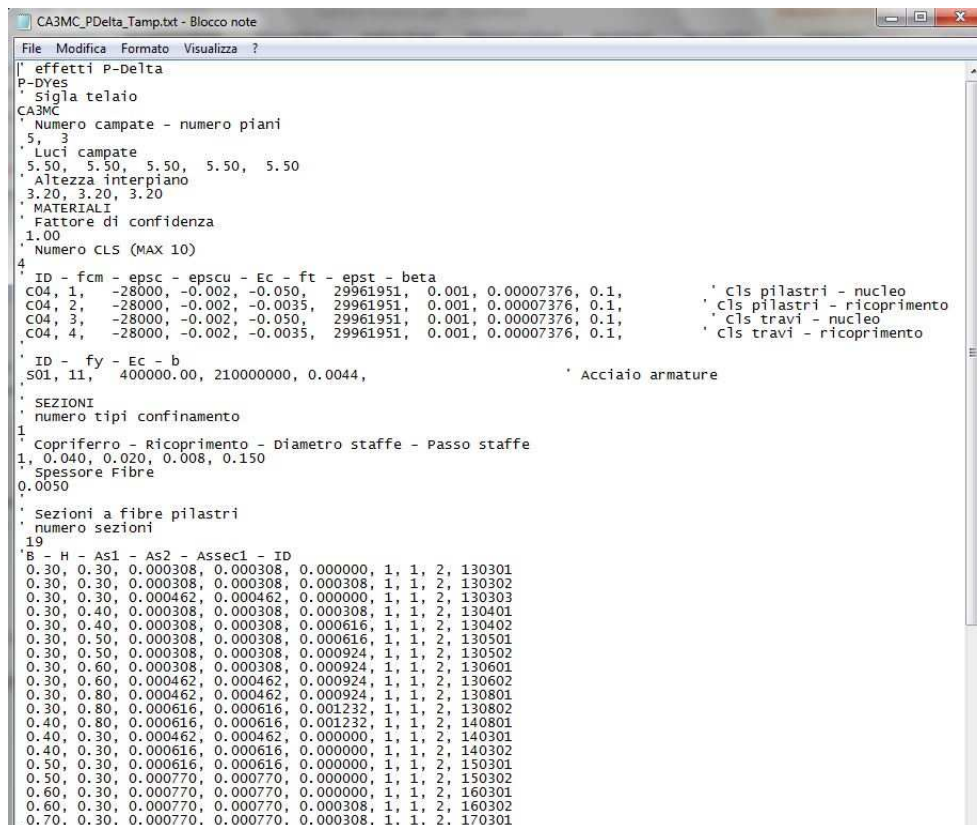


Figure 56 – Main frame of the ExeOS program

frame (number of storeys and spans, interstorey heights), (ii) the properties that are necessary to describe the constitutive laws of the materials in OpenSees, (iii) description of the geometrical and mechanical features of the fibre cross sections of columns and beams (height, depth, thickness of cover, area of rebars, materials assigned), (iv) description of the structural elements (columns and beams), (v) description of the mechanical properties of infill panels and their geometrical distribution, (vi) description of masses and loads (floor masses, loads on columns and beams, loads for P- Δ effects). All those data are read by ExeOS to build the tcl file of the frame. An extract of the tcl file is shown in Figure 58. It is noteworthy that the preparation of the data text file is a very basic task and it requires only few minutes of work. On the



```

CA3MC_PDelta_Tamp.txt - Blocco note
File Modifica Formato Visualizza ?
' effetti P-Delta
P-DYEs
' sigla telaio
CA3MC
' Numero campate - numero piani
5, 3
' Luci campate
5.50, 5.50, 5.50, 5.50, 5.50
' Altezza interpiano
3.20, 3.20, 3.20
' MATERIALI
' Fattore di confidenza
1.00
' Numero CLS (MAX 10)
4
' ID - fcm - epscu - epscu - Ec - ft - epst - beta
C04, 1, -28000, -0.002, -0.050, 29961951, 0.001, 0.00007376, 0.1, ' cls pilastri - nucleo
C04, 2, -28000, -0.002, -0.0035, 29961951, 0.001, 0.00007376, 0.1, ' cls pilastri - ricoprimento
C04, 3, -28000, -0.002, -0.050, 29961951, 0.001, 0.00007376, 0.1, ' cls travi - nucleo
C04, 4, -28000, -0.002, -0.0035, 29961951, 0.001, 0.00007376, 0.1, ' cls travi - ricoprimento

' ID - fy - Ec - b
S01, 11, 400000.00, 210000000, 0.0044, ' Acciaio armature

' SEZIONI
numero tipi confinamento
1
' Copriferro - Ricoprimento - Diametro staffe - Passo staffe
1, 0.040, 0.020, 0.008, 0.150
' spessore Fibre
0.0050

' Sezioni a fibre pilastri
numero sezioni
19
' B - H - As1 - As2 - Assecl - ID
0.30, 0.30, 0.000308, 0.000308, 0.000000, 1, 1, 2, 130301
0.30, 0.30, 0.000308, 0.000308, 0.000308, 1, 1, 2, 130302
0.30, 0.30, 0.000462, 0.000462, 0.000000, 1, 1, 2, 130303
0.30, 0.40, 0.000308, 0.000308, 0.000308, 1, 1, 2, 130401
0.30, 0.40, 0.000308, 0.000308, 0.000616, 1, 1, 2, 130402
0.30, 0.50, 0.000308, 0.000308, 0.000616, 1, 1, 2, 130501
0.30, 0.50, 0.000308, 0.000308, 0.000924, 1, 1, 2, 130502
0.30, 0.60, 0.000308, 0.000308, 0.000924, 1, 1, 2, 130601
0.30, 0.60, 0.000462, 0.000462, 0.000924, 1, 1, 2, 130602
0.30, 0.80, 0.000462, 0.000462, 0.000924, 1, 1, 2, 130801
0.30, 0.80, 0.000616, 0.000616, 0.001232, 1, 1, 2, 130802
0.40, 0.80, 0.000616, 0.000616, 0.001232, 1, 1, 2, 140801
0.40, 0.30, 0.000462, 0.000462, 0.000000, 1, 1, 2, 140301
0.40, 0.30, 0.000616, 0.000616, 0.000000, 1, 1, 2, 140302
0.50, 0.30, 0.000616, 0.000616, 0.000000, 1, 1, 2, 150301
0.50, 0.30, 0.000770, 0.000770, 0.000000, 1, 1, 2, 150302
0.60, 0.30, 0.000770, 0.000770, 0.000000, 1, 1, 2, 160301
0.60, 0.30, 0.000770, 0.000770, 0.000308, 1, 1, 2, 160302
0.70, 0.30, 0.000770, 0.000770, 0.000308, 1, 1, 2, 170301

```

Figure 57 – Part of the data text file

contrary, the construction of a tcl file of a fibre model of a frame is very time consuming and requires a much larger amount of data to be specified.

Afterwards, the analysis is set in the main frame of the program. With reference to Figure 59, the directory of the text data file and the directory of the output files are indicated in the boxes A and B. In box C, it is indicated the type of frame to be analysed (RC frame or steel frame) and some other modelling details. Box D allows the user to choose whether a nonlinear static analysis or a nonlinear dynamic analysis has to be run. In case of nonlinear static analysis is chosen, Box E is enabled and the user can choose to run:

```

CA3MC_1.TCL - Blocco note
File Modifica Formato Visualizza ?

#section Elastic $secTag      $E $A $Iz <$ $alpha>
section Elastic 199991      29961951      100      833

puts "sezioni"

# sezioni a fibre - travi

section Fiber 230601 {
  patch rect 3 110 1 -0.276 -0.126 0.276 0.126 # nucleo
  patch rect 4 110 1 -0.276 0.126 0.276 0.150 # ricoprimento //y, z>0
  patch rect 4 110 1 -0.276 -0.150 0.276 -0.126 # ricoprimento //y, z<0
  patch rect 4 5 1 0.276 -0.150 0.300 0.150 # ricoprimento //z, y>0
  patch rect 4 5 1 -0.300 -0.150 -0.276 0.150 # ricoprimento //z, y<0
  fiber 0.260 0.000 0.001090 11 # barre principali, y=0
  fiber -0.260 0.000 0.000462 11 # barre principali, y<0
  fiber 0.000 0.000 0.000308 11 # barre secondarie, y=0
};

section Fiber 230602 {
  patch rect 3 110 1 -0.276 -0.126 0.276 0.126 # nucleo
  patch rect 4 110 1 -0.276 0.126 0.276 0.150 # ricoprimento //y, z>0
  patch rect 4 110 1 -0.276 -0.150 0.276 -0.126 # ricoprimento //y, z<0
  patch rect 4 5 1 0.276 -0.150 0.300 0.150 # ricoprimento //z, y>0
  patch rect 4 5 1 -0.300 -0.150 -0.276 0.150 # ricoprimento //z, y<0
  fiber 0.260 0.000 0.001404 11 # barre principali, y=0
  fiber -0.260 0.000 0.000462 11 # barre principali, y<0
  fiber 0.000 0.000 0.000308 11 # barre secondarie, y=0
};

puts "Elementi - Pilastri"

geomTransf Linear 1
geomTransf Linear 2
geomTransf PDelta 3

# element beamwithHinges $eleTag $iNode $jNode $secTagI $lpi $secTagJ $lpi $E $A
element beamwithHinges 1101 001 101 140302 0.30 140301 0.30 29961951 0.120 0.0
element beamwithHinges 1102 002 102 130502 0.50 130501 0.50 29961951 0.150 0.0
element beamwithHinges 1103 003 103 130502 0.50 130501 0.50 29961951 0.150 0.0
element beamwithHinges 1104 004 104 130502 0.50 130501 0.50 29961951 0.150 0.0
element beamwithHinges 1105 005 105 130502 0.50 130501 0.50 29961951 0.150 0.0
element beamwithHinges 1106 006 106 140302 0.30 140301 0.30 29961951 0.120 0.0
element beamwithHinges 1201 101 201 130303 0.30 130301 0.30 29961951 0.090 0.0
element beamwithHinges 1202 102 202 130402 0.40 130401 0.40 29961951 0.120 0.0
element beamwithHinges 1203 103 203 130402 0.40 130401 0.40 29961951 0.120 0.0
element beamwithHinges 1204 104 204 130402 0.40 130401 0.40 29961951 0.120 0.0
element beamwithHinges 1205 105 205 130402 0.40 130401 0.40 29961951 0.120 0.0
element beamwithHinges 1206 106 206 130303 0.30 130301 0.30 29961951 0.090 0.0
element beamwithHinges 1301 201 301 130301 0.30 130301 0.30 29961951 0.090 0.0
element beamwithHinges 1302 202 302 130302 0.30 130301 0.30 29961951 0.090 0.0
element beamwithHinges 1303 203 303 130302 0.30 130301 0.30 29961951 0.090 0.0
element beamwithHinges 1304 204 304 130302 0.30 130301 0.30 29961951 0.090 0.0
element beamwithHinges 1305 205 305 130302 0.30 130301 0.30 29961951 0.090 0.0
element beamwithHinges 1306 206 306 130301 0.30 130301 0.30 29961951 0.090 0.0

element elasticBeamColumn 1107 007 108 1000 29961951 0.00000090 3
element elasticBeamColumn 1207 107 208 1000 29961951 0.00000067 3
element elasticBeamColumn 1307 207 307 1000 29961951 0.00000067 3

# element zeroLength $eleTag $iNode $jNode -mat $matTag1 $matTag2 $matTag3 -dir $dir1 $dir2 $dir3 <-
element zeroLength 71 107 108 -mat 101 101 100 -dir 1 2 6 -orient
element zeroLength 72 207 208 -mat 101 101 100 -dir 1 2 6 -orient

puts "Elementi - Travi"

```

Figure 58 – Part of the tcl file

- a classical pushover analysis in force or displacement control with a selected load distribution along the height;
- a multimodal displacement adaptive pushover (DAP) with a load vector evaluated from storey displacement or from storey drift and enveloping a selected number of modes of vibration;
- a modal pushover analysis according to Chopra's method, enveloping a selected number of modes of vibration.

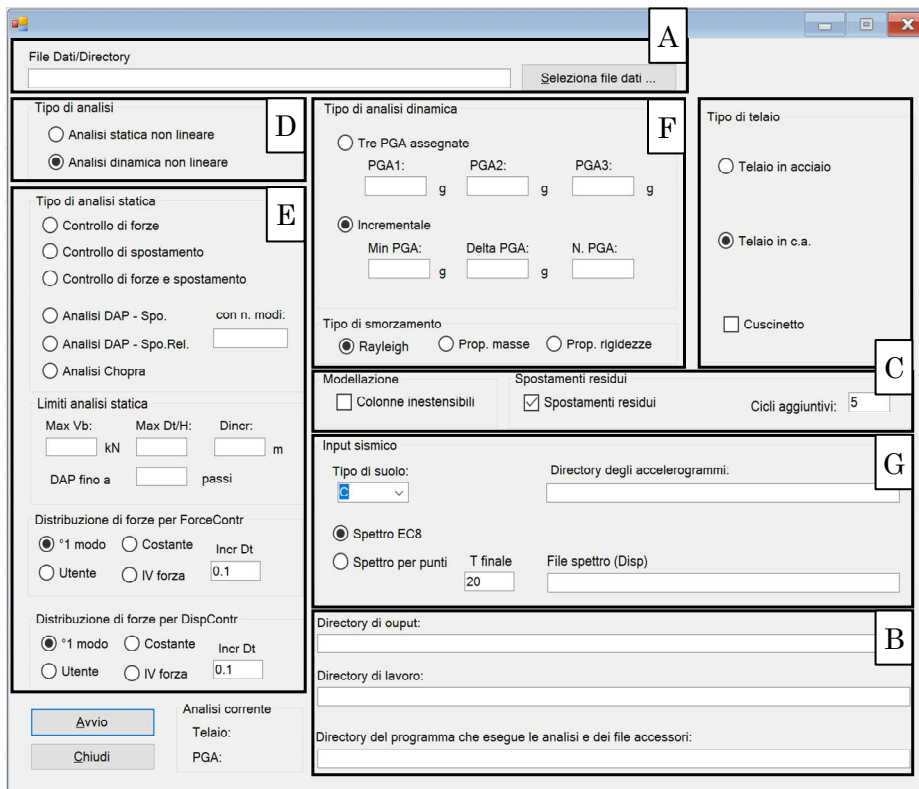


Figure 59 – Main frame of the ExeOS program with the boxes functions

For every nonlinear static analysis chosen, the final displacement or the maximum base shear to be reached, and the step size, can be indicated. Furthermore, box G allows the user to choose between the code response spectra or a response spectrum given by points.

In case nonlinear dynamic analysis, box F is enabled and the user can choose:

- to run three nonlinear dynamic analyses considering the three values of Peak Ground Accelerations (PGAs) indicated in the relevant text boxes;
- to run an incremental nonlinear dynamic analysis (IDA) with values of PGA increasing from a certain value to another, with a selected PGA step size.

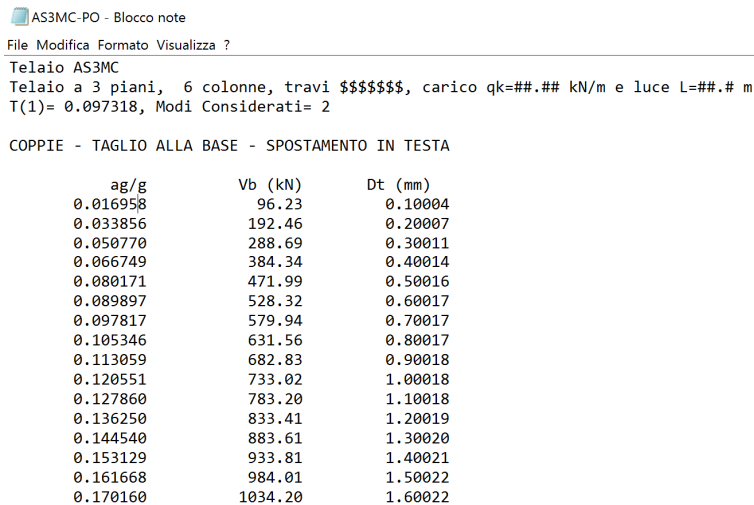
For every nonlinear dynamic analysis, in box G is necessary to indicate the type of Soil considered and the directory containing the accelerograms to be used.

Afterwards, ExeOS executes OpenSees to run the selected analysis. During the numerical analysis, OpenSees calculates the values of the response parameters at each step, and registers the results in text files. The values of local forces (axial force, shear force and bending moment) are calculated for all columns and for all the truss elements simulating the infill panels. For each storey two text files are produced to register separately the local forces of columns and infills. Another text file is produced to store the values of displacements of each storey. Thus, for every analysed frame the number of output files is equal to twice the number of storey plus one.

1.2. Elaboration of analysis results in post-processor phase

After the numerical analysis has been completed, ExeOS arranges the numerical results provided by OpenSees in synthetic files, which are easier to be interpreted and plotted.

Whichever analysis is conducted, ExeOS runs a preliminary elastic analysis, to evaluate the shape of the vibration modes, the periods of



```
AS3MC-PO - Blocco note
File Modifica Formato Visualizza ?
Telaio AS3MC
Telaio a 3 piani, 6 colonne, travi $$$$$$, carico qk=##.## kN/m e luce L=##.# m
T(1)= 0.097318, Modi Considerati= 2

COPPIE - TAGLIO ALLA BASE - SPOSTAMENTO IN TESTA
```

ag/g	Vb (kN)	Dt (mm)
0.016958	96.23	0.10004
0.033856	192.46	0.20007
0.050770	288.69	0.30011
0.066749	384.34	0.40014
0.080171	471.99	0.50016
0.089897	528.32	0.60017
0.097817	579.94	0.70017
0.105346	631.56	0.80017
0.113059	682.83	0.90018
0.120551	733.02	1.00018
0.127860	783.20	1.10018
0.136250	833.41	1.20019
0.144540	883.61	1.30020
0.153129	933.81	1.40021
0.161668	984.01	1.50022
0.170160	1034.20	1.60022

Figure 60 – Example of crp file

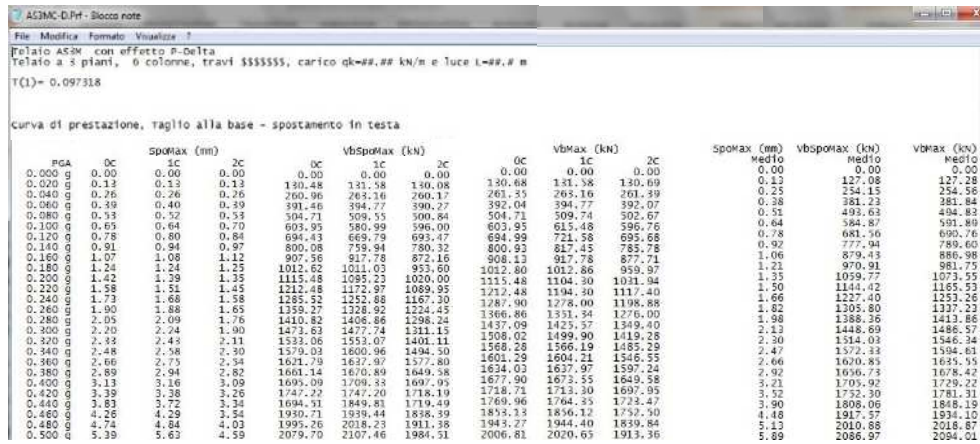


Figure 61 – Example of prf file

vibration of each mode and the modal masses. These quantities are reported in a dedicated file.

When a nonlinear static analysis is conducted, ExeOS provides the “.crp” file, briefly presented in Figure 60. This file reports the value of base shear and top displacement at each step of the pushover analysis. In addition to this, if a D-DAP analysis or a DAP analysis or a multi-modal pushover analysis are conducted, the .crp file associates the displacement demand at each step of the analysis to the corresponding value of PGA. Given those parameters, the performance curve of the frame can be expressed both in terms of base shear and top displacement and peak ground acceleration and top displacement.

In case of IDA, the main output file is the “.prf” file, partly shown in Figure 61. For each level of peak ground acceleration and for each of the *n* accelerograms applied, the .prf file provides (i) the maximum value of top displacement, (ii) the value of base shear corresponding to the maximum top displacement and (iii) the maximum value of base shear. To summarize those results, the mean value of each of the three aforementioned response parameters over the *n* number of accelerograms is reported. Furthermore, for each storey of the analysed frame the prf files provides (i) the maximum value of storey drift, (ii) the value of storey shear corresponding to the maximum storey displacement and (iii)

the maximum value of storey shear, for each peak ground acceleration and for each accelerogram. The mean values over the n accelerograms of these three response parameters are reported as well. The data reported in the .prf file allow the construction of the performance curve of the frame, both in terms of global (base shear, peak ground acceleration and top displacement) and local (storey shear, peak ground acceleration and storey drift) response.

In addition to the abovementioned files, ExeOS provides some secondary files listed in Table 15, for the analysis of specific response parameters.

ExeOS is a promising tool for the execution of nonlinear analysis of RC plane frames. Thanks to the quite large selection of analysis offered, the easy description required for whichever plane RC frame and the ready-to-use output files provided, the use of ExeOS has already been extended successfully beyond the limits of the present work.

Table 15 – List of the secondary synthetic files produced by

File	Description	IDA	DAP	MPA	PO
.Npi	Axial force in each column, for each accelerogram at each PGA, and corresponding mean values	✓	-	-	-
.Vpi	Storey shear force, for each accelerogram at each PGA, and corresponding mean values	✓	✓	✓	✓
.Vpp	Storey shear force without infill contribution, for each accelerogram at each PGA, and corresponding mean values	✓	✓	✓	✓
.Vpd	Storey shear force without infill contribution and neglecting P- Δ effects, for each accelerogram at each PGA, and corresponding mean values	✓	✓	✓	✓
.Spo	Absolute displacement of each storey at each step of the analysis	-	✓	✓	✓
.Drf	Drift of each storey at each step of the analysis	-	✓	✓	✓

List of abbreviations and variables

ACS	Advanced Capacity Spectrum method
CSM	Capacity Spectrum Method
DAP	Displacement Adaptive Procedure
D-DAP	OverDamped Displacement Adaptive Procedure
FAP	Force Adaptive Procedure
GL	Frames designed for gravity loads
GPA	Generalized Pushover Analysis
IDA	Incremental Dynamic Analysis
IO	Immediate Occupancy limit state
LS	Life Safety limit state
MDOF	Multi Degree Of Freedom
MMP	Multi-Mode Pushover analysis
MPA	Multimodal Pushover Analysis
NC	Near Collapse limit state
PGA	Peak ground acceleration
PRC	Pushover Results Combination
RC	Reinforced Concrete
SDOF	Single Degree Of Freedom
SR	Frames designed for seismic actions
SRSS	Square Root of Squares Summation
UMRHA	Uncoupled Modal Response History Analysis

D	Displacement of the MDOF system
D_t	Top displacement of the MDOF system
S_a	Spectral pseudo-acceleration
S_{ae}	Elastic spectral pseudo-acceleration
S_d	Spectral displacement
S_{de}	Elastic spectral displacement
T	Period of vibration
T_1	Fundamental period of vibration
T_B	Period corresponding to the beginning of the constant acceleration branch of the spectrum
T_c	Period corresponding to the beginning of the constant velocity branch of the spectrum
T_D	Period corresponding to the beginning of the constant displacement branch of the spectrum
T^*	Fundamental period of the equivalent SDOF system
V_b	Base shear
$V_{b,max}$	Maximum base shear
W_i	Weight of a generic i -th storey
W	Weight of the building
a_g	Value of the peak ground acceleration
$a_{g,ref}$	Reference value of the peak ground acceleration
c	Viscous damping coefficient
f_c	Compression strength of concrete
f_{ck}	Characteristic cylinder strength of concrete
f_{yk}	Characteristic yield stress of steel
h	Interstorey height
m	Storey mass
\ddot{u}_g	Horizontal ground motion acceleration
Γ	Modal participation factor
Δ	Storey drift
Δa_g	Increment of Peak ground acceleration

Δ_m	Mean value of maximum storey drifts along the height of the building
ΔD	Increment of displacement
ξ	Damping ratio
ξ_{eq}	Equivalent damping ratio
ξ_{hyst}	Hysteretic damping
ξ_{ref}	Reference value of the equivalent viscous damping
ξ_0	Nominal viscous damping
ξ_∞	Asymptotic limit value of the hysteretic damping
μ	Ductility demand
ϕ_{ij}	Eigenvector component of the j -th mode of vibration at the i -th storey
ω_n	Natural vibration frequency
ω	Input frequency

Lists of further symbols used in Chapter 1

A_n	Pseudo acceleration response
B	Scaling coefficient of the response spectrum according to Lin and Chang
D_{el}	Elastic displacement evaluated from modal response spectrum analysis with response spectrum
D_{req}	Displacement demand of the MDOF system
D'_i	Normalised modal scaling vector
D^*	Displacement of the equivalent SDOF system
D^*_{req}	Displacement demand of the equivalent SDOF system
D^*_y	Yielding displacement of the equivalent bilinear curve

E_D	Energy dissipated in a cycle of the response of a real structure
E_{SO}	Stored energy
F	Storey lateral force
F_i	Equivalent static lateral forces
F_y^*	Yielding force of the equivalent bilinear curve
F_{sn}	Resisting forces
F_{sny}	Yielding force of bilinear relation
F^*	Lateral force of the equivalent SDOF system
K_g	“Global” secant stiffness connecting the point of the performance curve corresponding to zero displacement to the displacement demand
K_s	Secant stiffness of the bilinear curve
K_l	Slope of the elastic branch of the bilinear curve
M	Storey bending moment
$M_{sys,k}$	Modal mass of the equivalent system
M^*	Effective modal mass of the considered mode shape
R_{μ}	Force reduction factor
$S_{a-cap,k}$	Equivalent system acceleration
S_n	Scaling factor of the base shear
T_e	Effective period
U	Loading vector
U_0	Nominal load vector
V	Storey shear force
V_B	Base shear estimated for the structure from static analysis
$V_{b,el}$	Strength demand evaluated from modal response spectrum analysis with response spectrum
a	Scaling coefficient of the response spectrum according to Lin and Chang
\mathbf{c}	classical damping matrix
\mathbf{f}_s	Lateral forces vector

\mathbf{i}	Unity vector
\mathbf{k}	Stiffness matrix
\mathbf{m}	Mass matrix
m^*	Mass of the equivalent SDOF system
\mathbf{p}_{eff}	Effective earthquake forces
q	Behaviour factor
r	General response quantity
r_{n0}	Peak value of a general response quantity relative to the n^{th} mode of vibration
r_n^{st}	General response quantity expressed as modal static response
r_{py}	Ratio between the post-yielding stiffness and the elastic stiffness.
q_n	Modal coordinate
s	Distribution of effective forces along the height of the frame
s	Modal force distribution
\mathbf{u}	Vector of lateral floor displacements
$\dot{\mathbf{u}}$	Horizontal floor velocity
$\ddot{\mathbf{u}}$	Horizontal floor acceleration
u_n	Response of the MDOF system in terms of top displacement
u_{rny}	Roof displacement at yielding point
u_{rn0}	Roof displacement due to the n^{th} mode of vibration
ΔD_{mod}	Increment of displacement caused by the modal shape
ΔF	Increment of storey force
$\Delta_{sys,k}$	Inverse of modal participation factor
ΔV_b	Increment of base shear
$\Delta \lambda_t$	Increment of load vector scaling factor
Φ	Displacement profile
Φ_n	Displacement profile at the top storey

λ	Scale factor of loading vector
$\bar{\phi}$	Equivalent mode of vibration

Lists of further symbols used in Chapter 2

S	Soil coefficient
T_{NC}	Period of the structure at near collapse
Ω	Scaling factor of absolute displacement of the D-DAP
η	Reduction factor of the response spectrum

Lists of further symbols used in Chapter 3

A_c	Actual cross section area of the column
$A_{c,req}$	Minimum cross section area of the column
A_s	Area of the longitudinal rebars
$A_{s,min}$	Minimum area of the longitudinal rebars
A_{tr}	Tributary area
C	Seismic coefficient
F_i	Design seismic force at a generic floor
F_h	Total design seismic force
K_{hi}	Scaling coefficient of storey weight
I	Coefficient of seismic protection
L_r	Tributary length
N	Design axial force
P_{self}	Self-weight load
P_{tot}	Total gravity load
S	Level of seismicity
R	Response coefficient
R_{ck}	Characteristic compressive cubic strength of concrete

n	Homogenization coefficient for rebars
s	Reduction factor of loads
β	Coefficient of structure
ε	Coefficient of foundation
γ_i	Coefficient that determines the distribution of seismic forces along the height of the building
ρ_l	Ratio of the longitudinal rebar area to $A_{c,req}$
$\bar{\sigma}_c$	Allowable stress of concrete

Lists of further symbols used in Chapter 4

A_w	Cross-sectional area of infill panel
E_c	Young modulus of concrete
E_s	Young modulus of steel
E_w	Young modulus of infill panel
F_{cr}	Shear cracking strength of infill panel
F_{max}	Maximum strength of infill panel
F_{res}	Residual strength of infill panel
G_k	Characteristic dead load
G_w	Elastic shear modulus of infill panel
I_c	Moment of inertia of RC column
K_{deg}	Degrading stiffness of the third branch of infill constitutive law
K_{el}	Elastic stiffness of the first branch of infill constitutive law
K_{sec}	Stiffness of the second branch of infill constitutive law
L_{pi}	Length of plastic hinge
L_w	Length of infill panel
P_{col}	Concentrated force on column
Q_k	Characteristic live load

b	Hardening ratio of steel constitutive law
b_w	Equivalent truss width
d_w	Clear diagonal length of the infill panel
f_{cm}	Average compression strength of concrete
f_t	Maximum tension strength of concrete
f_y	Yielding strength of steel
f_{ym}	Average yielding strength of steel
h_w	Clear height of infill panel
t_w	Thickness of infill panel
Δ_{step}	Displacement step size
Ψ_2	Coefficient for combination of dead and live load under seismic condition
α_1	Exponent in the equation of ξ_{hyst}
β_1	Parameter ruling the tension behaviour of concrete constitutive law
ϵ_c	Concrete strain corresponding to the maximum compression strength
ϵ_{cu}	Concrete strain corresponding to the ultimate compression strength
ϵ_t	Concrete strain corresponding to the tension strength
θ	Inclination of the diagonal truss
λ_h	Coefficient defined as a function of Young's moduli of the infill panel
τ_{cr}	Shear cracking stress of infill

Lists of further symbols used in Chapter 6

F_μ	Maximum friction force
N_g	Gravity load on column

<i>SF</i>	Short Flexible specimen
<i>SRig</i>	Short Rigid specimen
<i>TBB</i>	Top-Bottom Beam specimen
<i>TTB</i>	Top-Top Beam specimen
<i>a_b</i>	Acceleration of the lower mass
<i>a_{g,s}</i>	Ground acceleration corresponding to the first sliding
<i>a_t</i>	Acceleration of the top mass
<i>f</i>	Friction force
<i>k</i>	Lateral stiffness of the superstructure
<i>m_t</i>	Mass of the superstructure
<i>m_b</i>	Mass of the base of the separated structure
<i>u_g</i>	Horizontal ground motion displacement
<i>\dot{u}_g</i>	Horizontal ground motion velocity
<i>u_r</i>	Relative displacement between the top mass and the sliding base
<i>\dot{u}_r</i>	Relative velocity between the top mass and the sliding base
<i>\ddot{u}_r</i>	Relative acceleration between the top mass and the sliding base
<i>u_s</i>	Sliding displacement
<i>\dot{u}_s</i>	Sliding velocity
<i>\ddot{u}_s</i>	Sliding acceleration
<i>α</i>	Mass ratio
<i>μ_f</i>	Friction coefficient
<i>μ_d</i>	Dynamic friction coefficient
<i>μ_s</i>	Static friction coefficient
<i>v</i>	Amplification factor of the friction coefficient